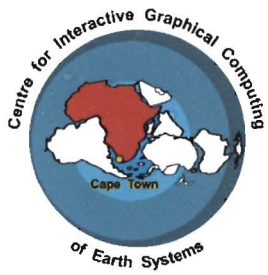

AFRICAN RIVER BASINS: THEIR PRESENT GEOMETRY AND RECENT PAST AS A FRAMEWORK FOR THEIR EVOLUTION

By: Jacek Stankiewicz

Submitted in fulfillment of the requirements for the PhD degree

University of Cape Town

Department of Geological Science

October 2004

Abstract

Fractals and scaling laws abound in nature, and it is said that geometry of river networks and basins is an epitome of this. This study investigates how on the tectonically unique African continent, scaling parameters, and in particular deviations from 'perfect fractal patterns' relate to parameters like underlying geology, climate, and vegetation through which the river flows. Stream and basin patterns are also used to reconstruct the past network geometry of rivers, and to shed some light on the drainage evolution of major African rivers.

A substantial amount of research has been concerned with treating river networks as fractals. A number of scaling laws and scaling parameters have been put forward, but it has been suggested that all river networks can be divided into universality classes represented by just 2 of these scaling parameters. One of these is the fractal dimension of individual streams, usually labelled d and having a value of ~1.1. The other parameter expresses how the dependence of stream length on drainage area changes with scale. This is Hack's Law, $l = ca^h$, where l is the stream length, a its drainage area, c a constant of proportionality, and h the Hack's exponent. Contrary to what might be expected, in African river basins h is almost never 0.5, and there is no universal value for it. Different networks often have different values for h, and inside a given network the parameter is often observed to change with scale. In most networks h decreases with increasing basin size. This decrease is not gradual, but consists of a series of thresholds. The regimes between these thresholds are analysed in this study. Horton-Strachler stream ordering is used to order networks, but it is found that real parameters, such as basin slope and aspect ratio are more productive in studying network geometry than order-based parameters, such as Hack's differentials. Furthermore, scaling regimes are more likely to be bound by basin sizes than stream orders. Thus while stream orders were used as guidelines for observing variations of h inside a network, these analyses had to be complemented by relating h to basin size, slope, aspect ratio and other such parameters.

At the smallest basin size scale, mountain streams are often non-convergent and parallel, and therefore have $l \sim a$, and $h \approx 1$. This was analysed in linear mountain belts from different geological settings: along the quartzite ridges of the Cape Fold Belt, down the

Drakensberg basalt escarpment, and in the linear basalt valleys of the Lesotho highlands. The spacing of these streams was found to be constant (with some random fluctuations) for belts in similar settings. The spacing is found to be dependant primarily of the underlying rock type, and independent of factors like mountain belt width, slope or elevation. In particular, sandstone/quartzite ranges in the Cape Fold Belt show wider spacing than basalt valleys in the Drakensberg Escarpment and in the flat-lying Lesotho highlands. Thus while h is very close to 1 in all settings, the constant c depends on local conditions.

The second regime starts when streams begin to converge and a network forms. This leads to a decrease in h. The following threshold is not fully understood, but another drop in h is observed when drainage areas reach between 400 and 1300 km^2. The two regimes on either side of this threshold are found to depend strongly on the mean basin slope in the network. Strong negative correlations are found between the slope and both the value of h in the network, and the difference in the exponent for basins on either side of the drainage area threshold. Thus basins with the lowest slopes have the greatest drop in h across the above mentioned threshold. Networks with very steep basins (mean sub-basin slope greater than 10m/km) sometimes produced anomalously high changes in h – this is interpreted as an extension of the linear regime into larger size basins. Combining these results with studies of slope and network connectivity led to the conclusion that h can be interpreted as the inverse of connectivity – the extreme case of this is observed in the hill-slope regime, where there is no stream convergence, and h has its maximum value of 1.

The last of the regimes is concerned with the continental-scale basins. It has been suggested that the shapes of these are controlled by tectonic activities, and the basins are self-similar ($h = 0.5$). This is not the case in Africa. The 11 largest basins give $h = 0.576$ with a 96.3 % correlation. The African continent is tectonically very different to the others, and one would expect this to be expressed through very different river patterns. The major basins of Africa are far from self-similar.

This thesis also shows that scaling laws and relations governing synthetic networks developed in laboratories are not necessarily observed in real networks. Approximations used in constructing theoretical networks make them unrealistic, and different to ones found naturally.

Drainage density describes what portion of land is covered by rivers. This parameter is often assumed to be constant, but this study shows this is not the case in Africa. Sections of the continent have no perennial drainage, and even the total channel density varies considerably. Using the database available, mean drainage density in Africa was measured as 0.068 km/km^2. The mean value in the Congo Basin is 0.086 km/km^2, with sections of the Congo Basin having values as high as 0.127 km/km^2. Southern Africa has a mean value of 0.076 km/km^2, while sections of the Sahara desert has channel density as low as 0.030 km/km^2, none of which is perennial.

Drainage density on the continental scale is positively correlated with the roughness of the topography in question. This correlation does not always hold on the regional scale – while in southern Africa it can be stated with 98 % confidence, it is not observed in the Congo Basin.

Drainage density of a given area is observed to play a role in the drainage organisation, as it is inversely proportional to h. Thus density is positively correlated with connectivity, as the latter is inversely proportional to h.

Drainage density, mean annual rainfall in the area and dominant vegetation type form a complex system. As climate change can result in droughts, the relationship between rainfall and density is of particular interest. It was found that most regions with annual precipitation under 400 mm have virtually no perennial rivers. Above that threshold density increases linearly with rainfall, up to a mean annual value of around 800 mm. Above that value, density becomes independent of rainfall, and is related more closely to dominant vegetation type than to rainfall. Drainage density is dependent on vegetation, not vice versa. Forested areas result in higher density than savanna. This is a guideline, not a direct relation – variations in vegetation do not explain density variations in the Congo Basin.

Given the threshold values above, regions that receive between 500 and 900 mm/year would be affected by a change in rainfall. Regions receiving 600 mm/y would have their drainage density halved if the rainfall dropped by 100 mm/y, while in regions receiving 500 mm/y such a drop would eliminate the little perennial drainage that did exist. Using climate forecasting models, water related conflicts that can potentially result from such a change can be addressed before they happen. A number of future climate models exist,

though these often differ. A worst-case scenario can be obtained and preparations for it can be laid in place. The CCCMA(A2) model predicts a decrease in annual rainfall across Africa of between 50 and 150 mm by the end of the 21st century, and this can significantly reduce the perennial drainage in the region, most of which is within the sensitive regime mentioned above.

Evolution of drainage patterns is also considered in the thesis. First, river patterns and surface trends in Central and East Africa were analysed. These, combined with fossil evidence and existing drainage evolution models led to the conclusion that before the Eocene, the Congo basin drained eastwards into the Indian Ocean, and that the Rufiji Delta was the most likely outlet of this network. Paleo-drainage of the Nile is also analysed. The old drainage lines in NE Africa are unique in that they are buried beneath a thick sand cover, and can only be observed with radar technology. A detailed analysis of this buried network can only be done if the whole area, not just sections of it, are surveyed. Such an analysis would shed more light on the history of north African drainage, and might give indications whether the Sahara will become vegetated again.

This thesis shows how drainage patterns contain information about the history of the river. These patterns can also hold clues about the future of drainage, which is very closely related with the development of climate, vegetation, and life. Water is a vital resource, and it must managed as such.

Acknowledgements

Prof. Maarten de Wit fulfilled with distinction the task of supervising this thesis. The project would not be possible without his guidance, constant interest in my work, enthusiasm and generosity.

Dr Moctar Doucoré, co-supervisor of this thesis, was spared having to deal with me on a daily basis after moving from UCT to De Beers Group in Centurion, but he remained involved in my project throughout, and continued to provide me valuable feedback.

At the beginning of this project I was lucky to spend some time with Prof. Dan Rothman at the Massachusetts Institute of Technology, an expert on river network geometry, and I would like to thank him for the time and effort he put into my project. I would also like to thank his research group: Norbert Schorghofer, Wes Watters and Josh Weitz for making my visit to MIT as not only as productive as possible, but also very pleasant.

African river databases used throughout this project were obtained from De Beers Group in Centurion. For this I would like to thank Dr Mike de Wit, with whom I also had a number of valuable discussion and Lindsay Urban. Dr Moctar Doucouré was a vital link between UCT and De Beers after his move.

Prof. Bruce Hewitson, from UCT Environmental and Geographical Science, provided me with a number of climatic forecasts and relevant literature, as well as giving me a crash-course on climate forecasting, and his valuable time is greatly appreciated.

While field work was not an integral part of this project, a number of field trips helped me make the transition from Theoretical Physics to Earth Science. I would therefore like to thank the people who invited me on their trips, and took time to help with this transition, in particular Prof. Maarten de Wit, John Decker, Danny MacPhee, Blair Schoene and Eugene Grosch. What some of these trips lacked in success was usually made up in entertainment. I never went on a field trip with Daud Jamal, but he often patiently explained simple geological problems in our lab. John Decker is also a member of the Carbon Cycle Group, though this research project was not a part of this thesis. He also makes excellent coffee every second morning at work.

I want to thank my parents not only for the usual parental support, but also for proof-reading this thesis – yes, they are qualified. Big Thank You to Sam for helping me to remain sane during this project.

Financially, this project would never happen without the generosity of Prof. de Wit. Prof. Craig Comrie from Physics at UCT very kindly allowed me to carry on being a physics lab demonstrator for a year, even though I was not in his department any more. The National Research Foundation provided financial support during this project.

Last, but certainly not least, Dr Marian Tredoux can never be thanked enough for luring me from Physics to Earth Science.

Table of Content

List of Figures

Chapter 1

Introduction

1.1. Importance of rivers and their basins

In our world water is essential for sustaining of life. Not just human life, but all animal and plant life. Terrestrial life, in most cases, is in particular dependant on fresh surface water. Thus rivers and their basins are of critical importance for life on Earth. The importance of rivers is clear in examining human history. The earliest civilizations were found near major rivers: The Egyptian Kingdom was absolutely dependent on the Nile, as Mesopotamia was on the Tigris and Euphrates. In Europe virtually all major cities have been built on the banks of a major river, while agricultural regions need water for irrigation. Today the importance of rivers is even greater than before, with energy provided by moving water being used to power many industrial plants, while fresh water fish are an important source of food.

Water, like all resources important to mankind, can also be a source of conflict. River channels and basin watersheds very often mark international boundaries. In southern Africa sections of each of the Orange, Nossob, Molopo, Limpopo, Cunene, Okavango, Cuando and Zambezi form such boundaries, as do the Drakensberg and Chimanimani Mountains watersheds. When water is scarce, disputes about access to the shared waters is bound to arise. One the most famous conflicts in history, between Israel and Palestine, has at least partially been about access to the Jordan river. In Africa the conflict over the Nile water supply dates at least as far back as the times of Nero, the Roman emperor, while a legend tells of an Egyptian Sultan during a famine in Egypt sending ambassadors to the Ethiopian King to ask him to stop interfering with the flow of the river near one of its sources. While that story sounds ridiculous, it bears close resemblance to actual events in the 20th century concerning European nations arguing over an African river, and all

conflicts related to building dams on the Nile (Collins, 1990). Water can be expected to be a source of conflict in the future unless international policies for river basin management are put in place. Even when such policies are attempted, the results are not always what should have been hoped for. In 1995 the Southern African Development Community[1] (SADC, a community of 14 independent states in southern Africa) adopted a protocol on shared watercourse systems aimed at cooperation in utilization of water. Vale (2004) comments on how each country's individual politics stand in the way satisfying the communities that need the water, and goes on to criticize the governments for not showing the imagination required for such a project to succeed. The importance of water is only going to increase in the future, and governments should not treat problems associated with it lightly.

1.2. Landscape and river basin evolution

By now scientists everywhere accept that landscapes are dynamic and continuously evolve. Mechanics associated with tectonic plate motion produce new mountain ranges, as do volcanic eruptions. Alterations in the landscape will clearly change the river system that drains it. The erosive effects of these rivers will continue changing the landscape. Even simple erosion with no input from tectonics can the change the landscape to a point where the drainage pattern will be significantly different (i.e., river captures). The first comprehensive model for landscape evolutions through erosion was proposed by Davis in 1889. It states that if erosion continues unchecked for a sufficiently long time, all topographic features will disappear, and the landscape will just be a low gradient surface (a peneplain) just above the sea level. Tectonic motions and volcanism rarely allow this to happen in reality. Thus landscape and drainage evolution is a dynamical system that can potentially be highly complex.

While drainage evolution is an interesting study area in its own right, its potential implications are from being purely academic. A series of studies by Cotterill (2003a, b, c, 2004; Broadley & Cotterill 2004) shows how it can account for observed spatial variations in animal life, while de Wit (1999) is but one example of the importance knowledge of drainage evolution has in identifying mineral placer deposits.

[1] www.sadc.int

Drainage evolution due to tectonics is not going to happen fast enough to be considered a threat to human population being dependant on a particular river system. Drainage is, however, also closely related to climate and vegetation, and these form a complex system capable of evolving in a time frame as short as decades. Climate changes in the Sahara were instrumental in both formation and demise of the Egyptian Old Kingdom (Claussen *et al*, 1999; Krom *et al*, 2002). If a small change in climate could have such far reaching consequences on vegetation and drainage, what effect can human induced changes in vegetation potentially have on the climate and water supply?

1.3 Network geometry

River networks form a wide variety of patterns. A description of their most common types can be found in any introductory book on geomorphology, usually accompanied by a brief description of the underlying terrain necessary to produce such a pattern.

A considerable amount of work has been done to attempt to describe river networks mathematically, using a series of numbers, each describing a particular property of the network. Some generalizations need to be made to achieve this, as no two real networks are identical. A question often asked first is whether networks are self-similar, i.e. does the network pattern depend on scale. To study the question of scale invariance the networks are often considered in terms of fractal geometry, where they are described by a series of scaling power laws. The exponents in these scaling laws are the numbers which scientists have used to describe networks numerically.

While a lot of work has been published concerning scaling laws and universality classes of networks, little has been done to relate the scaling exponents to geological and climatic conditions the river concerned flows through. This thesis will attempt to investigate whether real networks can be described numerically without gross over-simplifications, and how these parameters depend on the regional setting of the river basin.

1.4 Why Africa?

Africa is different to all other continents in a number of ways. The African plate is surrounded mostly (> 90 %) by extensional plate margins in the form of spreading ridges, and is the only plate relatively stationary with respect to mantle circulation (Burke &

Wilson, 1972). The only active mountain range resulting from orogeny is the Atlas range. Despite this Africa is host to some of the world's greatest elevated regions (Fig. 1.1). These are results of epeirogeny (e.g. vertical motion of continents; not associated with orogeny). The topography of Africa is also distinctly bimodal, with high, rugged regions in the south and east, and smooth, low-lying areas in the north and west. African topography is thus very different to ones on other continents. Such a topography might be expected to produce river networks different to ones on other continents, and it does (Fig. 1.2, and more detailed figures in later Chapters). A number of rivers flow away from the coast they are closest to, and what seems like a logical outlet (e.g. Niger, Zambezi, Orange). These have been suggested to be plume-related drainages formed above mantle hotspots (e.g. hot upwelling mantle - Cox, 1989). There are a number of plume-related failed rifts in Africa, and these often become major river valleys (e.g. Benue, Limpopo). Africa thus presents a fascinating natural laboratory of river networks apparently different to anywhere else in the world. A number of basins are landlocked (Okavango and Chad being the largest ones), though this is not unique to Africa (e.g. Caspian Sea).

Rivers in Africa are far from being just academic curiosities. Water conflicts are more likely in regions where the resource is scarce. A historical analysis of water conflicts (Wolf *et al.*, 2003) showed that conflicts are more frequent in 'marginal climates with highly variable hydrologic conditions'. Countries that do not have an effective water management scheme are also more likely to be involved in such a dispute. In developed countries not suffering from water shortage, sharing rivers is rarely an issue. Africa, unfortunately, is largely made up of dry areas and countries with no efficient water management schemes. Rivers form over 25,000 km (33%) of national boundaries in Africa, and major watersheds a further 5,000 km (6%). These are shown in Fig. 1.3. Conflicts often occur at these borders. Namibia and Botswana governments are currently arguing about the ownership of islands on the Chobe river (Ashton, 2002). The above percentages are lower than might be expected due to North African boundaries usually being arbitrary straight lines through the desert. These boundaries also experience water related conflicts, ranging from tribal fights over watering holes on the Mali-Mauritania border to the seemingly infinite series of conflicts and agreements over the 'ownership' of the Nile between Egypt and Sudan (e.g. Collins, 1990). The importance of water

management is being realized, and a number of international meeting regarding it have taken place, such as the Nile Basin Initiative[2] program started in May 1999 between countries sharing the Nile Basin. Unfortunately this has not been very successful. One of the major problems is the East African countries' refusal to surrender rights to water from Lake Victoria and Egypt's resulting military threats (Kimani, 2004).

Water and basin management is not just an international issue – it is clearly important for each country to mange the resources it does not share with other states. An example of this is the Working for Water program in South Africa (latest report: MacDonald, 2004). This program is a government initiative that addresses the problem of invasive plants, and their effect on water supply. This initiative, instead of attempting to randomly remove all vegetation, carefully calculates the impact of each alien plant species (e.g. Nel *et al.*, 2004), and provides scientific models for the most cost-effective water resource management (e.g. Görgens & van Wilgen, 2004). The attention this project receives from both the scientific community and government organizations shows the water management problem is given the attention it deserves.

1.5. Summary

It is clear that water is a vital resource. While the availability of clean water decreases, human population increases constantly, and with it the need for water. Water management schemes, both on national and international levels, are thus necessary. Water supply depends on regional climate and vegetation, and changes in either will affect the water supply. This thesis will attempt to relate the availability of river water to these parameters. In any water management scheme, future projections of the water supply of the river must be taken into account, and therefore river and basin evolution should be considered. This will be attempted by studying network geometry. In a flat world with uniform geology, climate and vegetation, networks would form perfect fractal patterns. In a real world, deviations from such 'perfection' result from different geology, topography and climate in different parts of the basin. They also hold clues about the river's past, and can therefore tell us something about their future. Before going into such an analysis, fractals must first be introduced.

[2] www.nilebasin.org

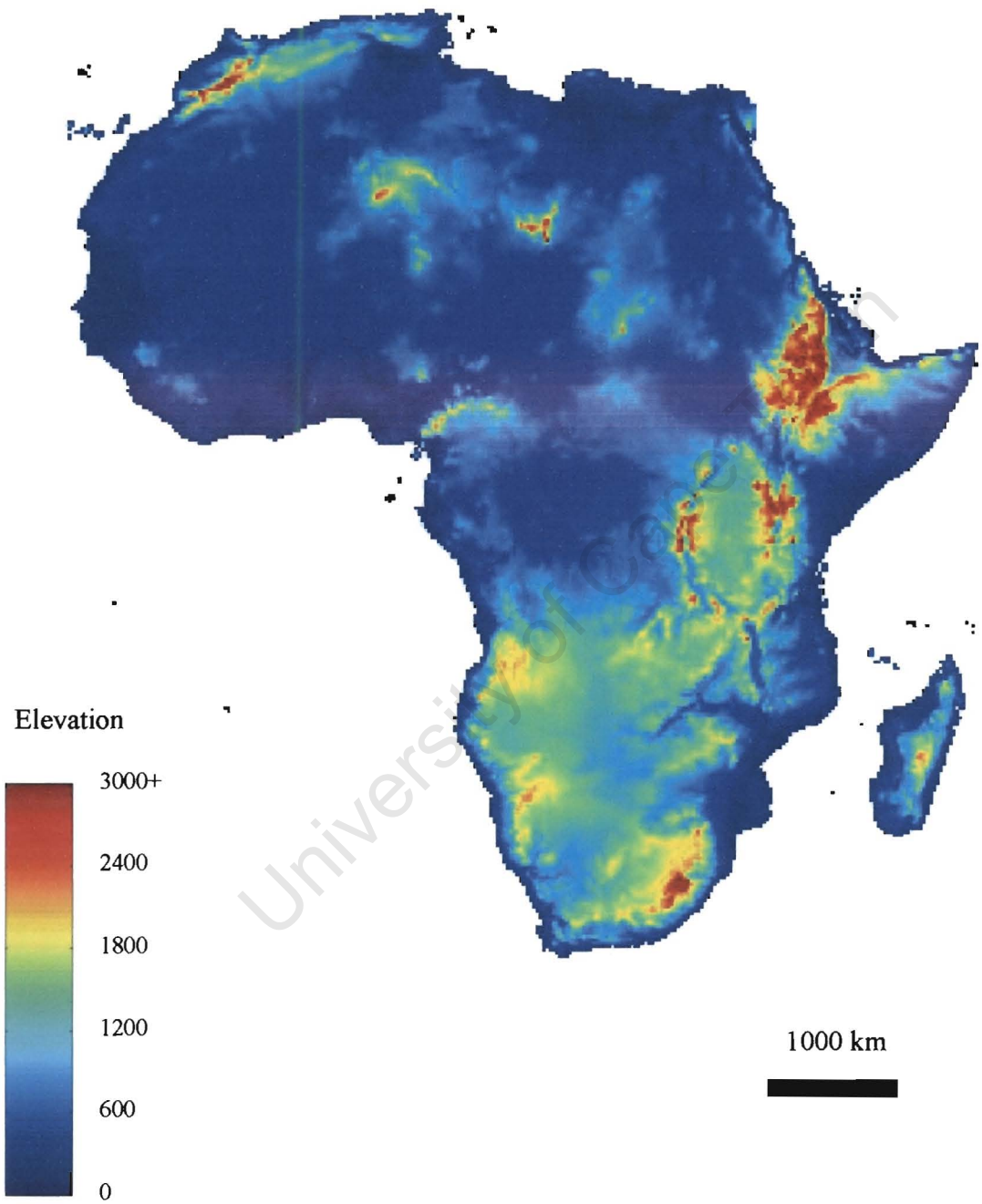

Fig. 1.1. Topography of Africa. Digital Elevation Model (30 km resolution) obtained from the U.S. Government website – see section 4.3. of this thesis for site address.

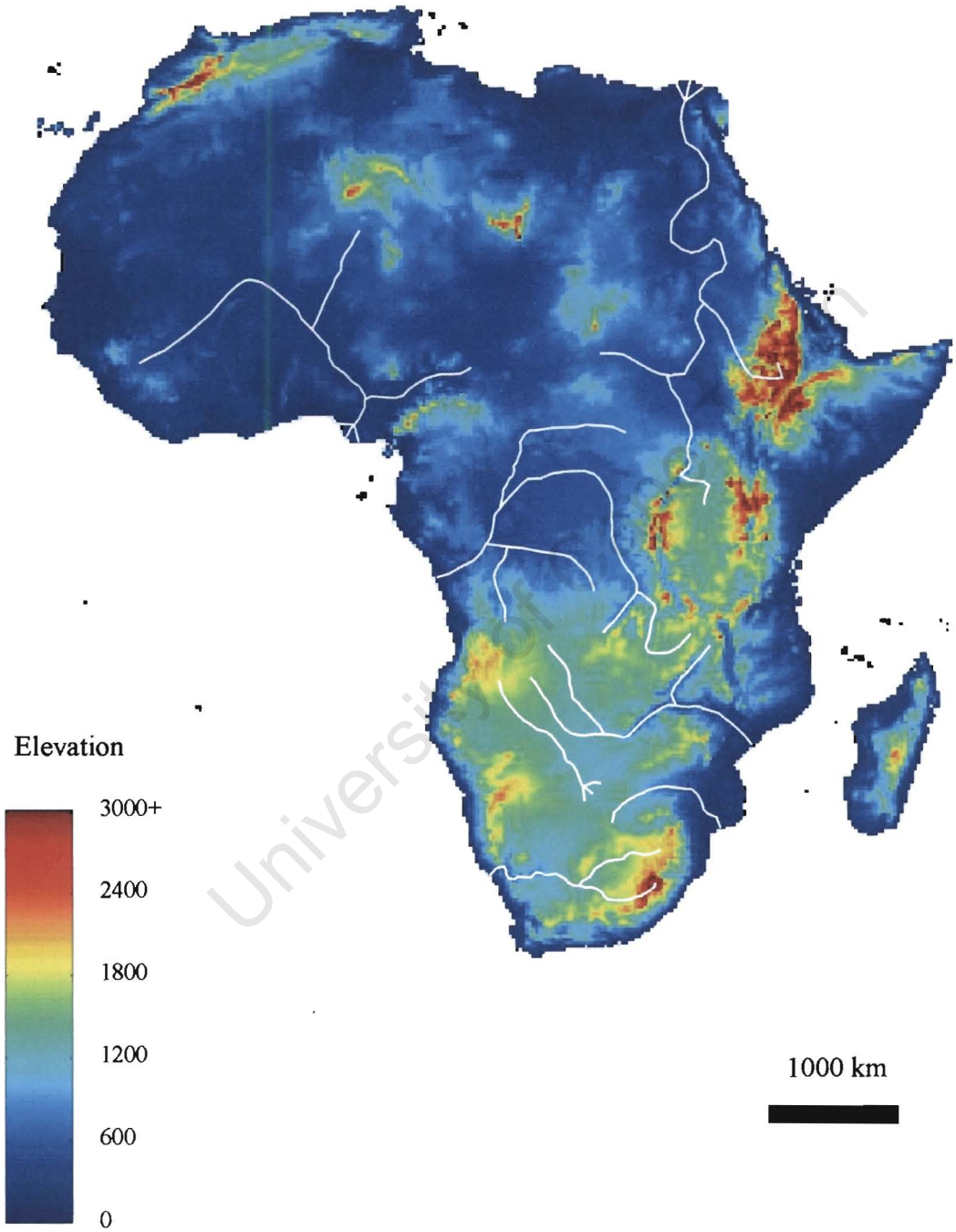

Fig. 1.2. Major rivers in Africa superimposed on Fig. 1.1 DEM.

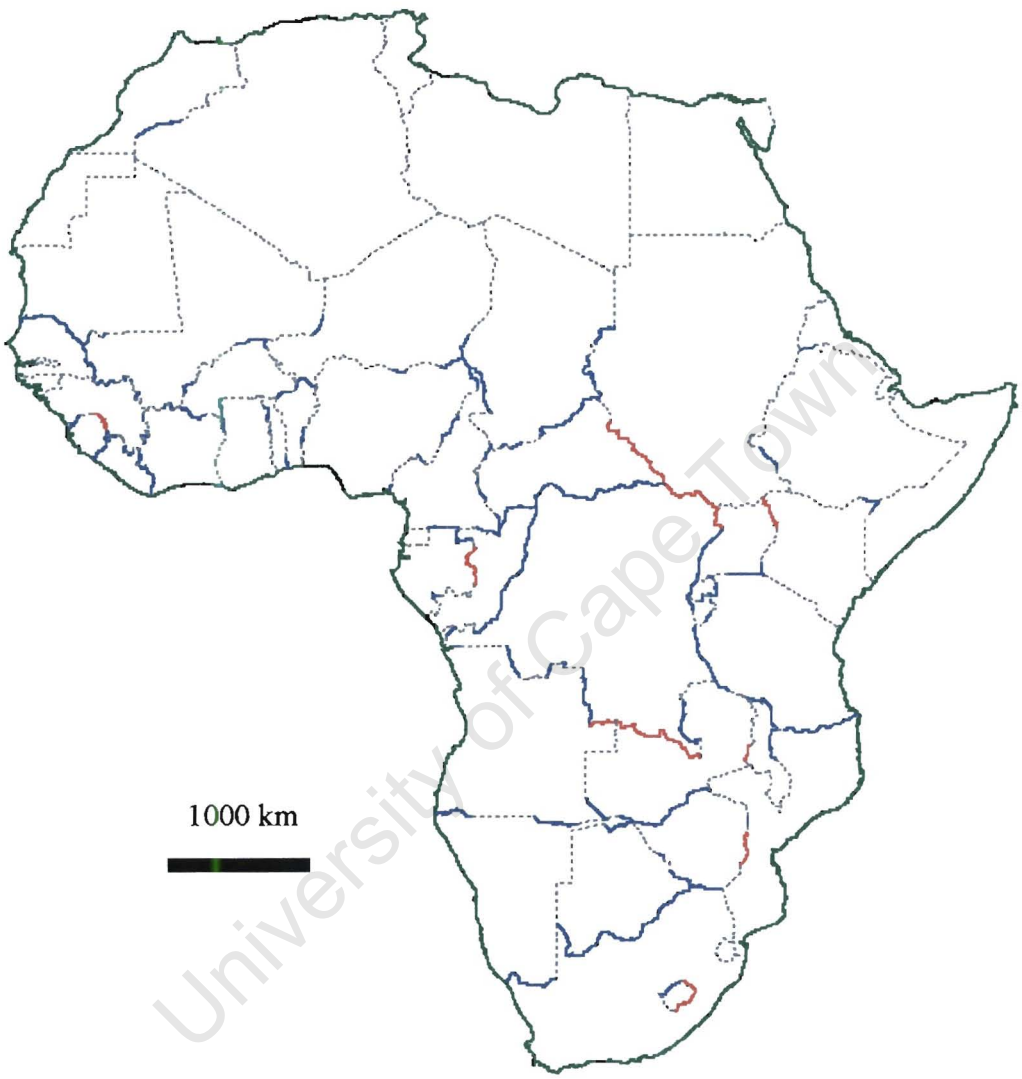

Fig. 1.3. National boundaries in Africa:
green: coastline: 40,300 km
blue: rivers: 25,900 km
red: watersheds: 5,000 km
gray: other: 47,300 km
Source: CIGCES data base derived from data of De Beers Group, Centurion.

Chapter 2

Introduction to Fractal Sets

2.1. Scale invariance

The scale invariance of geological phenomena has been experienced by nearly all earth scientists. When studying a photograph of a fold in rock strata, for example, it often cannot be determined whether it has an amplitude of 10 cm or 10 km. For this reason a scale defining object, like a coin, a rock hammer or a person, is usually included by geologists in their field pictures to give an idea of the scales involved. Another example is a photograph of a rocky coastline – without a reference object the scale cannot be determined. Objects that exhibit similar properties at a wide range of scales are said to be scale invariant.

It was in the context of the rocky coastline that Mandelbrot (1967) introduced the concept of fractals. The length of the coastline is determined using a measuring rod of a specific length. As the length of the rod decreases, the measurement becomes more accurate, and the measured length on the coastline increases. If the coastline is scale invariant, the measured length will increase according to a power law, which will be explained in the next section. This power law determines the fractal dimension of the coastline.

Scale invariance abounds in the geological world. It has been found in earthquake distribution (Gutenberg & Richter, 1954), thermal convection (Lorenz, 1963), rock fragmentation (Turcotte, 1986), and river networks which will be dealt with in great detail here, to name just a few.

2.2. Definition and examples

Since the original introduction of fractals (Mandelbrot, 1967), they have been applied to a wide variety of fields, from the most abstract mathematical concepts to the most empirical concepts of engineering. It is not clear that a single formula can encompass all the fractal sets, so following Turcotte (1992) a quantitative discussion can be started by defining a fractal set according to

$$N_n = \frac{C}{r_n^D} \tag{2.1}$$

where N_n is the number of objects (fragments) with a characteristic linear dimension r_n, C is a constant of proportionality and D the fractal dimension. Thus in the case of the rocky coastline mentioned above, r_n is the size of the measuring rod, and N_n the number of measurements with the rod. If the above power law holds for a given range of scales, the object is said to be scale invariant, or exhibit fractal statistics for those scales.

The fractal dimension D can be an integer, in which case it corresponds to the Euclidian dimension, and the object in study is then a point ($D = 0$), a straight line ($D = 1$), a square ($D = 2$) or a cube ($D = 3$). Usually, however, D is a fractional dimension, which is the origin of the term fractal.

Assuming Eq. (2.1) holds on a scale between given r_n and r_{n+1}, an expression for D can be obtained:

$$D = \frac{\ln(N_{n+1}/N_n)}{\ln(r_n/r_{n+1})} \tag{2.2}$$

It may now be instructive to consider simple examples of fractal sets. Consider a unit length line segment divided into three equal sub-segments, of which the outer two are retained and the middle one discarded. This process is repeated for all remaining segments. The first three iterations are shown in Fig. 2.1. The total length of the segments remaining in the set will tend to zero as the number of iterations tend to infinity, but consider how the measurements change with a decreasing rod length. Let $r_1 = 1$, $r_2 = {}^1/_3$, $r_3 = {}^1/_9$ and so on, the rod length decreasing by a factor of 3 with each iteration. From Figure 2.1 it is clear that $N_1 = 1$, $N_2 = 2$, and $N_{n+1} = 2N_n$. From Eq. (2.2) this gives $D = \ln 2 / \ln 3 = 0.6309$. This simple fractal in known as a Cantor set.

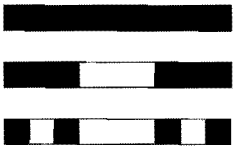

Fig. 2.1. The first three iterations for the construction of a Cantor set.

Another famous construction is the triadic Koch island illustrated in Fig. 2.2. It starts with a unit side length equilateral triangle, and each iteration consists of drawing an equilateral triangle on all straight lines available, facing outwards from a base of the central one-third of each line. To study its perimeter the obvious choice for measuring rods will again be a factor 3 decrease with each step, starting from unity. Then $N_1 = 3$, $N_2 = 12$ and $N_{n+1} = 4N_n$. This gives $D = \ln 4 / \ln 3 = 1.2619$.

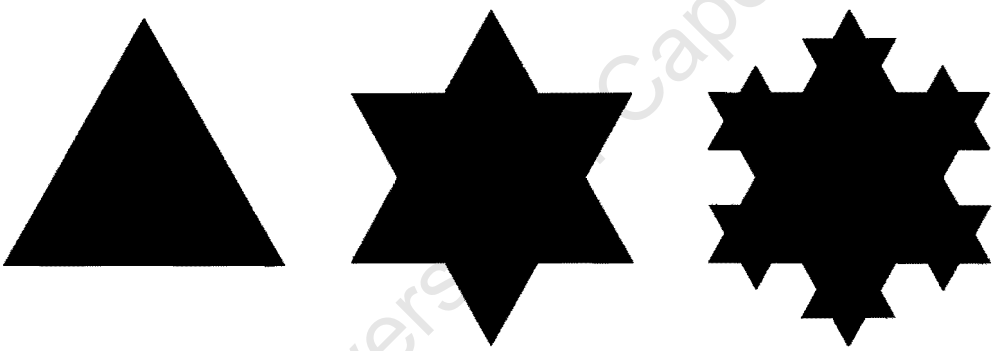

Fig. 2.2. The first three iterations in the construction of the triadic Koch island.

Mandelbrot's original question about the rocky coastline (Mandelbrot, 1967) is essentially similar to the Koch island model above. Using a measuring rod r_n the perimeter of the island is given by

$$P_n = r_n N_n \tag{2.3}$$

Combining this with Eq. (2.1) gives

$$P_n = \frac{C}{r_n^{D-1}} \tag{2.4}$$

which can be linearized to give

$$\ln P_n = (1-D)\ln r_n + \ln C \tag{2.5}$$

Thus the fractal dimension of a real coastline can be obtained from a logarithmic plot of the perimeter as a function of the measuring rod used. A straight line graph with slope m on a range $[r_1; r_2]$ implies scale invariance on that range of scales, with a fractal dimension $D = 1 - m$. Using this method Mandelbrot (1967) obtained $D = 1.25$ for the coast of Great Britain for scales between 1 and 100 km.

It is often useful to have an idea of the probability distribution of a fractal set in space, i.e. knowing the probability of a randomly chosen portion of space containing part of the set. For the example of the Cantor set (Fig. 2.1), consider the probability that a step of length r will include a line segment. At zero order the probability of $r_0 = 1$ encountering a segment is clearly $p_0 = 1$. At first order ($r_1 = {}^1/_3$) we have $p_1 = {}^2/_3$, at second order $r_2 = {}^1/_9$ corresponds to $p_2 = {}^4/_9$, and we can generalize

$$p_n = N_n r_n \tag{2.6}$$

where N_n is the number of line segments of length r_n. Combining this with Eq. (2.1), and taking $C = 1$ for normalization we can write the expression for the probability of a step of length r_n containing part of a fractal constructed from a straight line as

$$p_n = r_n^{1-D} \tag{2.7}$$

where D is the fractal dimension.

Similar expressions can be obtained for fractals in planes and volumes (and even in hypothetical d > 3 spaces). We note that for a given fractal set in a space of Euclidian dimension d

$$p_i = N_i r_i^d \tag{2.8}$$

which, combined with Eq. (2.1) gives

$$p_i = r_i^{d-D} \tag{2.9}$$

as the probability of a multi-dimensional step r_i containing part of the set.

2.3. Box-counting method

While the ruler method described above was the first one used to obtain fractal dimensions, it is not the most convenient one. The box-counting method (Pfeiffer & Obert, 1989) has a much wider range of applicability, as it can be used equally well to continuous curves, closed objects, and even distributions of points in two or three (or hypothetically even more) dimensions.

The method involves covering the space containing the set in study with same-size boxes (squares or cubes, depending whether the space in a plane or a volume), and counting how many boxes contain elements of the set. An investigation of how the number of 'full' boxes (N) changes as a function of length of the side of the box (r) can then reveal whether the set is a fractal, and what the corresponding equation is. A power law relation similar to Eq. (2.1)

$$N = \frac{C}{r^D} \tag{2.10}$$

will imply the set is a fractal on the range of scales for which the law holds, and D is the corresponding fractal dimension. This method can be used to measure the fractal dimension of a coastline by counting how many squares contain a piece of the coastline, as well as of a distribution of points (e.g. mineral deposits) by checking squares containing one or more deposit.

It is still debated (see Halsey & Jensen, 2004) for a review, whether this simple technique can be extended to more complicated sets, like multifractals introduced by Halsey *et al.* (1986). Such sets are well beyond the scope of this thesis. However, the standard, relatively simple box-counting technique described above continues being used even in the most advanced studies of fractal sets and chaotic systems (e.g., Gratrix & Elgin, 2004).

2.4. Self-affinity

All fractals discussed thus far were isotropic – if the object were rotated by 90 degrees (e.g. swapping the NS and EW axes of an island) the fractal dimension would not change. Not all fractals are like that – consider an island with a mountain chain. Both the coastline and the elevation of a cross-section can be fractals, but the vertical coordinate, while related to the horizontal, will have a much smaller scale.

A formal definition of an isotropic (or self-similar) fractal in a two dimensions xy-space is that $f(rx,ry)$ is statistically similar to $f(x,y)$ where r is a scaling factor. Thus if we need N_1 boxes of size x_1,y_1 to cover a set, and N_2 boxes rx_1,ry_1 then Eq. (2.2) implies that $N_2/N_1 = r^{-D}$.

An anisotropic fractal, also called self-affine, is defined as a set where $f(rx,r^H y)$ is statistically similar to $f(x,y)$, where the constant H is known as the Hausdorff measure. An example of a self-affine fractal is a random Brownian walk. A general motion in the horizontal consists of a random step up or down for every horizontal one. Three examples of such walks are shown in Fig. 2.3.

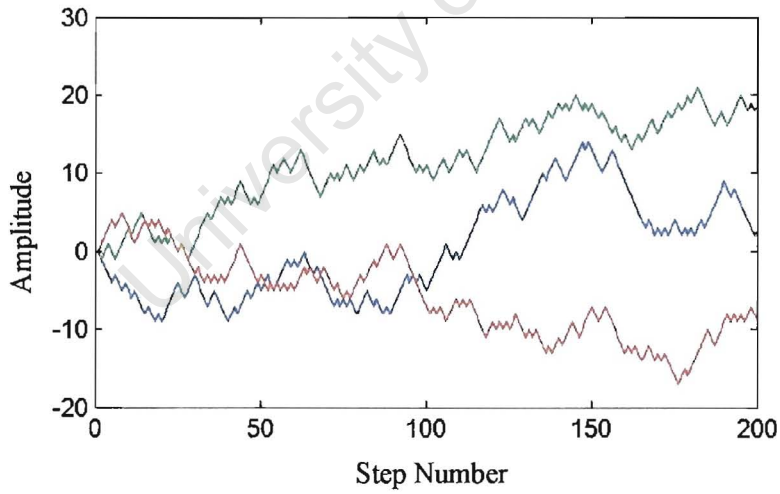

Fig. 2.3: Three examples of random Brownian walks of 200 steps each: at each time step the function randomly either increases or decreases by 1.

Self-affine fractals are generally treated quantitatively using spectral techniques (e.g. Turcotte, 1992). A detailed analysis is not necessary here, but an insight will be presented. Consider a single-valued function of a single variable *z(x)* that is random, but has a specified spectrum, such as dependence of topography on a distance along a linear track. This particular case will be important later in this thesis. A simple introduction is provided here, and a more detailed description is given in Appendix A. A fundamental consideration in such a series is the correlation between *z(x+x')* and *z(x)*. The larger the value of *x'*, the less the two values are expected to be correlated. For the series to be a self-affine fractal, it needs to satisfy the probability condition

$$p\left[\frac{z(x+x')-z(x)}{(x')^{H}} < z'\right] = F(z') \tag{2.11}$$

where H is the Hausdorff measure. While remaining random, the above equation states point values must be correlated with adjacent ones. If $H = 0$ there is no correlation and the series is white noise, while for $H = 1$ the fractal becomes isotropic (or self-similar) in z and x. A relation between H and D, the fractal dimension, can be derived (e.g. Turcotte, 1992):

$$H = d - D \tag{2.12}$$

where d is the Euclidean dimension of the space containing the fractal. Euclidean dimension is an integer number between 0 and 3 (inclusive) which corresponds to degrees of freedom the space containing a given set has. A point has $d = 0$, a straight line $d = 1$, a plane $d = 2$, and space $d = 3$. The exact derivation of this equation for $d = 2$ and $d = 3$ can be found in Appendix A. It can be calculated (e.g. Turcotte, 1992) that for random Brownian motion in 2-dimensional space (Fig. 2.3), $H = 0.5$, and hence $D = 1.5$. A more detailed discussion of fractals is beyond the scope of this work. An interested reader is referred to Mandelbrot (1967, 1975), Turcotte (1992) and Bak (1996).

We now turn to applications of fractals and scaling laws to African river networks, but first a table (Inset 1) is presented as a summary of scaling parameters that will be introduced in the next 2 Chapters.

Inset 1: Summary of River Network Fractal Parameters used in Chapters 3 and 4

Symbol	*Parameter*	*Section in text*	*Approx. value*	*Reference*
ω	Stream order	3.2	Integer	Horton (1945); Strahler(1957)
l	Stream length	3.2	N/A	N/A
a	Drainage area	3.2	N/A	N/A
Ω	Network order	3.2	Integer	N/A
$n(\omega)$	Number of streams of order ω in the network	3.2	N/A	N/A
$l(\omega)$	Mean length of streams of order ω	3.2	N/A	N/A
$a(\omega)$	Mean basin area of streams of order ω	3.2	N/A	N/A
R_n	Network's branching ratio	3.2	3-5	Horton (1945); Abrahams (1984)
R_a	Drainage area scaling with ω	3.2	3-6	Horton (1945); Abrahams (1984)
R_l	Stream length scaling with ω	3.2	1.5-3	Horton (1945); Abrahams (1984)
$L \equiv L_{\parallel}$	Basin length	3.2	N/A	N/A
$L_{\perp}$	Basin width	3.2	N/A	N/A
h	Hack's exponent (a-l relation)	3.2	0.5-0.7	Hack (1957)

D	*a*-L scaling exponent	3.2	1.5-2.2	Maritan *et al* (1996)
d	Individual stream fractality	3.2	~1.1	Maritan *et al* (1996)
κ	Basin aspect ratio	3.7	usually >1	Dodds & Rothman (2001)
H	Hurst exponent in self-affinity law	4.4	0.5-1.2	Rigon *et al* (1996)
h'	Hack's differential	4.4	0.3-0.9	Dodds & Rothman (2001)

Chapter 3

Fractal River Networks in Africa

3.1. Introduction

It is now said that if scaling laws exist in nature, river network geometries are an epitome of this phenomenon (see Dodds & Rothman, 1999, for a review). A number of laws describing how specific network parameters of real networks vary with scale have been uncovered (e.g. Horton, 1945; Hack, 1957; Tarboton *et al.*, 1988), and they have been used to validate a number of models for geomorphic evolution, and have even been suggested as evidence for self-organized criticality. However, very little is known about the origin of scaling laws of river networks.

In this chapter it will be explained how river networks can be viewed as fractals, and a number of scaling laws will be discussed. Following that, major African river basins will be introduced. While it is essential to recognize that evolution of river networks is a very important subject, in this chapter the discussion will be limited to networks 'frozen' in time. Drainage evolution will be dealt with later on.

3.2 Basic scaling laws for river networks

The first tool usually applied when studying a river network is stream ordering. The most common ordering scheme is the Horton-Strahler method, developed by Horton (1945) and later improved by Strahler (1957). In this scheme all source stream segments have order $\omega = 1$. When two source streams meet, the segment downstream from the junction has $\omega = 2$. The order increases by 1 when a stream joins another stream of the same order; when two streams of different orders meet, the segment downstream is assigned the higher of the two orders. Figure 3.1 illustrates this ordering scheme.

Natural quantities to measure in an ordered basin are:

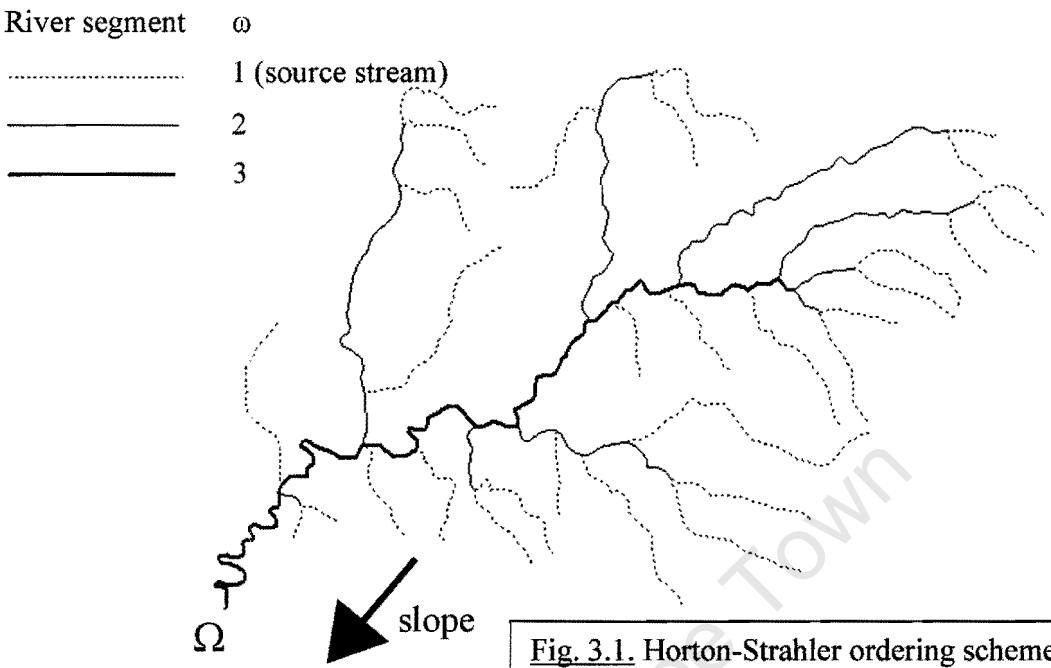

Fig. 3.1. Horton-Strahler ordering scheme for a river network (plan view).

- the number of streams of a given order: $n(\omega)$,
- average length of streams of a given order: $l(\omega)$,
- average drainage area (enclosed by the watershed) of streams of each order: $a(\omega)$.

The outlet of the network in study obviously has the highest order in the system, and is labelled Ω. Clearly $n(\Omega) = 1$, and $a(\Omega)$ is the network's total drainage area.

Horton (1945) introduced a number of measurements that follow the ordering scheme discussed above. The first was the bifurcation ratio, $R_n(\omega)$, defined as the ratio of streams of order ω to ones of order ω+1, i.e.

$$R_n(\omega) = \frac{n(\omega)}{n(\omega+1)} \tag{3.1a}$$

His suggestion that R_n is independent of ω was the first scaling law in the study of river networks. Two more ratios can be defined:

$$R_l(\omega) = \frac{l(\omega+1)}{l(\omega)} \tag{3.1b}$$

$$R_a(\omega) = \frac{a(\omega+1)}{a(\omega)} \tag{3.1c}$$

Horton's laws state that the three ratios are independent of order. Note the three ratios are defined in such a way that they are all greater than unity. Furthermore, Horton's early results showed that $R_a \equiv R_n$. This redundancy was also seen in the results of Hack (1957), but was not stated until Peckham (1995).

One of the most famous scaling laws for river networks is Hack's law (Hack, 1957), which relates main stream length (longest possible stream length from source to outlet) to its drainage area by the relation

$$l = ca^h \tag{3.2}$$

It could be expected from simple geometry that $a \sim l^2$, and therefore $h = ½$. However, an important property of this relation is that $h \neq ½$. Hack found the exponent equal to 0.6, but noted fluctuations from basin to basin, with some of them having h as high as 0.7. Further studies (e.g. Rigon *et al.*, 1996; Maritan *et al.*, 1996) found h typically in the range (0.55, 0.60). Rigon *et al.* (1998) show networks with h = 0.5 are "far from realistic", and quote a value of h = 0.57 for what they term "feasible optimum" of the network.

If we are to deal with drainage basin areas, it is important to consider the actual shape of the basin. To do this we define two parameters: $L_{\parallel}$, the length of the basin parallel to the main stream, and $L_{\perp}$, the width of the basin (Figure 3.2). As $L_{\parallel}$ is used far more often it is usually written as just L. This convention can be confusing (as by default $l > L$), but we will persist with it. As with l, L can be related to the drainage area (Maritan et al, 1996)

$$a \sim L^D \tag{3.3}$$

The exponent D shows how basin area changes with different values of L, and is found in nature to have a value very close to 2. It can be thought of as the fractal dimension of the network. However, it is necessary to point out that this dimension does not say anything about any single basin, only about how basin areas scale in the given area. All individual basins have a dimension of 2, and if the network has $D < 2$, it does not imply they are not space filling. For a further discussion of this point see Dodds & Rothman (1999).

It is also possible to relate L, the basin length, and l, the stream length (e.g. Maritan *et al.*, 1996)

$$l \sim L^d \tag{3.4}$$

This can be though of as fractality of individual streams, with the fractal dimension of approximately 1.1 for real networks.

Many more scaling laws have been suggested, with varying correlations to real networks. An interested reader is referred to, e.g. Rodriguez-Iturbe & Rinaldo (1997) or Dodds & Rothman (1999, 2000).

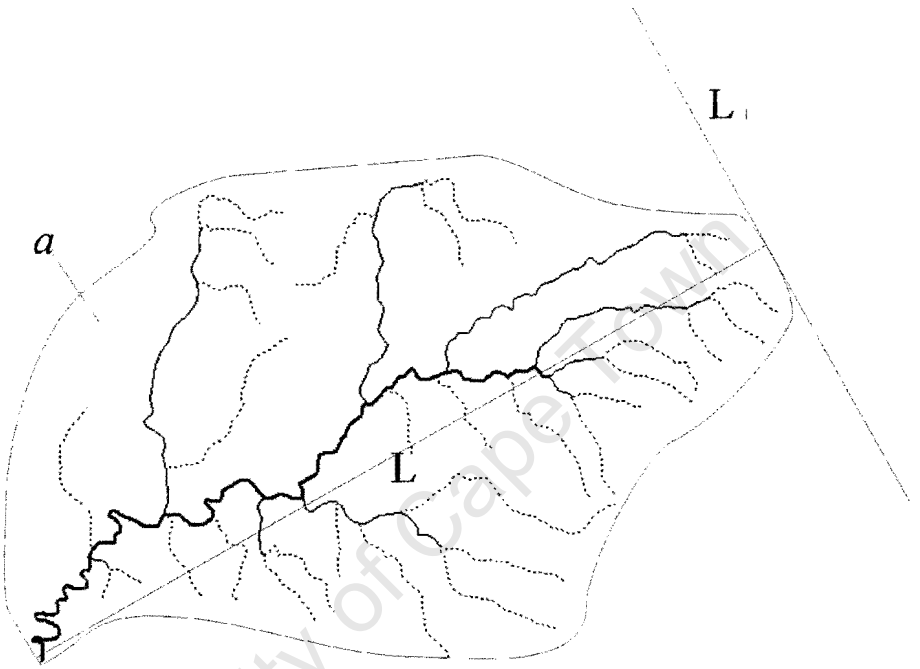

Fig. 3.2. Geometric quantities of a basin (plan view).

3.3. Universality

The idea behind universality is that phenomena (network parameters in the case of rivers) from vastly different scales often exhibit the same scaling laws (Dodds & Rothman, 2000). When common generic processes can be identified for the range, a universality class can be identified. Dodds & Rothman (2000) have shown that river networks obeying the scaling laws discussed above can be classified according to only two parameters: h and d. While obviously no two networks will ever be exactly the same, ones with similar values for these parameters will be statistically similar. Universality allows us to distinguish what different networks have in common in addition to what makes them different.

We now show the relations between scaling parameters described above. Assuming that Horton's ratios are independent of order, with a given ω_1, for all ω we have $\frac{l(\omega)}{l(\omega_1)} = R^{\omega-\omega_1}$ or $l(\omega) = \frac{l(\omega_1)}{R^{\omega_1}} R^{\omega}$. With all ω_1 terms being constant, and remembering that $R_n = R_a$ we have

$$l(\omega) \sim (R_l)^{\omega} = (R_n)^{\omega[\ln(R_l)/\ln(R_n)]} = (R_a)^{\omega[\ln(R_l)/\ln(R_n)]} \sim a(\omega)^{\ln(R_l)/\ln(R_n)} \tag{3.5}$$

combining this with eq.(3.2) we see that

$$h = \frac{\ln R_l}{\ln R_n} \tag{3.6}$$

Furthermore, combing eq.(3.2) and eq.(3.4) we see that

$$a^h \sim L^d \tag{3.7}$$

since they both are proportional to l. Combining this we obtain an equation for the fractal dimension of the network in terms of the two parameters defining the universality class:

$$D = d/h \tag{3.8}$$

It might be useful to remind the reader that D is not the fractal dimension of any individual basin, and therefore is not necessarily set to 2. A number of incorrect relations, including $d = 2h$, have been derived from this confusion (e.g. Rosso *et al.*, 1991).

3.4. Major river basins in Africa

Figure 3.3 illustrates major basins in Africa. These were obtained from a river database of approximately 40 km average stream separation, and the map contains 11 river networks that have $\Omega > 4$. Their properties are summarized in Table 3.1. By just looking at the figure, as well as the zoomed-in Figs. 3.4 to 3.7, one can notice interesting features within just about every basin. In southern Africa, the Orange river has its source about 200 km from the Indian Ocean, but flows west into the Atlantic 1400 km away (Figure 3.4). Cox (1989) claims this is a case of an inherited drainage pattern away from a lithospheric swell caused by a plume established in northern Moçambique at ~200 Ma. The Okavango (Figure 3.5) has a very unusual ending for a river – an inland delta in the Kalahari Desert. Wellington (1955) suggested that Okavango, Chobe and Limpopo were once the same river, before crustal flexuring truncated the Limpopo and Zambezi captured the Chobe. This is further explained in Chapters 8 and 9 (Figs. 8.8, 8.15, 9.4).

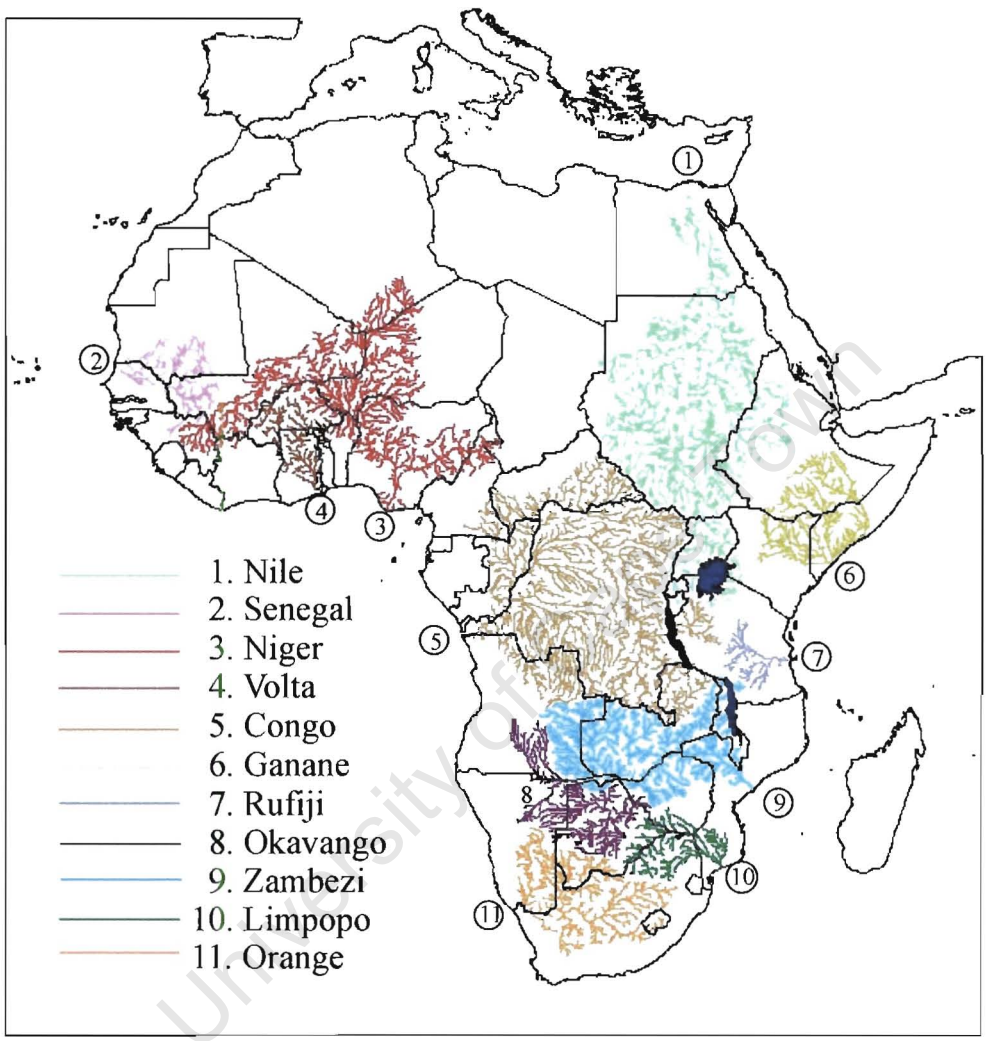

Fig. 3.3. Major river basins in Africa today. Note the Okavango (#8) has no outlet, but terminates in an inland delta.
Source: CIGCES river data base derived from data of De Beers Group, Centurion. Average stream separation in the database is ~ 40km. 'Major river' included here are rivers with order $\Omega > 4$.

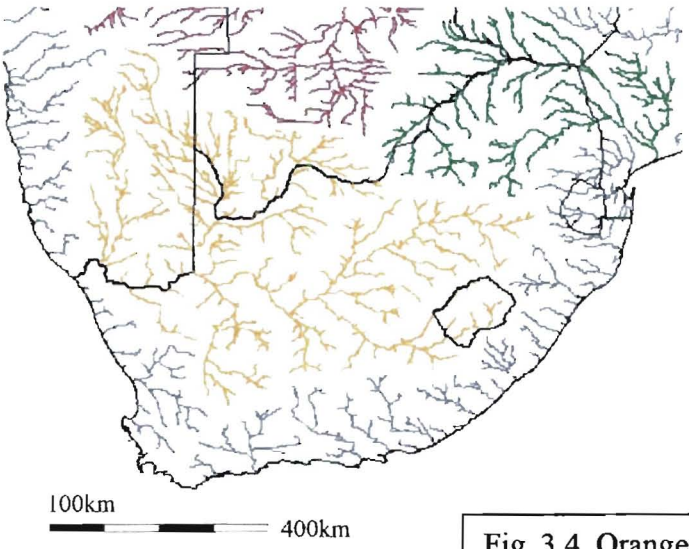

Fig. 3.4. Orange river network in southern Africa

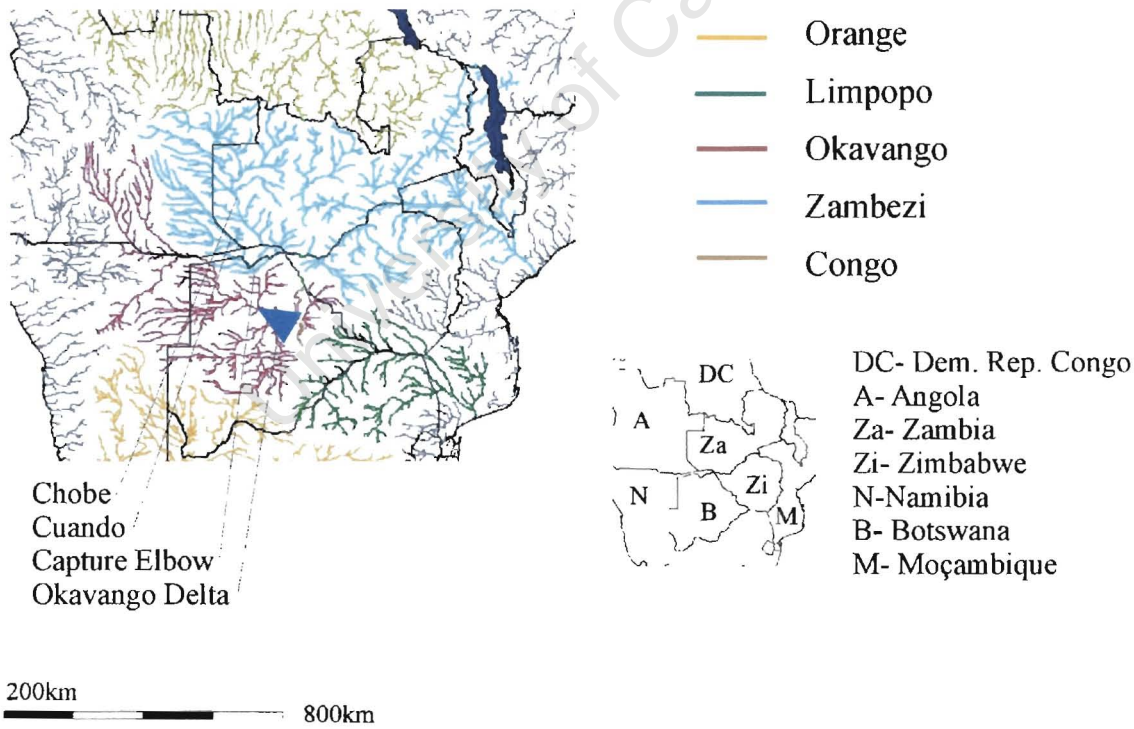

Fig. 3.5. Okavango-Zambezi-Limpopo 'system' is southern Africa

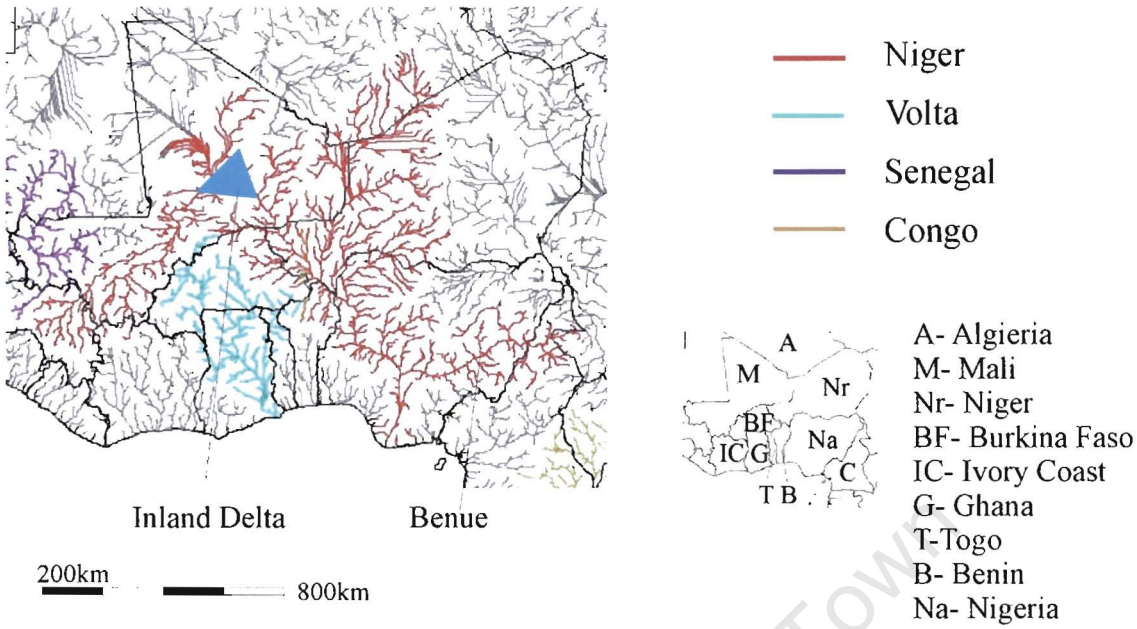

Fig. 3.6. Niger river network in western Africa. Blue triangle shows the site of the inland Niger delta described in the text.

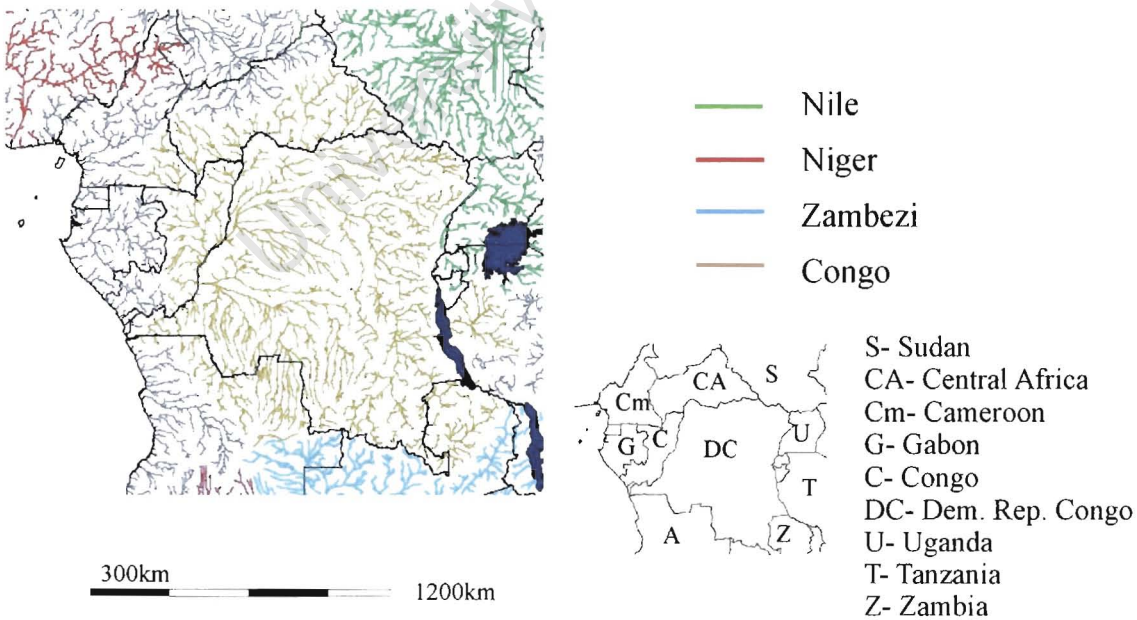

Fig. 3.7. Congo river network in western Africa

Further north, the continent's three biggest rivers could not be more different. The Congo drains the Congo Basin into the Atlantic. Evidence from marine fossils suggests the Congo Basin was episodically submerged below sea level throughout the late Mesozoic, and these marine waters reached the Congo Basin from the east in the Jurassic – Cretaceous (Sahagian, 1988 and refs. therein). This suggests that in the Jurassic the Congo network was flowing east (Shackleton, 1978) over the area where today the highlands of the East African rift system are found. While now mountains over 5000 metres high can be found there, at the time most of it was either low-lying land, and occasionally might have actually been flooded (Doucouré & de Wit, 2003, their Figure 9, reproduced here as Figure 3.8).

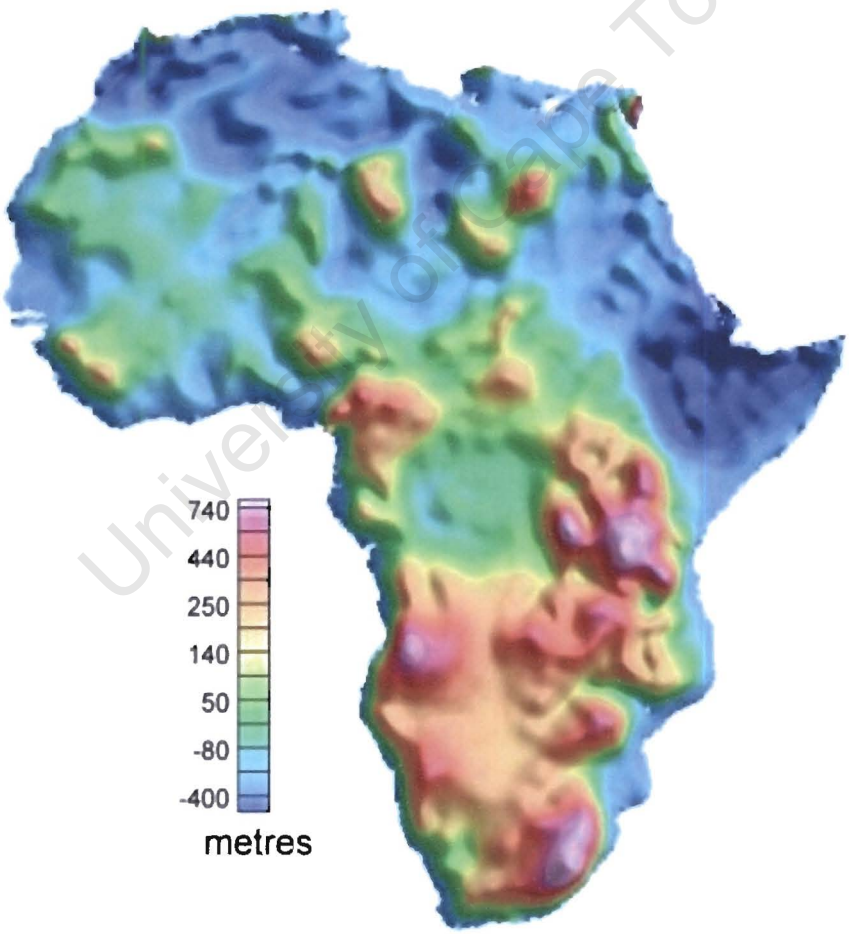

Fig. 3.8. Topography of Africa in the Cretaceous, modified from Doucouré & de Wit (2003). This map was obtained using gravity anomalies and the geoid.

There is some debate concerning the history of the Congo Basin. Topography of the African continent is unique in that it is almost completely devoid of folded mountain ranges, prompting Holmes (1965) to call it Basin and Swell topography. This has been suggested to be the result of the continent being stationary with respect to the underlying mantle for the last 30 Ma (Burke & Wilson, 1972; Burke, 1996). The Cretaceous topography reconstruction of Doucouré & de Wit (2003) shows that the basin is much older that 30 Ma, and its boundaries are in fact escarpment features. The northern and north-western of these boundaries are likely to be related to the West and Central African rifts and their shoulders (e.g. Fairhead, 1988l Sahagian, 1988; Fairhead & Binks, 1991).

Table 3.1: Summary of major African rivers

#	River	a (*1000 km^2)	l (km)	Ω
1	Nile	3360	6230	6
2	Senegal	413	1330	5
3	Niger	2210	3580	6
4	Volta	394	1680	5
5	Congo	3690	3700	7
6	Ganane	762	1900	5
7	Rufiji	192	792	5
8	Zambezi	1400	2820	5
9	Okavango	652	1800	5
10	Limpopo	405	1380	5
11	Orange	1040	2150	6

The Nile flows north from Lake Victoria, but around the border between Sudan and Egypt it suddenly stops being fed by overland tributaries, making the drainage basin look like a bottleneck in its northernmost section. Even the Ethiopian branch of the African Rift valley can be seen from the figure – the obvious uniform gap between the Nile and Ganane basins. The Niger (Fig. 3.6) is possibly the most interesting of all – its source is less than 300 km east of the Atlantic, but it flows northeast at first, before turning sharply

to the southeast in central Mali, and eventually, after over 3500 km, reaching the Atlantic in Nigeria.

The site of Niger's inland delta is still visible today (Reclus, 1888) close to the river's turning point mentioned above (Figure 3.6). It is possible that this stream was captured by a river parallel to the Volta, and now joins with the Benue just before reaching the coastal Niger delta. During very dry periods upper reaches of the Niger do not get past the inland delta, and the main section between that delta and the Benue can flow 'upstream' into the inland delta (Burke, 1996).

Today the Congo (Fig. 3.7) drains its huge basin through one narrow channel. This channel is believed (e.g. Burke, 1996) to have once been a short river that captured the Congo. It is also thought to be responsible for the cutting of the Congo's submarine channel, believed to be formed in the Miocene (Uenzelmann-Neben *et al.*, 1997).

As was mentioned in the introductory chapter, one of the major questions this thesis is concerned with, is how differences in river patterns, in different sub-regions of individual basins as well as between basins, can be expressed mathematically, using scaling laws and constants described above.

Figure 3.9 shows a logarithmic plot of stream length as a function of drainage area for the 11 major basins. The majority of the points lie on a straight line. Only the Volta and the Congo show significant deviations. If these two points are excluded from the analysis, the plot gives a value of 0.666 for Hack's exponent, with a correlation coefficient of 98.9 %. For all 11 points we obtain $h = 0.576$, with a 96.3 % correlation. Hack's original work (Hack, 1957) dealt with localized rivers in North America, and included data from sub-basins contained within a single basin. Dodds & Rothman (2000) suggest it is vital to discriminate between intra-basin and inter-basin measurements. They proceed to compute h for 37 of the world's largest rivers, which they find to be 0.50 ± 0.06, and go on to explain self-similar basins (i.e. with $h = ½$) are to be expected on continental scales, as these maximal basins shapes are controlled by geological structures related to predominantly horizontal tectonic forces. These maximal basins would have $L_{\perp} \propto L_{\parallel}$. Since Africa has been stationary for the past 30 Ma (Burke, 1996), and has had a history of significant vertical tectonics without horizontal plate motion since then, it is perhaps not surprising African river networks are different to rivers on other continents. One

might have expected maximal basins in a Basin and Swell topography to also have $L_{\perp} \propto L_{\parallel}$, but a glance at Figure 3.3 shows this is not the case for major rivers, except for the Congo. This suggests tectonics do indeed have a strong influence on river basin geometry. The Niger network has such a peculiar shape, that one is not sure how to measure the two parameters. This suggests that while Africa's topography is different to that of other continents (and thus has $h > 0.5$ for major river networks), it is a lot more complicated than the simple Basin and Swell structure.

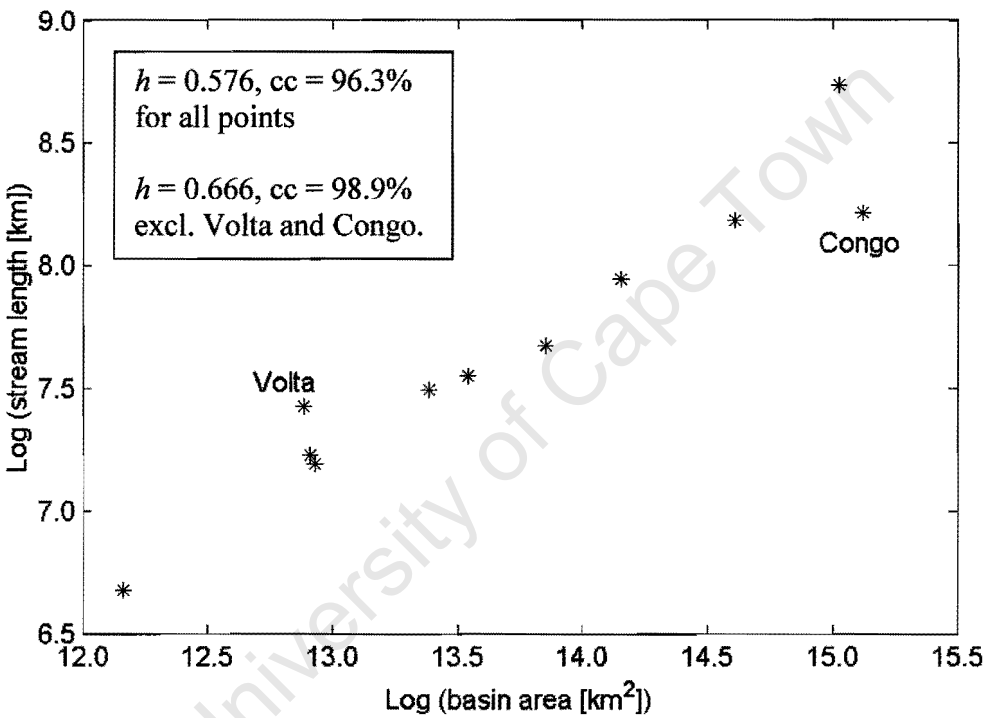

Fig. 3.9. Hack's Law plot for Africa's major rivers

The next step is to examine the validity of Hack's law inside the individual basins. For this the biggest three basins (Nile, Congo and Niger) were examined, using stream lengths and drainage areas of all tributaries with $\omega > 3$. Results are summarized in Table 3.2. It is clear that the relation is satisfied for all basins (correlation coefficients are all over 90 %), but the values for h are all significantly different. $N(\omega>3)$ gives the number of basins of order greater than 3 in each network.

Table 3.2: Summary of the 3 main African rivers

River	a (*1000 km^2)	l (km)	Ω	N(ω>3)	h	correlation of h
Nile	3360	6230	6	18	0.609	96.1 %
Niger	2210	3580	6	10	0.552	97.7 %
Congo	3690	3700	7	19	0.418	92.0 %

3.5. What do scaling laws actually tell us?

Can we make conclusions about the conditions through which the river flows from parameters governing the scaling behaviour of the network? Before attempting to answer this question, let us consider the converse: What natural parameters might control the fractal parameters of the network? For now we will concentrate on Hack's exponent – it was shown in the previous section that while the equation $l \sim a^h$ is obeyed for the major basins in Africa, h itself varies significantly. What can be the cause of this variation? Here we suggest three independent factors that can potentially determine characteristics of river networks:

- underlying geology
- topographic relief
- climate of the region.

These factors are obviously very complex, and in fact each can be thought of as a integration of sub-factors. For example, climate encompasses rainfall, temperature and many other parameters. On the other hand, vegetation will also have an effect on drainage, but can be considered as a function of local climate and geology. Seeing that from a given topography a unique network can be constructed, relief is the only factor for networks 'frozen in time'. Tectonic activity, climate, and its evolution, influence the development of this relief, as well as the evolution of the network directly. These will be dealt with at a later stage.

3.6. Simple river network models

In this section results of various simulations of resulting river networks from different synthetic topographies are presented. This will demonstrate how topographic relief affects resulting river networks.

In the first simulation topographies were constructed with a specified fractal dimension, D_{topo}, from 1.5 to 2.5 in increments of 0.1. D_{topo} values found in reality fall into that range. Topography fractality and fractal dimension was briefly introduced in Chapter 2, and is described in more detail in Appendix A (eq. A.28 shows how D_{topo} is computed). For each dimension 10 synthetic landscapes were produced, and Hack's exponent for all resulting networks was calculated. All landscapes were retained as horizontal, so that as a result a number of networks formed landlocked drainages rather than flow 'off the map'. The average values for h are plotted against D_{topo} in Figure 3.10. The straight line has a correlation coefficient of 99.8 %, clearly showing the linear relationship between the two fractal parameters. The values obtained for h in this simulation are larger than the values obtained for real network, but the range for D_{topo} chosen represents the values one expects to find in real topographies.

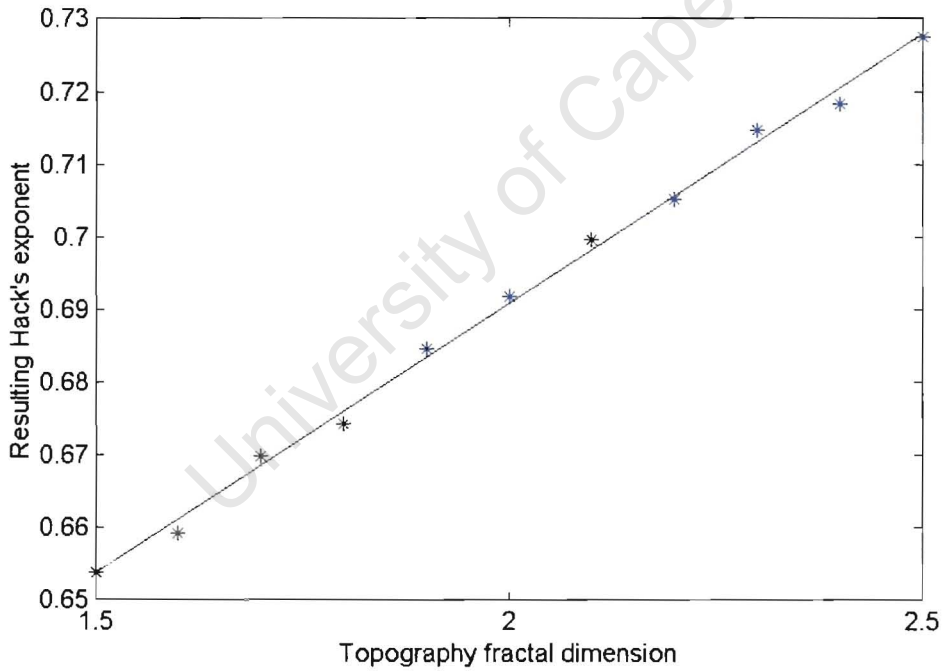

Fig. 3.10. Plot showing linear relationship between the fractal dimension of a synthetic topography and Hack's exponent of the resulting river network.

Next, the relationship between slope of the landscape and h was investigated. Topographies (elevation matrices 1000 pixels long and 500 pixels wide) with D_{topo} varied from 1.5 to 2.5 (in steps of 0.1) were progressively tilted. Units of slope are meaningless

here, as no constants of erodibility or flow rate are included in the model, and only relative slope is important. 10 values of slope were used, from 0.1 to 1.0, and each point had its elevation reduced by the product of the slope value (0.1 to 1.0) and its distance from the top horizontal axis (1 to 500). For each ordered pair of topography fractal dimension and relative slope, 10 landscapes were generated and the average Hack's exponent for the resulting network was calculated. Figure 3.11 shows how the resulting value for *h* varies with slope for each set value of topography fractal dimension. It is clear that while *h* increases with D, it does not appear to have an obvious dependence on the slope of the topography. This is confirmed by Figure 3.12, which shows dependence of *h* on D_{topo} for constant values of the slope – all lines show direct relationships between *h* and D_{topo} (correlation coefficients between 98.5 and 99.5 %), but individual lines (representing individual slopes) do not significantly deviate from each other. This is consistent with the results from the previous simulation. The presence of local discontinuities in the gradient of Figure 3.12 (at e.g. D_{topo} = 1.7, 1.9) suggests the relationship between the slope of the topography and the universality class of the resulting river network is very complex, but the variations it causes are small compared to varying the topography fractal dimension.

The last simulation in this section involved comparing drainages that develop in one topography mainly consisting of a basin, and another with a dome or free-standing hill (inselberg). Examples of each are shown in Figure 3.13 (a) – basin, and (b) – hill. For D_{topo} varied between 1.6 and 2.8 (in steps of 0.2) ten basin topographies were generated, and then each was simply inverted to produce the dome or inselberg. The resulting river networks were then examined, and average Hack's exponent was calculated for each D_{topo}. These plots are shown in Figure 3.14. While both graphs confirm the already stated *h*-D_{topo} relation, *h* is clearly higher for the basin topographies than for the dome. This simulation enabled us to describe a geographic property in terms of a single fractal exponent, which was the objective of this section. This result is the opposite of what one might have expected given the low *h* of the Congo network. The Congo is in fact not a typical centripetal drainage, and will be discussed in detail in later Chapters.

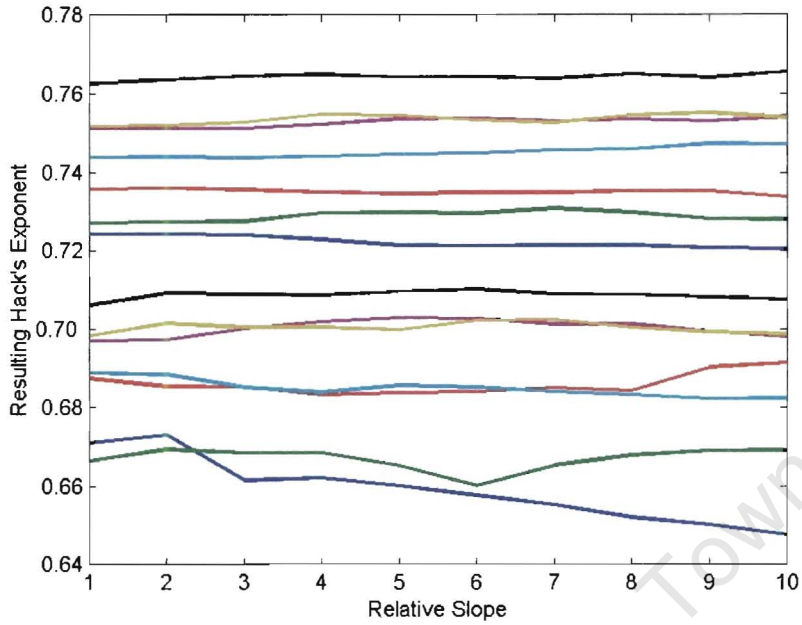

Fig. 3.11. Plot showing Hack's exponent of a network does not have a significant dependence on the regional slope of the topography. Different colours correspond to topographies with different fractal dimension.

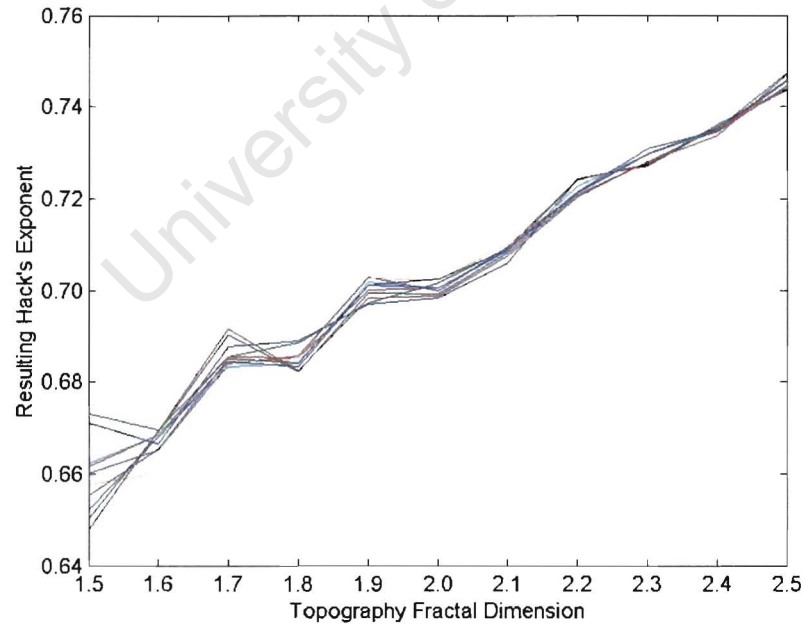

Fig. 3.12. Plot showing the influence of mean slope is much less significant than the fractal dimension of the topography in determining *h* of the resulting river network. Different colours correspond to different slopes of the synthetic landscape.

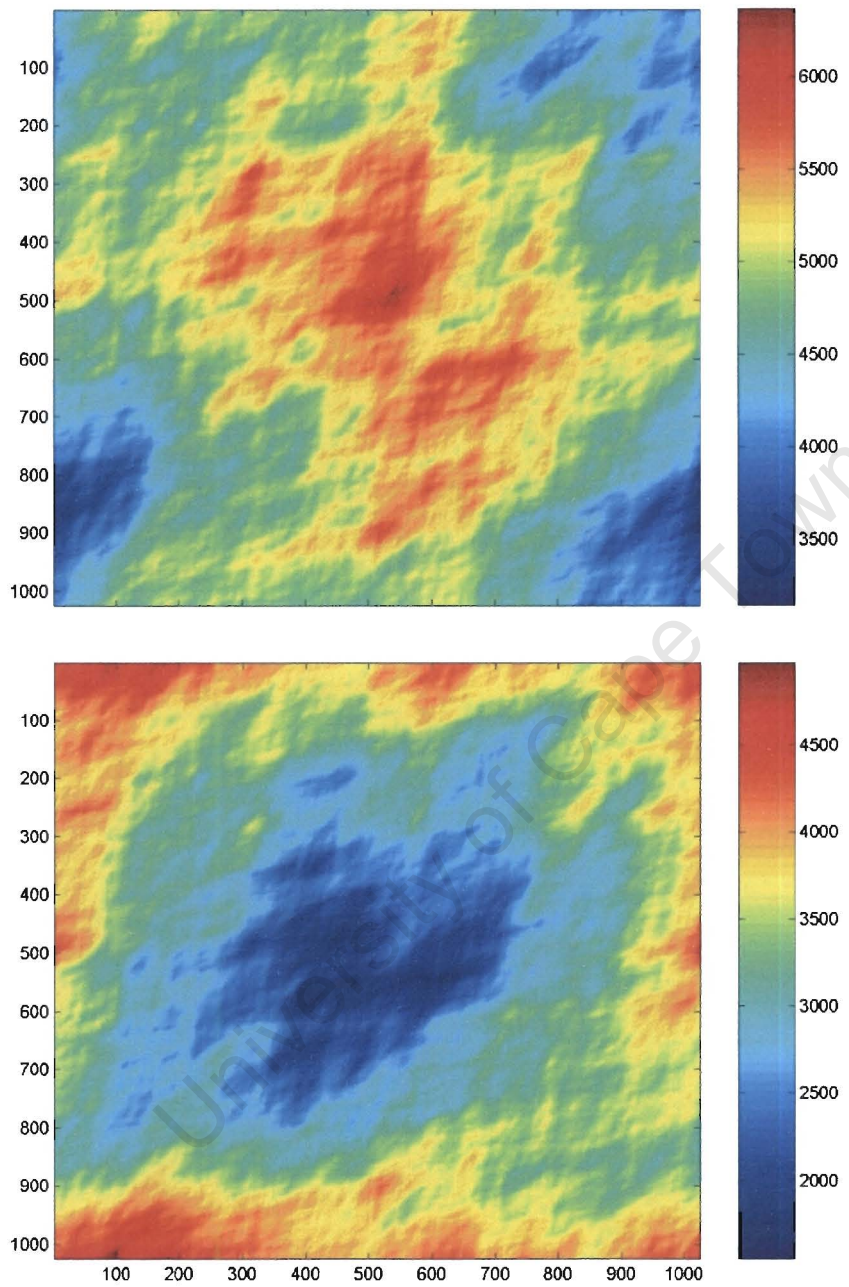

Fig. 3.13. Examples of synthetic topographies dominated by a dome (top) and basin (bottom). Units of 'maps' are distances in km, while scalebars show arbitrary height units.

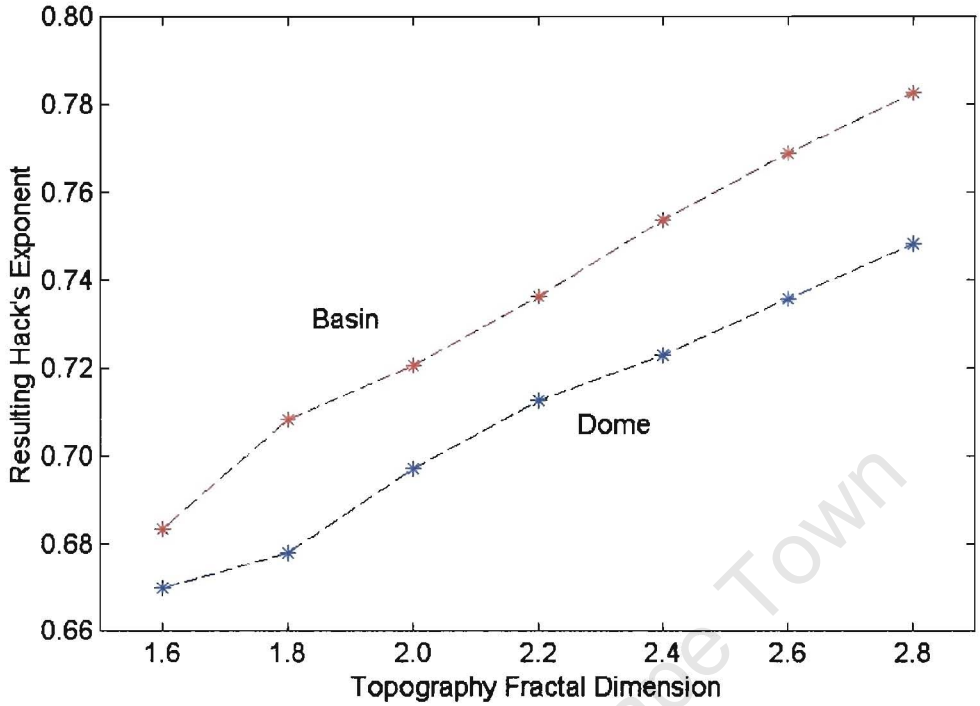

Fig. 3.14. Hack's exponents for network over a topography of given D dominated by either a basin or a dome.

3.7. Basin shapes

While a number of studies can be conducted relating basin areas to other parameters, this generalization can reduce the amount of information contained in the data set. From Figure 3.3 and Table 3.1 we can see the Nile and the Congo have almost similar areas, but the river basins are clearly very different geometrically. These differences need to be taken into account for any comprehensive study of river networks.

One way to mathematically describe the shape of a basin is to introduce the aspect ratio, κ. This is defined by (Dodds & Rothman, 2001)

$$\kappa = L^2 / a \tag{3.9}$$

Long, narrow basins will have $\kappa > 1$, and short, wide ones $\kappa < 1$. This last case is very unusual, and typically κ is around 2. This parameter now enables one to distinguish between the Nile ($\kappa = 4.55$) and the Congo ($\kappa = 1.50$), and will be used to describe basin shapes.

3.8. Summary

In this chapter it was explained how river networks can be viewed as fractals and basic scaling laws for networks were introduced. The major rivers in Africa were then briefly discussed, and examples of the scaling laws were demonstrated on them. Simple models were also constructed to show how different synthetic landscapes can yield river networks with different scaling parameters.

We shall now use these, and more advanced, scaling laws to examine river networks and their evolution on both regional scales and the continental scale.

Chapter 4

Analysis of River Networks in Southern Africa

4.1. Introduction to the region

This chapter deals with the river networks of southern Africa, a subcontinent comprising the Republics of South Africa, Namibia, Botswana and Zimbabwe, as well as the tiny kingdoms of Lesotho and Swaziland (Figure 4.1). The northern boundary of the subcontinent is chosen in an arbitrary way, political boundaries not having much correlation to geological features, and often parts of Angola, Zambia, Malawi and Moçambique are included in studies of southern Africa (e.g. Tankard *et al.*, 1982; Reeves, 1978; Moore & Larkin, 2001). In this chapter the boundary of the region will be the northern watersheds of the Orange and Limpopo networks.

Many books (e.g. King, 1963; Truswell, 1970; Tankard *et al.*, 1982) have been written on the geology and geomorphology of the area, and an interested reader is referred to them. Here only an insight to the subcontinent's fascinating history will accompany a description of various river basins.

4.2. Major river networks of southern Africa

The major river in the Republic of South Africa is the Orange (Figures 4.2 and 4.3). It is the 5th largest river in Africa, both in terms of main stream length (2150 km) and drainage area (1,040,000 km^2), and also drains parts of Lesotho, Namibia and Botswana. By looking at the drainage map of South Africa (Fig. 4.2) one of the main features of the region's geomorphology can be seen – the Great Escarpment, stretching from the Western Cape to the Limpopo basin near the South Africa – Zimbabwe border in an arc approximately 200km from the coast. All the drainage inland of this divide eventually joins the Orange and enters the Atlantic at Oranjemund. The zone between the

escarpment and the ocean is drained by rivers approximately perpendicular to the divide. Of the rivers in that band six are of particular interest in this study. They are the Olifants, Gourits, Gamtoos, Sundays, Great Fish and Kei (Figure 4.2). To reach the coast on their way down from the Great Escarpment they cross a band of mountains ranges known as the Cape Fold Belt. This belt (Figure 4.4) is the only place in the sub-continent where young (Mesozoic in age) mountain ranges related to horizontal tectonics are found. The mountains in the belt reach over 2000m in places, with Seweweekspoort Peak in the Swartberg being the highest point at 2324m. Other ranges in the belt are the Cederberg, Hex River Mountains, Langeberg and many other smaller ranges. These ranges have been extensively faulted and folded at ~250 Ma (i.e. before the break-up of Gondwana), and a trellis river pattern has developed across them. Main river segments have formed in the weaker shales, leaving the hard Table Mountain Sandstones (often quartzites) as vertical ridges. Lower order streams then flow down these steep ridges to join the main (higher order) stream. This environment is not found anywhere else in Southern Africa, hence our interest in how and why river network geometry differs between this and other areas.

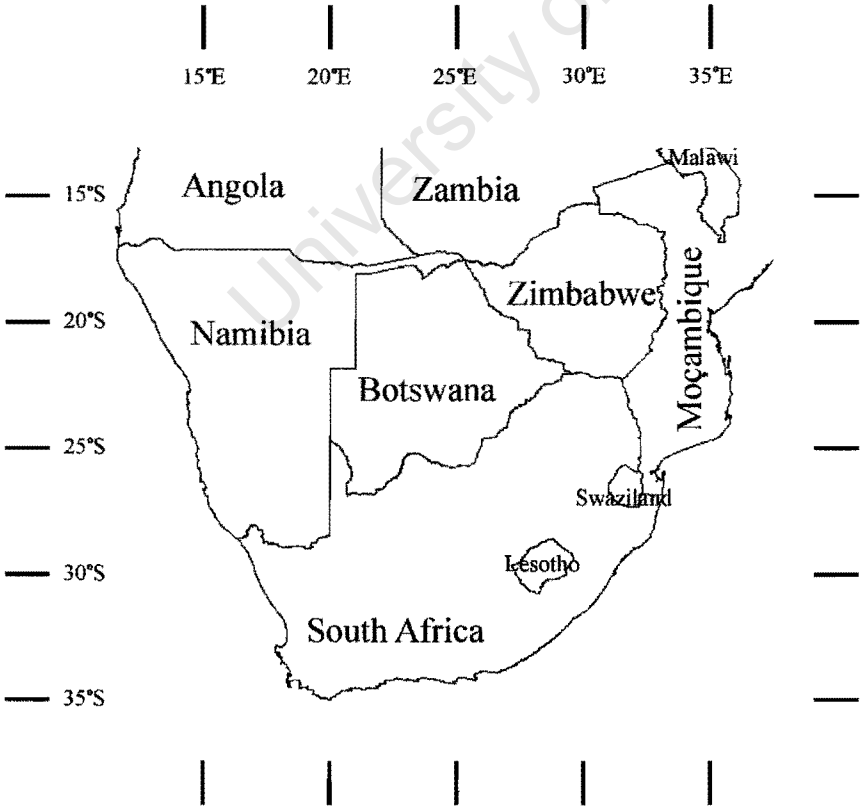

Fig. 4.1. Southern Africa

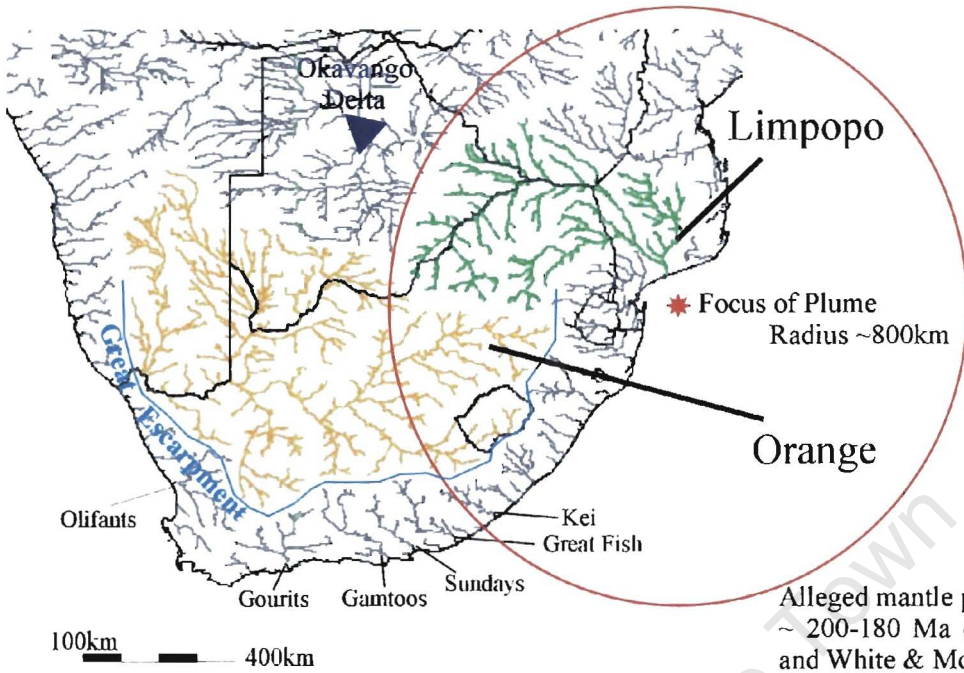

Fig. 4.2. River networks in southern Africa

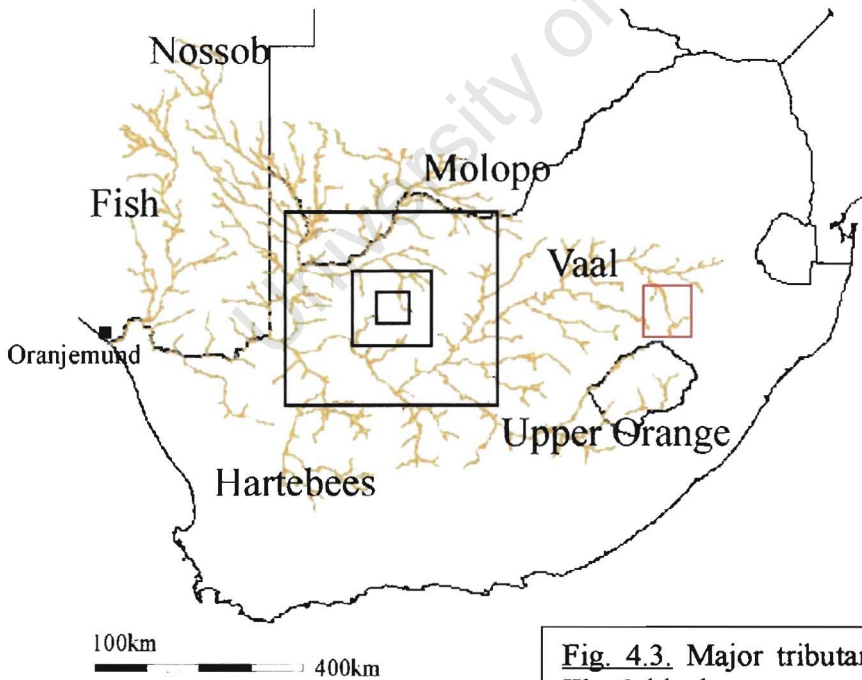

Fig. 4.3. Major tributaries of the Orange river. The 3 black squares correspond to logarithms of areas (in km^2) of 8, 10 and 12, to give an idea of scales used in this study. Red square shows the study area of Tooth *et al.* (2002, 2004) discussed in Chapter 6 in this thesis.

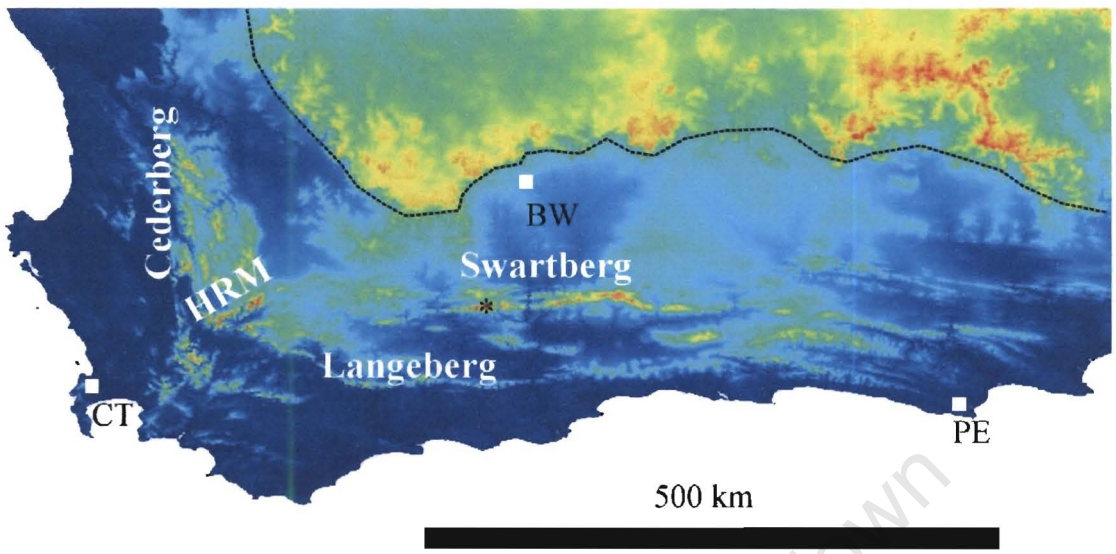

CT: Cape Town
BW: Beaufort West
PE: Port Elizabeth
HRM: Hex River Mountains
* Seweweekspoort Peak
------ Great Escarpment

Elevation [m]
0 500 1000 1500 2000 2500

Fig. 4.4. Digital Elevation Model of the Cape Fold Belt

The Limpopo river flows east forming the boundary between South Africa and Zimbabwe, before reaching the Indian Ocean through a delta in Moçambique. Du Toit (1933) suggested that the Limpopo was originally linked with the Okavango, a theory supported by Wellington (1955) who attributed the drainage evolution to stream capture (discussed in detail in later Chapters).

Major tributaries of the Orange drain totally different geological and climatic terrains. Large part of the drainage comes from the Orange-Vaal system sources in high ground inland of the Drakensberg escarpment. This high ground (reaching 3482 metres at its highest point, Thabana Ntlenyana in Lesotho) has been suggested to be inherited from a deep mantle plume that brought about the break-up of Gondwana ~180 Ma (White & McKenzie, 1989). The fact that the Orange has its sources just 150 km west of the Indian Ocean, but flows to the Atlantic 1400 km away, has been seen as a case of drainage away

from the new (Indian) ocean, supporting the plume hypothesis (Cox, 1989). There are, however, problems with this hypothesis. Burke (1996) argues that if the age of the escarpment corresponded to the age of the break-up of Gondwana it should have since been completely eroded away, given average erosion rates. He therefore suggests uplift in the area only started ~30 Ma, and relates it to the present day mantle anomaly below southern Africa (e.g. Nyblade *et al.*, 1990; Silver *et al.*, 2001; Stankiewicz *et al.*, 2002) and the African Superswell associated with it (Nyblabe & Robinson, 1994). The Limpopo flows through a similar geological setting, but in the opposite direction. Cox (1989) suggests, however, that the Limpopo drainage is rift-inherited, related to the failed spreading axis in the Kalahari postulated by Reeves (1972, 1978). While that debate is fascinating in its own right, the important fact for this study is that the Orange-Vaal system flows from altitudes of over 3000 metres in the general western direction of the Atlantic.

The Fish River flows south through the arid Namibia, and the only perennial part of the network is the few kilometers upstream from its confluence with the Orange. The most dramatic feature of this network is the famous Fish River Canyon in the river's lower reaches. There the river has cut into the horizontal quartzitic sandstones and shales of the Eocambrian Nama Group (500 – 700 Ma) to reach the underlying Precambrian schist and granite gneiss of the Namaqua complex (1000 – 1200 Ma; Buckle, 1978). In places the canyon is over 500 metres deep.

The Molopo and Nossob rivers drain (technically speaking) the Kalahari basin. Neither network has a record of permanent flow during living human history (Bootsman, 1997). When water is transported in the channels, overland flow never reaches the Orange river – transport takes place by groundwater. The two networks are therefore not strictly tributaries of the Orange, but have been included in the analysis nonetheless. The presence of river terraces indicates that both these rivers were perennial in past history during more fluvial stages of the recent African climate (de Wit, 1993).

The Hartebees River, also known as Sak River, is the last major tributary included here. Its headwaters drain the Upper Ecca and Lower Beaufort Group sediments north from the south-western edge of the Great Escarpment. Most of this network is also non-perennial, but as with the Molopo and Nossob, the presence of terraces suggests this has not always

been the case. On these terraces there is today a number of 'vleis' (local name for wetlands) that characterize the river. Fossil evidence further indicates that as recently as the Middle Miocene (10-15 Ma) the Hartebees flowed through a wet and wooded environment (de Wit, 1990 and 1993).

4.3. Preliminary fractal analysis

In this section a Digital Elevation Model (DEM) of Southern Africa was used. This was obtained from the U.S. Government Public Information Exchange Resource website[1]. The horizontal resolution of the model is a 1km grid (North-South and East-West), with vertical elevations given to the nearest meter at the lattice points. A program was written to model the flow of water over any given landscape, similar to the one used in the models of section 3.6. The streams are derived by dividing the whole area into individual basins (using the *watershed* function in Matlab[2]) – because of this first order stream lengths and numbers cannot be uniquely determined, and have been left out of the analysis. The exact description of the computing process used to obtain the river network from the DEM can be found in Appendix B.

We first list the preliminary results for the Orange river network. After the streams have been ordered, the network was found to have $\Omega = 8$. Table 4.1 below shows the results for Horton's laws of stream numbers, lengths, and drainage areas.

Table 4.1: Horton's Laws of numbers, lengths and drainage areas for the Orange river

ω	$n(\omega)$	$R_n(\omega)$	$l(\omega)$ [km]	$R_l(\omega)$	$a(\omega)$ [km^2]	$R_a(\omega)$
2	3,195	4.64	19.6	3.01	188	4.83
3	689	4.28	59.2	2.48	908	4.44
4	161	4.13	146	2.01	4,030	3.87
5	39	3.90	294	2.17	15,600	4.92
6	10	3.33	637	1.52	76,700	2.75
7	3	3.00	970	2.22	211,000	4.93
8	1		2,150		1,040,000	

[1] URL: http://edcdaac.usgs.gov/gtopo30/gtopo30.html
[2] Matlab is software package from The MathWorks (http://www.mathworks.com)

While it is obvious there are deviations in the ratios, some patterns can are observed. R_l is always smaller than the other 2 ratios, and fluctuates between 1.52 and 3.01. Up to the ratios of $\omega = 4$ and 5, R_n and R_a are decreasing with increasing order, and for each order the 2 ratios are within 7% of each other's value, supporting the relation $R_a \equiv R_n$ stated in Chapter 3. The discrepancies at higher orders can be attributed to having much fewer data points.

The next step in our analysis is examining the relationship between stream length and drainage area, or Hack's Law. Figure 4.5 illustrates the logarithmic plot of these values for the 4098 basins of order greater than 1 inside the Orange network. The plot shows an obvious power law relation (linear on a log-log plot) between the stream length and drainage area. Linear regression yields $h = 0.685 \pm 0.004$ with a correlation coefficient of 92.5 %. It should be noted, however, that the graph is slightly concave, or the slope decreases with increasing area.

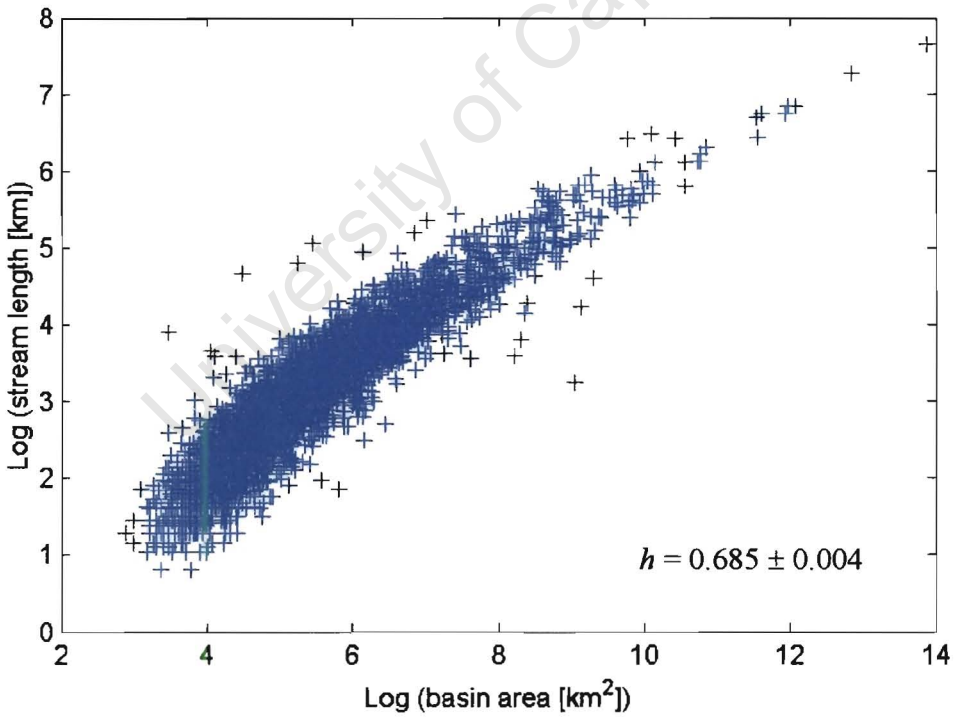

Fig. 4.5. Hack's Law plot for the Orange river network

Looking at the results presented in Table 4.1 and Figure 4.5 above, it is satisfying to note that they agree well with the theoretical models of networks and previous studies, but because of this agreement, we are not able to make any conclusions about the Orange river network, other than "it's just another river". We shall therefore come back to study individual sub-basins of the network, and compare them with other networks.

The six Cape Fold Belt rivers are much smaller than the Orange, with basin areas between 20,000 and 70,000 km^2, and can therefore supply us with much less data, but not necessarily less insight – some interesting analyses can be performed, though any results will have much larger error bars. After ordering the streams, their numbers, lengths and drainage areas were tabulated with corresponding Horton's Ratios. These can be seen in Table 4.2. It is immediately clear that there is considerably more variation in the ratio than was the case for the Orange. R_n is greater than 5 at least once for each basin (except the Kei), and in the Gamtoos basin $\frac{n(\omega=2)}{n(\omega=3)}$ is as high as 8.50. Similarly R_a is very high (>10 at times) for a number of cases. These anomalies can be partially attributed to less data points available, but can also be a reflection of a real phenomenon. If a trunk stream flows through a soft shale valley with lower order streams draining the hard quartzite mountainsides on either side of the valley, the branching ratios can be affected, and Horton's ratio R_n will be larger than usual. There would, in fact, be a direct relation between this ratio and the length of the valley. The ratio of basin areas, R_a, and of stream lengths, R_l, may be similarly affected. This is illustrated in Figure 4.6. Hack's Law plots were drawn for each of the basins (Figure 4.7). Despite having fewer data points than for the Orange river plot, they all give excellent correlation for h in power law plots. Values for h in each basin vary slightly (0.585 - 0.665), but not significantly so. It is interesting to note that they are all smaller than the exponent for the Orange network (0.685).

Finally, an analysis was done on the Limpopo river. Horton's numbers are listed in Table 4.3. The ratios resemble those in the Orange network, with slightly more variation, probably due to a smaller data set. The logarithmic basin area – stream length plot (Fig. 4.8) has an excellent correlation of 92.7 %, and yields $h = 0.642 \pm 0.008$. This value for h is similar to the ones obtained for most CFB networks, suggesting the rift-inherited pattern is similar to one developed in parallel mountain ridges.

Table 4.2: Horton's Laws of numbers, lengths and drainage areas for the CFB rivers

ω	$n(\omega)$	$R_n(\omega)$	$l(\omega)$ [km]	$R_l(\omega)$	$a(\omega)$ [km^2]	$R_a(\omega)$
Olifants						
2	157	4.24	21	2.76	246	4.71
3	37	5.29	58	2.05	1160	2.95
4	7	3.50	119	3.88	3420	10.67
5	2	2.00	462	1.24	36500	2.02
6	1		572		73800	
Gourits						
2	110	5.24	22	2.50	272	4.45
3	21	3.50	55	2.64	1210	5.52
4	6	3.00	145	1.63	6680	3.85
5	2	2.00	236	1.40	25700	2.09
6	1		330		53700	
Gamtoos						
2	88	5.18	23	2.65	261	4.87
3	17	8.50	61	4.08	1270	9.76
4	2	2.00	249	2.02	12400	3.31
5	1		502		41100	
Sundays						
2	41	3.73	24	2.38	381	3.02
3	11	5.50	57	1.67	1150	3.38
4	2	2.00	95	3.65	3890	6.81
5	1		347		26500	
Great Fish						
2	70	4.67	21	2.62	300	3.77
3	15	3.75	55	1.69	1130	2.83
4	4	4.00	93	5.41	3200	11.38
5	1		503		36400	
Kei						
2	34	4.25	23	2.78	360	4.39
3	8	4.00	64	1.78	1580	3.06
4	2	2.00	114	2.55	4830	4.74
5	1		291		22900	

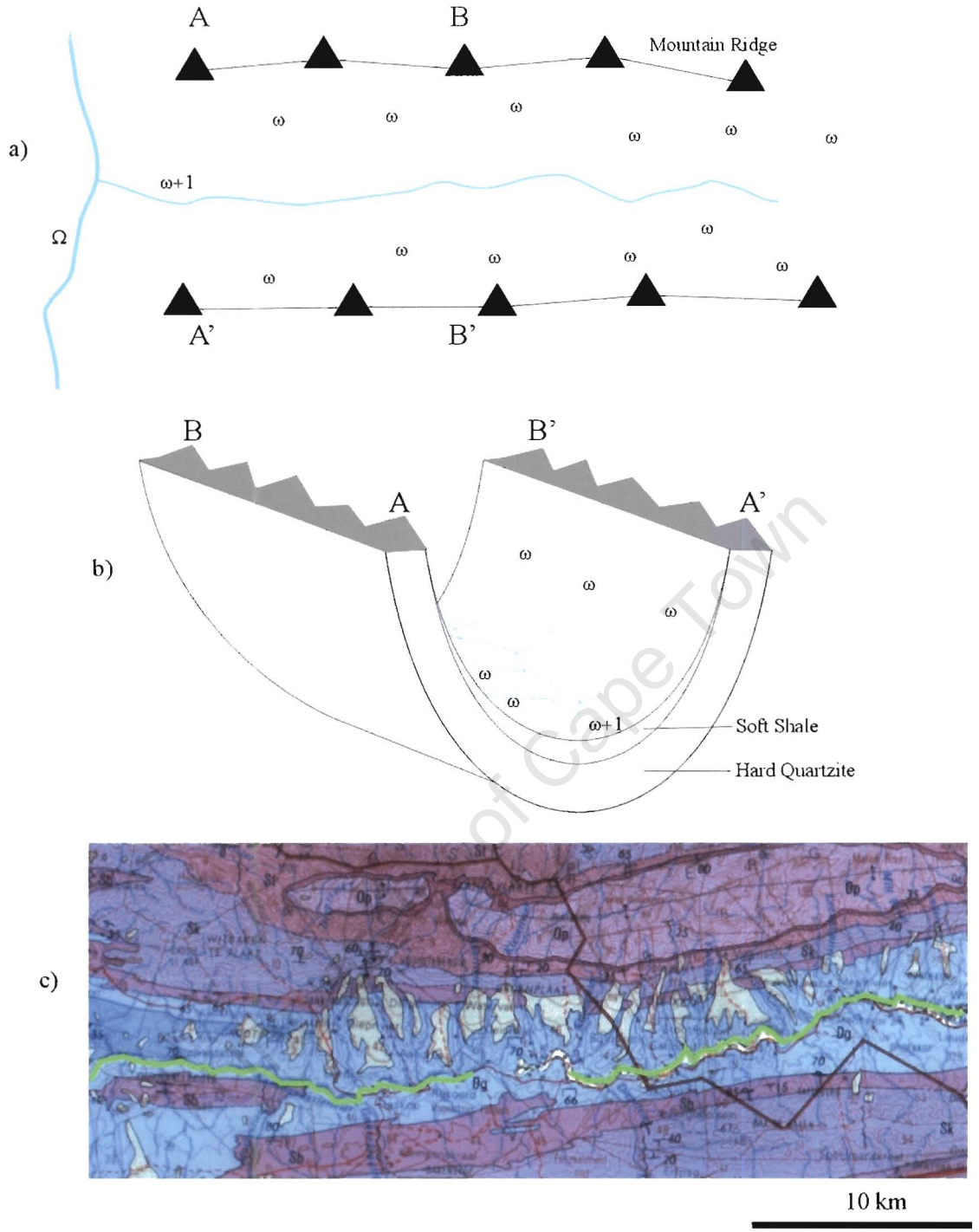

Fig. 4.6(a). Drainage pattern between 2 parallel mountain ranges, similar to the pattern found in the Cape Fold Belt. Low order streams (ω) drain the hard quartzite ridges into the order ω+1 trunk stream in the shale valley, which in turn drains into the mainstream (order Ω) which crosses the mountain belt.
Fig. 4.6(b). A cross-section through the area illustrated in (a).
Fig. 4.6(c). Section of a geological map (South African Geological Survey, 1979) of the Swartberg area in the Gourits River drainage basin. The pattern in (a) and (b) is shown - 2 rivers (marked in green) drain in opposite directions in the shale valley (blue) and are fed by streams draining quartzite and sandstone ridges (different shades of purple) that bind the valley. Yellow represents aeolian sands.

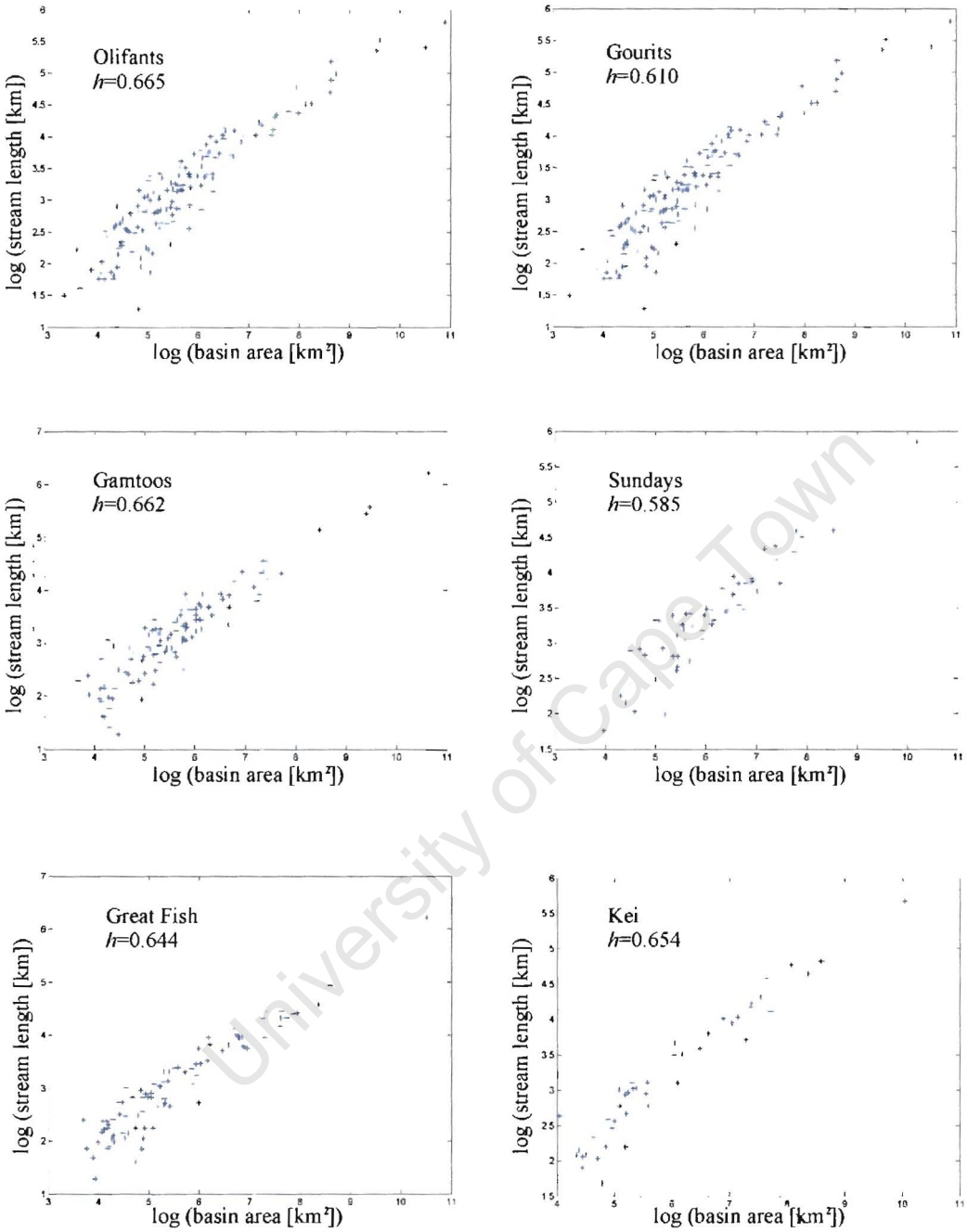

Fig. 4.7. Hack's Law plots for the CFB networks. Value of h for each network is shown on the corresponding plot. For combined data $h = 0.639$. Note that all graphs are concave, with a decrease in slope for $\log(a)$ between 5 and 7.

Table 4.3: Horton's Laws of numbers, lengths and drainage areas for the Limpopo river

ω	$n(\omega)$	$R_n(\omega)$	$l(\omega)$ [km]	$R_l(\omega)$	$a(\omega)$ [km^2]	$R_a(\omega)$
2	830	5.29	22	3.06	262	5.67
3	157	4.76	69	2.67	1490	5.49
4	33	4.71	183	1.94	8140	3.81
5	7	3.50	354	2.81	31100	6.14
6	2	2.00	995	1.52	191000	2.02
7	1		1510		386000	

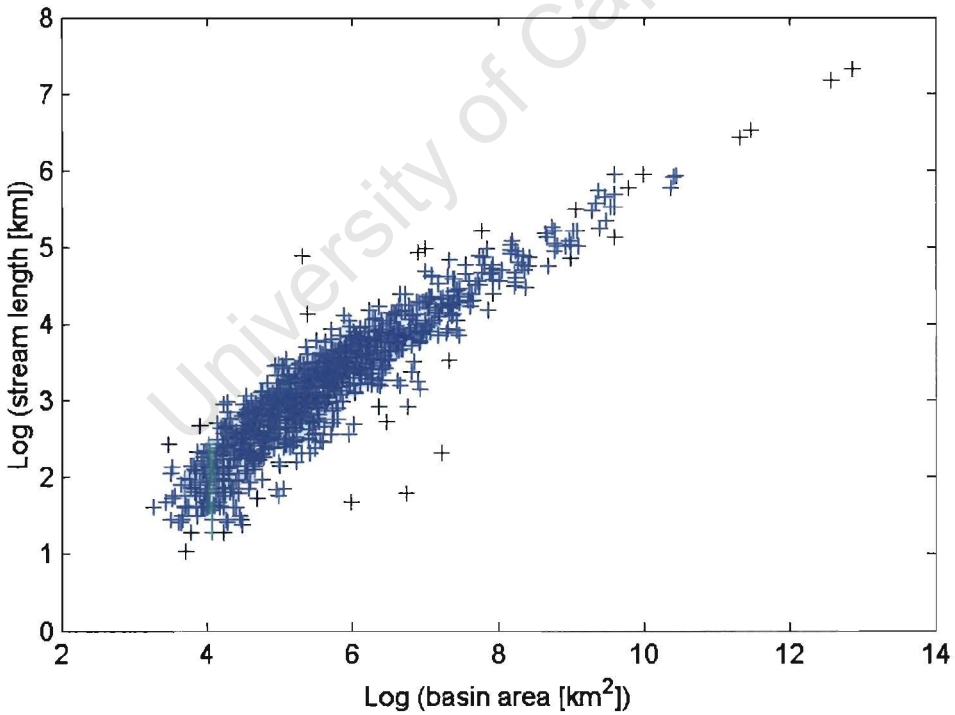

Fig. 4.8. Hack's Law plot for the Limpopo river network

4.4. Hack's Law and basin shapes

There is a lot more to Hack's law that the simple equation $l \sim a^h$. Seeing there is no universal value for h, we need to ask what causes its variations. Does h vary from network to network, or is it different for different scale basins in a single network? We therefore turn our attention to asking what Hack's law, and in particular variation in its scaling exponent, tells us about basin shapes. Following Rigon *et al.* (1996) we assume basins are self-affine, and therefore

$$a \sim L_{\perp} L \tag{4.1}$$

and

$$L_{\perp} \sim L^{H} \tag{4.2}$$

where H is the Hurst exponent (e.g. Meakin *et al.*, 1991). It is the river basin geometry equivalent of the general Hausdorff measure described in the introduction to self-affine fractals (section 2.4). Combining this with the aspect ratio introduced in section 3.7 ($\kappa = L^2 / a$), we have

$$\kappa \sim L / L_{\perp} \sim L^{1-H} \tag{4.3}$$

Alternatively, using Hack's Law (eq. 3.2) and stream fractality (eq. 3.4)

$$\kappa = \frac{L^2}{a} \sim \frac{L^2}{l^{1/h}} \sim \frac{L^2}{L^{d/h}} \sim L^{2-d/h} \tag{4.4}$$

Combining eqs. (4.3) and (4.4) and expression for H can be obtained:

$$H = d/h - 1 \tag{4.5}$$

or, using eq. 3.8

$$H = D - 1 \tag{4.6}$$

Thus, if basins are to have a scaling dimension of $D = 2$, as might be expected from a naïve geometrical intuition, they must remain self-similar, i.e. $H = 1$ and $L/L_{\perp}$ must remain constant. If $D < 2$, and thus $H < 1$, κ increases with increasing basin size, and conversely it decreases if $D > 2$.

The above derivation assumes constant h and d for the basin. However, whenever we average any data over a range of scales, we lose information about its distribution. Therefore, following Dodds & Rothman (2001), we define an order-based Hack's differential

$$h'(\omega_1,\omega_2)=\frac{\log\left[\frac{l(\omega_1)}{l(\omega_2)}\right]}{\log\left[\frac{a(\omega_1)}{a(\omega_2)}\right]} \tag{4.7}$$

where $l(\omega_x)$ is the average length of streams of order ω_x inside a given basin of order ω and a their average area, with $\omega_1 \leq \omega$ and $\omega_2 < \omega_1$. This differential can be thought of as a measure of how Hack's exponent changes inside the main basin when one moves from the scale of ω_2 to ω_1.

Assuming for streams of order ω_1 Hack's law holds with an exponent h_1, and for those of ω_2 with h_2, and further assuming log(c), the constant in eq. (3.2), is negligible compared to log of any average area (in km^2) we can write

$$h'=\frac{h_1 \log a_1 - h_2 \log a_2}{\log a_1 - \log a_2} \tag{4.8}$$

or

$$h'=h_1+(h_1-h_2)\frac{\log a_2}{\log a_1 - \log a_2} \tag{4.9}$$

Since $a_1 > a_2$, $h_1 > h_2$ will give $h' > h_1$, and $h_1 < h_2$ implies $h' < h_1$. Thus, a high value of h' will mean h is increasing with order, and a low value a decreasing h.

4.5. Scaling regimes of Hack's Law

A question associated with h changing with scale inside a basin is whether the changes are gradual or abrupt. Mueller (1973) identified 3 regimes where h was 0.6 at the smallest scale, 0.5 at the intermediate (20,000 – 250,000 km^2) and 0.466 for the largest basins. Dodds & Rothman (2000) suggest networks consist of up to 4 scaling regimes and, for each, Hack's Law holds with a different exponent. The regimes they identified were:

- *Hill slopes*. The smallest basins belong to non-convergent streams running down hill slopes. This regime will be more pronounced in areas that have long, parallel channels. Since streams in this regime do not converge, $l \sim a$, and thus h_{hill}, or h_h has a value close to 1.
- *Short range*. This regime starts when streams begin to converge. While the first order streams are roughly parallel, and second order ones can be similarly, but to

a lesser degree, positioned, at higher orders more sinuous formations can be found. The crossover between the hill slopes and the short range can therefore be quite a gradual one.

- *Randomness*. At larger scales correlations in stream and basin shape decrease, suggesting at this scale streams belong to a random universality class.
- *Geologic constraints*. Eventually, basin reach shapes of geologically constrained maximal basins. As these are controlled by tectonic processes, they are likely to be self similar, and therefore have $h_g = 0.5$.

A logarithmic plot of l against a would then look something like Figure 4.9.

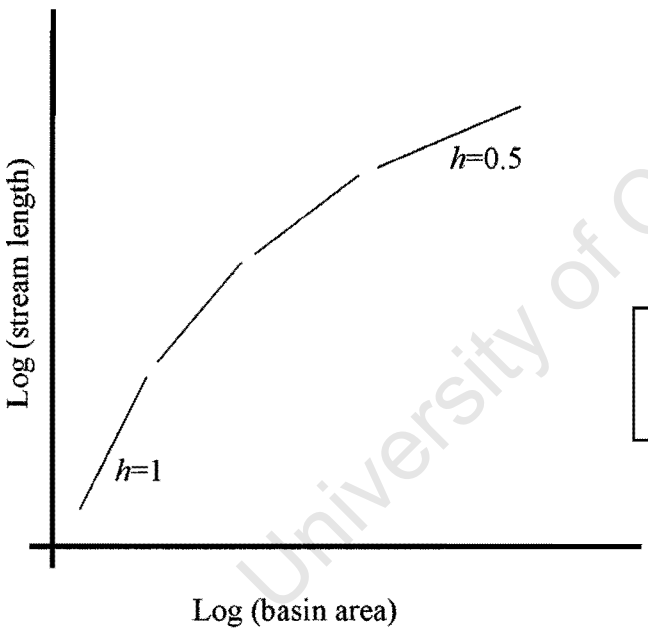

Fig. 4.9. Theoretical plot of Hack's Law showing regimes proposed by Dodds & Rothman (2000).

It was mentioned earlier that the African continent differs from the other ones with respect to tectonic activity. Since Burke & Wilson (1972) first suggested the African plate is relatively stationary, and has been since 30 Ma, all evidence studied since then (e.g., McKenzie & Weiss, 1975; Thiessen *et al.*, 1979; Ashwal & Burke, 1989; all reviewed by Burke, 1996) confirms this observation. Absence of mountain belts resulting from active horizontal plate motion led Holmes (1965) to suggests Africa's topography is thus a unique 'basin and swell' structure. The geological constraints on maximal river

basins would thus be different in Africa than in continents where basins are bounded by such tectonically active belts. A recent study of Africa's topography (Doucouré & de Wit, 2003) shows, however, that most of these basins and swells have a long and complicated history, and that not simply the result of the continent being stationary with respect to the underlying mantle. The fact remains, however, that maximal basins of Africa are constrained by different tectonic features than those on other continents – predominantly epeirogenic motion as opposed to horizontal plate tectonics.

4.6. Further analysis of Hack's Law for real networks

The major sub-basins of the Orange network are the Vaal, the upper Orange (before its confluence with the Vaal), Hartebees, Fish, Molopo and Nossob (Figure 4.3). Sub-basins in these main sub-networks were examined separately. Figure 4.10 shows Hack's law plots for each of the 6 main sub-networks. For basins in each of them the correlation coefficient for a logarithmic plot of stream lengths and drainage areas is over 90%, so Hack's law is always satisfied. These values have been included in Fig. 4.10. The individual values of h inside the 6 networks are slightly different – this will addressed in detail in Chapter 6. What is potentially significant is the sharp discontinuity in the slope at $\log a \approx 7$ on all (most notably for Molopo and Nossob) graphs. Similar breaks can be seen in some Cape Fold Belt river networks (Figure 4.7). This is possibly the crossover from short range to randomness mentioned above. Figure 4.11 shows a Hack's law plot for the entire Orange basin similar to Figure 4.5, except basins of different orders are represented by different colours. From the figure one can see that at $\log a \approx 7$ we have mostly orders 3 and 4, as well as some of the larger order 2 and smaller order 5 basins. We shall therefore turn our attention to Hack's differentials at those scales.

Table 4.4: Hack's exponents for basins of a specific order.

ω	Orange	Limpopo	CFB
2	0.751 ± 0.008	0.679 ± 0.015	0.676 ± 0.018
3	0.585 ± 0.016	0.577 ± 0.022	0.586 ± 0.026
4	0.547 ± 0.035	0.496 ± 0.046	0.558 ± 0.051
≥4	0.514 ± 0.017	0.516 ± 0.024	0.538 ± 0.030

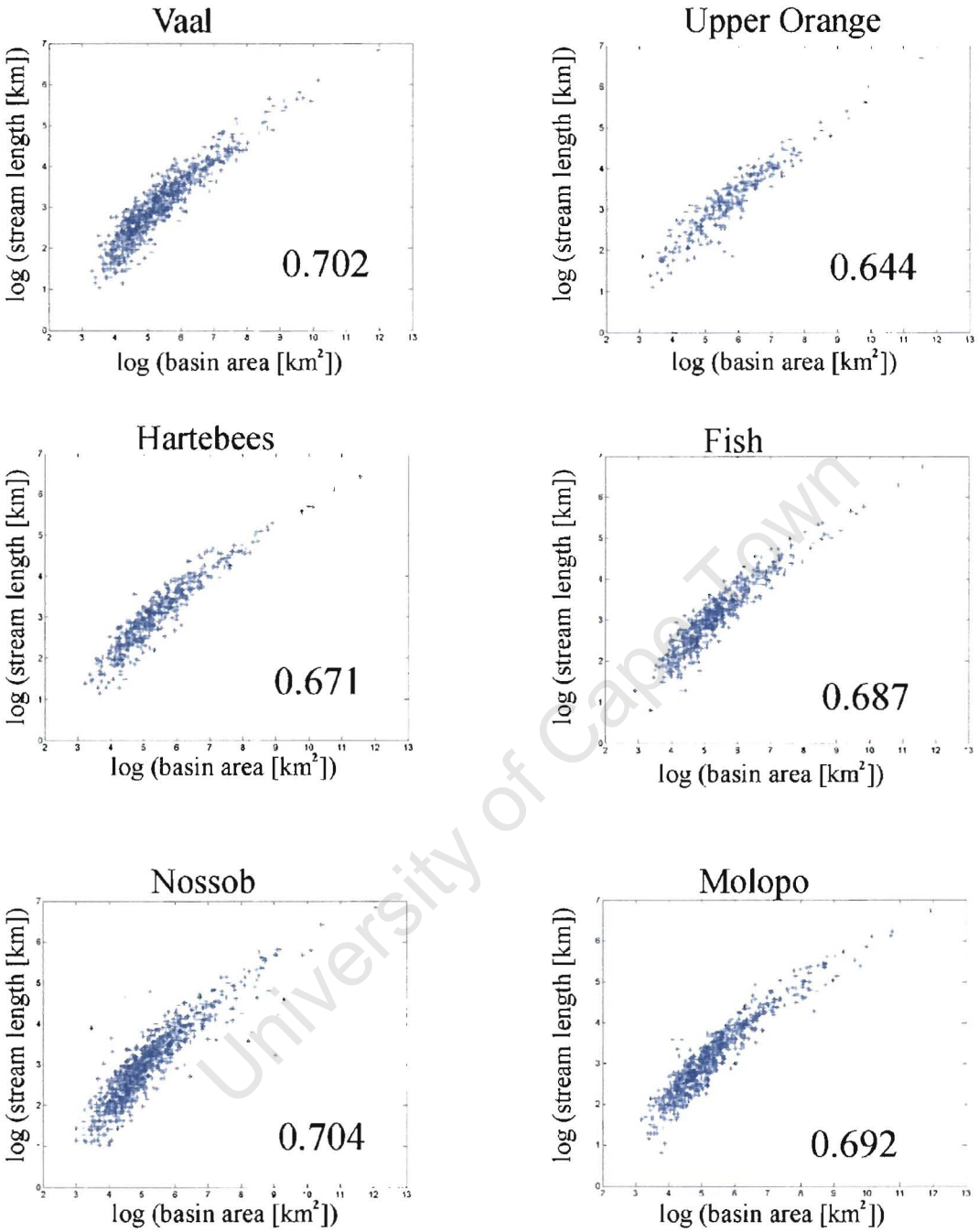

Fig. 4.10. Hack's Law plots for the 6 major sub-basins of the Orange. Number on each graph is the Hack's exponent inside the sub-basin.

First, it is important to demonstrate that h does in fact change with order, or alternatively, basin size. Table 4.4 shows how the exponent varies for basins of a given order for the Orange and Limpopo networks, as well as for the Cape Fold Belt rivers (averaged over the 6 networks). The constant decrease in the value of h is clear to see. At this point it might be important to point out that while the order of a given basin in a network puts constraints on its size, it is essential to realise Horton's ratios apply to average basin sizes in the entire network. In other words, basin order is not necessarily an indication of basin size for individual basins. For example, it can be seen from Fig. 4.11 that some 2nd order basins have larger areas than some 5th order basins. As scaling regimes are more likely to have thresholds or cross-overs corresponding to a given size, not order, of the basins, it is important to complement all studies of how scaling laws vary with order with observations how they vary with size.

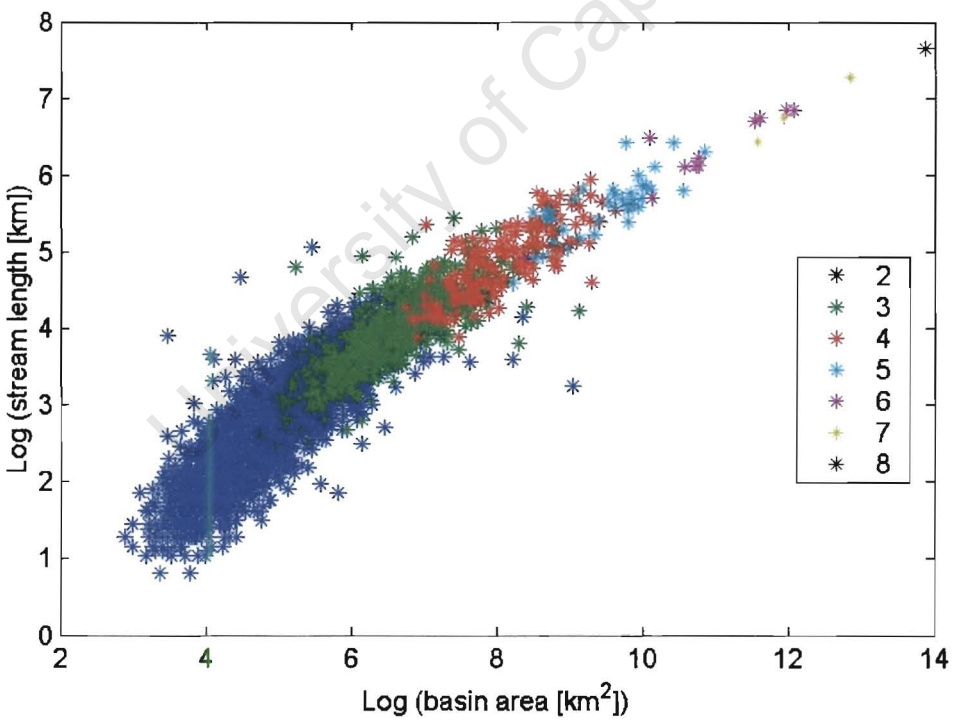

Fig. 4.11. Hack's Law plot for the Orange network with basin orders in different colours.

With that in mind, Figure 4.12 shows a plot of local values for h. For each value of the natural logarithm of the basin area a_0 (in km^2), the graph shows the best fit value for Hack's exponent for basins with area a within a natural order of magnitude of the given area, or $a \in [\log a_0 - 1; \log a_0 + 1]$. A general trend of h decreasing with increasing basin size is evident, but a number of secondary features can be seen in the graph. The most notable one is the drastic increase at $\log a \approx 9.5$, and a less prominent one at $\log a \approx 7.5$. The bizarre features for $\log a > 11$ have no significance, and are purely the result of very few data points for these maximal basins (as is evident from Fig. 4.5).

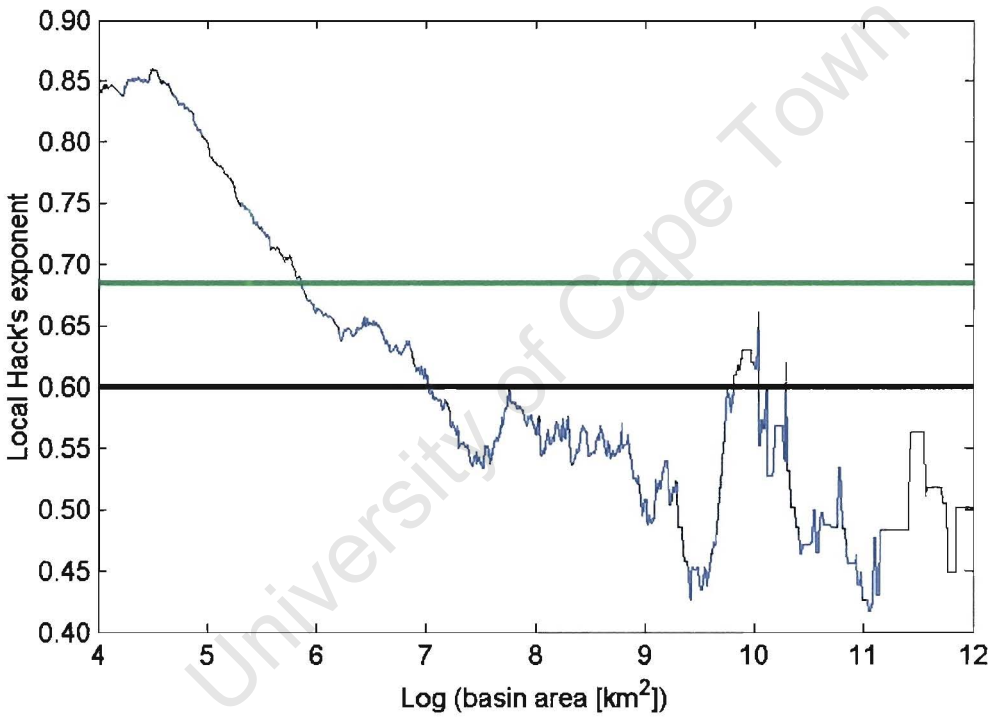

Fig. 4.12. Local Hack's exponent (within a natural order of magnitude) for the Orange network. Green line corresponds to the value of h for the network, 0.685. Black line corresponds to $h = 0.6$, the original value quoted by Hack (1957).

4.7. Analysis of Hack's differentials

For all 161 4th order basins in the Orange network, $h'(4,3)$, $h'(4,2)$ and $h'(3,2)$ were determined using eq. (4.7). It might be helpful to explain what the differentials h' mean in non-mathematical terms. Inside a given basin of order ω, with $\omega = 4$ in this case, we are interested to find out how the relationship between basin area and stream length changes with order. $h'(4,3)$ tells us how scaling of basin area and stream length changes from 3rd order streams to the maximal $\omega = 4$ basin. As shown by eq. (4.9) a high value of h' implies h increasing with order, and a low h' – a decreasing h. Similarly, $h'(4,2)$ shows how scaling changes at the transition from 2nd order to 4th order, and $h'(3,2)$ from 2nd to 3rd inside a given $\omega = 4$ basin. The mean values for $h'(4,3)$, $h'(4,2)$ and $h'(3,2)$ were found to be 0.606, 0.664 and 0.714. Hack's exponent for basins of order 4, 3 and 2 in the Orange network is 0.707, and for orders 3 and 2 it is 0.726. The differentials are therefore smaller than mean values of h at this scale, confirming what we have seen before, namely that the value of h is decreasing.

These differentials potentially hold the answer to scaling regimes, and cross-overs between them. To see what factors influence the differentials, we follow Dodds & Rothman (2001) in comparing h' with the basin's aspect ratio, κ, and furthermore with the average slope and relief of the basin.

The plots of each $h'(4,3)$, $h'(4,2)$ and $h'(3,2)$ against the aspect ratio of the 4th order basin concerned are shown in Figure 4.13. Positive correlation between the $h'(4,3)$ and $\log(\kappa)$ is clear to see, and a correlation coefficient of 57.7 % confirms it. For the $h'(4,2)$ – $\log(\kappa)$ plot the correlation is even better (67.2 %), while the correlation between $h'(3,2)$ and the logarithm of the aspect ratio is poor (18.8 %). The significance of these correlations can be analysed using Student's t distribution. Starting with a null hypothesis H_0 that 2 variables are independent of each other, a two-sided significance p_s can be determined – if this value is sufficiently low ($p_s < 0.05$ for the most commonly used 95 % confidence interval), the null hypothesis is rejected, which in turn suggests significant correlation between the two variables in question. For the first 2 plots mentioned above we have $p_s < 10^{-10}$, which all but conclusively proves relationships between the two differentials and $\log(\kappa)$. For the last plot we have $p_s = 0.017$, which still falls within the 95 % interval. It therefore seems that changes in h depend of the aspect ratio on the basin

concerned – in long, narrow basins h' tends to be higher than in short wide ones. Having already established h is decreasing with increasing order, the above correlations suggest it would decrease by a higher factor in wide basins, which have lower κ, and therefore lower h'.

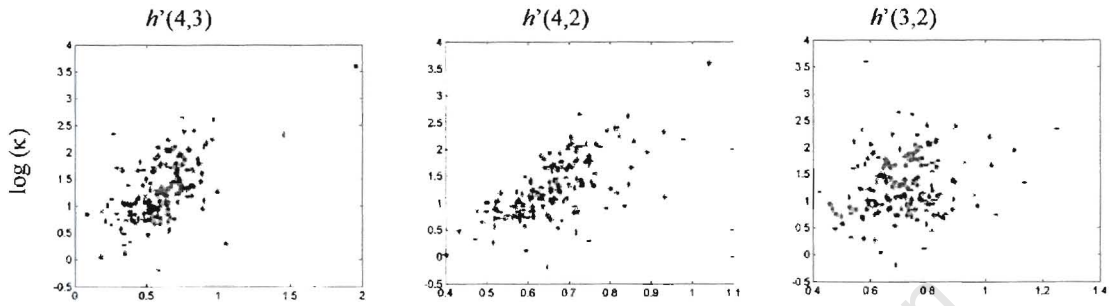

Fig. 4.13. Hack's differentials in the Orange network plotted against logarithms of 4th order basin aspect ratios.

As stated before, it is necessary to complement any analysis involving basin orders with one considering actual sizes. A correlation coefficient of 1.4 % between $h'(4,3)$ and the area of the 4th order basin makes it clear the two parameters are independent. The corresponding statistical significance p_s is 0.986.

Plots for the same differentials against log(κ) for the combined Cape Fold Belt (CFB) networks are shown if Fig. 4.14. The correlation coefficients between log(κ) and $h'(4,3)$, $h'(4,2)$ and $h'(3,2)$, respectively, are 65.5 %, 60.4 % and –10.8 %. The corresponding values for p_s are ~ 10^{-3} for the first two correlations, and 0.622 for the last. It is clear $h'(4,3)$ and $h'(4,2)$ depend on the aspect ratio in a similar way to basins in the Orange network. The last correlation cannot be accepted, suggesting no dependence on κ in transition between orders 2 and 3.

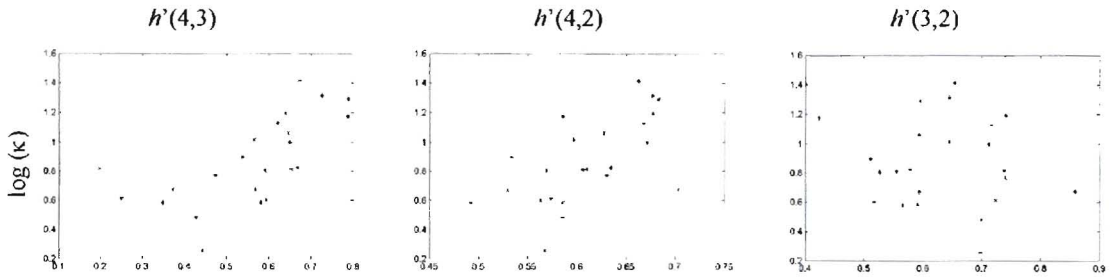

Fig. 4.14. Hack's differentials in the CFB networks plotted against logarithms of 4th order basin aspect ratios.

The corresponding plots for the Limpopo network are shown in Fig. 4.15. The correlations are similar to those in the Orange network. They, together with ones from the Orange and CFB networks, are listed in Table 4.5.

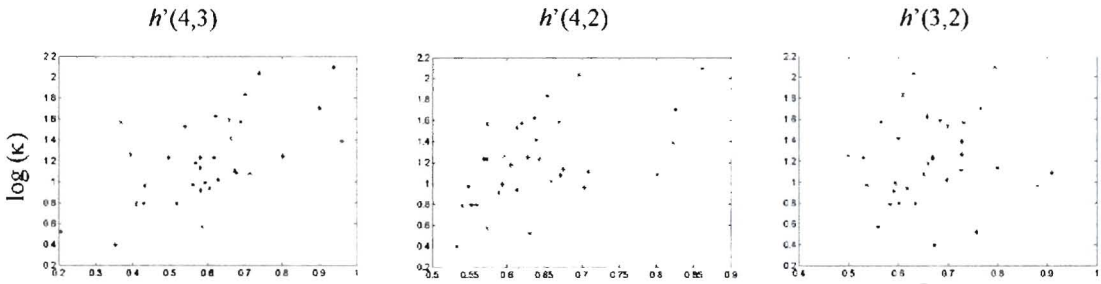

Fig. 4.15. Hack's differentials in the Limpopo network plotted against logarithms of 4th order basin aspect ratios.

Table 4.5: Correlation coefficients between Hack's differentials and basin aspect ratios.

variables examined	Orange		Cape Fold Belt		Limpopo	
	corr	p_s	corr	p_s	corr	p_s
$h'(4,3)$-log(κ)	57.7 %	$<10^{-10}$	65.5 %	0.001	62.3 %	$< 10^{-4}$
$h'(4,2)$-log(κ)	67.2 %	$<10^{-10}$	60.4 %	0.002	53.2 %	$\sim 10^{-3}$
$h'(3,2)$-log(κ)	18.8 %	0.017	-10.8 %	0.622	11.3 %	0.529

We next examine the relationship between the differentials and average slope of the basin. The correlation coefficients, as well as their statistical significance, are summarised in Table 4.6.

Table 4.6: Correlation coefficients between Hack's differentials and basin slopes.

variables examined	Orange		Cape Fold Belt		Limpopo	
	corr	p_s	corr	p_s	Corr	p_s
$h'(4,3)$-log(slope)	-23.1 %	0.003	-50.8 %	0.012	20.4 %	0.254
$h'(4,2)$-log(slope)	-29.8 %	<0.001	-29.4 %	0.172	26.8 %	0.131
$h'(3,2)$-log(slope)	-12.5 %	0.114	19.5 %	0.372	21.6 %	0.227

It is clear to see the correlation is not as strong as was the case with aspect ratios of basins. However, we can suggest these are negative trends between the logarithm of the mean slope and $h'(4,3)$ and $h'(4,2)$, respectively, in the Orange network, and between $h'(4,3)$ and log(slope) in the Cape Fold Belt networks. This would suggest h decreases faster in gently sloping basins than in steep ones. For the Limpopo network there appears to be no significant (or even suggestive) correlation between any differential and basin slope.

It is interesting to compare mean values of Hack's differentials as well as basin aspect ratios and their mean slopes in the different networks studied here. These are summarised in Table 4.7.

Table 4.7: Mean Hack's differentials and $\omega = 4$ basin aspect ratios and mean slopes

Network	$h'(4,3)$	$h'(4,2)$	$h'(3,2)$	κ	slope [m/km]
Orange	0.606 ± 0.223	0.664 ± 0.103	0.714 ± 0.131	4.33 ± 3.52	2.81 ± 1.96
Limpopo	0.600 ± 0.166	0.642 ± 0.085	0.668 ± 0.096	3.63 ± 1.58	3.37 ± 1.61
CFB	0.557 ± 0.157	0.610 ± 0.056	0.636 ± 0.100	2.49 ± 0.75	6.93 ± 2.85

Despite fairly large standard deviations for all the values tabulated above, some clear differences in the basin geometry can be seen between the networks. The mean slope of the 4th order basins in the Cape Fold Belt networks is more than twice as steep as in the Orange or the Limpopo basins. This is hardly surprising, as the relatively small basins draining this Belt descend over 2000 metres in places. At first it might seem surprising that the mean aspect ratio is smaller in the Cape Fold Belt basins, as one usually expects steep basins to be long and narrow. This low aspect ratio is probably a result of the trellis pattern. When narrow basins meet at right angles, the resulting basin will have a main stream length comparable to that of the lower-order basins, but also their combined area, and therefore a low aspect ratio. The values for the individual differentials are smaller in the Cape Fold Belt networks than in the Orange and Limpopo, but the differences are relatively small, especially given the standard deviations associated with them. It therefore seems studying aspect ratios and slopes of basins can be more productive in the study of network geometry than examining Hack's differentials would be.

4.8. Sub-networks of the Orange

We now return to take a closer look at the 6 sub-networks of the Orange, mentioned earlier in Section 4.6 and shown in Figure 4.3. We have already mentioned they drain different geological and climatic terrains, and there is variation in Hack's exponent for each of the sub-networks. Following the finding from the last section that basin slopes and aspect ratios vary more than Hack's differentials, and that they both display correlation with these differentials, Table 4.8 was constructed. In it, for each main sub-network of the Orange, values for h (using basins of $\omega > 2$), mean aspect ratio, and slope of those basins, as well as $h'(4,3)$. All values are accompanied by standard deviations. These deviations are sometimes very large, in particular for the mean slope. This should not be particularly surprising – basin slope is expected to vary significantly in any realistic network. Despite these variations some clear differences can be seen from basin to basin. The Upper Orange, which drains the highest (3000m+) parts in the highlands has, not surprisingly, by far the steepest mean slope, as well as the smallest aspect ratios. This is perhaps unexpected – it was mentioned earlier steep basins are expected to be narrow. However, similar 'anomaly' was encountered with the Cape Fold Belt networks – despite their steep slopes, the basins on average had aspect ratios much smaller than those in the Orange and the Limpopo networks.

Table 4.8. Parameters of sub-networks of the Orange river

Network	h	κ	slope [m/km]	$h'(4,3)$
Nossob	0.704 ± 0.012	2.77 ± 2.14	1.60 ± 1.47	0.634 ± 0.204
Molopo	0.692 ± 0.010	2.79 ± 1.93	2.03 ± 1.60	0.550 ± 0.232
Hartebees	0.671 ± 0.012	2.08 ± 1.32	4.22 ± 2.45	0.614 ± 0.143
Vaal	0.702 ± 0.011	2.15 ± 1.60	4.41 ± 2.90	0.616 ± 0.260
Fish	0.687 ± 0.012	2.24 ± 1.43	5.56 ± 4.15	0.587 ± 0.142
Upper Orange	0.644 ± 0.015	1.84 ± 1.03	7.94 ± 6.98	0.587 ± 0.199

Table 4.9 shows correlation coefficients between each pair of parameters listed above, as well as the statistical significance of these correlations. The first thing one notices from the table is the mean value of *h'* in each sub-network is not correlated with any other parameter. This is perhaps surprising, seeing individual values of *h'* seemed to display correlation with individual values for both slope and aspect ratio of basin.

It is interesting to note that with as few as 6 data points there is clear correlation between any two of mean basin slope, mean aspect ratio and Hack's exponent. Given that from a given topography a unique river network can be constructed, we assume that of these three parameters, slope is the first order one. *h'* and k then are dependant on the slope, and both show strong negative correlation, i.e. they increase as slope decreases.

Table 4.9: Correlations between parameters in Table 4.8 and their significance

	κ		slope		*h'*(4,3)	
	corr.	p_s	corr.	p_s	corr.	p_s
h	75.5 %	0.061	-82.7 %	0.026	27.5 %	0.589
κ			-89.4 %	0.007	-26.3 %	0.605
slope					11.9 %	0.818

4.9. Climate and Drainage Patterns

In this section variation in climatic conditions across southern Africa is compared to drainage pattern parameters in the region. Two principal parameters that can be used to define climate are the mean rainfall and temperature. The data used here was obtained from De Beers Group in Centurion, based on the studies of Legates & Willmott (1990a, 1990b) and are shown if Figures 4.16 and 4.17, respectively. The region has then been subdivided into squares 500 km across, as shown in Figure 4.18. Three of the squares (A5, F4 and F5) did not contain any land, and were not used in the analysis. Furthermore, blocks A4, F3 and E5 did not contain enough land to produce any reliable data, and were therefore incorporated into A3, F2 and E4, respectively.

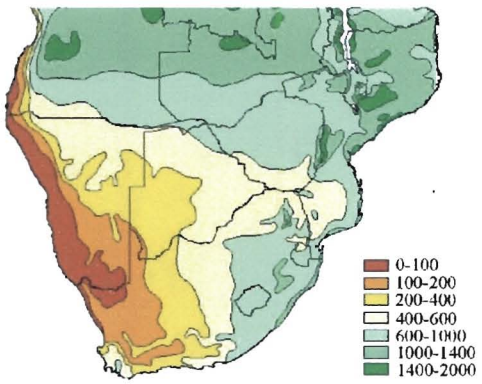

Fig. 4.16. Mean Annual rainfall [mm]

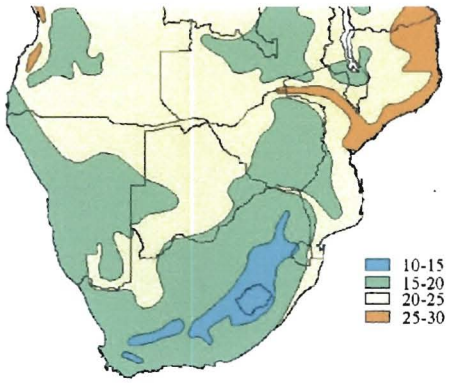

Fig. 4.16. Mean Annual temperature [°C]

For each block the average annual rainfall and temperature were computed by measuring relative areas of regions in Figures 4.16 and 4.17. Using a database of rivers in Africa, the total length of perennial and non-perennial streams in each block were computed. These values were in turn used to determine drainage density of all channels, as well as of only perennial ones, and the ratio of non-perennial streams to perennial ones. Drainage density is defined by (Horton, 1945):

$$\rho = \frac{\sum l}{a} \tag{4.10}$$

where $\sum l$ represents the total length of streams in the given area a. Using a 1 km resolution DEM of the sub-continent, Hack's exponent was computed for each block. Only basins fitting within a given 500 km square were taken into account, so the value for h computed here corresponds to scaling of small-scale basins. All results are summarised in Table 4.10.

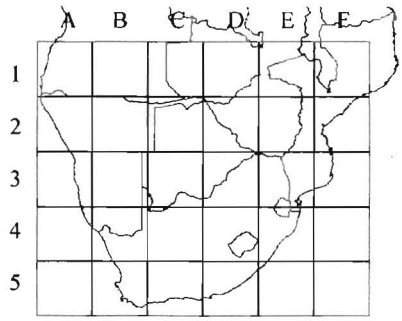

Fig. 4.18. Grid used for the climatic analysis of the region.

Table 4.10. Climatic and drainage parameters of each block

block	area	temp	rain	perennial	non-per	density	per dens	non-p/p	*h*
A1	215	21	730	17300	400	0.082	0.080	0.023	0.702
B1	250	22	950	16800	50	0.067	0.067	0.003	0.731
C1	250	23	970	18700	100	0.075	0.075	0.005	0.764
D1	250	21	1000	25900	50	0.104	0.104	0.002	0.624
E1	250	21	1050	31600	0	0.126	0.126	0.000	0.664
F1	240	20	1180	28800	0	0.120	0.120	0.000	0.647
A2	190	19	260	1800	8400	0.054	0.009	4.667	0.654
B2	250	21	480	1900	6300	0.033	0.008	3.316	0.738
C2	250	22	540	4400	2200	0.026	0.018	0.500	0.732
D2	250	21	690	12900	1500	0.058	0.052	0.116	0.568
E2	250	18	780	22400	0	0.090	0.090	0.000	0.684
F2	165	24	980	11000	0	0.067	0.067	0.000	0.646
A3	110	17	60	20	4200	0.038	0.000	210.000	0.680
B3	250	18	230	200	10600	0.043	0.001	53.000	0.712
C3	250	21	340	400	4200	0.018	0.002	10.500	0.765
D3	250	19	540	10800	4700	0.062	0.043	0.435	0.658
E3	238	18	620	18300	100	0.077	0.077	0.005	0.696
B4	228	19	90	2600	13900	0.072	0.011	5.346	0.671
C4	250	19	320	3100	11200	0.057	0.012	3.613	0.684
D4	250	15	680	23700	1000	0.099	0.095	0.042	0.683
E4	150	18	890	18800	0	0.125	0.125	0.000	0.700
B5	120	16	270	13000	1100	0.118	0.108	0.085	0.653
C5	200	16	270	19800	4300	0.121	0.099	0.217	0.649
D5	145	16	640	18900	300	0.132	0.130	0.016	0.679

area = area of land in block [*1000 km^2]
temp = mean annual temperature
rain = mean annual rainfall
perennial; Non-per = length [km] of perennial and non-perennial rivers in block
density = drainage density (km/km^2) of all channels
per dens = drainage density of perennial channels
non-p/p = ratio of non-perennial to perennial drainage
h = Hack's exponent

By just looking at the table one gets the impression the variations in temperature across the region are not significant enough to justify any change in drainage. A statistical analysis confirms this – correlation coefficients between mean temperature and perennial river density, river channel density, and Hack's exponent are: –19.8%, –39.4% and 19.4%, respectively. The only result that could be considered suggestive is the temperature – river channel density, and even here a t-distribution analysis gives the significance $p_s = 0.056$. The result therefore lies just outside the 95% confidence interval, and certainly does not provide conclusive evidence for any trends. The plot of the two variables (Figure 4.19) further indicates there is no significant correlation. We must therefore conclude that no relationship between temperature variations and river network geometry can be seen in southern Africa.

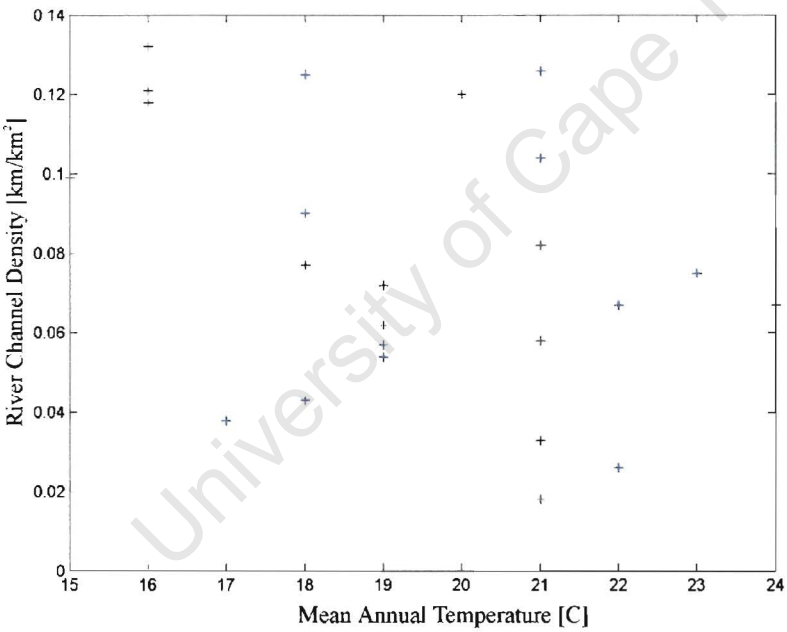

Fig. 4.19. Plot of river channel density against mean annual temperature, showing no significant correlation.

Comparing network parameters with rainfall is much more successful. Correlation coefficients between mean annual rainfall and perennial river density, river channel density, and Hack's exponent are: 67.1%, 44.7% and –7.4%, respectively. The corresponding t-table significance values p_s are $3*10^{-4}$, 0.027 and 0.504. The last of these numbers shows there is absolutely no correlation between rainfall and Hack's exponent,

and Figure 4.20 confirms this. However, there is strong correlation between rainfall and drainage density, particularly when only perennial rivers are taken into account. The positive correlation suggests the drainage density is higher in areas with more rainfall. This should not come as a surprise, as all the water coming down as rain must leave the area as rivers or evaporation (although some can be stored in underground reservoirs). It is also interesting to note that perennial density gives better correlation to rainfall than all river channels combined. It is possible that the number of non-perennial streams present in a given area today is an indication of what the climate, or in particular the rainfall, was in the area at the time the drainage pattern developed.

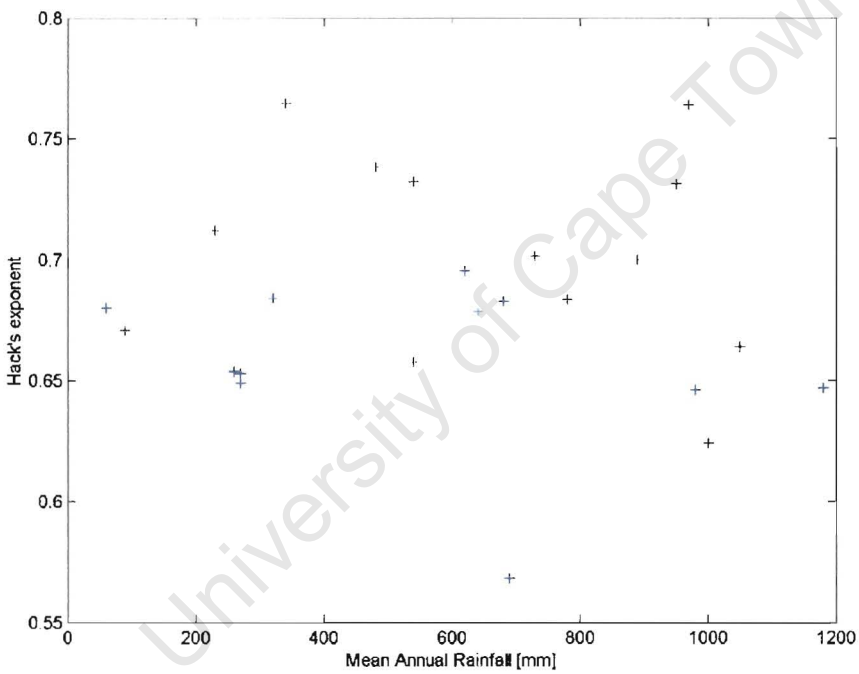

Fig. 4.20. Plot of Hack's exponent against mean annual rainfall, showing no significant correlation.

The above result might seem trivial, but a number of river network scaling laws have been derived from an assumption that drainage density is uniform, or that its local variations are negligible (e.g. Dodds & Rothman, 1999). As is shown here, this is not necessarily the case, particularly in arid regions.

Looking at the plot of perennial density against rainfall (Figure 4.21) some outliers can be seen, and have been marked in red and circled. These three points correspond to the

southern-most blocks, B5, C5 and D5. These blocks correspond to the Cape Fold Belt, which has geology and relief vastly different from the rest of the sub-continent. Despite having low annual rainfall the perennial density is relatively high, suggesting another mechanism, related to geology or relief, is more influential than climate in forming river networks in that area. When the three point are removed from the analysis, rainfall – perennial density correlation jumps up to 88.2%, with $p_s \sim 10^{-8}$, suggesting a very direct relationship between the two parameters.

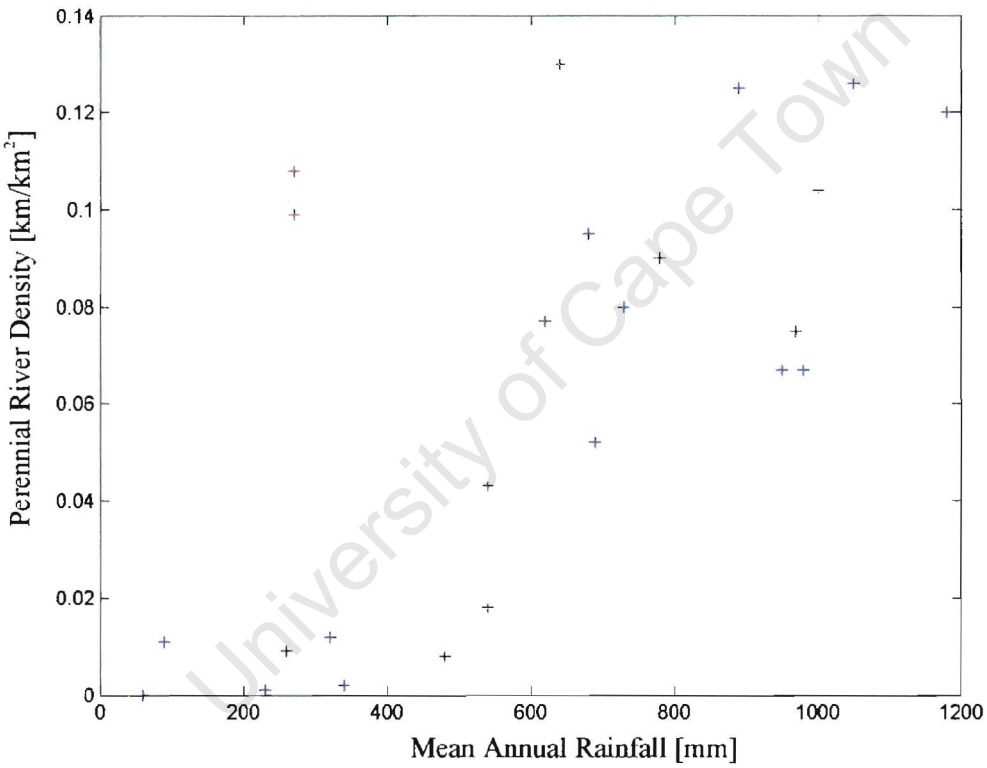

Fig. 4.21. Plot of perennial river density against mean annual rainfall. Correlation is increased significantly if points corresponding to the Cape Fold Belt (circled) are excluded.

It also appears from the figure that a minimum amount of rainfall is necessary for the perennial density to start increasing with rainfall. For all areas where mean annual rainfall does not exceed 500 mm, the perennial density varies between 0 and 0.01 km/km^2 with

no particular pattern. From 500 mm to 1200 mm it increases gradually up to 0.13 km/km^2. This pattern does not include the aforementioned 'anomalous' data points from the Cape Fold Belt.

4.10. Summary

In this chapter large scale drainage patterns in southern Africa were analysed using scaling laws. Basic laws, such as Horton's Law and Hack's Law were obeyed by local networks. To see if there is a relationship between scaling exponents and 'real' properties of river basins, such as underlying geology or climatic conditions in the area, we turned our attention to variations in these exponents. We have found some anomalous Horton's ratios in the Cape Fold Belt, which are probably results of drainage being dominated by long parallel valleys joined by streams cutting through mountain belts at roughly right angles to the valleys. This area will de dealt with in more detail in later chapters.

It was also found that Hack's exponent, h, decreases with increasing basin size in all networks. In networks small enough to neglect large-scale variations in climate and geology it seems this change in h is not gradual, but rather abrupt. This led us to the notion of scaling regimes. In an attempt to examine those, we have, following Dodds & Rothman (2001), introduced Hack's differentials h'. The individual values of these showed correlation to the basin's aspect ratio, and, to a lesser degree, to basin slope. Their regional averages, however, showed no correlation to any other parameter discussed.

An analysis of other parameters showed strong correlation between any 2 of: mean regional aspect ratio, mean regional basin slope and Hack's exponent for basins in the region. This leads us to conclude aspect ratios of basins, as well as h, which can be expressed in terms of branching ratios (eq. 3.6), depend on basin slope, which is a result of local relief and underlying geology. Thus in following chapters attention will be given to variations of h to attempt to understand the scaling regimes. Networks at different scales and regional settings will be examined to see what variations in h are inevitable, irrespective of the topography, and which are results of specific geological settings or particular landforms.

Lastly, the role of climate on drainage geometry was examined. Temperature variations in the region were not significant enough to detect any relationships, but the study of rainfall was more productive, with a strong positive correlation between perennial drainage density and mean annual rainfall. The correlation became even stronger when data points corresponding to the Cape Fold Belt were removed from the analysis. This region was found to have perennial density much higher than expected from rainfall, when compared to the rest of southern Africa.

Chapter 5

Drainage Spacing of Linear Mountain Belts

5.1. Introduction

Many mountain belts have simple drainage patterns transverse to their structural trend. This kind of drainage, and many aspects associated with it (such as sediment erosion and deposition, its response to climatic changes, and even human impact on it) have been studied for mountain belts all around the world (e.g., Seeber & Gornitz, 1983; Adams, 1985; Jones, 2002). The best examples for such transverse patterns are found in active mountain ranges with linear crests and an approximately constant width (e.g. Hovius, 1996). Such a hypothetical mountain ridge is shown in Figure 5.1.

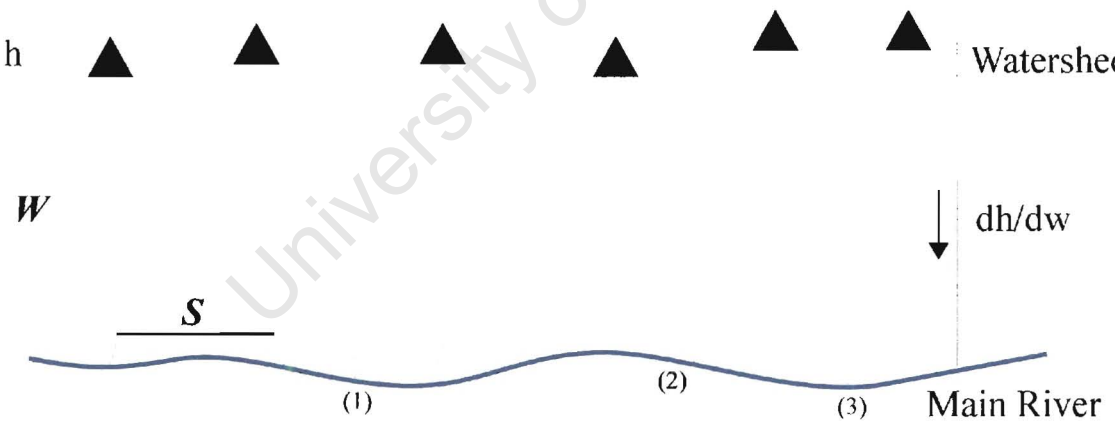

Fig. 5.1. Hypothetical drainage of the slope of a linear mountain range

(1) Not included in study: source more than half-way down between Watershed and Main River
(2) Counted as two streams: each drains more than half the slope before confluence
(3) Counted as one stream: confluence more than half-way up.

h: average height of Range above Main River
H: highest point in range
dh/dW: average slope between Watershed and Main River

In the global study of such drainage by Hovius (1996), no rivers on the African continent have been included. The major reason for this is that due to its unique position in the plate tectonic jigsaw, the African Plate is virtually stationary (Burke & Wilson, 1972), and mostly surrounded by divergent margins. The only active mountain belt is the Atlas Mountains in the north (Figure 5.2), with the exhumed Cape Fold Belt (Figures 5.2 and 5.3) approximately 250 Ma in age being the only other significant folded mountain range.

In this study the regularity of the transverse drainage in the Cape Fold Belt is examined, and the results are compared to the aforementioned global study of Hovius (1996), who studied 11 mountain belts varying between 200 and 1600 km in length.

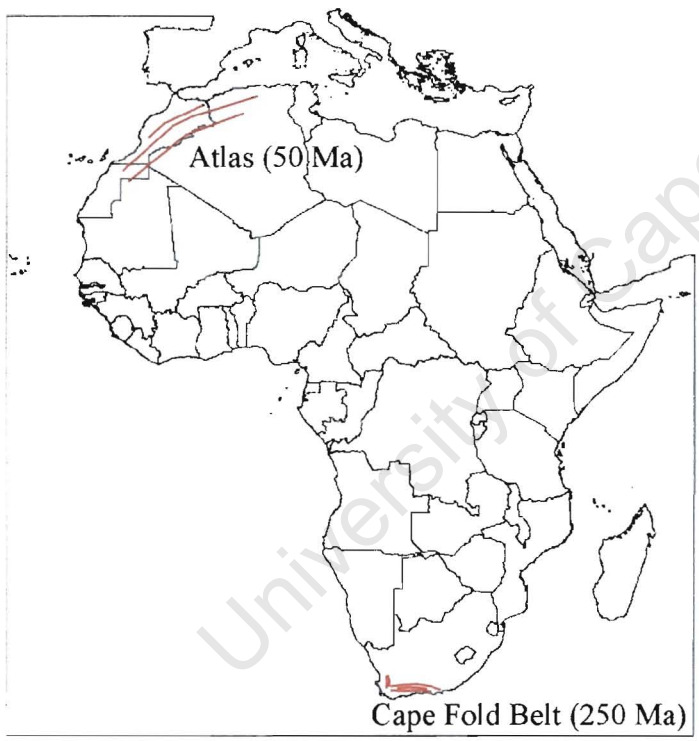

Fig. 5.2. Relatively young folded mountains in Africa.

Parallel first order streams can, however, be found in any linear mountain range, irrespective of its rock type and age. Other linear structures found in southern Africa that exhibit such drainage are on either side of the Drakensberg Escarpment. Outwards from Lesotho rivers flow down the escarpment. In sections where that divide is linear, a pattern of parallel first order streams is observed.

Inland of the escarpment, on the flat lying basalt surface of Lesotho, the drainage pattern is completely different. Trunk streams that combine to form the Orange river flow in almost any direction, but have cut deep valleys into the basalt (some of them over 1000 m deep but less than 10 km across). When these trunk streams, and hence the valleys, are straight, parallel first order streams are once again observed on the valley slopes.

5.2. Data Acquisition

Topographic maps with 1:250,000 scale were used to find linear mountain ranges with transverse drainage. The Cape Fold Belt consists of a number of primary parallel quartzite ridges separated by valleys often containing softer shale (Fig. 4.6). The large scale drainage pattern of the area is thus trellis – the transverse streams draining the mountain belts join main rivers in the shale valleys (parallel to the ridges, and therefore roughly perpendicular to the transverse streams), which then find their way into the Indian Ocean.

Only ranges with at least 11 streams (10 intervals between streams) were considered in this study. Eight mountain ridges (or section thereof) were found to be linear enough for our purposes. These are the Baviaanskloof, Groot-Winterhoek, Suuranysberg, 2 sections of the Swartberg, Langeberg, Kareedouwberg, and a small nameless range draining into Blourivier, labeled Blouberg for this study (Figure 5.3). Smaller or less prominent ranges not included in the study have been excluded from this figure, but such ranges keep the drainage pattern of the network trellis. There is no mountain range immediately to the south of the eastern section of the Swartberg (labeled Swartberg 1 here), and therefore no trellis patter. The mountain front there was defined at the sharp discontinuity in the slope, obvious from the contours on the topographic map. From the belts examined, the distance, *S*, between adjacent streams was measured. This spacing distance could be determined on the maps to the nearest 1mm, which corresponds to 250 metres in reality.

Interpretative ambiguities may arise with streams draining the mountainside converging before meeting the main river in the valley. In this study streams that joined up before flowing halfway down the slope were taken as one stream. Similarly, streams with sources less than halfway up the mountain slope were not considered here. All these features are illustrated in Figure 5.1.

For each of the eight belts, the half-width of the mountain belt, W, was measured. This parameter is defined as the distance between the watershed on top of the mountain range and the base of the mountain front (Hovius, 1996). Here a mean value for W was used for each belt. In each belt the highest point, H, was also recorded, as well as the average slope, dh/dW, and the average height of the mountain range above the valley, h. The stream spacing ratio of each belt, R, was calculated using the definition of Hovius (1996): R=W/S, where S is the mean spacing ratio for each belt. The assembled data are listed in Table 5.1a.

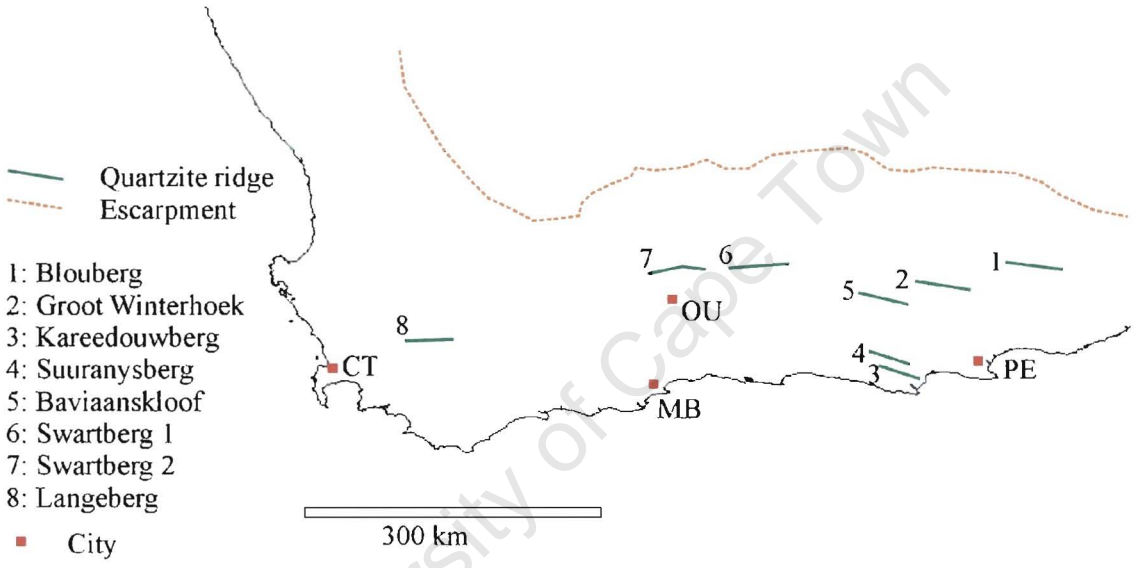

Fig. 5.3. CFB quartzite ridges used in this study

Collection of data from the Drakensberg was a process similar to the one described above, but some differences existed due to the different nature of the mountain belts. Five linear sections of the escarpment were found (Fig. 5.4), from Mount Amery to the Twelve Apostles, Popple Peak to Giant's Castle, Giant's Castle to Mkhomazi Pass, Mzimkulu Pass to Thaba Ntso and Mount Fred to Quachasnek Border Post. What was described as the half-width of a folded mountain range was very difficult to describe or measure here, as there is no convenient trunk stream parallel to the mountain range, and even the mountain front is not necessarily linear. Some of the first order streams join with their neighbours in valleys less than 3 km from the divide, others have a length of well over

10km and only join other rivers in the plains below the Drakensberg. Thus for the escarpment drainage all streams with sources less than 2 km from the divide, and with a stream length of at least 2 km were included in the study. The assembled data are listed in Table 5.1b.

In the Lesotho highlands Orange river headwaters cut deep valleys into the soft, horizontal, vertically jointed basalt volcanic bedding planes. When these are straight for a sufficiently long distance, the trunk streams in these valleys are fed by short parallel streams draining the steep valley slopes (Fig. 5.5). The resulting drainage pattern is similar to that in the Cape Fold Belt, and all the parameters described there could also be measured here. The spacing of these short parallel streams was the 3rd dataset included in this Chapter. Eight trunk rivers were examined: Sehonghong, Mashai, Khubelu, Moremoholo, Semenanyane, Mokhotlong, Mantsonyane and Mokhabong (Fig. 5.4). The difference from the Cape Fold Belt was that most valleys widened downstream, with the half-width often more than doubling in the section examined. Occasionally, the valley narrowed downstream just before its confluence with another valley. The data assembled here can be seen in Table 5.1c.

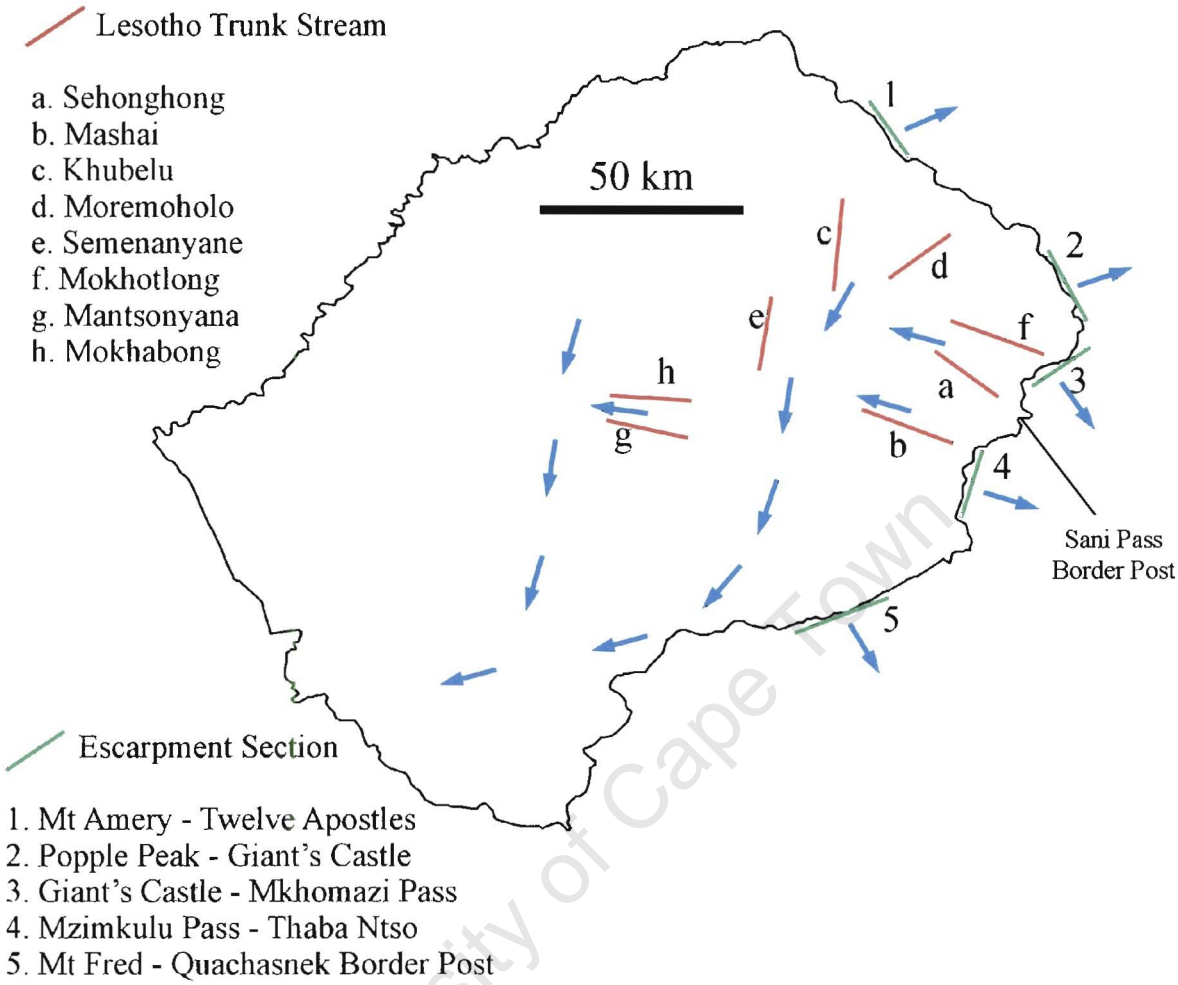

Fig. 5.4. Lesotho trunk streams (red) and linear escarpment sections (green) where regular spacing was observed. Black line is the Lesotho – SA border. On the east this coincides with the Drakensberg escarpment, which acts a major watershed between the Orange and short rivers flowing to the Indian Ocean. The main drainage directions are shown in blue.

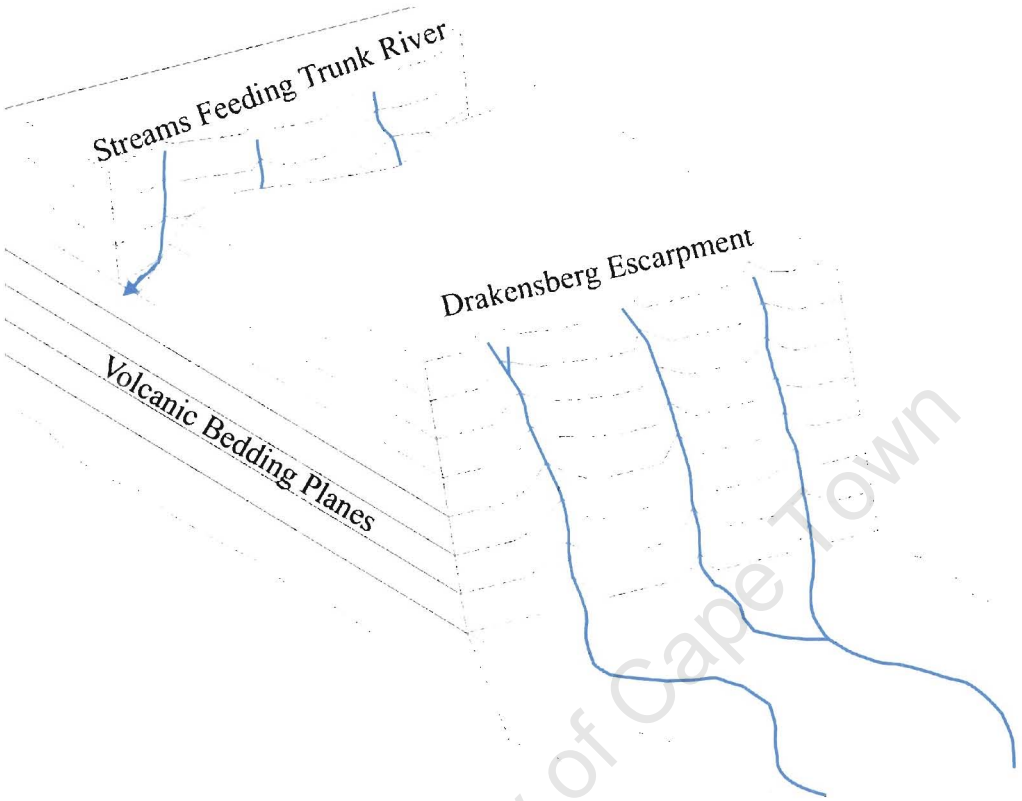

Fig. 5.5. Schematic figure showing two types of linear drainage in the Drakensberg. Streams run off the steep Escarpment to reach the gently sloping rivers that flow to the Indian Ocean. On the other side of the watershed deep valleys have been cut into the basalt, and the trunk river in these are fed by streams draining the steep valley slopes. These are the headwaters of the Orange River.

Blouberg	**Groot Winterhoek**	**Kareedouwberg**	**Suuranysberg**	**Baviaanskloof**	**Swartberg1**	**Swartberg2**	**Langeberg**
33d15m S	33d35m S	34d S	33d55m S	33d35m S	33d25m S	33d20m S	33d40m S
25d40m E	25d E	24d25m E	24d15m E	24d10m E	22d45m E	22d15m E	19d45m E
north-flowing	*north-flowing*	*north-flowing*	*north-flowing*	*south-flowing*	*south-flowing*	*south-flowing*	*north-flowing*
0-Witwater	0-Bosrivier	0-Kareedouwpas	0-Canaga	0-Donkerkloof	0-Doring	0-Swartbergpas	0
6	7	9	9	7	9	6	7-Langdam
15	13	14	24	14	19	18	15
22-Irene	22	25	40	19	31	23-Grobbelaar	18-Jakkelsvlei
30	26-Wilgerivier	30	45	26	39-Grootkloof	31	24
39	35	35	54-Liekloof	31	44	45	27
46	42	40	61	42-Skuinspadkloof	50	52-Hoeksrivier	32
52	52	48-Lomoenfontein	71	55	57	65	34
55-Lynton	61	60	78-Holgatkloof	59	60	81	42
59	71	71	87	67	69	87-Boesmankloof	59
64	76	77	92	77-Erasmusboskloof	74-Groot Doring	94	67
67	82	80	100	90	77	103	70
74	89	91-spot505	109	96	85	108	77
79-Viewlands	94-Tierhoek		118	101	93	115	82-Olifantskop
86	99		124	106-Sipreskloof	103-Snykoloof	127-Meulrivier	88
93	106		132-Vryheid	115	114	140	92
101	112			121	119	153	98
110	115			128	130	157	106
117-Klipkuil	121			132	133	162-Huisrivier	109-spot1401
	132			139	139-Tierkloof	177	
	140			146-Grysdraaikloof	145	188-Outol	
	147				150		
	156				154-Pardekloof		
	162						
	172-Krompoort						
	177						
	183						
	192						
	201-Kantiens						
	211						
	219-Vermaakskop						

Table 5.1a. Drainage spacing for 8 mountain ranges in the Cape Fold Belt.
Latitude and longitude of each range's centre are given in degrees and minutes, as well as flow direction.
All ranges are aligned east-west, for each range it is indicated if north or south-flowing streams are used.
Numbers are distances in mm between successive streams on 1:250,000 topo maps. 1mm=250m in reality.
If a stream is named, or flows past a named point marked on the map, this name is given as reference.
Distance 0 is always on the West edge of the range's section used.

Mt Amery	Popple Peak	Giant's Castle	Mzimkulu Pass	Mt Fred
28d50m S	29d15m S	29d20m S	29d40m S	30d5m S
29d E	29d25m E	29d25m E	29d10m E	28d50m E
0	0-spot2327	0	0	0
4	3	5	5	5
14	8	13-Lotheni	10	12
17	14	17	16-Mlambonja	19
21	18	21	20	27
29-Cidi	20	27-Masihlenga	25	32
35	25-Gypaetus	35	28	37
37	32	40	31	39-Uplands
45-Mbundini	35	44	39	49
53	42	51	41	54
60	49	57	48	64
67	52-Kambule	65	57	68
		73	61	72
		80	66	
			71	
			75-Ngwangwane	

Table 5.1b. Drainage spacing for 5 linear sections of the Drakensberg Escarpment.
Latitude and longitude of each range's centre are given in degrees and minutes.
Numbers are distances in mm between successive streams on 1:250,000 topo maps. 1mm=250m in reality.
If a stream is named, or flows past a named point marked on the map, this name is given as reference.
Distances increase from 0 as the mountain range goes clockwise along the escarpment.
Ranges are referred to by the peak or pass next to distance 0.

Sehonghong	Mashai	Khubelu	Moremoholo	Semenanyane	Mokhotlong	Mantsonyane	Mokhabong
29d30m S	29d45m S	29d5m S	29d10m S	29d15m S	29d25m S	29d35m S	29d30m S
29d15m E	29d10m E	29d E	29d20m E	28d45m E	29d15m E	38d30m E	28d30m E
0	0-spot 3431	0	0	0	0	0	0
7	8	9	7	6	5	7	7
13	15	16	13	11	10	13	14
20	19	21	20	18	18	17	20
25	25	28	26	21	25-Ha Mohale	21	25
31	37	34	32	27	32	26	28
37	46	39	38	34	40	33	37
43	52	43-Mafulane	46	38	44	37	42
53	60	48	51	42	50	42	46
58	67	54	55	49	58	46	50
67	74-Matsoetsoe	58	62	54	66	49	58
73	79	63		61	72-Linotsing		67
79	83	69-Popa			79		73
	86	76			84		
	92	80					
		87					
		95					

Table 5.1c. Drainage spacing in 8 linear valleys in Lesotho.
Latitude and longitude of each range's centre are given in degrees and minutes.
Numbers are distances in mm between successive streams on 1:250,000 topo maps. 1mm=250m in reality.
If a stream is named, or flows past a named point marked on the map, this name is given as reference, though this was vary rare in this region.
Distances increase from 0 at the head of the trunk valley, and increase downstream.

5.3. Results

5.3.1. Cape Fold Belt

From the eight mountain ranges examined in the Cape Fold Belt there was a total of 153 intervals between their total transverse mountain streams. The mean value for this distance, S, was determined to be 1.864 km, with a standard deviation of 0.747 km. Figure 5.6 shows a histogram of the values for *S*. The mean spacing in each individual basin varied from 1.553 km in the Langeberg to 2.395 km in the second section of Swartberg. The mean of the 8 averages for each belt was 1.880 ± 0.284 km. It is of particular interest to find out whether the variations in *S* are just random fluctuations, or if they depend on characteristics of individual belts.

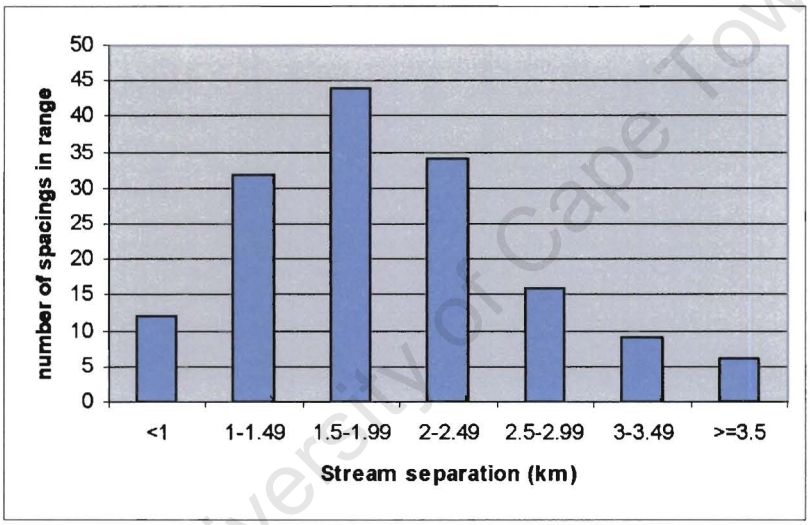

Fig. 5.6. Drainage Spacing Histogram for combined data from the Cape Fold Belt.

All of the mountain ranges included in this study have similar geology – the lithology is the same (quartzite), but there are some differences in the exact geological setting, like the dip of the bedding of the quartzite: this will be explored later in this Chapter. Furthermore, their proximity to each other rules out significant variations in climate or vegetation. Whether the northern or southern part of a range is analyzed also does not seem to play a role, as the mean value for northern slopes separation is 1.798 km, not significantly different to 1.975 km for the southern slopes. Thus the only parameters that could control the drainage spacing are the ones discussed in the previous section, and shown in Table 5.2. Number of spacings in each range, n, has also been included in the table.

Table 5.2. Summary of results for the eight CFB mountain belts analysed.

Range	n	W (km)	H (m)	h (m)	dh/dW (m/km)	S (km)	R=W/S
Blouberg	18	2.75	931	300	110	1.625	1.69
Groot-Winterhoek	30	4.30	1758	690	160	1.825	2.36
Kareedouwberg	11	3.47	919	490	140	1.864	1.86
Suuranysberg	15	2.73	1073	440	160	2.200	1.24
Baviaanskloof	20	5.23	1626	890	170	1.825	2.87
Swartberg1	22	4.50	2084	720	160	1.750	2.57
Swartberg2	19	5.50	2132	1100	200	2.395	2.30
Langeberg	18	2.65	1698	620	230	1.553	1.71

First, the relationship between S and W, the belt half-width, is examined. This relation is of particular interest here, and will be discussed in much detail later on. Figure 5.7 shows a plot of the average spacing for each belt as a function of the half-width. The graph seems to suggest the spacing remains constant irrespective of the value of W. The slope of the linear best-fit curve is 0.037. The fact it is positive would normally suggest a direct relation between the two parameters, but its small size means the difference in S over the range in W available from the data would be 0.104 km, less than one eighth of the range observed in S. Furthermore, a correlation coefficient of 14.9 % for the best fit curve means the slope obtained cannot be taken seriously. We must therefore conclude that we see no evidence for variation of the drainage spacing as a function of the mountain belt's half-width. The correlation coefficient between S and h, the average height of the belt above the valley, was slightly higher at 27.3 %. However, with just 8 data points this correlation gives the Student t-distribution probability p_s as 0.513. This number can be seen as the probability the 2 variables concerned are not correlated, and to accept a relationship between variables one usually needs $p_s<0.10$, or even <0.05. We thus conclude the spacing of mountain streams does not depend of the height of the belt above the valley any more than it does on the width of the mountain belt. The plot of S as a function of h is shown in Figure 5.8.

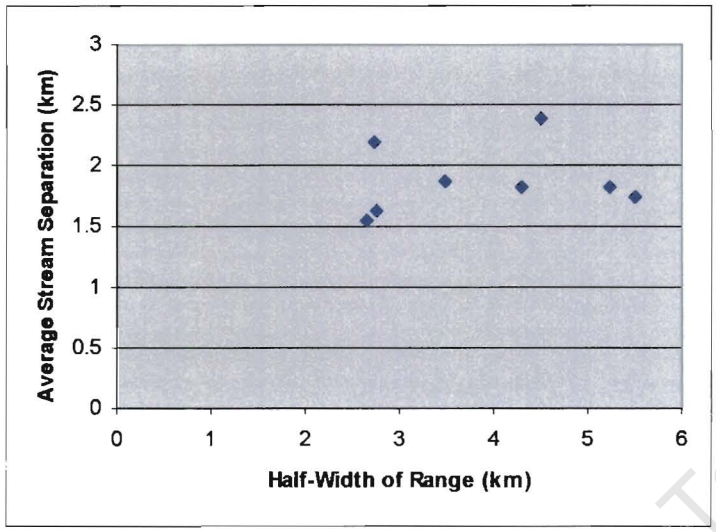

Fig. 5.7. Average stream separation as a function of each CFB range's half-width.

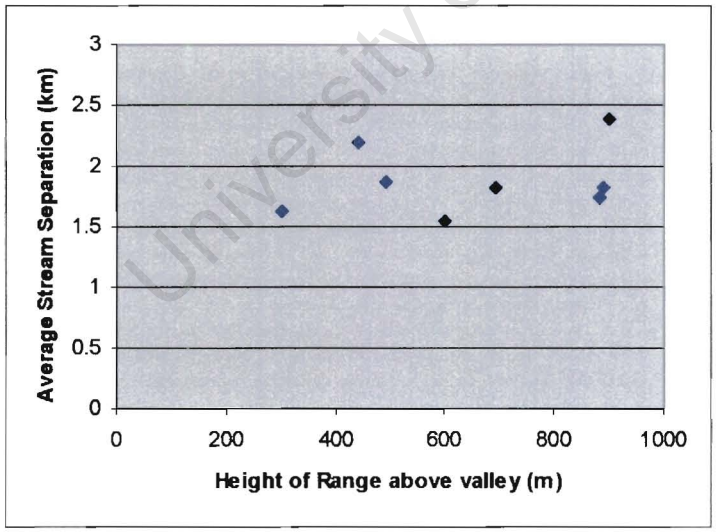

Fig. 5.8. Average stream separation as a function of each CFB range's relative height.

The above correlations (or lack thereof) should not be surprising. Intuitively one would expect the drainage pattern to rather depend on the slope of the ridges, which is just the ratio of the height to the width, rather than the individual parameters. With this in mind Figure 5.9 was constructed, showing S as a function of the slope, dh/dW. The result was a correlation coefficient of 14.3 %, lower than for either of the parameters needed to compute the slope.

The last dependence examined here was between S and the highest point in the ridge, H (Figure 5.10). This gave the correlation coefficient of 18.6 %. This low correlation should not be surprising, as one would expect the height above the foot of the mountain front (h) to be more significant than that above sea level. Since no correlation between spacing and h was observed, it would be strange to say the least to have significant correlation between the spacing and H.

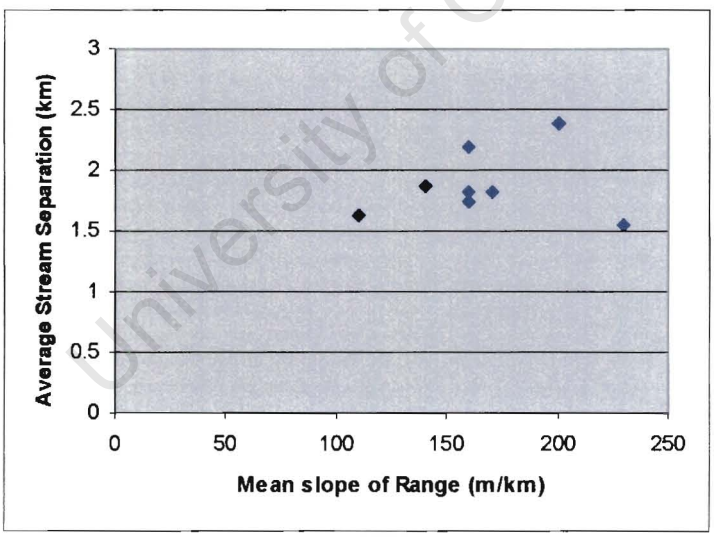

Fig. 5.9. Average stream separation as a function of each CFB range's mean slope.

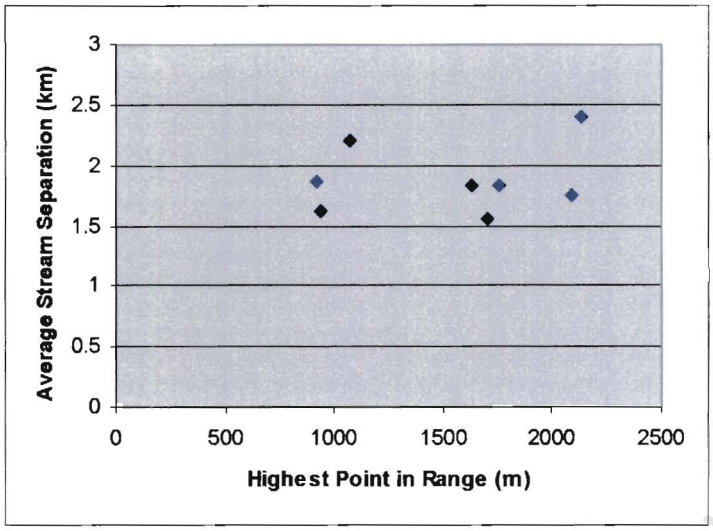

Fig. 5.10. Average stream separation as a function of each CFB range's highest

5.3.2. The Escarpment

From the five linear sections of the Drakensberg escarpment 62 spacings were obtained. The mean value of these was 1.395 km, with a standard deviation of 0.523 km. Figure 5.11 shows the histogram of the individual values. While all five sections have essentially identical geology, the mean spacing varies from 1.182 km to 1.538 km in individual sections. These mean spacing values are shown in Table 5.3, along with the mean slope of the first 3 km from the watershed, and the elevation above sea level of the watershed.

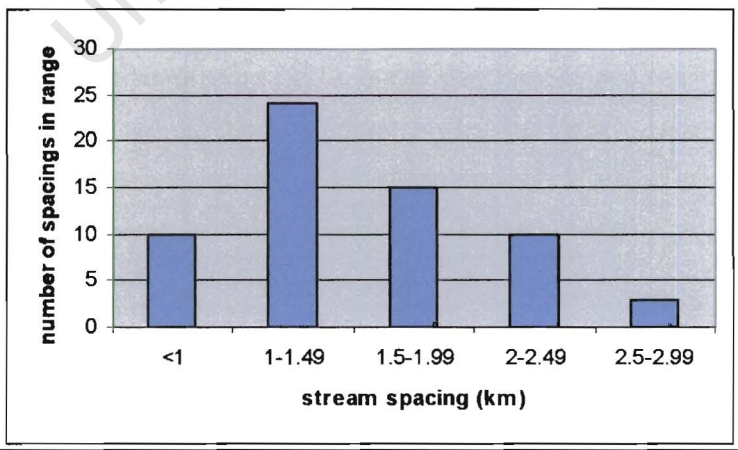

Fig. 5.11. Drainage Spacing Histogram for combined data from 5 linear sections on the basalts of the Drakensberg Escarpment.

Table 5.3. Summary of results for the five escarpment sections analysed.

Section (north margin)	n	slope (m/km)	[$H_{min} - H_{max}$]	S (km)
Mt Amery	11	400	2950-3229	1.523
Popple Peak	11	270	2950-3325	1.182
Giant's Castle	13	290	2800-3314	1.538
Mzimkulu Pass	15	270	2500-3313	1.250
Mt Fred	12	150	2050-2517	1.500

From the table one can see the spacing, *S*, does not depend on either the mean slope, or the elevation of the escarpment above sea level. This can be confirmed by the correlation coefficients between the spacing and slope, and between spacing and mean elevation (taken as halfway between H_{max} and H_{min}). These were found to be 11.3 % and –29.2 %, respectively. With just 5 data points, these values show *S* to be independent of either of the 2 parameters.

5.3.3. Lesotho

From the eight river valleys in the Lesotho highlands considered here, 98 spacing values were obtained. The mean spacing was 1.518 km, with a standard deviation of 0.416 km, with the mean spacings for each valley varying between 1.225 km and 1.646 km. The histogram of the data is shown in Figure 5.12. Parameters of individual belts are listed in Table 5.4.

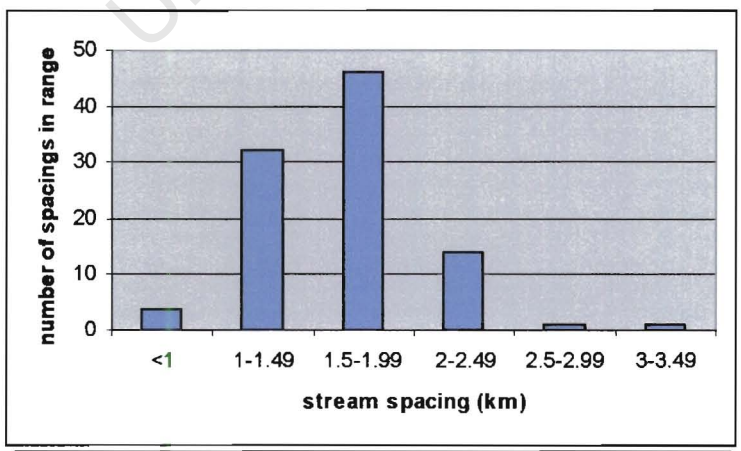

Fig. 5.12. Drainage Spacing Histogram for combined data from 8 linear valleys in Lesotho.

Table 5.4. Summary of results for the eight Lesotho valleys analysed.

Valley	n	W range (km)	slope (m/km)	H (m)	S (km)
Sehonghong	12	3-8	140	~3200	1.646
Mashai	14	2-4	150	3431	1.643
Khubelu	16	4-5	140	~3000	1.484
Moremoholo	10	3-5	140	3352	1.550
Semenanyane	11	3-5	130	~2950	1.386
Mokhotlong	13	4-5	150	~3200	1.615
Mantsonyane	10	3-5	100	~3000	1.225
Mokhabong	12	3-5	80	~3000	1.521

As was mentioned earlier, the half-width of the belt ranged considerably more than in the Cape Fold Belt, and mean values would thus be pointless. These valley widths all have similar values, one can see from the table there is no correlation between them and the spacing ratio. Similarly, except for the last 2 trunk streams, the slope values are very similar, and therefore differences in slope would not be able to account for variations in the spacing. As all Lesotho data were assembled from similar geological and climatic settings, it must be concluded spacing variations of first order streams does not directly depend of any topographic or climatic parameter.

5.4. Is spacing constant?

5.4.1. Summary of results

Assuming that stream separation distance follows a normal distribution, spacing distribution curves were drawn for each of the three main regions using the mean value and its standard deviation from each region. These are shown in Figure 5.13. The curves are normalised to a unit integral, so the maximum probability is lower for distributions with a higher standard deviation.

The normal curves show there is some variation in the assembled data. The data from Lesotho had the smallest standard deviation, and this can also be seen in the normal curve corresponding to that region. The Escarpment data produced a mean spacing of marginally less than the Lesotho data, and the standard deviation was slightly larger – both these

features can be seen on the bell curve (Fig. 5.13). The difference between the mean values of spacing in Lesotho and the Escarpment is so small compared to the standard deviation in either curve, however, that it cannot be concluded stream spacing is greater in Lesotho. Instead, it must stated that both settings exhibit similar spacing. This is very interesting, as while the underlying rock type of both regions is the same (basalt), the geomorphology is vastly different (near-vertical escarpment compared to valleys cut into volcanic bedding planes). In the Cape Fold Belt the mean drainage spacing was considerably larger than in the basalts, as was the standard deviation associated with that mean. However, even in that region 56% of the data lie between 1.5 and 2.5 km (inclusive of these points). Furthermore, we could not conclusively find any parameter which could account for these variations inside each of the 3 regions. It should also be noted that while mean spacing for each range was used in the analysis above, these values were not constant. A glance at Table 5.1 shows there was considerable variety in stream separation in each range. If error bars were to be put on a plot that yields little correlation as it is, it would make the independence of S on any of the parameters examined here even more obvious. It is thus concluded that in linear mountain belts the most important parameter controlling stream separation is the underlying rock type.

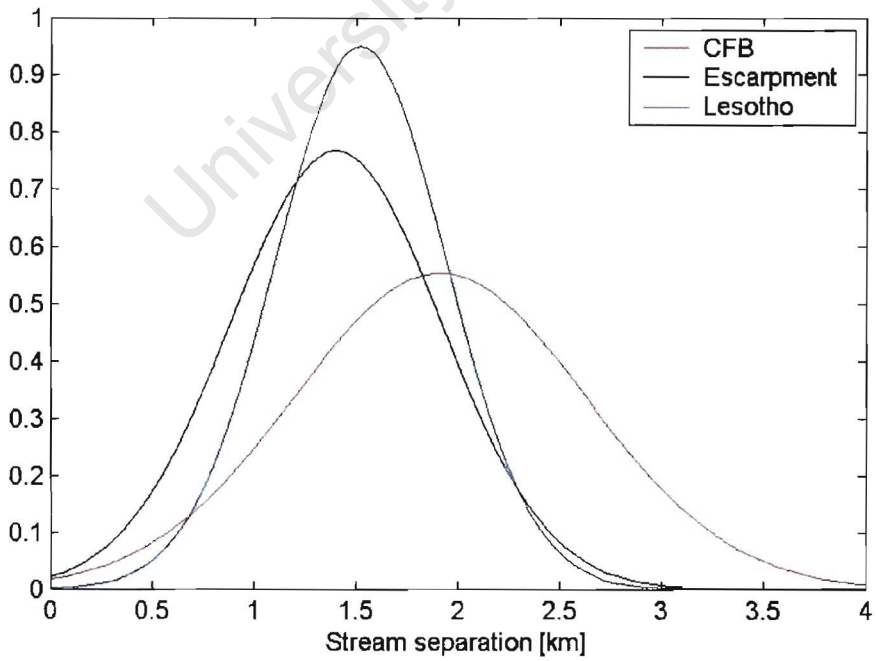

Fig. 5.13. Normal curves for stream spacing distribution in the 3 regions in Southern Africa. Vertical axis scaled to give a unit integral for each curve.

In his study of drainage in linear mountain belts, Hovius (1996) found a direct relationship between drainage spacing S and belt half-width W. This would imply a constant value for R, which he found varied from 1.91 to 2.23, with a mean value of 2.07. Such a relationship is not observed in the ranges of the Cape Fold Belt, which was the only region where W could be measured accurately, and exhibit variation among different ranges. Using mean values from the eight mountain ranges examined, the ratio of the standard deviation to the mean value for S is a very small 0.15, while for R such ratio is twice as large at 0.30. It is clear the aspect ratio R varies much more than the spacing itself, and, as was discussed earlier and is shown by Figure 5.7, S is not seen to be directly proportional to W. Instead, S appears constant for the given range of W. In the 2 regions on either side on the Drakensberg watershed, S cannot be discussed as a function of W. However, the variations in the spacing are considerably less than in the Cape Fold Belt, prompting the suggestion that first order stream separation in linear mountain ranges is constant. The value of this spacing depends on the regional conditions, as do the fluctuations associated with the stream spacing distribution. It was found that in folded quartzite/sandstone mountains, the stream separation (1.864 ± 0.747 km) is greater than in basalts. In basalts the separation was smaller in the drainage off the steep escarpment (1.395 ± 0.523 km) than in the less steep valleys on the flat-lying basalt surface (1.518 ± 0.416 km), but the difference between these was much smaller than between either basalt setting and the folded quartzite ranges. The valleys in the basalt surface have slopes similar to the folded mountains, but their separations are very different. It is therefore concluded here that linear mountain belts exhibit regular drainage spacing, with the value of the spacing being determined by the underlying rock type.

5.4.2. Structural Controls

A possible link to regular stream spacing is fracturing and jointing in the underlying rocks. It might be of use to quote some definitions regarding these structures, so the following are quoted from Ramsey & Huber (1987): Joints are fractures of geological origin along which no appreciable displacement has occurred. Joints occur generally in parallel or sub-parallel joint sets, and where differently oriented sets cross, the resulting geometric pattern is known as a joint system.

The fact that joints influence drainage has been documented for at least a hundred years (Hobbs, 1905). Streams form where erosion is the easiest – it was shown here how in the Cape Fold Belt most trunk streams form in the soft shale valleys between hard quartzite. On a smaller scale, where the underlying rock type is the same, other lines of weakness will be followed, and joints are the most likely structure to provide such lines.

To examine the jointing in the areas studied here, sample aerial photographs have been obtained from the Chief Directorate of Surveys and Mapping (South Africa), and are presented here as Figures 5.14 a-b. It is clear from these photos that first order streams in 1:250,000 maps are in reality higher order streams. This fact does not change any of the results in this chapter – a question of what exactly qualifies as a stream is very complex (e.g. Montgomery & Dietrich, 1988), and any study of drainage must present a clear definition of what it considers a stream. For the analysis in this chapter this was done in section 5.2, but in an attempt to explain the stream spacing observed here, it is necessary to zoom-in and examine the geometry of the network that leads to forming the 'first-order-on-1:250,000-map' streams.

The basalt capping both the Lesotho Highlands and the Drakensberg Escarpment is characterized by vertical jointing. This often leads to spectacular columnar structures near the top of the Escarpment (e.g. Fig. 5.15). Due to the escarpment forming a national border (South Africa – Lesotho) aerial photographs were difficult to obtain, and only the vicinity of the Sani Pass border post was available (Fig. 5.14a). This photo did not coincide with any of the escarpment sections measured here, but some information can be gained from examining it. Streams would originate in the vertical joints, but one can see that each joint does not produce a river flowing perpendicular to the escarpment. Instead, several small streams originating in such joints join to form the famous headward eroding V-shaped valleys (e.g. Buckle, 1978). The width of these valleys corresponds to the number of joints in each of them. This is the definition of normal distribution: each measurement (valley width) is the sum of a number of independent increments (joint spacing). However, the streams from such valleys are still not the streams studied in this chapter. On can see they flow parallel to each other for around 500-1000 metres, but then some of them join. Smaller streams originating on buttresses separating valleys can also be seen as parts of these networks. When streams from 3 or 4 valleys join, the resulting

river is the 1st order stream marked on the 1:250,000 topographic maps. Examples of such streams have been drawn on the aerial photograph (Fig. 5.14a). Unfortunately the escarpment section is not long enough to illustrate the regular spacing, but as was explained earlier photos of other sections are difficult to obtain.

For the same reason no detailed aerial photographs of the highland valleys could be obtained, but the same joint-related process is likely to exist. Before this regular transverse drainage could develop, however, the trunk valley needed to form. These have been formed by the upper reaches of the Orange, cutting steep gorges into the vertically jointed basalt. Once these existed, the tributaries would cut their own gorges. The similarity in their spacing to the Escarpment suggests the mechanism was the same.

The geology of the Cape Fold Belt is completely different from the Drakensberg. Fig. 5.14b is the aerial photograph of the area near Swartberg Pass, i.e. range Swartberg2 in this chapter. The northern and southern slopes of the range are completely different, even though the lithology is obviously the same. This is also illustrated in Fig. 5.16, a photograph taken from an unnamed peak immediately west of Swartberg Pass looking east. Jointing in such heavily folded structures is very complicated, and different types of joints occur, (e.g. extension joints, shear joints – see McClay, 1991 for descriptions).

Near Swartberg Pass the bedding planes dip towards the south (Fig. 5.14b. 5.16). Thus the southern slopes intersect them at a very slight angle, while northern ones are almost perpendicular to them, resulting in a different drainage pattern on either side. To the south a number of straight valleys form very close to each other. These usually join at very narrow angles for form what appears as a first order stream on the 1:250,000 topographic maps. Occasionally a vary narrow valley goes all the way down the mountain without joining with another one. These obviously carry very little water (due to their narrow catchment area) and are usually not marked on the maps. This again brings up the question of what classifies as a stream. On the northern side, the hill-slope drainage is almost a miniature of the large-scale Cape Fold Belt trellis pattern. Streams flow down until they meet a particularly resistant bedding plane, which on this side of the mountain is almost orthogonal to the slope. The stream then turns and almost follows a contour until a breach in the obstacle is found. At such a breach a number of streams are of course likely

to join, and each of the resulting rivers flowing down corresponds to the 1st order streams which were marked on the topographic maps.

The two hill-slope drainage patterns found on either side of the Swartberg are not the only possible scenarios. Bedding planes can be (and in the Cape Fold Belt often are) vertical or virtually have any angle to the ground. They are also often folded and faulted. Combining this with the possible types of jointing, a lot of hypothetical run-off patterns can be constructed. While these might all produce regular spacing of major streams, the spacing is likely to be different in each structural setting. A detailed structural analysis of each of the analysed ranges would be a very interesting study, but falls beyond the scope of this thesis. Unlike the basalts, the underlying rock type is not sufficient to explain hill-slope drainage here. The geometry of the sedimentary layers is also important. The different spacings in different settings may explain the relatively large standard deviation for the combined data of the Cape Fold Belt.

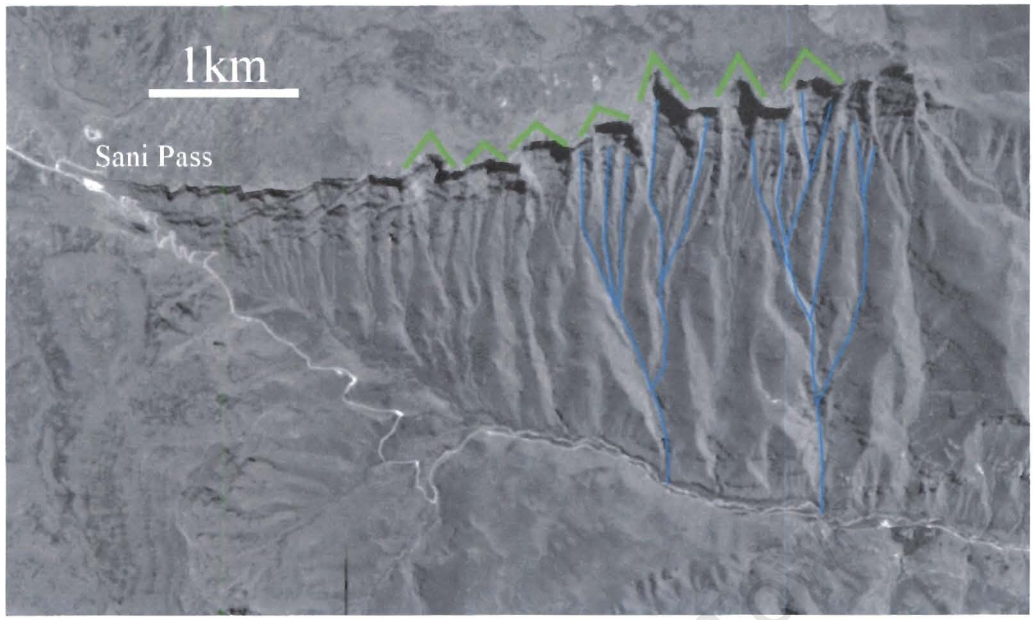

Fig. 5.14a. Aerial photograph of the Drakensberg Escarpment near Sani Pass (see Fig. 5.4). Green curves mark the most prominent V-shaped valleys, while the detailed network structure of what were treated as 1st order streams here are marked in blue.

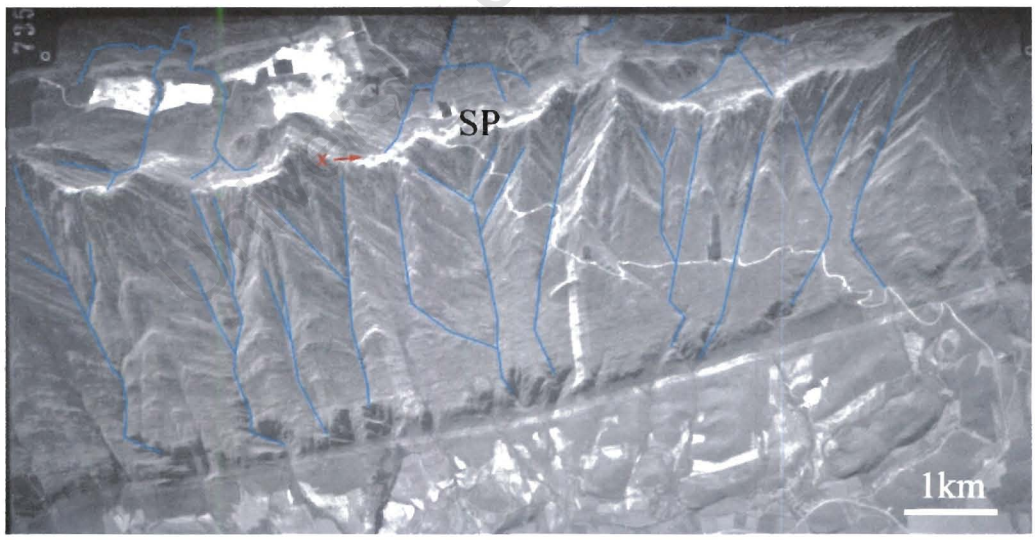

Fig. 5.14b. Aerial photograph of the Swartberg near Swartberg Pass (SP). Rivers on either side of the watershed are marked in blue. Note the completely different drainage patterns on the northern and southern slopes resulting from the dip of bedding planes. Red x and arrow show position and direction of the camera when the photograph shown when Fig. 5.15. was taken.

Fig. 5.15. Examples of spectacular columnar structures near the top of the Drakensberg Escarpment as a result of vertical jointing. A column over the Organ Pipes Pass (left) and the Organ Pipes (right). Prominent joints marked in green, volcanic bedding planes in blue. Both photographs taken just north of Escarpment section 2 in Fig. 5.4.

Fig. 5.16. Panorama of the Swartberg (see Fig. 5.13b for location). Note how the dip of the bedding planes (marked in blue) makes the 2 sides very different, though the mean slope on either side is similar.

5.5. Drainage organization

Drainage geometry has been discussed in detail in Chapter 3, so only a very quick overview will be presented here. In a given river basin, the basic quantities that can be defined are the area of the basin (a), the longest continuous river course in the basin from a source to the outlet (l), and the length of the basin, measured in the straight line from source to outlet (L). Of interest are relationships between these parameters.

Hack (1957) observed dependence between stream length and basin area:

$$l \sim a^h \tag{5.1}$$

His original study found $h = 0.6$, and since then different values have been suggested, though no complete explanation for the law's origin or the variation in its exponent has been forthcoming.

Fractality of individual streams can be defined by (e.g. Maritan *et al.*, 1996):

$$l \sim L^d \tag{5.2}$$

where d usually has the value of 1.1 (e.g. Dodds & Rothman, 1999 and references therein). The above relations can be combined to give:

$$a \sim L^D \tag{5.3}$$

where $D = d/h$, which has often been used to represent the fractal dimension of the network (e.g., Rosso *et al.*, 1991; Maritan *et al.*, 1996; Dodds & Rothman, 1999), and usually has a value of ~2 for real networks.

For the case of streams draining a linear belt presented here, the half-width of the belt, W, is equivalent to L, while a can be expressed as the product of W and S (spacing). Making these substitutions to equation (5.3) we obtain an expression that relates drainage spacing to a fractal dimension of the network:

$$S \sim W^{D-1} \tag{5.4}$$

From the findings of Hovius (1996), which show S~W, the corresponding value for D in equation (5.4) is 2 which, assuming $d = 1.1$, gives $h = 0.55$, a value often found for real networks.

A detailed analysis of real networks by Dodds & Rothman (2000) suggests rivers show up to 4 scaling regimes for the relation between a and l. For each of those regimes, defined by the basin area or stream being between 2 threshold values, the relationship $l \sim a^h$ is satisfied, but the value of h in each domain is different.

The first of these regimes that the aforementioned authors describe, is the hill-slope run-off at the smallest scale, before streams begin to converge. As these first (or at most second) order streams are roughly parallel to each other, drainage area is proportional to the length of the stream, and h has a value of close to 1. This gives a value of D similar to that of d, marginally above 1. From equation (5.4) it is clear for that regime the value for S will be dependant on W by a very insignificant factor. The results presented here show that indeed S does not vary as a function of W. The vastly different results from this study and that of Hovius (1996) illustrate that basins studied came from different scaling regimes. It was mentioned earlier that belts examined by Hovius varied in length from 200 to 1600 km, and that all had half-widths of at least 20km. By contrast, the Cape Fold Belt ranges varied in length from 20 to 50 km, and were no wider than 6 km.

Another aspect of drainage geometry often discussed in literature is drainage density (e.g., Horton, 1945; Shreve, 1967; Tokunaga, 1978; Dodds & Rothman, 1999). In its simplest form it is defined as the ratio of total stream length to basin area:

$$\rho = \frac{\sum l}{a} \tag{5.5}$$

This density is often assumed to be constant. Unfortunately (for geologists), most of these studies are concerned with topological controls on theoretical rivers. Discussions of what happens "in the absence of geological controls" in "networks that for practical purposes are essentially infinite" (Shreve, 1967) are not very helpful to studies of real networks, so the density's spatial variations will be analysed in detail in Chapter 7 of this thesis. However, in an area small enough to assume no significant variations in climate, and in a study of streams draining mountain belts that are all a part of single geological foundation and structure, there seems no reason to suggest drainage density should not be uniform. If a belt has n individual spacings between parallel streams, equation (5.5) can be written in terms of familiar parameters:

$$\rho \approx \frac{nW}{nWS} = \frac{1}{S} \tag{5.6}$$

It is obvious that for ρ to be constant, the spacing S must be constant.

5.6. Conclusion

Regularity of drainage spacing was investigated for 3 different regions in Southern Africa: eight sections of linear mountain ranges in the Cape Fold Belt in South Africa, five linear sections of the Drakensberg Escarpment, and eight linear valleys in the Lesotho highlands. The mean stream spacing for each of the 21 ranges studied was calculated, and compared with other parameters measured for the individual ranges. The mean value in each of the 3 regions was also computed.

Each of the three regions had a different mean value for the spacing. Different ranges in each of the regions also had different spacing. Of all correlations examined, none was even suggestive for variations inside a given region. In fact it appeared that no measurable parameter included in this study has any effect on the mean spacing between adjacent streams in the belt. While some variety exists in mean spacing between belts, there is also variety in the spacing within each of the individual belts. The latter variety is nearly impossible to attribute to any measurable parameter, as the slope of any range did not vary considerably, and there could not be serious variations in geology inside each linear mountain range. With no parameter to relate to the varieties observed, we conclude that drainage spacing in the studied ranges is constant with a degree of random fluctuations. That constant value, however, differs, and it is suggested here that underlying geology is the most significant factor in mean stream separation. In the Cape Fold Belt the differences in local bedding plane geometry can account for some of the variations between different ranges in the spacing in that region. The results presented here are further interpreted as evidence for the lowest scale, hillslope, regime of Hack's Law being a universal law. Hack's exponent, h, in that regime is very close to 1, and the constant of proportionality between stream length and basin area was shown to depend on local conditions in the mountain range.

This conclusion is thus shown to be consistent with the theory of scaling regimes, as well as with the theory of constant drainage density in a region with uniform geological and climatic parameters.

Chapter 6

More About Scaling Regimes

6.1. Hack's Law

The relationship between stream length and basin area in river networks has been extensively discussed in earlier chapters, and only a brief review will be presented here. Termed Hack's Law, after the man who first analyzed the relation (Hack, 1957) it is usually expressed as

$$l = ca^h \tag{6.1}$$

where l is the stream length, a the corresponding basin area, c a constant of proportionality, and h the exponent in the scaling law. Hack's original work found the exponent at 0.6, and since then many different values have been found in different studies. This study (Chapter 4) found the Sundays river has $h = 0.585$ while the Nossob has $h = 0.704$, while a value as low as 0.466 has been quoted by Mueller (1973).

It is therefore clear there is no universal value for h. Furthermore, the value for the exponent varies not only between networks, but as has been shown earlier in this study, inside networks it varies with scale and place. The general trend seems to be for h to decrease with increasing basin size, while its spatial variation is not obvious.

6.2. Scaling Regimes

It has been suggested (Dodds & Rothman, 2000) that the change in h across different scales is not gradual, but that a network orders itself into up to 4 scaling regimes. Inside each of those, different factors control the network geometry and, while Hack's law is satisfied in each regime, the respective values for h are different. The summary of this "regime hypothesis" was given in section 4.5.

The regime at lowest scales corresponds to non-convergent flow on hillslopes. Here streams are parallel to each other, and l is proportional to a, and therefore $h = 1$. This regime was discussed in the analysis of small-scale drainage spacing in the Cape Fold Belt in the previous chapter. The second regime starts when first order streams begin to converge, and clearly the value of h drops. The cross-over between the second and third regime is not clearly understood, and its analysis will be attempted here.

6.3. Data

In this section combined data has been used from the 3 areas discussed separately earlier: the Orange river network, the Limpopo, and 6 major rivers draining the Cape Fold Belt. This yielded 5770 basins of order greater or equal to 2. The river networks were calculated from a 1km resolution DEM of southern Africa. This resolution is not sufficient to see the hillslope regime clearly, but the cross-over we are concerned with is clearly visible. Figure 6.1 shows the Hack's Law plot for the entire data set. A decrease in the slope with increasing area is clear to see. The point at which the slope changes the most is near $\log a \sim 7$, but the exact value is difficult to pick up – it was shown earlier that this break is more clear in some basins than others, and is not always found at the same place. Some basins (most notably the Upper Orange before its confluence with the Vaal) do not seem to have a significant change in the slope at all.

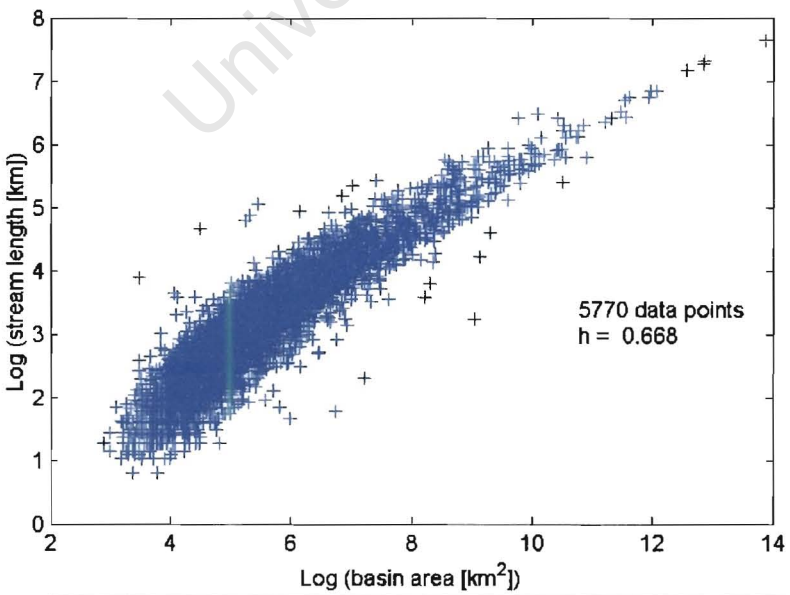

Fig. 6.1. Hack's Law plot for the combined data set.

6.4. Analysis

To find the "threshold" basin area at which the cross-over seems most likely, a statistical analysis was performed. Using the data shown in Figure 6.1, the uncertainty in correlation of the ordered pairs was computed for all basins with the logarithm of the area less than a given value. This maximum was varied between 5 and 10 in steps of 0.01, and the plot of correlation uncertainty as a function of this upper bound is given in Figure 6.2.

It is clear that the larger the upper bound, the more points are taken into account. Should the plot be a linear regression, increasing the number of points would decrease the correlation uncertainty. This trend is present over ~2 natural orders of magnitude, where the uncertainty starts to increase. The suggestion made here is that we have now entered a different scaling regime, and are attempting to correlate points on two adjacent regression lines, which causes an increase in the uncertainty. The area which corresponds to the lowest correlation uncertainty (log a = 7.20, or $a \approx 1300$ km^2) is then the value at which the cross-over takes place. There are some local minima present in the graph, which support the suggestion the cross-over does not always happen at the same basin size threshold, but varies with local conditions. The two most prominent of these minima are placed at log a = 5.92 and 6.73, respectively, which correspond to $a \approx 400$ and 800 km^2.

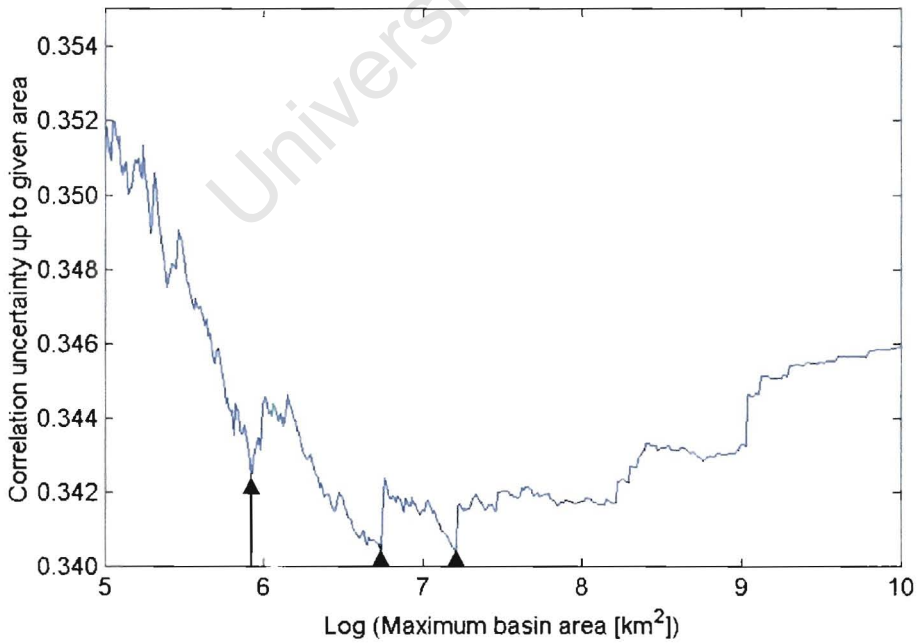

Fig. 6.2. Correlation uncertainty plot. The minimum at log(a) = 7.20 and local minima at log(a) = 6.73 and 5.92 are shown by arrows.

To determine what causes the change in scaling, we must ask what parameters can influence the network geometry. The most obvious suggestion is some property connected with the topography over which the river flows. We turn our attention to the simplest of those, namely the average slope of the river basin. The collective data (5770 basins) was divided into 10 bins on basis of average basin slope. The properties of each bin (some of which will be explained later) are given in Table 6.1. The slope thresholds for each bin seem arbitrary, but were chosen so that each bin has a similar number of streams in it.

Table 6.1. Combined data divided into bins by basin slope

slope (m/km)	mean slope	# streams	h	$\Delta h_{5.92}$	$\Delta h_{6.73}$	$\Delta h_{7.20}$
0-0.9	0.59	588	0.703	0.352	0.377	0.387
0.9-1.5	1.19	558	0.639	0.316	0.290	0.226
1.5-2.2	1.84	561	0.631	0.278	0.249	0.241
2.2-2.9	2.54	593	0.664	0.266	0.247	0.219
2.9-3.6	3.24	581	0.675	0.306	0.276	0.232
3.6-4.4	3.99	582	0.651	0.227	0.210	0.267
4.4-5.4	4.87	597	0.665	0.202	0.188	0.209
5.4-6.9	6.11	578	0.678	0.201	0.082	0.182
6.9-9.9	8.26	575	0.671	0.197	0.163	0.049
9.9+	16.01	557	0.685	0.215	0.310	0.206

6.4.1. Hack's exponent as a function of basin slope

The value for Hack's exponent was calculated for the basins inside each of the bins. The plot of these as a function of the mean slope in each bin is seen in Figure 6.3. The slope axis is logarithmic to prevent the data points of less steep basins from clustering. No obvious regression line to accommodate all the data points seems to exist. The point corresponding to the least-steep basins has the highest value for h, but the remaining points seem to suggest an increase in h with increase in slope. The correlation coefficient of this trend (with the first data point excluded) is 70.4 %. This 'trend', however does not appear as simple linear relationship, but seems to involve thresholds between which

individual trends exist. Nonetheless, with the correlation coefficient mentioned above, using t-distribution tables we can accept a positive correlation between h and slope with a 95 % confidence. Thus there appears to be a slope threshold of somewhere between 1 and 2 m/km. 'Flat' basins with slopes below this threshold have a decreasing value of h as they get steeper, while above the threshold h increases with slope. Thus the highest value of h is exhibited by steepest and flattest basins, while the lowest value is found at the above mentioned threshold.

A computer model study of river flow over synthetic topographies (Schorghofer & Rothman, 2001) found the convergence of the network decreases with increasing slope. However, for real river networks they found this pattern is reversed for the least steep basins, and thereafter the connectivity does not decrease steadily, but the curve contains secondary features (their Figure 3). This is exactly the opposite of the behaviour found here for h as a function of slope, which suggests a negative correlation between the value of h and network connectivity. The extreme case of this relation is in the hill-slope run-off regime: h is at its maximum when there is no convergence of flow.

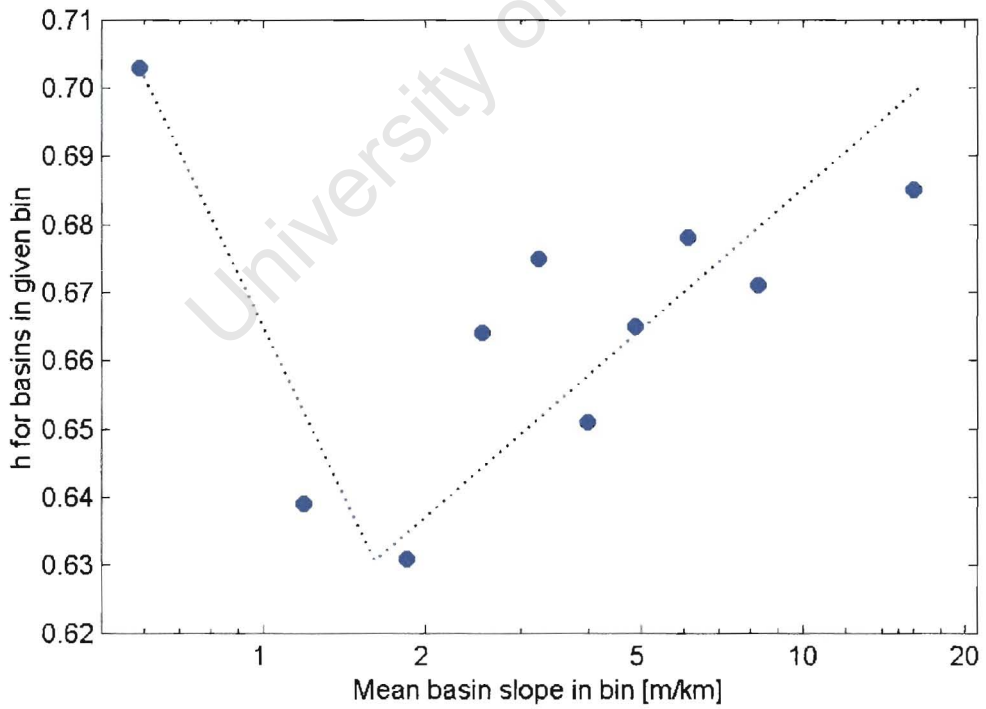

Fig. 6.3. h-slope relation for combined data grouped into bins by basin slope.

The slope threshold mentioned earlier thus correspond to the slope at which network connectivity would be highest. In really flat areas rivers can meander 'aimlessly' without forming networks, while in very steep areas we find the hill-slope regime of parallel streams with no convergence of flow.

6.4.2. Variations in Hack's exponent

For each bin, values for h were computed for basins on either side of the area threshold. Three different thresholds, $\log a = 5.92$, 6.73 and 7.20 were used. For each of them Δh, defined as the difference between h for basins smaller than the threshold and those larger, was computed. The plot of these differentials is plotted against mean slope in each bin in Figure 6.4. Differentials obtained from the 5.92 threshold originally decrease with increasing slope (except for one obvious stray point), before settling at approximately $\Delta h = 0.2$ for slopes greater than 4 metres per km. The plot from the 6.73 threshold is similar for the lower slope values, but Δh decreases to below 0.1 at slope of 6 metres per km, before increasing with slope for steep basins. The last of the 3 plots, corresponding to the 7.20 threshold, varies between $\Delta h = 0.2$ and $\Delta h = 0.3$ for slopes under 4 metres per km (except for the least steep bin, there Δh is just less than 0.4). It then decreases to less than 0.05 for the second-steepest bin, before going back to $\Delta h \approx 0.2$ for the steepest one.

The $\log a = 7.20$ threshold plot shows more variation from a specific pattern than the other two, suggesting it might not be a real threshold, and the trough visible in Figure 6.2 at that area may be an artifact of a statistical analysis rather than a real phenomenon. We thus concentrate our analysis on the other 2 points. The primary difference between graphs 6.4*a* and *b* is that *a* (corresponding to $\log a = 5.92$) levels off in the second half of the slope range. In the 5 steepest bins Δh varies between 0.197 and 0.227 with no obvious increasing or decreasing trend. Figure 6.4*b* (results of the $\log a = 6.73$ threshold) does not settle near any value, a steady decrease for the first 8 points is followed by a clear increase in the last 2.

To explain the results presented above, we present the following hypothesis. The cross-over between the second and third scaling regime is gradual, taking place over approximately a natural order of magnitude. The first evidence for the change in scaling can be seen in southern Africa in basins with $\log a$ just under 6 (5.92 was the value

obtained in a statistical analysis). The difference in the value of h on either side of this threshold seems to depend on the slope of the basins concerned, decreasing with increasing slope from ~0.35 to ~0.2, a value at which the difference remains constant for basins steeper than 3.6 m/km. The last evidence of the second scaling regime is visible around $\log a \approx 7$. The exact value obtained here was 6.73, but it could be as high as 7.20. The change in h across these thresholds shows a more complicated dependence on the slope, suggesting it depends more on local conditions. We therefore turn our attention to variation in Hack's exponent in individual basins.

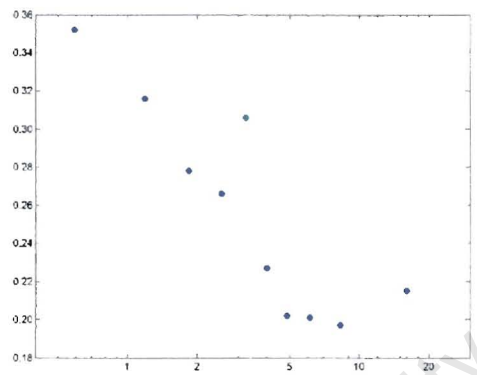

(a)

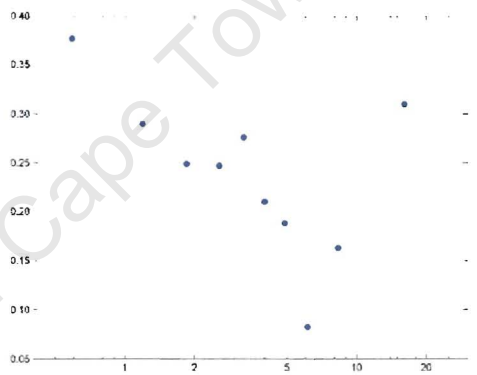

(b)

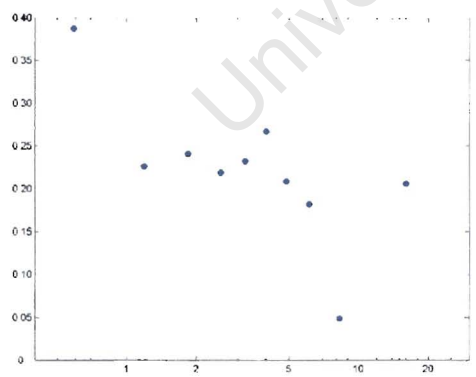

(c)

Fig. 6.4. Change in h inside each slope-bin across the area threshold of $\log a$ =
a) 5.92
b) 6.73
c) 7.20
x-axis: mean slope in each bin, logarithmic to prevent clustering.

6.4.3. Individual networks in Southern Africa

In this section we look at Hack's exponent, and its variation, in 14 separate networks. We use data from the 6 sub-basins of the Orange mentioned before (Fish, Nossob, Molopo, Vaal, upper Orange and Hartebeest), the 6 Cape Fold Belt rivers also discussed earlier (Olifants, Gourits, Gamtoos, Sundays, Great Fish and Kei), as well as 2 basins in the Limpopo network, the Elands and the main Limpopo before the confluence. The properties of all these networks are given in Table 6.2. For all graphs in this chapter involving networks summarized below, Orange sub-networks are plotted in blue, the Cape Fold Belt rivers in green, and the Limpopo tributaries in red. These colours are also indicated in the table below next to the basin name

Table 6.2. Networks used in this study. Slopes are given in m/km

River	log (a)	h	maximal basin slope	mean sub-basin slope	maximal basin κ	mean sub-basin κ
* Vaal	12.0	0.702	0.68	4.41	2.98	2.15
* Upper Orange	11.5	0.644	2.60	7.94	3.58	1.84
* Hartebeest	11.6	0.671	1.58	4.22	2.09	2.08
* Fish	11.6	0.687	1.94	5.56	3.78	2.24
* Nossob	12.1	0.714	0.95	1.60	2.75	2.77
* Molopo	11.9	0.692	0.79	2.03	2.18	2.79
* Olifants	11.2	0.664	2.67	9.02	2.16	1.95
* Gourits	10.9	0.610	3.12	11.44	1.17	1.87
* Gamtoos	10.6	0.662	2.79	6.35	3.47	1.99
* Sundays	10.2	0.585	4.53	10.24	2.99	1.93
* Great Fish	10.5	0.644	2.98	9.80	3.73	1.72
* Kei	10.0	0.654	4.88	14.03	3.12	1.61
* Elands	11.5	0.680	2.29	7.91	3.01	2.53
* Upper Limpopo	12.0	0.630	1.14	4.86	2.11	2.21

It was first examined how the value of *h* for each basin depends on the slope. Figure 6.5 shows *h* as a function of the mean slope of all-sub-basins used to determine *h*, and Figure 6.6 as a function of the slope of each maximal basin. Each of the 2 graphs has a very strong negative correlation, using the t-distribution table we can confirm a trend with 99% confidence. This is perhaps surprising, as in the previous section it was shown that basins from different networks grouped in bins of similar slopes scale in the opposite way, *h* increasing for steeper basins. The two results are not a contradiction, but merely reinforce the suggestion of Dodds & Rothman (2000) mentioned earlier in the study that it is vital to discriminate between intra-basin and inter-basin measurements when investigating the basin area – stream length relation.

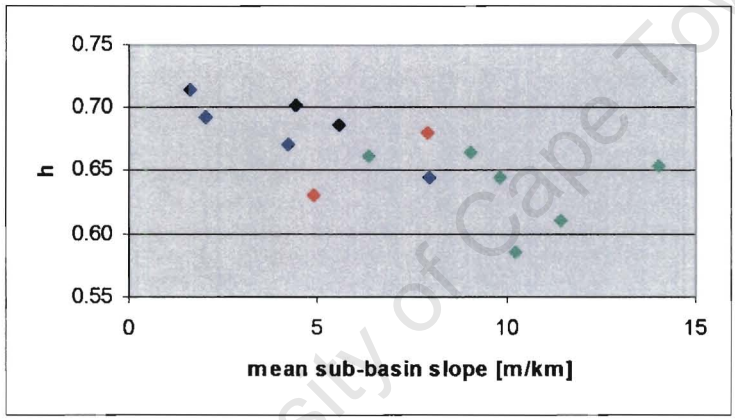

Fig. 6.5. *h* for each network as a function of mean sub-basin slope in it.

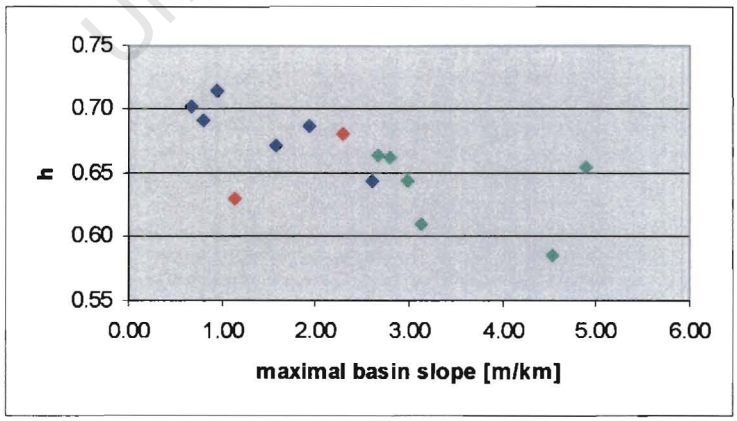

Fig. 6.6. *h* for each network as a function of the main basin's slope.

Relationship between *h* and basin aspect ratio, κ, is investigated below. Fig. 6.7 shows the exponent as a function of mean sub-basin aspect ratio, while Fig. 6.8 shows *h* against the maximal basin's κ. A positive correlation exists in Fig. 6.7, but it is not as strong as the either of the negative ones seen in the exponent's dependence on slope (Fig. 6.5 and 6.6). Hack's exponent and the maximal basin's aspect ratio appear to be independent of each other. This leads to the conclusion that *h* is a function of basin slope rather than aspect ratio. This makes intuitive sense, as one would expect a network parameter to depend firstly on the topography that produces this network, not another network parameter, like the aspect ratio. Thus for the remainder of this chapter mean sub-basin slope will be considered as the parameter most likely to control variations in *h*.

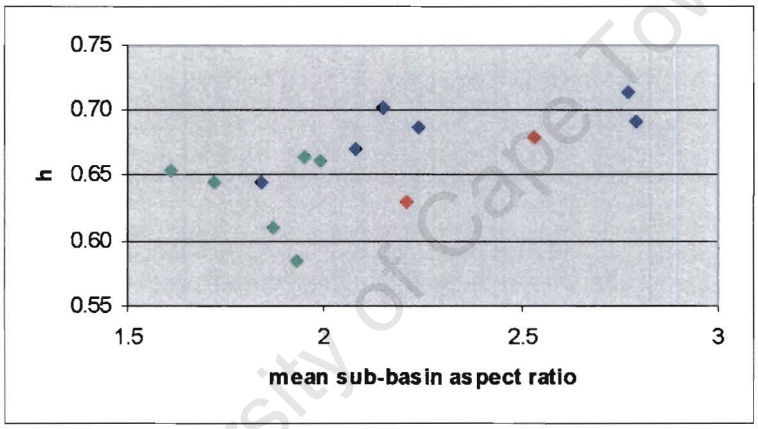

Fig. 6.7 *h* for each network as a function of mean sub-basin aspect ratio

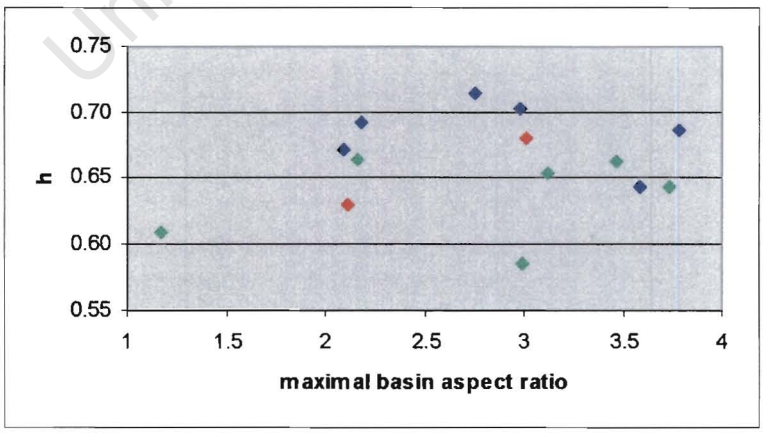

Fig. 6.8 *h* for each network as a function of maximal basin's aspect ratio

The next step is to investigate the cross-over between scaling regimes in the individual basins listed above. The differences Δh (defined in the previous section) were computed in each of the 14 networks for each of the 3 possible area size thresholds. These are listed in Table 6.3, and are plotted against mean basin slope inside each network in Figure 6.9.

Table 6.3. Δh across different thresholds in all networks

River	$\Delta h_{5.92}$	$\Delta h_{6.73}$	$\Delta h_{7.20}$	River	$\Delta h_{5.92}$	$\Delta h_{6.73}$	$\Delta h_{7.20}$
* Vaal	0.239	0.213	0.195	* Olifants	0.057	0.120	0.158
* Up. Orange	0.095	0.089	0.062	* Gourits	0.200	0.247	0.245
* Hartebeest	0.250	0.266	0.245	* Gamtoos	0.130	0.124	0.096
* Fish	0.236	0.227	0.221	* Sundays	-0.006	-0.003	0.004
* Nossob	0.363	0.358	0.307	* Great Fish	0.129	0.131	0.072
* Molopo	0.303	0.323	0.321	* Kei	0.160	0.175	0.136
				* Elands	0.247	0.232	0.219
				* Up. Limpopo	0.207	0.158	0.155

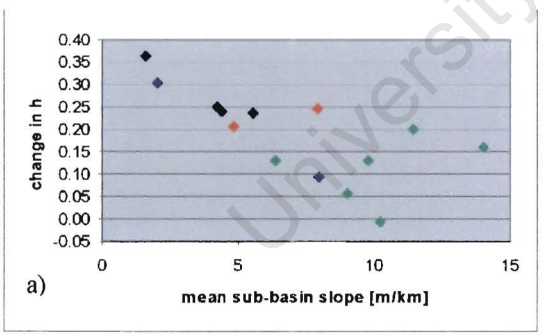

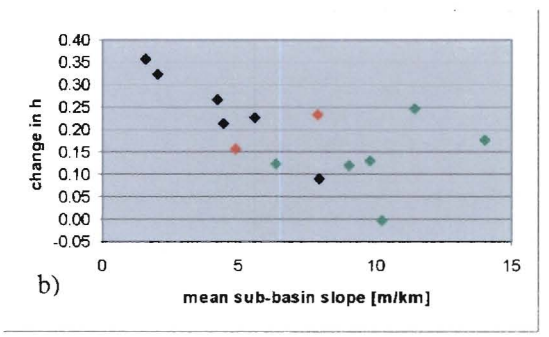

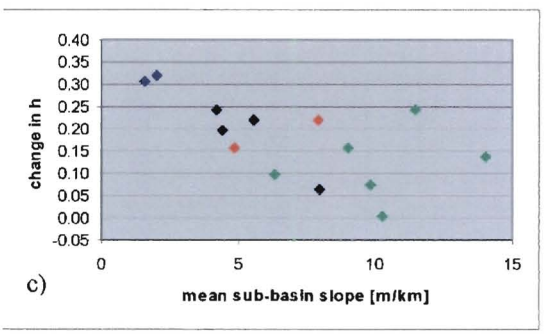

Fig. 6.9. Change in h across possible thresholds inside each network as a function of mean sub-basin slope. Thresholds used: $\log(a)$=
a) 5.92
b) 6.73
c) 7.20

All 3 plots showing Δh as a function of mean slope have a strong negative trend, with the one corresponding to log a = 5.92 looking like the best fit. This is confirmed be the correlation coefficient of 67.4 %, compared to 58.3 % and 58.4 % for log a = 6.73 and 7.20, respectively. These coefficients are high enough to conclude the relationship between Δh and slope exists with 95 % confidence, but each graph has some outliers that need to be discussed.

The obvious feature of the graphs in Figure 6.9 is that all the outliers lie 'above' the trend line, or the only anomalies are found where the change in h is greater than one would expect from the slope. One also notices the 2 greatest outliers are the 2 basins with the largest mean slope (Gourits and Kei rivers in the CFB). If these basins were to fit the trend of the other 12 data points, the necessary Δh would need to be negative. The network with the 3rd highest mean slope, the Sundays river, actually has $\Delta h < 0$ for two of the three thresholds. However, these values are –0.003 for log a = 6.73, and –0.006 for log a = 5.92, which combined with Δh = 0.004 for log a = 7.20 clearly shows there is no significant change across our area of interest. Some other networks (less steep than the Sundays) in the Fold Belt show minor deviations from the trend in selected graphs, but not as significant ones as the Kei and Gourits. A possible explanation for those anomalies is with such high slopes the first (hillslope) scaling regime will be found for larger basins than elsewhere in the sub-region, and this $h \approx 1$ trend will share part of the second regime's domain. The values for h for basins smaller than a given threshold will thus be larger than the scaling exponent of the second regime, causing an high Δh. Even if the basin slopes are not very high, but the trellis pattern characteristic of the CFB is particularly well defined with long shale valleys between well exposed quartzite ridges, the presence of these parallel trunk streams would make the $h \approx 1$ regime visible at larger scales, causing a similar effect on Δh. Another persistent outlier is the Elands river from the Limpopo drainage.

6.4.4. Fractal Properties of basin topography

We now turn our attention to a more subtle topography parameter, namely its fractal dimension. This is computed from the DEM using spectral methods described in Appendix A. The DEMs were divided into blocks of 32 * 32 data points (optimal size for

spectral analysis according to Turcotte, 1992), and the fractal dimension of each block was computed. While the slope of the power spectrum corresponds to the arithmetic inverse of the fractal dimension, the intercept can be thought of as a representation of the roughness of the area in study, and this parameter was also calculated. The dimension and roughness of each basin was taken as the average of individual values of blocks that overlap with that particular basin. The results are given in Table 6.4.

Table 6.4. Fractal dimension (D) and roughness (R) of each network's topography

Network	*D*	R	Network	*D*	R
* Vaal	2.18	16.4	* Olifants	2.24	18.2
* Up. Orange	2.32	17.8	* Gourits	2.09	19.4
* Hartebeest	2.22	16.5	* Gamtoos	2.21	18.3
* Fish	2.23	16.9	* Sundays	2.20	18.7
* Nossob	2.29	14.1	* Great Fish	2.26	18.8
* Molopo	2.13	14.9	* Kei	2.30	18.9
			* Elands	2.19	17.8
			* Up. Limpopo	2.13	17.0

Figure 6.10 shows a plot of h as a function of the fractal dimension in each network. It is clear there is no relationship between the 2 parameters – the correlation coefficient is as low as 22 %. The fractal dimension also has no influence on the values of Δh across any of the 3 basin size thresholds (Figure 6.11).

Roughness of the topography does, however, seem to be related both to the overall value of h of the network and to the changes in the exponent (Figures 6.12 and 6.13). The effect it has on Hack's exponent looks similar to that the mean basin slope has on it. This should not come as a surprise, as one would expect roughness to be closely correlated to mean basin slope – this is confirmed in Figure 6.14, where the 2 parameters are plotted against each other. For low values there is a clear linear relationship, but once roughness reaches a value of 18, it does not change much while slope increases further. It is interesting that the correlation coefficients between roughness and Δh are about 10% higher than those between slope and Δh: for log a = 5.92, 6.73 and 7.20, respectively,

they are 76.7%, 70.7% and 68.9%, compared to 67.4%, 58.3% and 58.4% for slope values. It therefore seems that some information about the topography can be lost in averaging basin slopes, while the mean roughness value preserves it. The outliers present in the slope – Δh graphs (Figure 6.9) are, however, still visible in Figure 6.13.

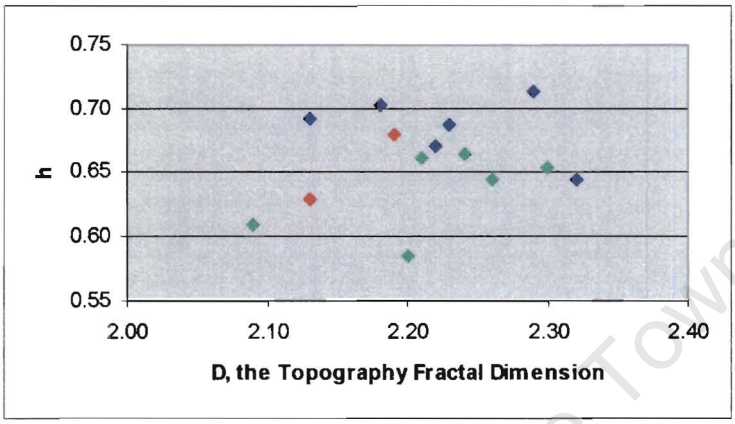

Fig. 6.10. h in each network as a function of topography fractal dimension.

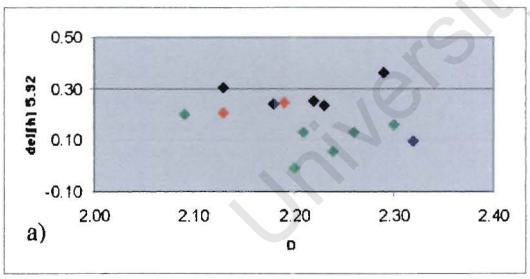

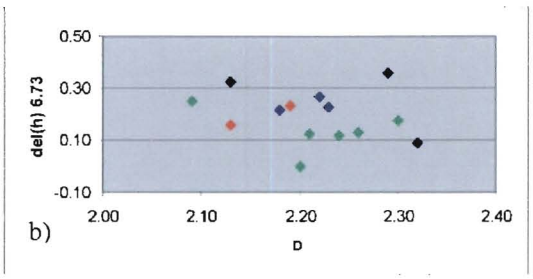

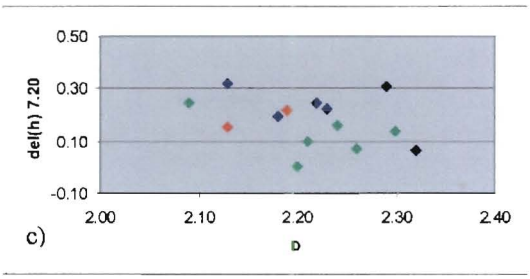

Fig. 6.11. Change in h across possible thresholds inside each network as a function of topography's D.
Thresholds used: log(a)=
a) 5.92
b) 6.73
c) 7.20

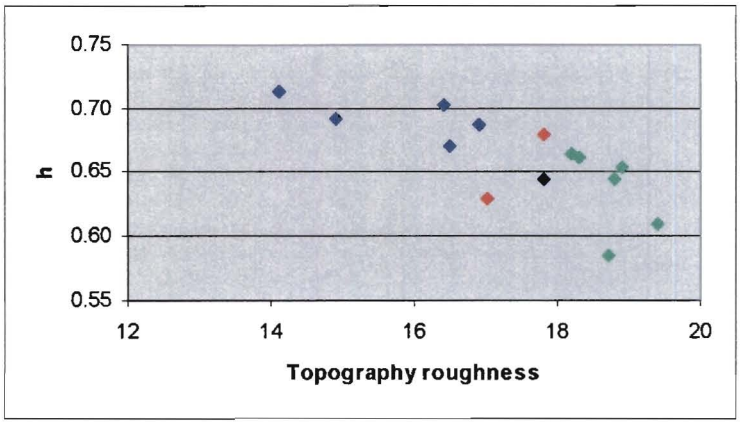

Fig. 6.12. *h* in each network as a function of topography roughness.

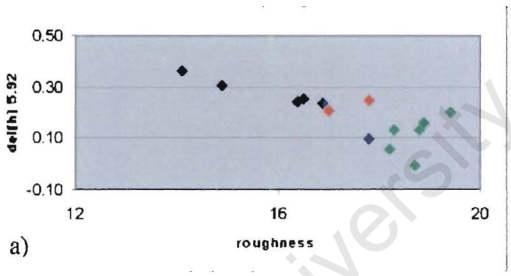

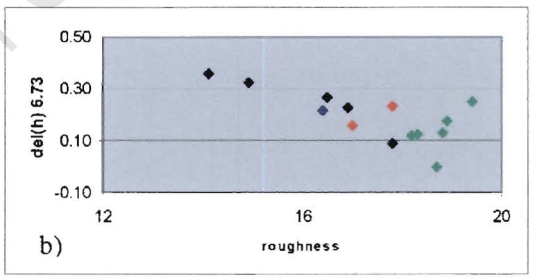

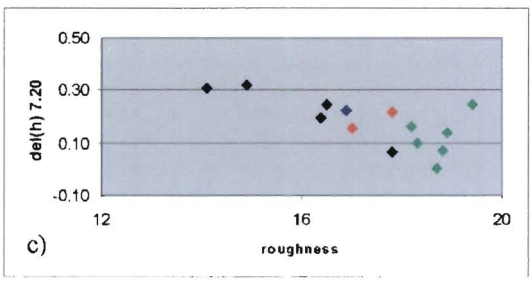

Fig. 6.13. Change in *h* across possible thresholds inside each network as a function of topography's roughness. Thresholds used: log(*a*)=

a) 5.92
b) 6.73
c) 7.20

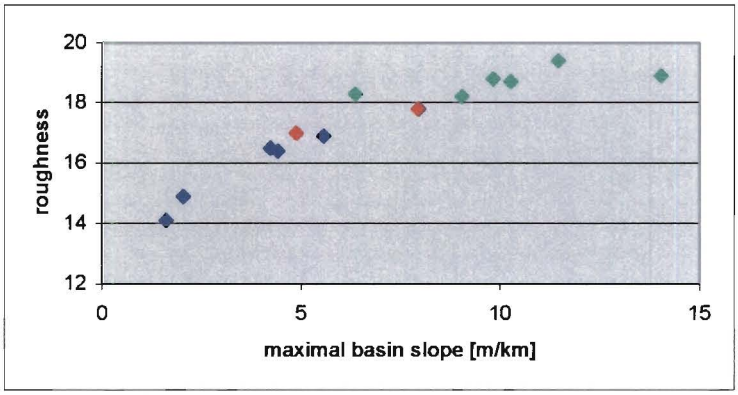

Fig. 6.14. Topography roughness – mean sub-basin slope correlation.

6.4.5 Variations inside individual networks

Whenever data is averaged, information about its distribution it is invariably lost. While mean basin slope values have yielded excellent correlations with scaling parameters in previous sections, it is vital to point out that mean slope can be a misleading term. As an example, 3 theoretical river profiles are shown in Fig. 6.15, all of them having the same mean slope.

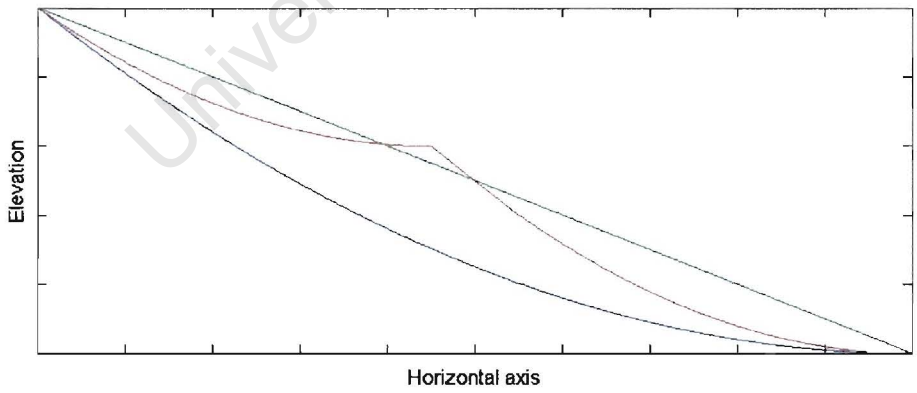

Fig. 6.15. Three hypothetical river profiles. Blue line shows the accepted model for a mature stream in a relatively stable environment, with the slope decreasing downstream. Green line shows a constant slope, which is what one might find on the dip slope side of a mountain. Red line shows a river that experienced a significant change in base level. Note all streams have the same mean slope.

It is therefore suggested that while the mean slope provides an approximation of the river good enough for the analyses above, variations in the relationships discussed earlier are not random fluctuations, but can be attributed to variations of the parameters inside the basin.

An example of geological controls on river network geometry was given in Chapter 4, where it was explained how steep, parallel mountain ranges account for a trellis pattern with some very high values for certain Horton's ratios. Results from this study, however, found that the values and variations in h in these networks have a similar dependence on slope to other networks. The steepest of such basins showed deviations from the observed pattern, but this anomaly was also explained here.

Another example of geological constraints on river geometry is presented in two studies by Tooth *et al.* (2002, 2004), which examine the influence of local geology on the behaviour of left bank tributaries of the Vaal river (see Fig. 4.3 for location). These authors examine drainage basins with log a between 5.8 and 7.0, i.e. very close to the threshold examined in this chapter. The region consists of easily erodible sandstone/shale layers and is intruded by a number of hard, more resistant, dolerite dykes and sills (Fig. 6.16a). These intrusions act as barriers for rivers, forming local base levels for drainage upstream. Vertical erosion at the weak sandstone cannot proceed faster than the erosion of a dolerite, and the resulting river profile consists of a series of floodplains separated by knickpoints. On these floodplain the stream meanders and wetlands form. When a knickpoint is breached (Fig. 6.16b) the base level is lowered to the next downstream barrier, and channel incision, possibly accompanied by channel straightening, takes place. The former floodplain stops receiving regular flooding, resulting in gradual wetlands desiccation natural donga (gully) formation. This runs counter to the traditional explanations that these phenomena are results of poor land management (e.g. King, 1963) and susceptible soil characteristics (e.g. Bell & Maud, 1994).

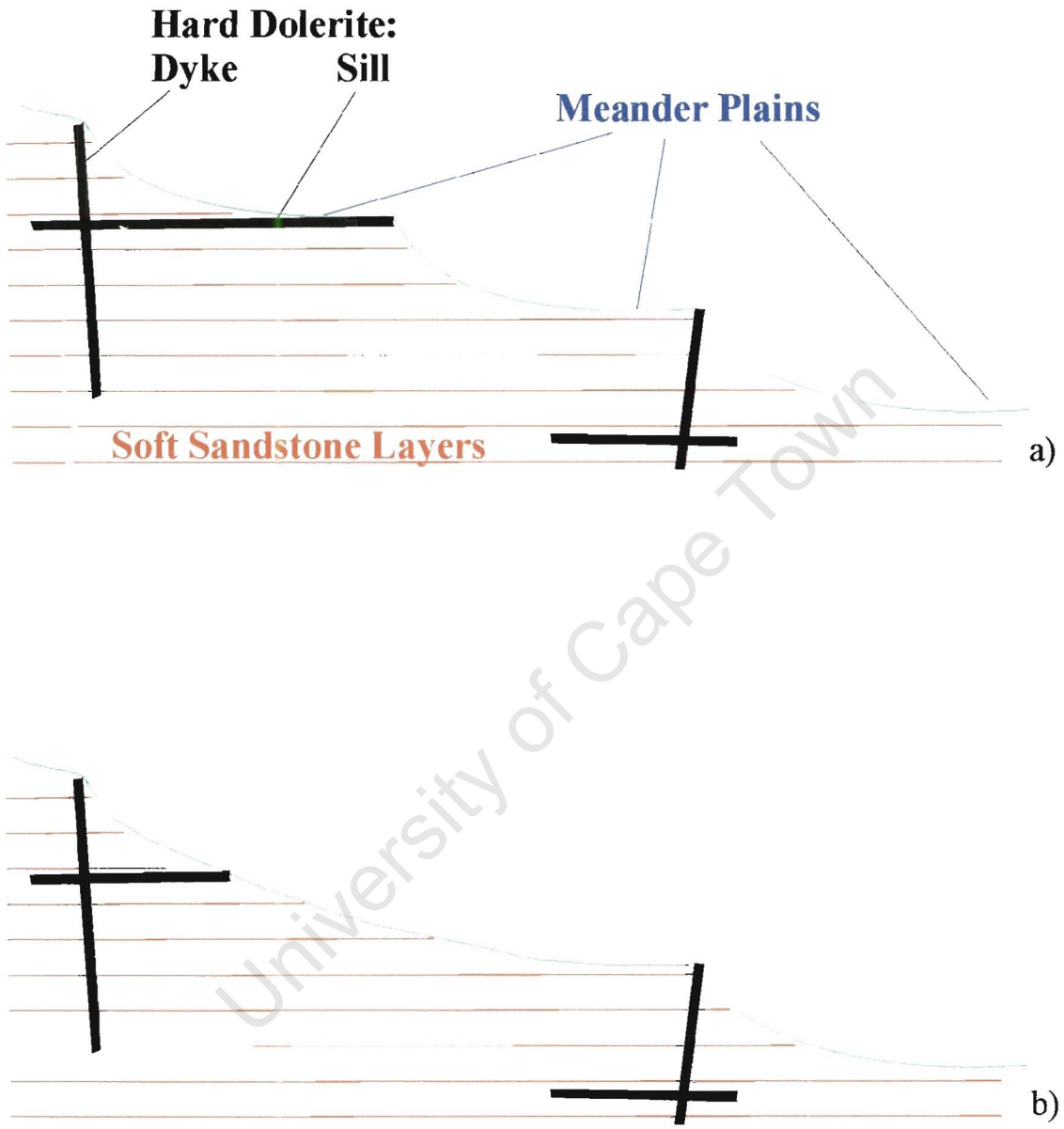

Fig. 6.16. a) Schematic diagram of the structure underlying the study area of Tooth *et al.* (2002, 2004). Dolerites form barriers for rivers, creating local base levels and resulting in a number of meander plains (floodplains). Lister (1967) presents a similar diagram (her Fig. 38) to show how waterfalls are frequently caused by intrusive bands of hard rock.
b) When a knickpoint is breached the base level immediately above it has a lowered base level, and the river profiles changes accordingly. With the elimination of a meander plain, the river channel upstream from the beach would straighten.

Changes in the network described in the above-mentioned studies would affect the Hack's exponent in two ways. Firstly, when a meandering channel is straightened, its stream length decreases, while the drainage area remains the same. The dongas are said to be initiated as gullies on the steepened banks of the incising channel, and then extend headwards (Tooth *et al.*, 2004). Thus one would expect them to belong to the hillslope scaling regime, similar to linear mountain belt drainage discussed in Chapter 5, and having $h \approx 1$. Some of the dongas are separated by as little as 100 metres, and any drainage evolution on that scale will not be detected on a 1km resolution DEM. Thus the formation of dongas will not have any effect on the results in this study. The channel straightening will, however, be picked up. The effect this will have on the value and variations of h is not straightforward, but depends on the size of drainage area of the channel concerned. To examine this, the basin size – stream length data for the Vaal river (Fig. 4.10) were used. The value for h using the 649 basins was found in Chapter 4 to be 0.702. Let us now assume that a single channel experienced straightening by 25 % of its stream length, while retaining its drainage area. The new value for h was computed for each channels being straightened. The 649 values are plotted in Fig. 6.17 as a function of the drainage area of stream that was changed. One can see that if the stream that is straightened has a large drainage basin, h will decrease, while a straightening of a small basin will result in an increase in h. If the stream has $\log a = 5.39$, or $a = 220$ km^2, no change in h will be observed.

The scale variations in h are even more interesting. A plot of Δh across $\log a = 5.92$ (the smallest of the 3 thresholds computed here) as a function of the shortened basin's area is shown in Fig. 6.18. It is clear that the effects drainage evolution described here will have on h and its variations are very difficult, if not impossible, to predict. The calculations here are naturally simplified – shortening of one stream will also change stream lengths in basins that contain the original basin in question. The purpose of this section, however, was not to predict such changes, but to show how one should expect such changes to occur, even if the mean slope and aspect ratio of all basins remain unchanged.

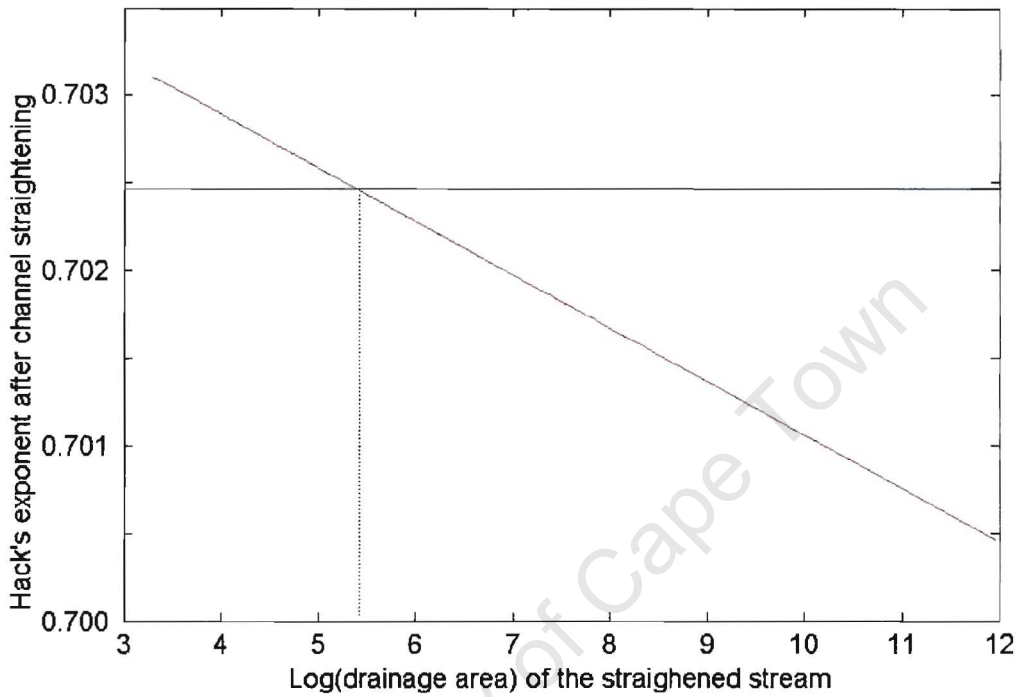

Fig. 6.17. Resulting Hack's exponent for the Vaal river network after straightening of a single channel by 25 % (red line), as a function of the particular's channels drainage area. Blue line shows h for the unaltered Vaal network. When the channel has $\log(a) = 5.39$ (dashed line), the value of h does not change.

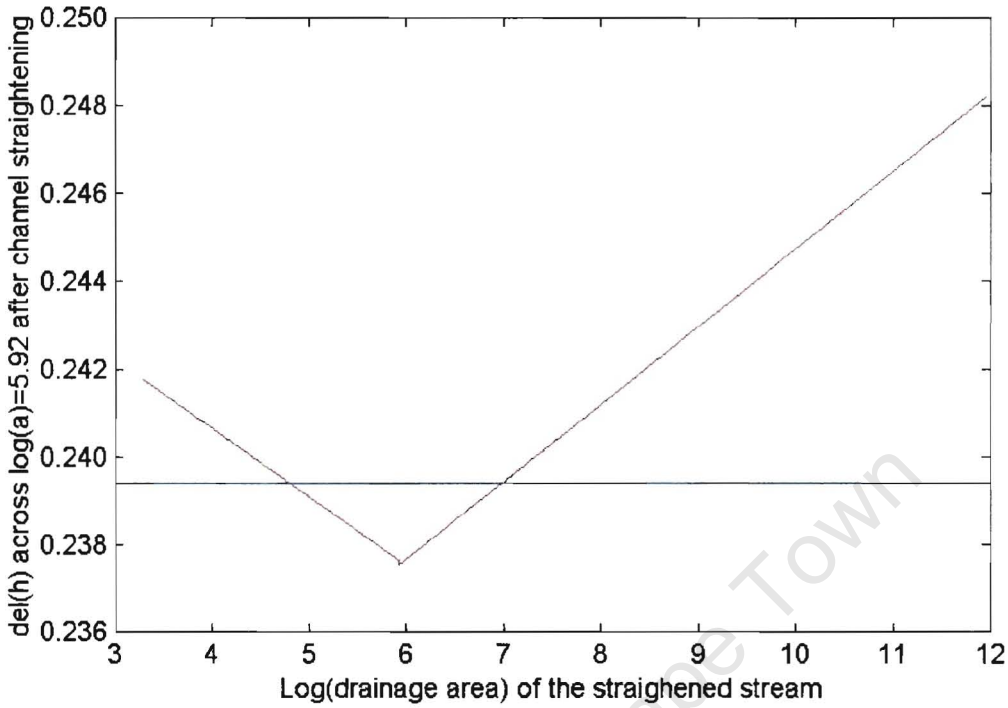

Fig. 6.18. Δh across log (a) =5.92 after straightening of a single channel by 25 % (red line), as a function of the particular's channels drainage area. Blue line shows Δh for the unaltered Vaal network.

6.5. Conclusion

The exponent governing the power law describing the relationship of stream lengths and their drainage areas, h, changes at scales between log a = 6 and 7, where a is the basin area in km^2. We believe basin scaling on either side of this threshold is controlled by different parameters: basins belonging to the smaller scaling regime correspond to hill-slope runoff becoming convergent, while at the larger scale streams belong to a random universality class. This chapter investigated at which point this cross-over takes place, and what effects the topography has on the change in h.

It was found that when basins from different networks are grouped together by their slopes, there exists a slope threshold around 1-2 m/km. For basins steeper than this the value of h increases with increasing slope, but below this threshold it decreases with

increasing slope. However, when h is computed for each network using all basins in it, the exponent decreases for networks with higher mean slope. This emphasises the necessity to distinguish between intra-basin and inter-basin studies of Hack's Law. It was also shown how the exponent h can be thought of as the inverse of network connectivity.

Using uncertainty in the correlation coefficient of parts of the basin area – stream length data set we found the most likely places where h changes are at $\log a = 5.92$, 6.73 and 7.20. The difference in h on either side of any of these potential thresholds was analyzed as a function of mean basin slope, and a general trend of Δh decreasing with increasing slope was found. Best correlations for that plot were found for $\log a = 5.92$, suggesting that scaling regime cross-over starts at approximately that point in most basins, and the magnitude of the change in h is inversely proportional to the slope. The regression lines obtained for this analysis (Figure 6.7) show Δh should drop to zero at slope $\approx$ 10 m/km. Basin steeper than that (and some less steep in that, too) do not lie on the regression lines, and have $\Delta h > 0.1$, and sometimes as high as 0.25. This anomaly is possibly caused by steep basins having an extended hill-slope scaling regime where $h \approx 1$, overriding the value of h for the convergent flow.

The fractal dimension of the topography was found to be uncorrelated to the value of h as well as to changes in it. The roughness parameter accompanying the fractal dimension did, however, show correlations to h and Δh. The trends found were similar to those found when examining dependence of mean basin slope on h, but correlation coefficients were significantly higher, suggesting roughness is a more meaningful parameter than mean slope. The plot of roughness against mean basin slope showed strong linear correlation for lower values, but above a certain value of slope the roughness settled near a constant value of approximately 19. This slope threshold was difficult to measure with a limited number of data points, but was somewhere between 6 and 8 m/km.

Finally, a case study of some of the Vaal's tributaries showed that variations from relationship between the scaling parameter and the slope are not necessarily random, but can be explained by geological controls on stream evolution. With the computer software and detailed databases available today it is very easy to get carried away with theoretical modeling and neglect field observations, which should be incorporated into even the most theoretical study in earth science.

Chapter 7

Drainage Density in Africa

7.1. Drainage density

Drainage density is a parameter describing what portion of land is covered by rivers. It is usually defined as (Horton, 1945):

$$\rho = \frac{\sum l}{a} \tag{7.1}$$

where $\sum l$ is the total length of rivers in a given surface area a. This formula is clearly an approximation, as width of river channels is not taken into account. The exact value of the total length, and thus of the density, will depend on the resolution of the map from which the streams were obtained. There are also many finer points of what exactly constitutes a stream – an interested reader is referred to Montgomery & Dietrich (1988) for a discussion of this issue. For this reason the same resolution and standardized parameters need to be used throughout a given analysis, otherwise density variations could be observed where none really exist. A commonly used parameter related to the density (e.g. Horton, 1945; Rodriguez-Iturbe & Rinaldo, 1997) is the stream separation, defined as the inverse of the density:

$$s = \frac{1}{\rho} \tag{7.2}$$

There is some debate whether the density is uniform in real networks (Dodds & Rothman, 1999, and refs. therein). Shreve (1967) notes drainage density must be uniform in "mature topography developed in a homogeneous environment". Real topographies, however, are often very dynamical, and one can never assume a "homogeneous environment" over a continental scale. Gregory (1976) observed variations over 3 orders of magnitude in assembling data for 44 regions around the world. This data set can hardly

be considered global, as 21 of the data points came from USA, 5 from Britain, and just 1 from Africa. The data came from a number of different sources, it is unlikely the resolution of the study areas, and other finer points of stream definition were the same in each case, but these factors are unlikely to account for the vast variations observed.

7.2. Density variations on the continental scale

7.2.1. Introduction

To observe river density variations in Africa, the continent was subdivided into 38 blocks, as shown in Figure 7.1. The usual grid size was 1000 km, which would give a box area of 1,000,000 km^2. With a number of boxes being on the coastline, which quite obviously is not made up of 1000 km line segments, only 14 of the boxes actually covered a million square kilometres. When a box covered less than 400,000 km^2 it was combined with a neighbouring box. The island of Madagascar was counted as a 'box' by itself.

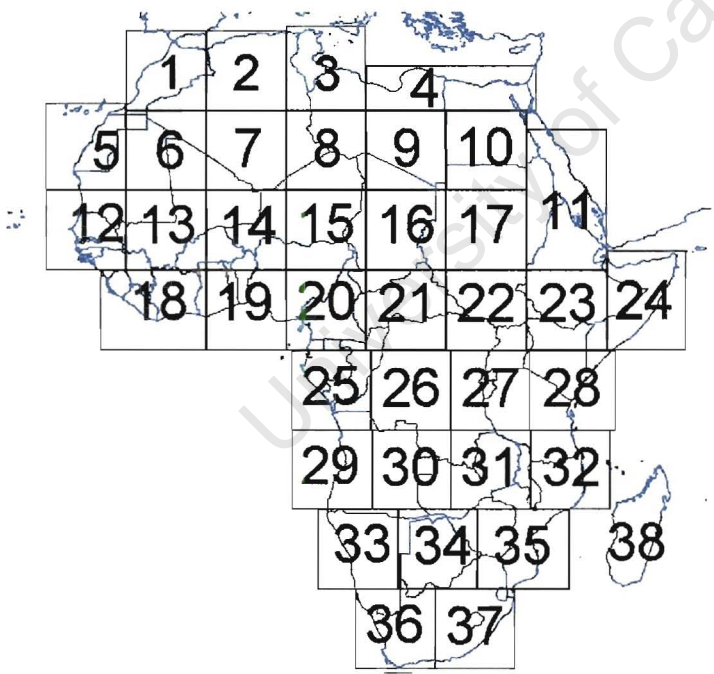

Fig. 7.1. Africa subdivided into 38 boxes using a grid of 1000 km.

The database of African rivers was obtained from De Beers Group in Centurion. The resolution of the set gives a mean density of 0.068 km/km^2, and thus an average stream separation of ~15 km. All rivers in the set are also described either as perennial or non-perennial, and the total length of each of the 2 types was computed in every block. A

number of other parameters in each block were computed, such as the mean annual rainfall (also using data obtained from De Beers, based on results of Legates & Willmott (1990a), who used average values between 1920 and 1980 – shown here in Figure 7.2), the mean elevation of land, and roughness of the topography, the latter two obtained using a 3km resolution Digital Elevation Model. To obtain the roughness, each block was divided into squares of 96 km sides, which corresponded to 32 pixels on the DEM, optimal size for fractal analyses of surfaces (Turcotte, 1992). Roughness of each square was calculated (as described in section 6.4.4.), and the mean of these values was taken to be the roughness of the block. All these, and other, parameters are given in Appendix C.

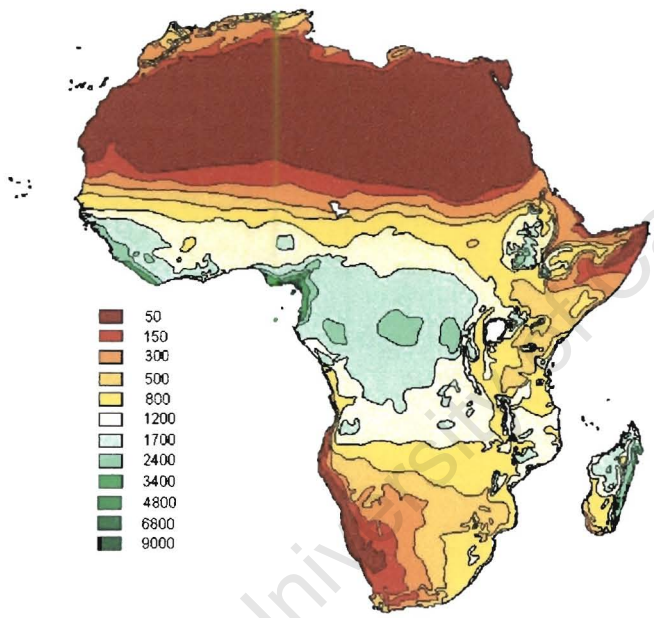

Fig. 7.2. Mean annual rainfall in Africa (mm)

7.2.2. Preliminary analysis

To study in detail the spatial variation of drainage density in Africa, 3 different parameters relating to river spacing were defined. These were:

- perennial river density, obtained by using total length of perennial rivers in eq. (7.1).
- channel density, obtained by using all river channel lengths in eq. (7.1).
- perennial percentage, showing what fraction of all channels is perennial.

All these parameters are provided in Appendix C.

To examine what relationship these might have with mean annual rainfall, mean elevation and topography roughness, correlation coefficients were computed between each of them and the 3 'density' parameters. These are shown in Table 7.1, along with the corresponding t-distribution probabilities p_s. These values show the probability of the 2 parameters in question being un-correlated. To accept correlation between 2 sets of values, a 95 % confidence interval is used most commonly, i.e. the value of p_s must be less than 0.05.

Table 7.1: Correlations between primary features and drainage parameters.

	perennial density		**channel density**		**perennial %**	
	corr.	p_s	**corr.**	p_s	**corr.**	p_s
mean rainfall	81.1 %	<1e-9	64.4 %	<1e-4	86.7 %	<1e-11
mean elevation	26.2 %	0.112	30.4 %	0.064	26.5 %	0.108
surface roughness	29.3 %	0.074	33.1 %	0.043	22.5 %	0.173

From the results in Table 7.1 one can safely assume a correlation between mean annual rainfall and any of the 3 drainage parameters. One also notices the relationship is stronger when perennial rivers are recognised as such. The correlations with surface roughness are not strong, but its relationship with the total channel density can be stated with the 95 % confidence mentioned earlier. No correlations can be concluded between the mean elevation and any of the 3 drainage parameters.

7.2.3. Rainfall and drainage density

While the tests above can suggest whether or not parameters are related to each other, they do not confirm a linear relationship. The plot of perennial density as a function of mean rainfall (Figure 7.3) consists of 2 clusters of points rather than a continuous linear distribution. For low rainfall (up to approximately 800 mm/year) the perennial density does appear to be linear function of rainfall (with the exception of block #36, corresponding to western South Africa, which will be discussed later). For higher values, however, there is virtually no correlation between the 2 parameters. It thus appears there exists a threshold minimum rainfall below which perennial density increases with

increasing rainfall. Above that threshold the density is independent of rainfall – it is not constant (varying from 0.054 to 0.127 km/km^2), but depends on other parameters. The exact value of this threshold is not obvious, as some blocks receiving as much as 850 mm of rain belong to the linear low rainfall regime, while the eastern South Africa block (#37) receives 674 mm per year but has a relatively high density (0.101 km/km^2). This threshold's value probably depends on other local parameters, but lies somewhere between 650 and 850 mm/year.

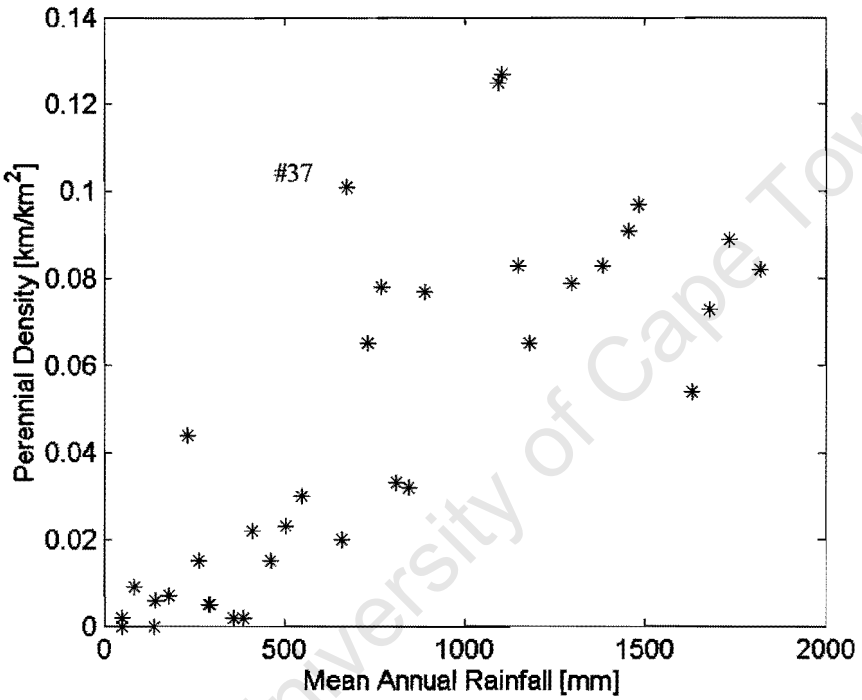

Fig. 7.3. Perennial density as a function of mean rainfall

Figure 7.4 shows the plot of the perennial percentage as a function of mean annual rainfall. This cannot obviously be a linear relationship for all possible rainfall values, as the percentage has an upper bound of 100. Once again the points can be classed into two regimes, with the rainfall value separating them around 800 mm/year. Below this value there is a clear trend by which the perennial fraction increases with more rainfall. For areas with rainfall higher than this threshold the fraction is close to 100 %, and is never below 80 %.

In conclusion, it is suggested here that perennial density increases with rainfall in dry areas receiving less than approximately 800 mm/year. The percentage off channels that are perennial also increases with rainfall, up to the same threshold value, beyond which most streams are perennial. It is noted that in both of the above relationships there are data points receiving up to 400 mm/year (half the threshold value) that have virtually no perennial streams. This will be returned to in regional analyses. It is furthermore suggested that mean rainfall does not influence channel density directly, though this density might be a reflection of what the rainfall was in a different epoch. Figure 7.5 shows a plot of channel density against today's rainfall. If the cluster of points with low rainfall and density was removed from the plot, the 2 variables would appear to be independent of each other. That cluster corresponds to points on one of the Sahara, Namib or Kalahari deserts, where unused waterways can get covered by sand a lot quicker than they would erode in an equally dry, but rocky, landscape.

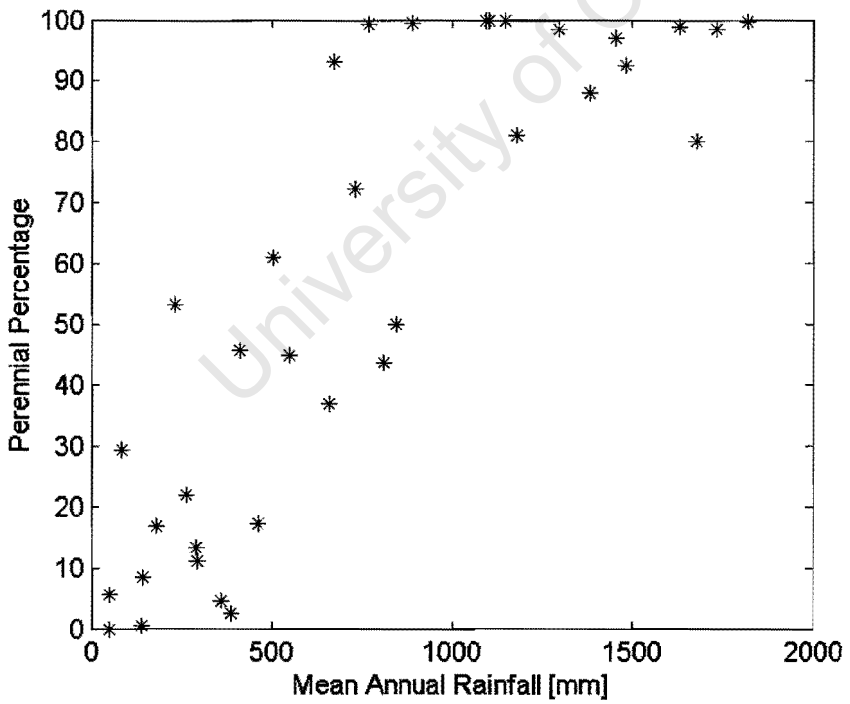

Fig. 7.4. Perennial percentage as a function of mean rainfall

In his study, Gregory (1976) found the drainage density to increase with increasing rainfall up to a threshold value of around 800 mm/year, decrease with increasing rainfall between that threshold and around 1000 mm/year, and be independent of rainfall for areas receiving over 1000 mm annually. He also observed considerably more variation in the densities for rainfall areas below the first threshold than in the wetter areas. This pattern is similar to the perennial density plot in this study (Figure 7.3), though not enough data points are available here to convincingly state the existence of the Gregory's decreasing regime between 800 and 1000 mm/year.

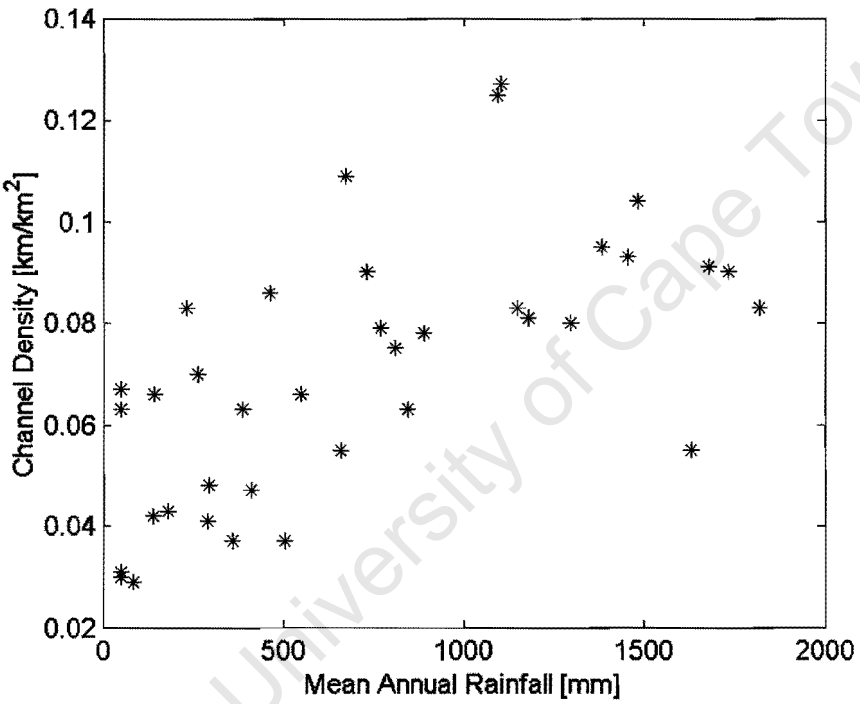

Fig. 7.5. Channel density as a function of mean rainfall

7.2.4. Deviations from the rainfall – drainage density relation

Mean annual rainfall is not the only factor that would influence drainage density. It was shown earlier that roughness of the topography is strongly related to the channel density. A rough topography will have more steep slopes for river channels to form, and run-off will be more likely than seepage. In Chapter 6 it was noted how certain river basin

characteristics have similar relationships with mean basin slope as they do with topography roughness.

A problem with dividing the continent into blocks and representing any parameter with one number in each block, is that by taking average values across the block, data is invariably lost. For example block #18 (containing Ivory Coast and Liberia) has one of the highest mean rainfalls, but only 80 % of rivers there are perennial. This is because the north-eastern section of the block is a low rainfall region, and most rivers there are non-perennial. Similarly data can be lost when computing the roughness of the block's surface. Southernmost blocks, #36 and #37, each have the same value for roughness, 27.5, while the average over the 38 blocks is 27.4. Both these blocks, however, have higher channel and perennial densities than one would expect given their mean annual rainfall. Topography of block #37, the eastern of the two, is dominated by the Great Escarpment, in places over 3000 m high. Inland of it are the sources of the Orange River, while the actual escarpment is drained by a number roughly parallel rivers that drain into the Indian Ocean. Away from this spectacular drainage divide the topography is not particularly rough, but with steep slopes in the upper-most reaches of drainage basins the channels are well defined, and the amount of precipitation is enough to keep the rivers flowing. The western block, #36, receives only 231 mm/year, but has comparatively high values for all 3 drainage parameters. This is probably due to the belt of folded mountains (the Cape Fold Belt) in its southern section. These mountains consist of soft shale valleys between hard quartzite ridges. The shale valleys erode much faster and become river channels. The high slopes of the mountains, and low absorption of quartzite, ensure the rivers in that particular section of the block are perennial.

7.2.5. Vegetation and drainage density

When studying the relationship between drainage density and vegetation one must be careful to distinguish between the cause and the effect. Is the density dependant on the vegetation, or is vegetation cover a direct result of the amount of rivers in the area?

Major vegetation zones of Africa are shown in Figure 7.6 (data from De Beers, based on the study of Matthews, 1983 and 1984). All types have been grouped into 6 major zones: deserts, forests, savanna, combination of forests and savanna, grasslands and floodplain

vegetation. This might seem rather generalized, with deserts and semi-deserts, as well as rainforests and open woodlands being grouped together, but it presents a starting point for an analysis. Distinctions such as ones mentioned above can be used later for a detailed analysis. Percentage of each vegetation zone inside each of the 38 blocks is listed in Appendix C. For the zones containing a combination of forests and savanna it was assumed each of the two types takes exactly half the area. All numbers were rounded off to the nearest 5%.

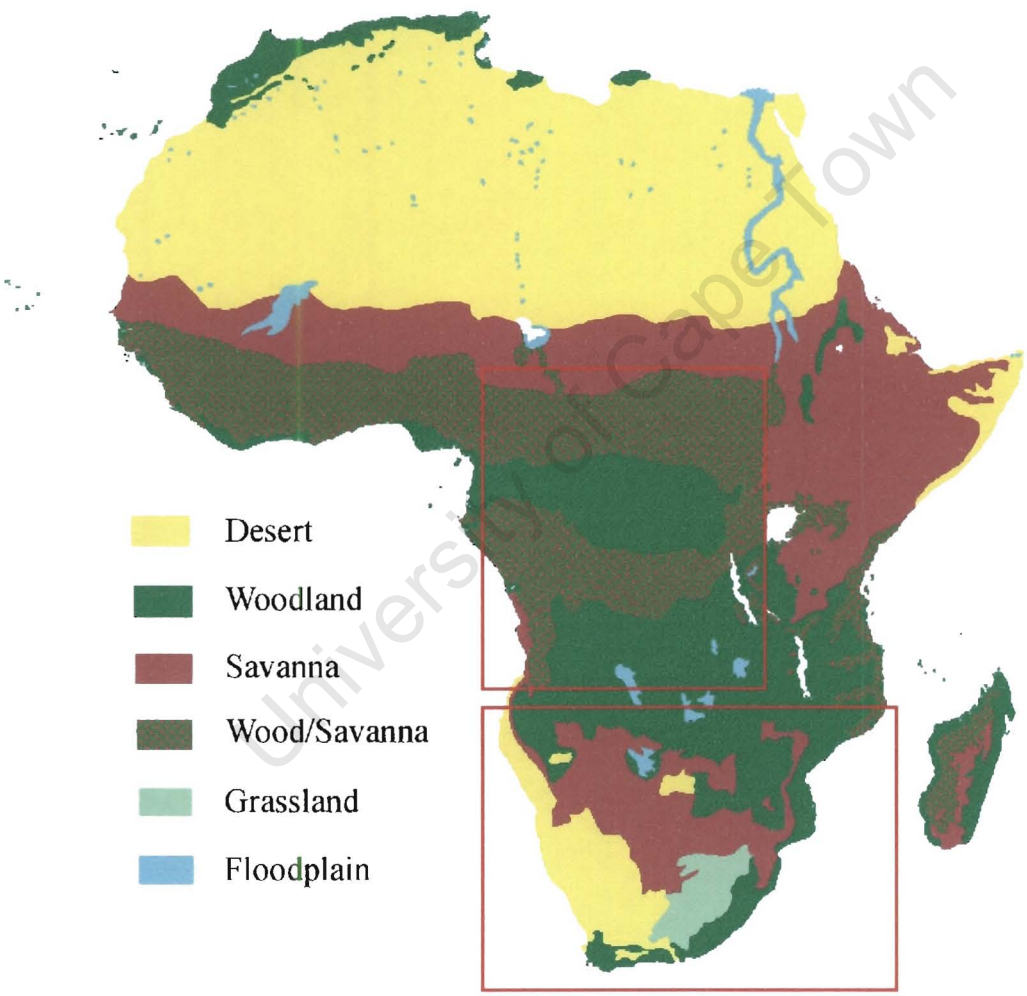

Fig. 7.6. Major vegetation zones of Africa. The regions studied in detail later, the Congo basin and Southern Africa, are shown by the red rectangles.

From Figure 7.6, as well as the appendix, one can see 2 of the zones are very rare. Floodplain vegetation is only found near the Nile and around major swamps, like the inland deltas of Okavango and Niger, as well as in many tiny oases in the Sahara. Grasslands are only found in south-eastern Africa, and made up more than 5% of only one block - #37.

Figure 7.7 shows the plot of what percentage of each block is taken up by each of the 3 main vegetation zones. Fig. 7.7a is a function of block's mean annual rainfall, and 7.7b of the perennial density. The most obvious pattern in these figures is the inverse linear dependence of the desert percentage on the rainfall – this is hardly surprising. For blocks with a mean rainfall of under 800 mm/year the percentage decreases with increasing rainfall, the correlation coefficient for the relationship being 93.6 %. Areas with rainfall over 800 mm/year, contain no desert vegetation – again this should have been obvious. From Figure 7.7b one can see areas with perennial density under 0.03 km/km^2 are dominated by desert vegetation, but the trend there is not obvious. For areas with a mean annual rainfall above 800 mm, or perennial density above 0.03 km/km^2, the dominant vegetation zones are the forests and savanna.

Percentages of areas thas these zones occupy in the blocks seem to depend more on the perennial density inside the block than on the rainfall. Amount of forests increases with increasing density, while the savanna areas decrease. The trends in Fig. 7.7a are much less clear. This is confirmed by a statistical analysis: considering only points above the aforementioned thresholds, the correlation coefficients for percentage of wooded and savanna areas as functions of perennial density are 74.8 % and 62.3 %, respectively. As functions of rainfall the corresponding values are 31.5 % and 20.2 %, it is suggested here that the amount of rainfall influences the amount of desert vegetation, but for areas with higher rainfall, the distribution of main vegetation zones, forests and savanna, is directly related to perennial drainage density, and not the rainfall.

It has been suggested that vegetation is responsible for the existence of the threshold rainfall at which the density stops increasing (e.g., Moglen *et al.*, 1998; Tucker & Bras, 1998). In the absence of any vegetation cover, one would expect the wetter the climate, the greater the degree to which the topography would be dissected by the drainage network (Moglen *et al.*, 1998). Vegetation provides a balance between the erosive forces

of precipitation and stabilizing forces of vegetative growth. The threshold thus corresponds to the amount of rainfall below which no significant vegetation cover can exist. The results of this study confirm that below the value of ~ 800 mm/year perennial density is directly proportional to the rainfall (Fig. 7.3), and at approximately the same value the desert scenery ceases to be the dominant vegetation zone (Figure 7.7a).

a)

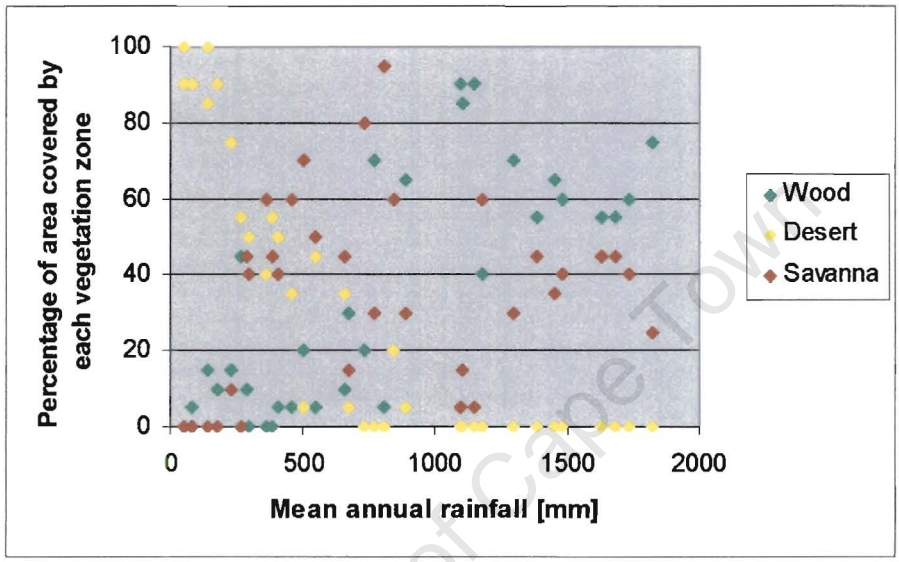

b)

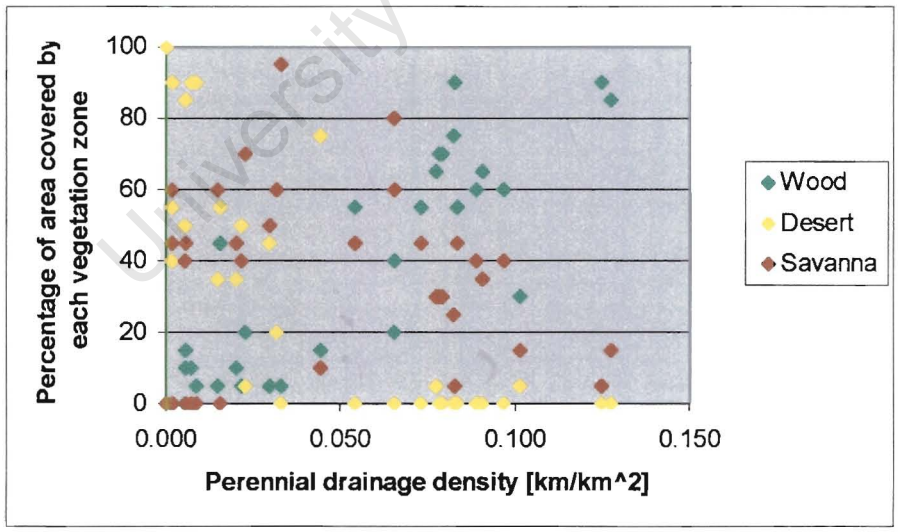

Fig. 7.7. Fractions of each block in Fig. 7.1 occupied by the 3 main vegetation zones as a function of:
a) mean annual rainfall
b) perennial drainage density

If vegetation is indeed responsible for the threshold in the rainfall – drainage density relation, it seems likely that the type of vegetation will influence the density beyond that threshold. In other words, the density would be dependent on the vegetation, not vice versa. From the previously mentioned strong linear correlations between perennial density in the are and the distribution of forests and savanna in the area it is concluded that forested areas result in higher drainage densities than savanna.

It was shown earlier that non-perennial rivers are only found in the dry areas belonging to the first density regime. These values are dominated by desert vegetation, which makes a further analysis of channel density's relationship with vegetation pointless – channel density and perennial density are only significantly different in desert environment.

7.2.6. Drainage evolution

Having established a number of trends relating drainage density to local parameters, it would be interesting to establish how the density would change if any of these parameters were changed. This question is far from being purely academic – a change in natural water supply can potentially have far reaching consequences not just on local wildlife, but on the human population in the area.

In their study of drainage density response to climate changes Moglen *et al.* (1998) derive a theoretical model for the density as a function of mean rainfall. In this model the density increases sharply with rainfall, but the curve smoothes out as it approaches a threshold value, and thereafter decreases slowly beyond this value. This decrease is not observed here (nor in the results of Gregory, 1976), but these authors present an interesting analysis of what they refer as the 'sensitivity of drainage density', which is the derivative of their density curve as a function of rainfall. This will be positive in low rainfall regions, and will decrease as it approaches the threshold, at which it will be zero. Beyond the threshold it will have a negative value, but its absolute value would be small compared to the sensitivity under the threshold.

The implications of this sensitivity curve are that for dry areas a small change in rainfall will have a large effect on the drainage – density would increase with increasing rainfall, and if the rainfall was an oscillating function in time, the oscillations of the density would be in phase with the rainfall curve. In wet areas, changes would be much smaller, but

perfectly out of phase with the rainfall. In the intermediate regions, where the rainfall value is close to the threshold, a change in climate could result in crossing the threshold into the other regime, and the density variations are quite complicated functions of rainfall change.

While there might be a dependence of drainage density on the rainfall in wet areas, for the African data presented here it is overridden by the density's dependence on vegetation. It is suggested here that the density variations exist in 2 separate regimes – in the dry areas density is a function of rainfall, in wet areas of the vegetation type. These regimes are separated by a threshold rainfall value below which there is not significant vegetation cover. This threshold is somewhere between 650 and 900 mm/year. With this model the variations with rainfall would be similar to those of Moglen *et al.* (1998) in dry areas – a change in rainfall produce an 'in phase' change in density, but changes in rainfall would not directly influence density in wet areas. Density changes in these areas would be brought about by change in the vegetation covering the area. The general trend for this would be an increase in density with replacement of savanna with forest areas, and decrease for the reverse process.

Evolution of drainage, climate and vegetation clearly forms a complex system. This topic will be re-addressed in the concluding chapter of this thesis.

7.3. Detailed analysis of the Congo Basin

7.3.1. Introduction

The rivers forming the Congo Network were selected from the above-mentioned data base, and ordered using the now familiar Horton-Strahler ordering scheme. With the available resolution the network had an order $\Omega = 8$, and is shown in Figure 7.8. The figure also shows how the network has been sub-divided into 25 blocks, in a similar style to Figure 7.1. These blocks usually squares 400 km across, but as with the division of Africa, outside ones have been shifted, stretched or combined. The mean density of the drainage in the Congo is considerably higher than the mean value for Africa – from the data used here it is 0.086 km/km^2, which corresponds to stream separation of 12 km, compared to 15 km for the entire continent.

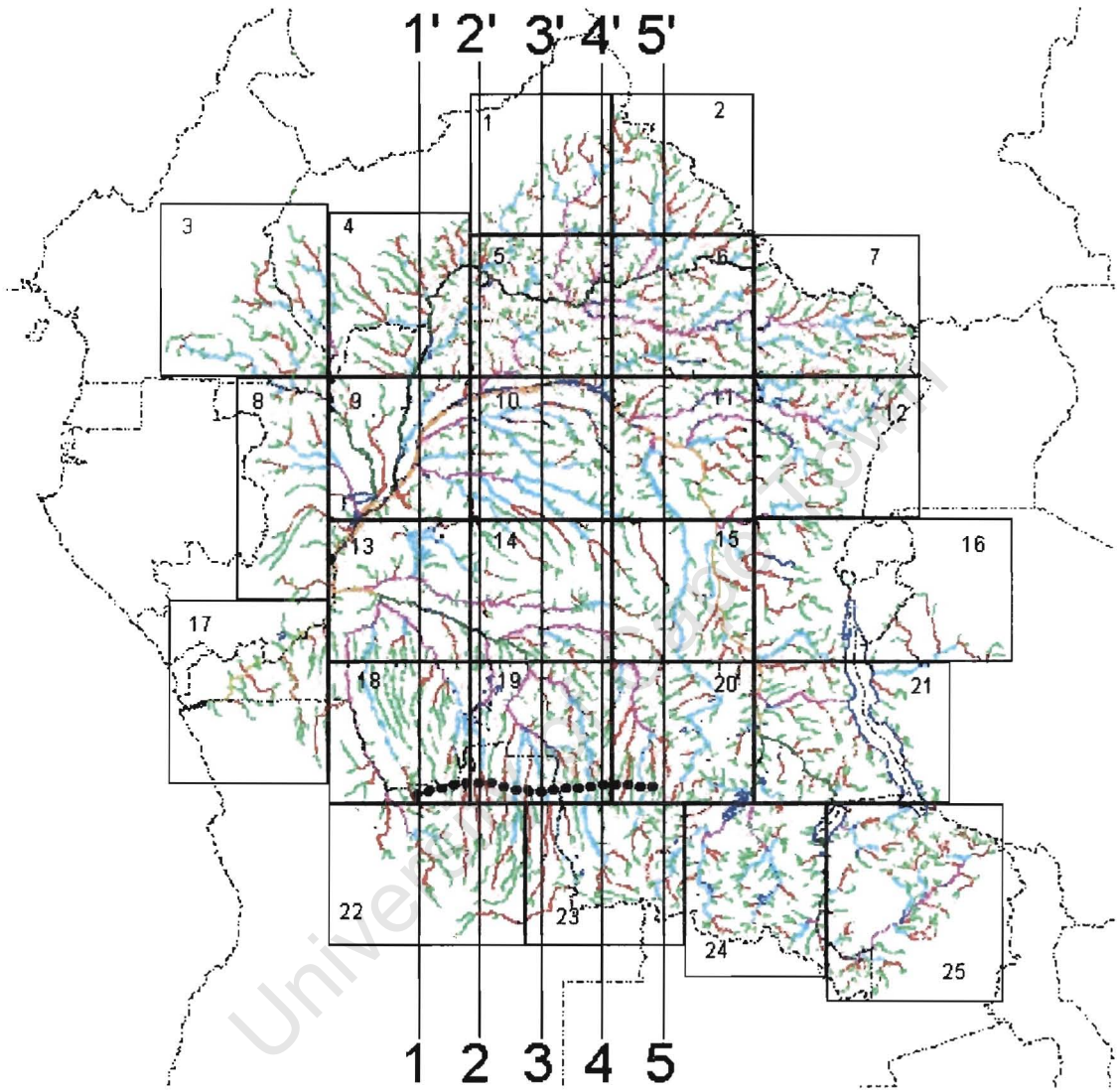

Fig. 7.8. Ordered streams in the Congo River network. Subdivision of basin into 400 km * 400 km blocks is shown, though some blocks on the edge of the basin have been extended or joined with others – see text for explanation. 5 North-South lines show where the cross-sections in Fig. 7.9 were taken. Thick dashed line shows where the streams from the south reach the 610 m plain, changing the drainage pattern.

Inside each block the length of all rivers was computed, and from it, the drainage density. No distinction was made between perennial and non-perennial rivers – 99.2 % of the network stream length is perennial, so a separate analysis would have been useless. The total length of streams of each order was also determined, and from it the 'order density'. The number of streams of each order was counted inside each box for the 3 lowest orders only – 4th order streams often flowed through more than one square. Using the total stream lengths for each order and stream numbers it was also possible to determine the mean stream length of the 3 lowest orders inside each box.

Using the 3km resolution Digital Elevation Model the mean elevation of each block was calculated, as well as the roughness of the surface. Mean annual rainfall was not computed for each box, as there is relatively little variety in the rainfall across the basin, and no part of it receives less than 800 mm annually. The low-rainfall regime described earlier is thus not expected to exist in the Congo, though as will be mentioned in the next section, this was not always the case. The relevant parameters for all boxes can be seen in Appendix C.

7.3.2. Analysis

From the data in the appendix, or even from just looking at Figure 7.8, it is obvious there is considerable variation in drainage density in the Congo Basin. The densities in different blocks vary from 0.065 to 0.136 km/km^2, and are clearly regional. The densest drainage is found in the north-eastern part of the basin. The density decreases as one goes south, until the area with the least rivers is reached. This is a west-east orientated band going across the middle of the network. Immediately south of that the density increases again, with a completely different pattern of long, narrow, parallel basins in the south-west producing a relatively low density. These channels occupy the northern-most reaches of the Mega Kalahari Sand Sea. Stokes *et al.* (1997) identified four arid phases in the Sand Sea in the last 115,000 years. During these phases the drainage density would be low (and perennial density possibly 0). With the area being dominated by sand (Stokes *et al.*, 1997, report dune-building environment), with the onset of aridity surface channels would be quickly covered by sands. With the next wet phase there would be no existing drainage network in place, possibly explaining the simple, parallel drainage pattern.

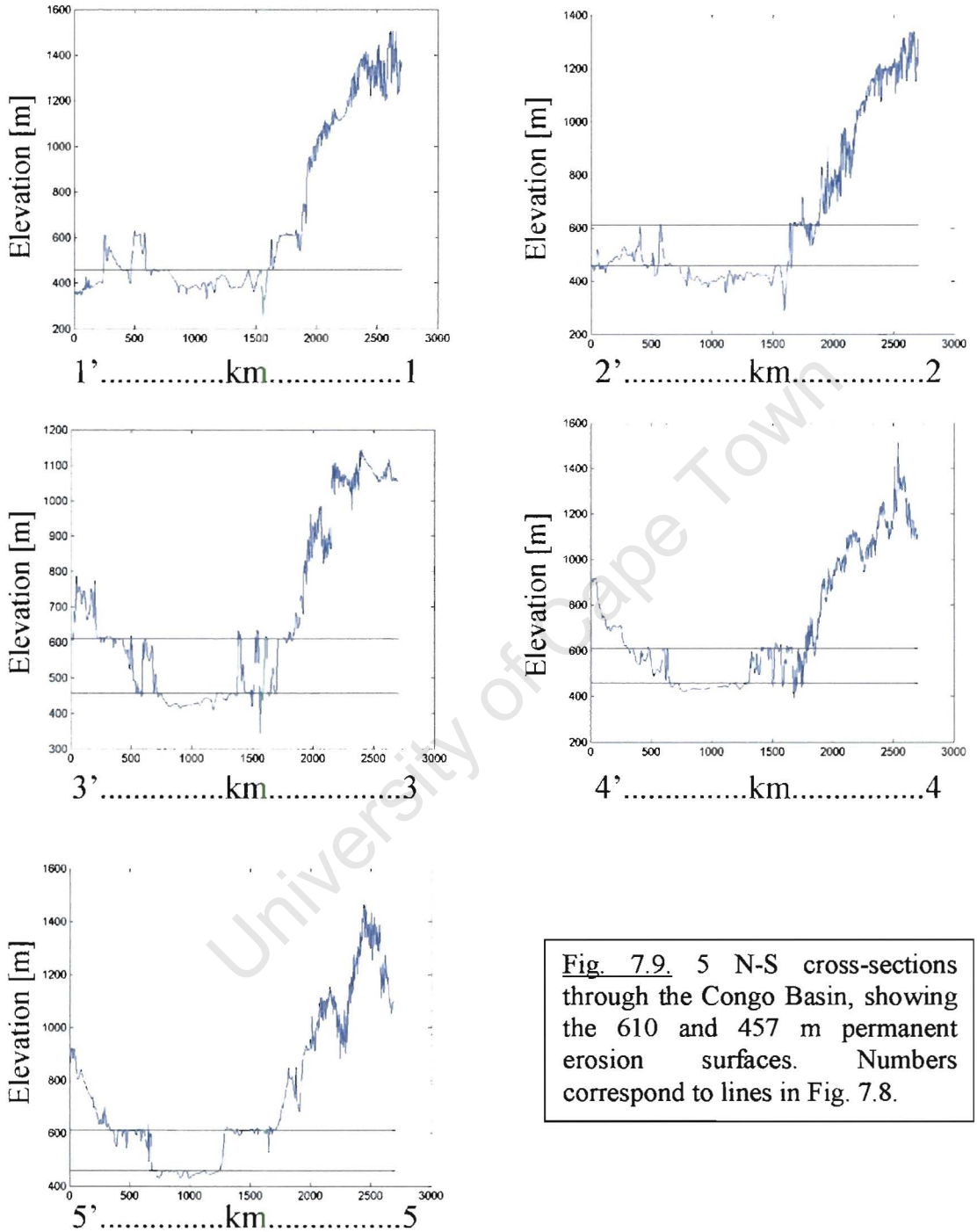

Fig. 7.9. 5 N-S cross-sections through the Congo Basin, showing the 610 and 457 m permanent erosion surfaces. Numbers correspond to lines in Fig. 7.8.

There does not seem to be even a hint of relation between the density and the mean elevation of the topography – correlation coefficient here is 3.4 %. Between the density and surface roughness it is -19.7%, which for 25 data points gives a t-distribution p_s = 0.342, showing the correlation has no significance. The parameters controlling the drainage density are therefore more subtle. Figure 7.9a shows some N-S cross-sections through the basin. Examples of E-W sections are shown in the next chapter (Fig. 8.5), which deals with the Congo Basin in more detail.

An interesting feature of the Congo Basin is the existence of large peneplains, or, in places, remnants of them. Virtually all of them have an elevation of either 610 or 457 metres above sea level. These surfaces are discussed in more detail in the next chapter. These elevations have been marked on all cross-sections, and the peneplain areas are clear to see. These cross sections are constructed using the 3 km resolution DEM containing the Congo Basin. This DEM is a square with 900 data points (2700 km) along each side.

In the south-western areas of the basin, the streams start at the elevation between 1100 and 1600 metres and flow north, following the slope down. These are the long parallel streams mentioned earlier. Due to the constant slope all flow is directed north, and the streams have virtually no perpendicular tributaries – all junctions have very narrow angles. When these rivers drop to the height of approximately 610 metres, they reach the higher peneplain. This can be seen on the cross-sections between 1800 and 1850 km from the northern boundary of the Congo network. This corresponds to the point at which the rivers start having regular first order tributaries, the great decrease in slope presumably making it possible for rivers to forge their channels in different directions.

The corresponding 610 m surface in the northern parts of the basin ends somewhere between 600 and 700 km from the northern limit (Fig. 7.9), where it drops to the 457 m surface. This corresponds to about two-thirds down (south) in boxes #5 and #6 (Fig. 7.1), where a slight but clear drop in density is visible. This might suggest the higher of the 2 surfaces has lower absorption than the lower surface, and all water received by rainfall is drained overland, while in the lower surface groundwater transport also takes place. These surfaces cannot explain the more significant change in drainage density (in boxes #10 and #11), and the reason for it remains uncertain.

7.3.3. Density and vegetation

Vegetation in the Congo Basin can be divided into 4 areas (Figure 7.6). Furthest north is a combination of seasonally wet forest and savanna. South of that zone is the equatorial rainforest, with another band of seasonally wet forest and savanna south of it. The boundary between the rainforest and the forest / savanna zones coincides with the escarpment between the 610 m and 457 m plains mentioned above. Seeing the two forest / savanna zones are on different sides of the equator, they receive majority of their rainfall at different times – they are both summer rainfall areas. The southern-most section of the basin is covered by dry forest and open woodland. In the continental scale analysis in section (7.2) no distinction was made between such forest and the equatorial rainforest, but for a detailed regional analysis a distinction is necessary. Drainage density was computed inside each of these zones – the results are in Table 7.2 below.

Table 7.2: Drainage density in vegetation zones

#	**Vegetation**	**Area (km^2)**	**Density (km/km^2)**
1	Seasonally wet forest and savanna (North)	710,000	0.111
2	Rain forest	1,097,000	0.073
3	Seasonally wet forest and savanna (South)	898,000	0.081
4	Dry forest and open woodland	871,000	0.086

All zones had similar areas, which were also similar in size to the blocks used in the continental scale analysis. There is some variety in the densities above, but not as much as between different blocks. This suggests there is a lot of uncertainty in the mean density values for the vegetation zones. This is confirmed when boxes contained within vegetation zones are examined: box #1, totally inside the northern forest/savanna has a density of 0.089 km/km^2, while box #9, virtually all inside the rainforest, has a similar value - 0.088 km/km^2. Boxes #22 and #25 are both contained in the dry forests in the far south of the basin, but their densities are 0.076 and 0.119 km/km^2, respectively. Furthermore, zones 1 and 3 in the table are described as having the same vegetation in the data base, but they produce significantly different drainage densities. All this leads to the conclusion that in the Congo Basin variations in the drainage density cannot be explained using vegetation zones alone, which admittedly do not exhibit significant variation.

Another local parameter that can potentially influence drainage is the soil type. A database of basic soil types similar to the vegetation one was available (Zobler, 1986), and Figure 7.10 shows the soil map of the Congo Basin and its surroundings. Only isolated areas larger than 100,000 km^2 were considered. Ten such areas existed, and the results are summarized in Table 7.3 below.

Table 7.3: Drainage density in soil type zones

#	Soil Type	Area (km^2)	Density (km/km^2)
1	medium loam	186,000	0.113
2	sand and loamy sand	135,000	0.098
3	heavy loam and clay	353,000	0.123
4	medium loam	159,000	0.089
5	medium loam	320,000	0.073
6	sand and loamy sand	430,000	0.069
7	medium and heavy loam	131,000	0.074
8	sand and loamy sand	430,000	0.084
9	medium and heavy loam	230,000	0.110
10	medium loam	102,000	0.106

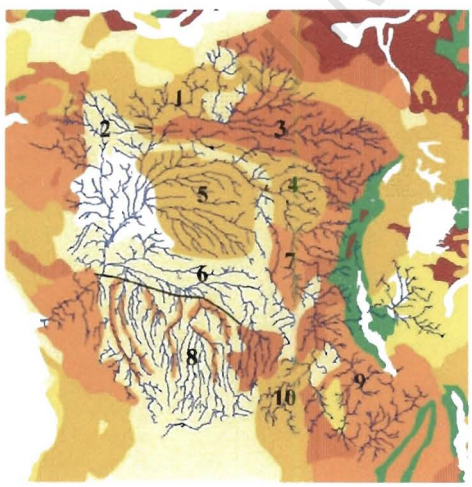

Fig. 7.10. Major soil types in the Congo basin. Numbers correspond to those in Table 7.3, from where types and areas can be read.

As with vegetation, it seems impossible to explain drainage density variations in terms of soil types. Each type that was recorded in more than one area shows fluctuations between these areas, with densities on either side on the basin's mean value (0.086 km/km^2) being recorded for each soil type. The highest density was recorded in the area containing heavy loam and clay, but as this was the only area with this soil type in the basin, and given the fluctuations for other soil types, it must be concluded that drainage density does not depend on soil type in the Congo basin.

7.3.4. Hack's Law

Knowing the stream numbers and mean stream lengths in each block for the 3 lowest orders, it was possible to determine Horton's ratios (Horton, 1945) over 2 changes in order: from 1st and 2nd, and from 2nd to 3rd. Given that most of 4th order basins had larger drainage areas than the box size studied here (not more than 1600 km^2), only these orders were taken into account. The weighted means for the ratios were computed across these 3 orders:

$$R_l = \frac{\frac{n(\omega=1)}{n(\omega=2)} * \frac{l(\omega=2)}{l(\omega=1)} + \frac{l(\omega=3)}{l(\omega=2)}}{\frac{n(\omega=1)}{n(\omega=2)} + 1} \qquad (7.3a)$$

$$R_n = \frac{\left[\frac{n(\omega=1)}{n(\omega=2)}\right]^2 + \frac{n(\omega=2)}{n(\omega=3)}}{\frac{n(\omega=1)}{n(\omega=2)} + 1} \qquad (7.3b)$$

These numbers were used to represent Horton's ratios of stream lengths and stream numbers, respectively, and have been listed for each block in the appendix. In Chapter 3 of this text it was shown that (with the assumption that $R_n \equiv R_a$) Hack's exponent h, relating stream length to basin area, can be expressed using these ratios:

$$h = \frac{\log R_l}{\log R_a} \qquad (7.4)$$

This exponent was also computed and values for each box are listed in the appendix. Most values are under the 0.6 originally found by Hack (1957), and some are even under 0.5. Using stream numbers and mean lengths for the entire network, the mean value for h in the entire network is 0.548.

These values for h are rather low when compared to both results earlier in this study and references quoted in it. In Chapter 6 it was shown how the exponent can be viewed as an inverse of the connectivity of the network, so most areas of the Congo have a high connectivity. The highest values for h were found in blocks #18, #22 and #23, which are dominated by long parallel streams, which one would expect to have low connectivity.

Figure 7.11a shows a plot of h as a function of drainage density. There seems to be strong negative regression, though some outliers are present. The correlation coefficient is 40.0%, and using the t-distribution one finds the probability p_s of the 2 parameters being un-correlated to be 4.8 %. The existence of the relation between the 2 can thus be assumed within a 95 % confidence interval. Neither of these parameters can be thought of as a primary feature of the landscape, so it can be difficult to decide which of them depends on the other. Here h was assumed to be a function of the density.

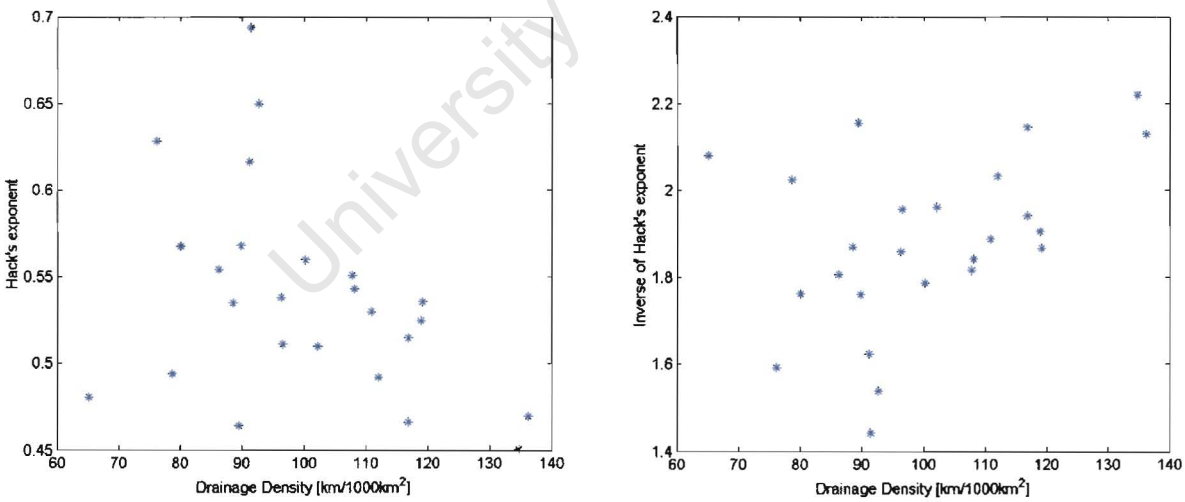

Fig. 7.11. a) Plot of Hack's exponent against drainage density.
b) Plot of the inverse of Hack's exponent against drainage density.

The negative correlation means an area with a lower density will have a higher value for Hack's exponent. It is interesting to note that all stray points of the plot correspond to areas with a relatively low drainage density. If only boxes with a density higher that 0.095 km/km^2 are considered, the correlation coefficient goes up to 65.6 %, and the t-distribution probability p_s drops to 1.1 %. Noting that a negative linear regression would require negative densities to produce values of h above 0.7 (which was the case quite often in this study alone), a plot of the inverse of h as a function of density was drawn (Figure 7.11b). This eliminated some of the outliers, and increased the correlation to 41.4%. We therefore propose the drainage density of a given area plays a role in the drainage organization, as it is inversely proportional to Hack's exponent h.

7.4. Southern Africa

7.4.1. Recap of previous results

A study of climate's influence on drainage patterns in Southern Africa was performed earlier in this thesis (section 4.9) in Chapter 4, which dealt with an analysis of river networks in the sub-region. To recap, the conclusions of that study were:

If an areas receives less than 400 mm/year of precipitation, it will contain virtually no perennial rivers. Above that threshold value, the perennial density increases linearly with mean rainfall. Areas containing the Cape Fold Belt mountains were outliers for this fit (Figure 4.21), having more perennial drainage than the amount of rainfall they receive would suggest. It was further concluded temperature does not influence drainage parameters, while Hack's exponent h (obtained from simulating water flow over a 1km resolution DEM of the area) is independent of climatic parameters.

7.4.2. Closer look at the rainfall-density relation

The perennial density – annual rainfall relationship described above is significantly different from what was observed in the continental analysis of Africa, and which compared favourably to the results of Gregory (1976) and Moglen *et al.* (1998). However, all regions in this study received less than 1200 mm of rain annually, so the wet-areas regime was not well exposed. Looking at the plot (Fig. 4.21) one can see that the perennial density stops increasing around 800 mm/year, consistent with earlier

findings. The significance of this was not realized when the analysis in Chapter 4 was performed. The other anomaly, the threshold below which there are no perennial streams, is obviously different from the continental model. 8 of the 24 blocks in the study have perennial densities under 0.02 km/km^2, despite their rainfall varying between 60 and 540 mm/year. These blocks cover the entire Namibia, western Botswana and north-western South Africa, areas covered by the Kalahari and Namib deserts. Whatever rainfall these areas receive is in their summer (December-February). With virtually no rain for the rest of the year it is impossible for rivers caused by the summer rain to keep flowing through the rest of the year.

7.4.3. Vegetation

The generalized vegetation zones of southern Africa can be seen in Figure 7.6. There is considerably more variation in the vegetation cover than in the Congo basin, with deserts, forests, savanna and grasslands all making up significant portions of the sub-region. Some fluvial plane vegetation exists near the Okavango swamps, but did not make a significant fraction of any block. Percentages of each block covered by each vegetation zone are listed in Appendix C. The way the sub-region was divided into blocks was shown in Figure 4.18 in Chapter 4.

Figure 7.12 shows how the percentage that a vegetation zone occupies in a block correlates with the mean annual rainfall of the block (Fig. 7.12a) and with the perennial density of the block (Fig. 7.12b). These figures are similar to Fig. 7.7 of the continental study. It was found that better regressions are observed when woodlands and grasslands are combined to form a single zone. The patterns observed here are similar to the ones in Figure 7.7, but some differences can be seen. For low rainfall regions the percentage of desert vegetation decreases with increasing rainfall, as was observed in section 7.2, but the rainfall value above which desert cover becomes insignificant is between 500 and 600 mm/year (though it might to be less in some regions), compared to the ~800 mm/year in the continental study. From Fig 7.12b it also appears high density corresponds to wooded/grassland areas, and low density to savanna. These relationships are not straightforward. First, it is interesting to note the distribution of perennial density is not continuous. In 8 blocks with a density of less than 0.02 km/km^2, no blocks have a value

between 0.02 and 0.04 km/km^2, and only 2 blocks between 0.04 and 0.06 km/km^2. The areas with perennial density above 0.06 km/km^2 are dominated by woodlands and grasslands – no block with density of 0.08 km/km^2 or higher is more than 20 % savanna.

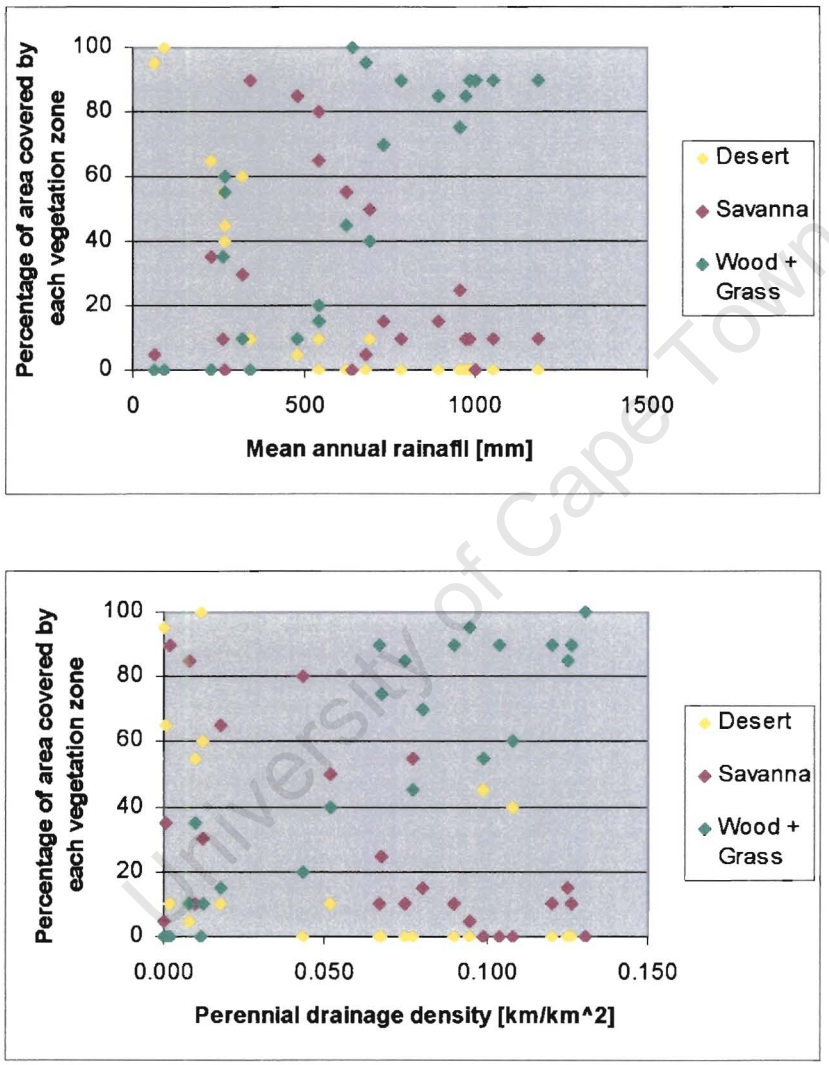

Fig. 7.12. Fractions of each block in Southern Africa occupied by the main vegetation zones as a function of:
a) mean annual rainfall
b) perennial drainage density

Another difference between this local analysis and the continental one is that low rainfall regions are not dominated by desert vegetation, some of them being covered by savanna. Reference must also be made to the 2 blocks that are nearly half covered by desert, but have high perennial densities of ~0.1 km/km^2. These blocks correspond to the extreme south, where the Cape Fold Belt mountains were found, though these mountains form the not-desert parts of the block. These are the points that have unusually high densities for the low mean amount of rainfall they receive, discussed in Chapter 4. This anomaly was explained in section (7.2.4) as probably being due to well defined waterways in the steep valleys of the Cape Fold Belt.

7.4.4. Density relationships with other parameters

A 1km DEM of the sub-region was used to model flow of water over the landscape. A detailed analysis of fractal properties of rivers in the area was conducted in Chapter 4, while a description of how networks are obtained from the DEM can be found in Appendix B. In Chapter 4 Hack's exponent was computed using all basins that fit into a particular block. This exponent was found to be independent of climate properties. Here it was tested against river density.

The correlation coefficient between h and total channel density was found to be -34.6 %, considerably higher than with the perennial density, -27.0%. The higher value gives a t-distribution $p_s = 0.06$, just outside the 95 % confidence interval. It does suggest, though, a negative trend between h and channel density, or a positive one between the density and connectivity of the network. This result is similar to the one obtained for the Congo network in the previous section.

The final two parameters compared to the drainage density were related to the topography: mean elevation of the block and its surface roughness. Even though a 1km DEM of the area was available, to be consistent with the results from earlier sections 3km resolution was used for the roughness. The mean elevation was found to be un-correlated with the any density parameter, but there was a 47.9 % correlation coefficient between channel density and roughness. This corresponds to a t-distribution $p_s = 0.018$, suggesting a direct relationship between the parameters.

7.5. Conclusion

In this chapter variations in drainage density in Africa were examined. Two different densities were defined: one including all total channels, the other only perennial rivers. The two were only significantly different in dry regions receiving less than approximately 800 mm/year. The total channel density was found not be dependant on present day rainfall, though areas with the lowest density were in fact low rainfall regions. These regions, however, correspond to sandy deserts, where any unused waterway is likely to be covered up by easily movable sand. In regions underlain by harder rock, the channel density is independent of rainfall. Instead, channel density shows convincing correlation with topography roughness for the continental study, as well as the regional analysis of southern Africa. A rough topography would have more slopes and valleys than a smooth one, and thus be more conducive to the run-off of whatever water was precipitated. However, there was no correlation between channel density and roughness in the Congo basin. Relatively high densities of non-perennial river networks in what today are extremely low rainfall regions suggests the climate in these regions must have at some point in the recent past been significantly different.

The perennial density was found to have a strong dependence on mean annual rainfall, at least in dry regions. Up to a threshold value of ~ 800 mm/year, the density increases with increasing rainfall. In some areas (e.g. south-western Africa) there exists another threshold, ~ 500 mm/year, below which the perennial density is extremely low, and above which it increases with rainfall, but only up to the higher threshold. This lower threshold is a result of seasonal precipitation – if the entire annual rainfall occurs in one or two months, and perhaps even cause a flood, if it is below the threshold it will not keep the rivers flowing throughout the year. The existence of two thresholds close together means the distribution of perennial density values will not be continuous – there will be a number of very dry areas (with virtually no perennial rivers) below the first one, as well as a number of well watered regions above the second threshold, but very few values between the extremes will exist. An example of this 'gap' can be seen in southern Africa.

The 800 mm/year is the threshold corresponding to rainfall value below which no significant vegetation cover can exist, and the dry regions below that threshold are dominated by deserts. Plant cover is responsible for terminating the direct relationship

between density and rainfall, balancing the erosive power of precipitation with stabilizing forces of vegetative growth. The perennial density in these high rainfall regions will depend on the type of vegetation dominating the area, with forests and grasslands corresponding to higher densities than savanna. This is not a direct relationship, but more a guideline. In the Congo basin, for example, different vegetation types could not explain the variations of density.

Regional studies of the Congo basin and southern Africa found an inverse correlation between channel density and Hack's exponent. As h can be thought of as an inverse on network connectivity, this relationship suggests the connectivity is positively correlated with drainage density.

Chapter 8

Drainage Evolution in Central Africa

8.1. Central Africa Today

Figure 8.1 shows the 3 km resolution Digital Elevation Model of Central Africa. Features not usually associated with Central Africa (such as the Cameroon Volcanic line and the Tibesti Highlands in Chad) can be seen, but the areas we are concerned here are the vast Congo Basin on the west and the East African Rift Valley in the east. The vertical scale used in the figure has been truncated at 3000 metres above sea level – this is barely over half the maximum elevation in the region (Kilimanjaro – 5895 metres), but it makes geomorphic features in the low-lying areas visible much more clearly.

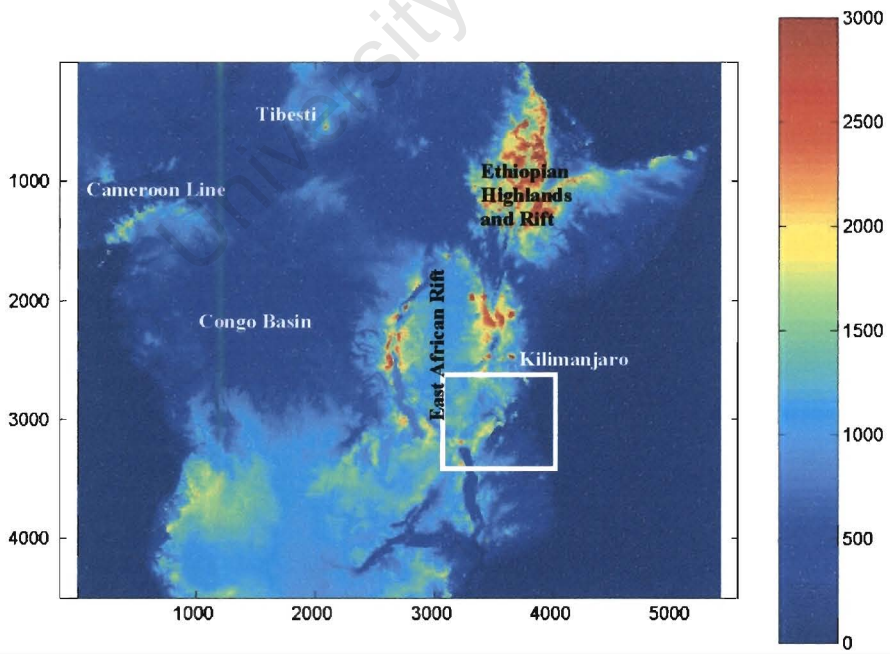

Fig. 8.1. DEM of Central Africa. Horizontal distances in km, elevation scale in m. Note how the East African Rift consists of 2 (Western and Eastern) branches. Area of Fig. 8.8 (the Rufiji river area) is highlighted with the white block.

The drainage pattern observed today in the region is shown in Figure 8.2a. It is dominated by the Congo river (Figure 8.3) with its sub-circular basin. It is, however, not a classic centripetal drainage pattern one would expect from a circular depression. In Chapter 3 it was shown the Congo river network has a very low Hack's exponent. Later in that chapter models of radial drainage away from a dome and centripetal drainage into a sink showed that the sinks have consistently higher values for h than patterns associated with domes. An examination of the river pattern in Figures 8.2 and 8.3 confirm there is no convergence of drainage into a central point. In the southern one-third of the basin most of the drainage is directed north. While that does not sound particularly unusual, it is very interesting to note there is relatively little convergence of these north-flowing streams. Instead they mostly seem to join west-flowing streams. The main Congo stream, and the lower reaches of Oubangui and Zaire before their confluence flow south-west. The areas where eastwards and southward drainage is dominant are comparatively small – these are in Congo, Cameroon and the Central African Republic. In this study the Congo refers to the river downstream from the junction of the Zaire with Oubangui (Fig. 8.3), though other studies often describe the entire river as either Congo or Zaire.

South of the Congo Basin are the Zambezi and Okavango networks, both having general eastward drainage direction. This is particularly notable for the Zambezi, as its sources are 3 times as far from the Indian Ocean as from the Atlantic. Even more unusual, however, is the Okavango, which after flowing for nearly 2000 km ends in an inland delta another 1000 km from the Indian Ocean.

North-east of the Congo basin the Nile basin starts, where rivers start their long journey north (see Chapter 9). The drainage in the Rift Valley is quite complicated between the two branches (Western and Eastern Rifts – Fig. 8.1). A number of landlocked sinks form small lakes, but most streams find their way into one the 3 Great Lakes, Victoria, Tanganyika and Nyassa. Interestingly these all drain in opposite directions: towards the Mediterranean, the Atlantic, and the Indian Ocean, respectively (Fig. 8.2b). Outwards off the two main ridges of the East African Rift the drainage is fairly straightforward – west into the Congo basin, and east into the rivers going straight to the Indian Ocean, of which the Rufiji is the largest. North of these lakes the Rift turns slightly east – this can be clearly seen on the drainage map as the uniform gap between the Nile and Ganane basins.

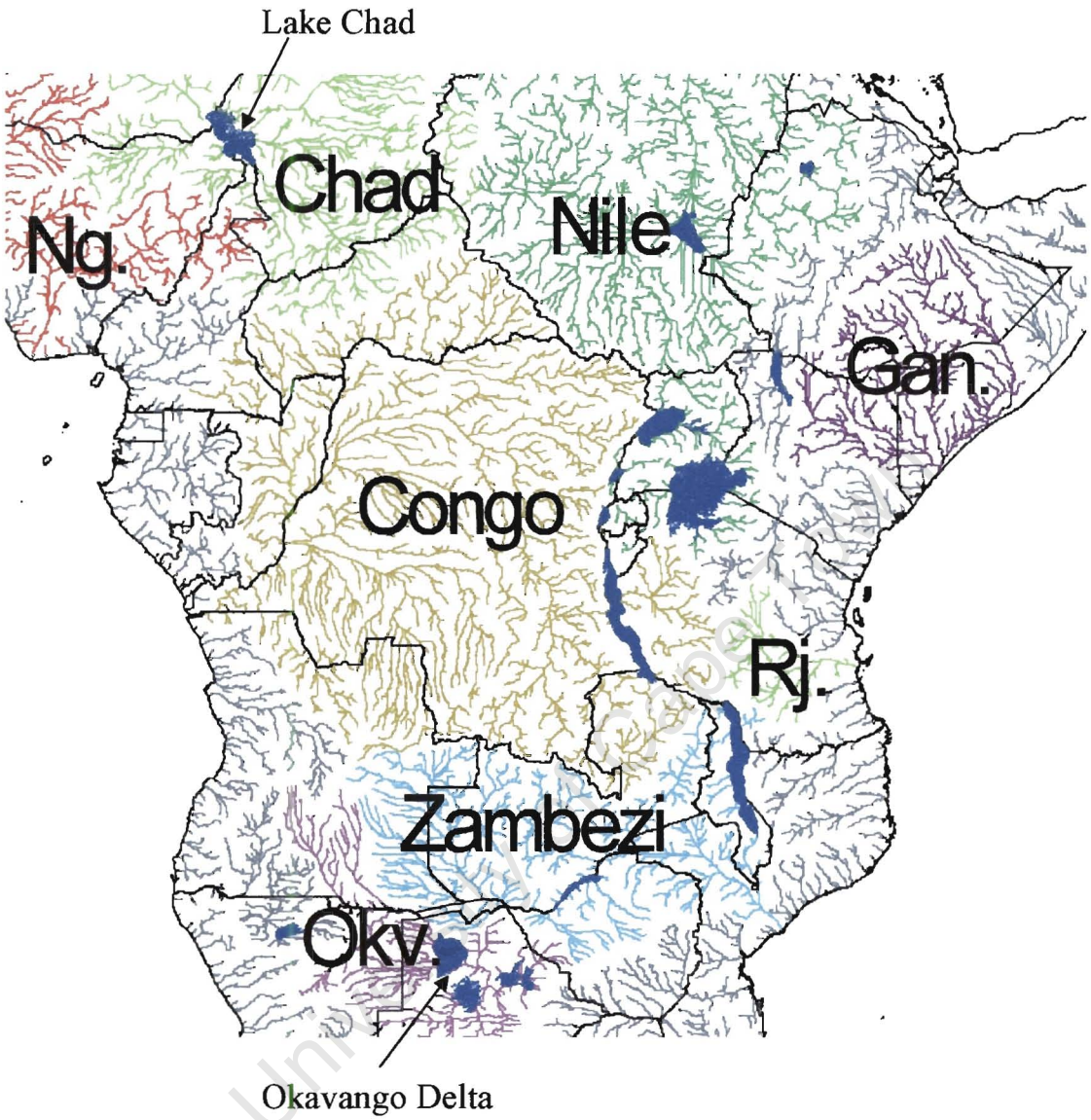

Fig. 8.2a. Drainage pattern observed in Central Africa today. Abbreviations of major basins: Ng.= Niger, Gan.=Ganane, Rj. = Rufiji, Okv. = Okavango. Note that the Okavango and Chad basins are landlocked, draining into the Okavango Delta and Lake Chad, respectively.

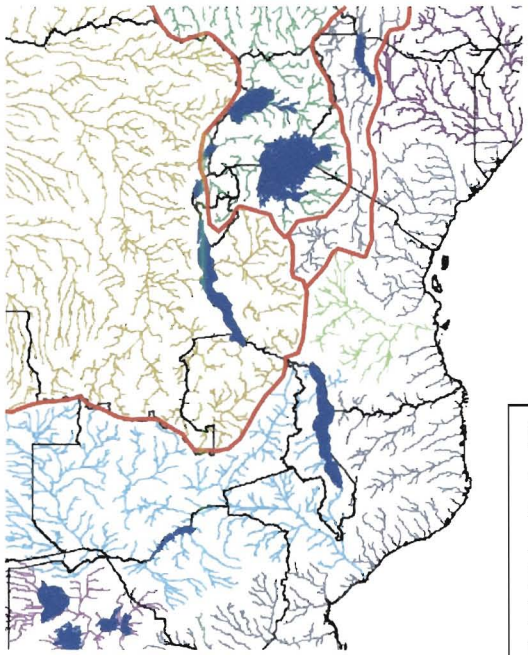

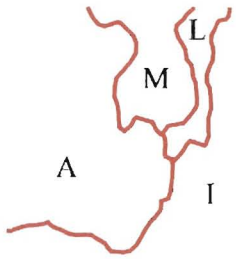

Fig. 8.2b. Major watersheds in East Africa. Note the 3 Great Lakes drain into different catchments:
A: Atlantic Ocean
I: Indian Ocean
M: Mediterranean Sea
L: Landlocked

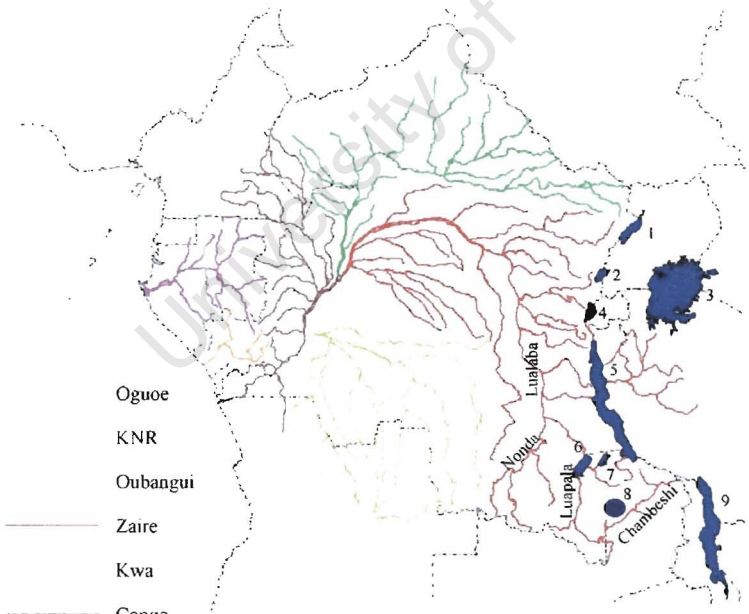

Lakes

1: Albert	2:Edward	3:Victoria
4:Kivu	5:Tanganyika	6:Mweru
7:Meru Marsh	8:Bangweulu	9:Nyassa

Fig. 8.3. Main streams in the Congo network, as well as Oguoe and KNR.

8.2. Mesozoic-Cenozoic Congo Basin History

A more detailed DEM of the Congo basin (still at 3 km resolution, but with the elevation range truncated at 1200 m) is shown in Figure 8.4. Marine fish fossils recovered from the north-east of the basin suggest the Congo Basin was submerged below sea level throughout the Upper Jurassic and Lower Cretaceous, i.e. ~ 200-120 Ma (Sahagian, 1988 and refs. therein). Presence of similar fossils on the east coast of Africa and their absence on the west coast suggest these marine waters reached the Basin from the east in the Cretaceous (Doucouré & de Wit, 2003). The implication of this is that once the land was elevated above the sea level in the Cenozoic, the Congo network was flowing across over where today the East African rift system is found (Shackleton, 1978).

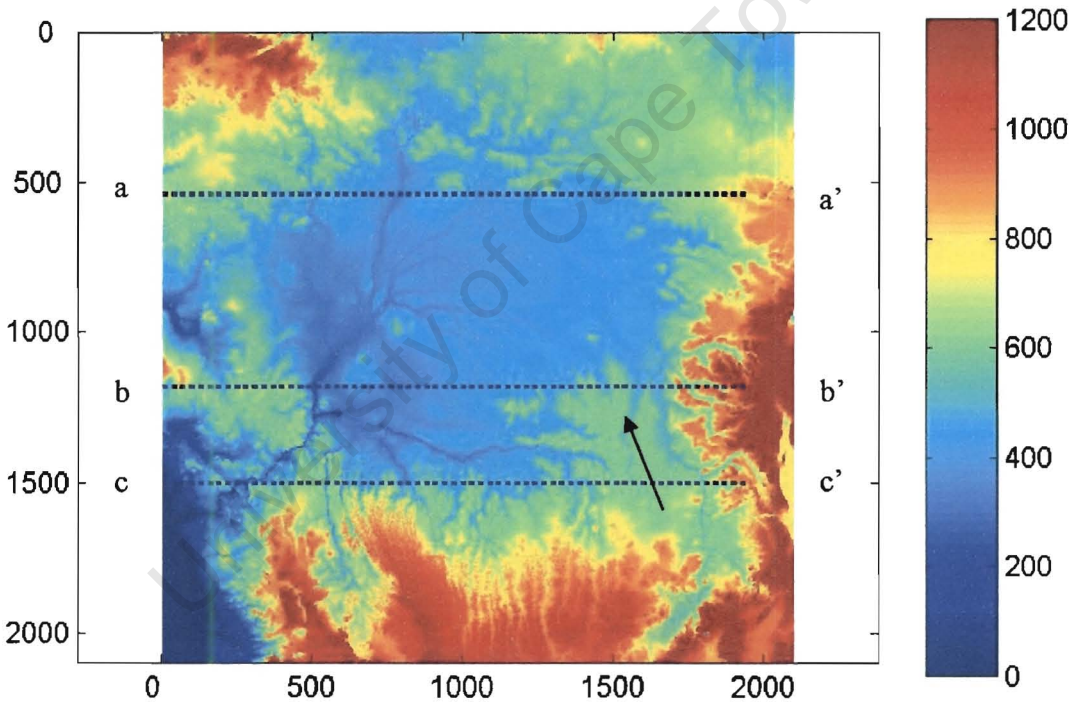

Fig. 8.4. DEM of the Congo Basin. Horizontal distance in km, elevation scale in m (truncated at 1200m). Cross-sections in Fig. 8.5 are along west-east dashed lines marked a-c. The black arrow marks the Lualaba valley.

Seismic studies of the offshore Congo Fan (Uenzelmann-Neben *et al.*, 1997; Uenzelmann-Neben, 1998) produced a history of deposition off the Atlantic coast near today's outlet of the Congo river. These studies found that in Late Paleogene / Early Neogene (~ 30-20 Ma) the only source of sediment was the Kouilou-Niari river system (KNR – Fig. 8.3). In Middle-Late Miocene (~ 15-5 Ma) the Congo and the KNR were both active sources of sediment, but from the Early Quaternary, the Congo has been the prevailing sediment source. This is consistent with the evidence presented above that the Congo drained into the Indian Ocean prior to that time. It is perhaps surprising that the KNR, which today has a drainage area of 60,000 km^2, should deposit a significant amount of sediment. Burke (1996) suggests the drainage of the western area of today's Congo basin consisted of numerous rivers similar to the present Oguoe (Figure 8.3), perhaps not unlike the south-east coast of South Africa. The Oguoe has an area of 210,000 km^2, much larger than the KNR, but still hardly comparable to today's Congo basin of 3,690,000 km^2. It is, however, possible that the Miocene river ending at today's outlet of KNR was significantly larger than Oguoe today.

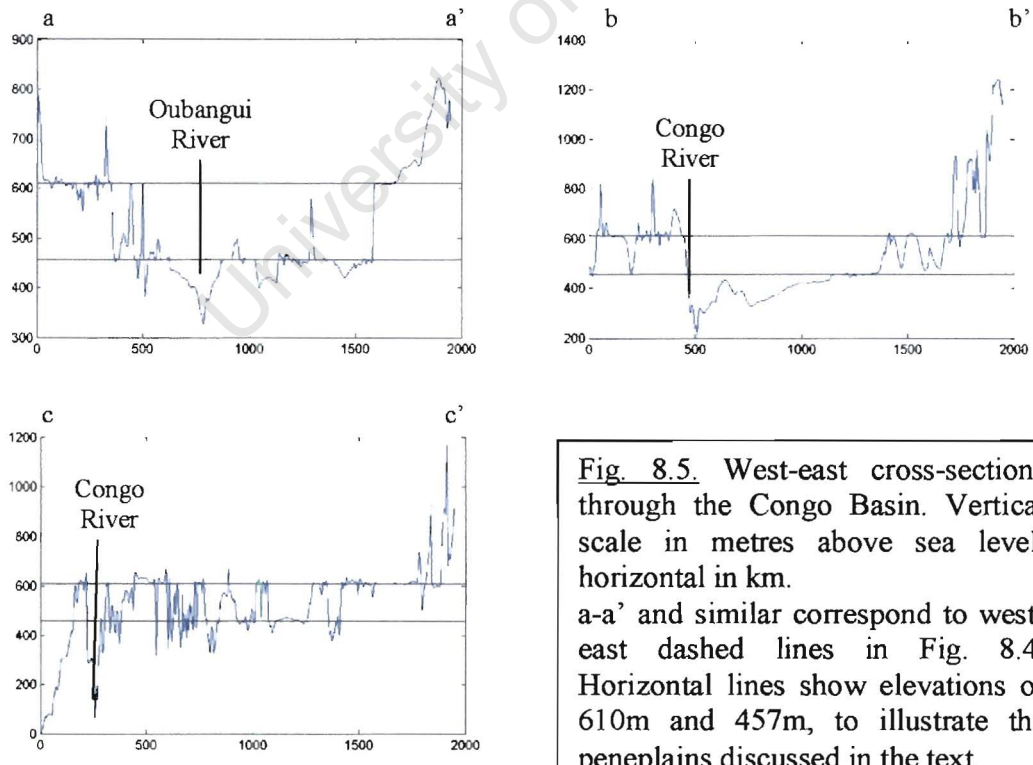

Fig. 8.5. West-east cross-sections through the Congo Basin. Vertical scale in metres above sea level, horizontal in km.
a-a' and similar correspond to west-east dashed lines in Fig. 8.4. Horizontal lines show elevations of 610m and 457m, to illustrate the peneplains discussed in the text

While it is probably impossible to suggest, let alone prove, the exact shape of the river networks that covered today's Central Africa in the past, it would be of great interest to identify the place where a river system as large as the Congo had its outlet prior to the mid-Tertiary uplift in East Africa. This will be attempted later, after other areas in the region have been introduced in detail.

It is also possible that there exists more than one of these former outlets into the Indian Ocean. If the drainage pattern could change so significantly, a drastic change could have occurred more than once. From studying cross-sections of the DEM in Figure 8.4, a number of flat erosion surfaces (peneplains) can be seen. These are often incised by today's streams and major rivers, but remnants of these peneplains are obvious. Examples of these cross-sections are given in Figure 8.5. As was mentioned in the previous chapter, it is interesting that throughout the huge basin these plains have only 2 distinct elevations: 610 and 457 metres above present day sea level. Fig. 8.6 shows the Congo basin DEM with the same boundaries as Fig. 8.4, but only 5 contour intervals have been included to highlight these surfaces. The 457m heights (and elevations within 10m of it) are in blue and the 610m (± 10m) in yellow. Elevations between these surfaces are in green, while black and red show areas below 447m and above 620m, respectively. The 457m plains, dissected by today's channels of the Congo network, seem bounded by the 610m plains, with an occasional inselberg rising out of the lower plain (such as the ones at ~500 and 1300 km in Figure 8.5a). These are obviously prone to erosion, and their elevations are usually just under 610m. The boundary of Cuvette Centrale (Daly *et al.*, 1992) corresponds at least partially to the boundary between these 2 surfaces. This "Central Basin" is largely covered by Cretaceous and Tertiary sediments, with Jurassic and Permo-Triassic sediments exposed along its eastern rim. It is surrounded by crystalline rocks of Proterozoic thrust belts of a variety of ages (some as old as Archean) and structural styles. Their details are beyond the scope of this study – an interested reader is referred to, e.g., Cahen & Snelling (1984); Daly *et al.* (1984, 1992).

Doucouré & de Wit (2003) reconstructed Africa's paleotopography for the Cretaceous. They find the Congo Central Basin is a topographic low, not more than 50 metres above the relatively high Cretaceous sea level (from which the basin was just uplifted), surrounded by higher ground. If this high ground is indeed a peneplain (today's 610 m

plain), it corresponds to a tectonically stable period considerably before the Cretaceous. There is evidence from Permo-Carboniferous glacial deposits in the area (Daly *et al.*, 1991) for positive surface relief across central Africa at the end of the Paleozoic (Doucouré & de Wit, 2003), so the higher peneplain is unlikely to be part of the Mesozoic-Cenozoic history of the basin, but instead represents a much older erosion surface. The lower (457m) plain probably corresponds to the coastal plain of the east-flowing Cretaceous paleo-Congo.

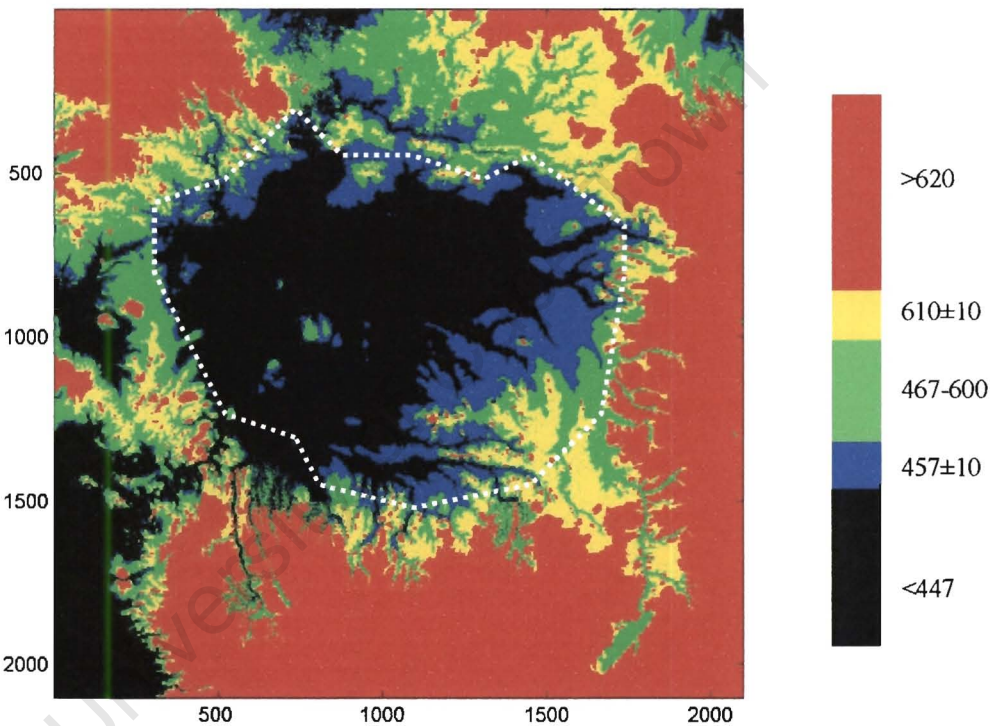

Fig. 8.6. Congo basin map highlighting the 457m (blue) and 610m (yellow) peneplains. Horizontal distance in km. Dashed white line shows the approximate boundary of the Cuvete Centrale (Daly *et al.*, 1992).

8.3. Southern Flank of the Congo Basin: Zambezi-Okavango-Limpopo System

Some sections of this river system might have belonged to the paleo-Congo network in the past, while parts of today's Congo have been suggested to reach the Indian Ocean at the Limpopo delta in the Jurassic (e.g. Moore & Larkin, 2001). Thus this river system should be carefully analyzed when trying to reconstruct the drainage history of the Congo. The three networks are shown in Figure 8.7.

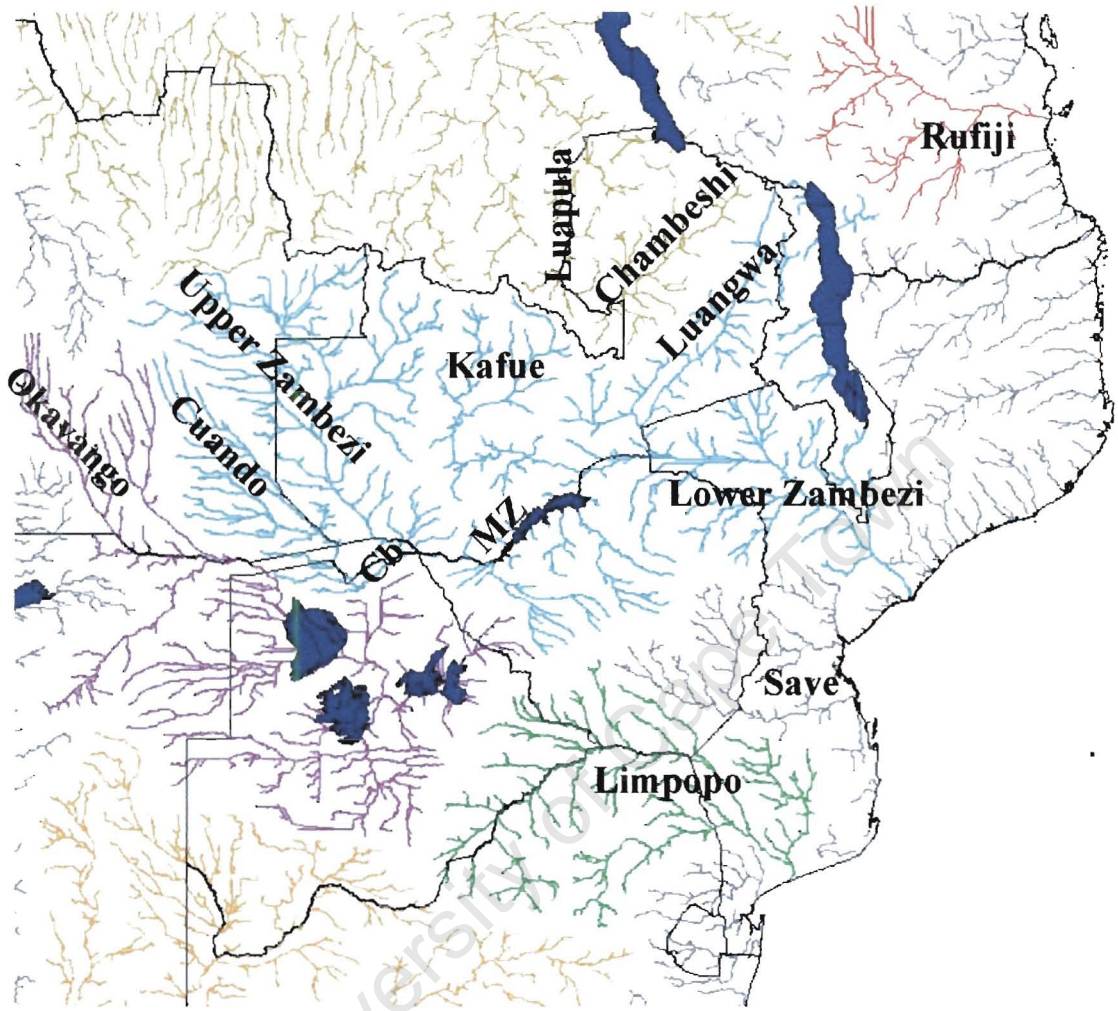

Fig. 8.7. Zambezi-Okavango-Limpopo System today.
Cb = Chobe, MZ = Middle Zambezi

A drainage evolution model has been put forward by Moore & Larkin (2001) based on a palaeo-drainage reconstruction of Thomas & Shaw (1991). This model (illustrated in Figure 8.8) suggests that in the Jurassic and Cretaceous the Okavango, Cuando and upper Zambezi flowed south-east parallel to each other for well over 1000 km with each of them eventually joining the Limpopo river, all draining into the Indian Ocean. The Kafue and Luangwa were major left bank tributaries of the upper Zambezi. The lower Zambezi would have been a network similar in size to today's Save. During the early Tertiary

crustal flexuring along the Okavango-Kalahari-Zimbabwe axis (OKZ – Moore, 1999) severed the links of the Okavango, Cuando and upper Zambezi with the Limpopo. Until the Eocene (~38 Ma) the three rivers formed a major landlocked system draining into the Kalahari Basin. The model goes on to suggest that in the Oligocene headward erosion of the Lower Zambezi (initiated by the OKZ flexuring) would have captured the Luangwa. In the Lower Pleistocene continued headward erosion of the Lower Zambezi would capture the Gwembe Trough (location of Lake Kariba), forming a link between the Upper and Lower Zambezi. At a similar time what would then have been the Upper Kafue (Chambeshi today) is said to be captured by the Luapula tributary of the Congo. In the Upper Pleistocene captures of the Cuando and Kafue by tributaries on the main Zambezi would have produced a drainage pattern observed today.

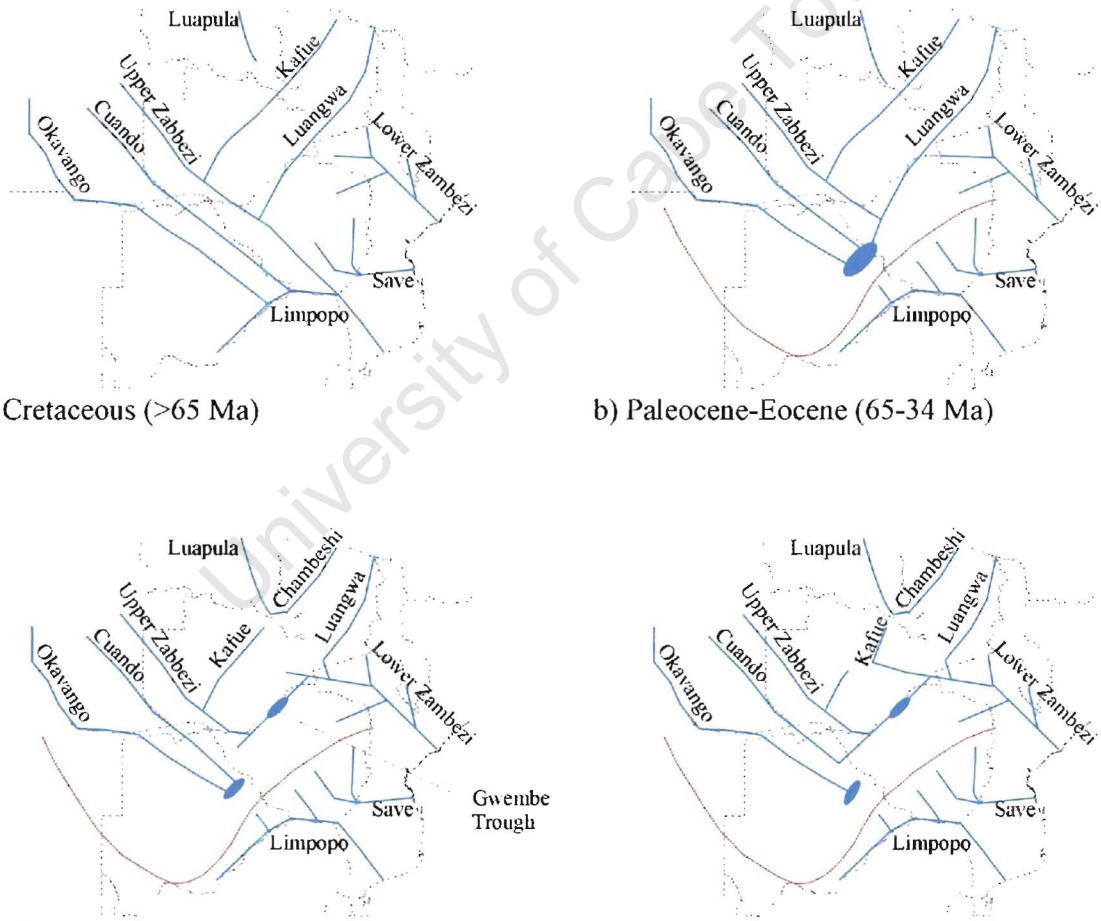

a) Cretaceous (>65 Ma)

b) Paleocene-Eocene (65-34 Ma)

c) Pleistocene (~1 Ma)

d) Present

Fig. 8.8. Drainage evolution model of the Zambezi-Okavango-Limpopo system based on Moore & Larkin (2001). Brown line shows the Okavango-Kalahari-Zimbabwe (OKZ) flexuring. It is possible that in the future the Okavango will be captured by tributaries of the Nossob or Molopo rivers cutting through the western side of OKZ, and drain to the Atlantic via the Orange river.

8.4. Eastern Flank of the Congo Basin: East African Rift Region

The uplift and rifting in East Africa was not an instant event (even on the geological time scale), but consisted of multiple episodes (e.g. Shackleton, 1978; Ebinger & Ibrahim, 1994). At 35 Ma, during Oligocene, basalts were erupted in southwest Ethiopia and northwest Kenya from fissures in the Afar and the Ethiopian Rift, while the youngest lavas dated in the area are as young as 0.63 Ma (Baker *et al.*, 1971).

The proximity of the rift to the Indian Ocean makes the development of any significant drainage patterns east of the highlands impossible, but the largest of the rivers found there, the Rufiji (Figure 8.2), deserves some attention. Despite its relatively small size (drainage area of just under 200,000 km^2, less than half the size of Limpopo's basin) a delta more than 500 km wide can be seen at its outlet on the DEM in Figure 8.1. A close-up of Rufiji's basin is shown in Figure 8.9, with the old delta clearly visible. However, today the Rufiji has a single outlet, with the outer reaches of the 'delta' containing outlets of short (~200 km in length) separate rivers. This suggests that at some time in the past a river much larger than Rufiji today had its mouth (delta) at that spot.

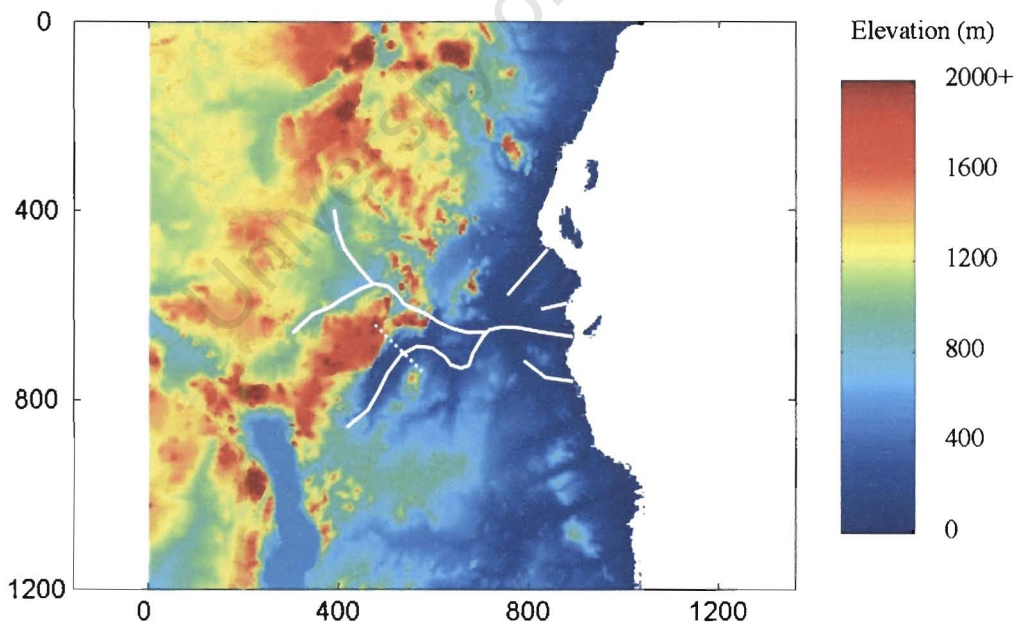

Fig. 8.9. DEM (truncated at elevation of 2000m) of the Rufiji Area. Solid white line show the main streams (from North to South: Kisiga, Ruaha and upper Rufiji). Small streams suggesting a former delta are also shown. Dashed line shows where the cross-section in Fig. 8.10 was taken.

Another interesting feature of the Rufiji is the prominent valley of its major southern tributary, the upper Rufiji. A cross-section of the valley is shown in Figure 7.9. The valley is over 50 km wide, but the headwaters are only 150 km upstream of where the cross-section was taken. It seems reasonable to assume its headwaters were once considerably further from the wide valley. The presence of a river terrace, albeit only on one side, further suggests the flow volume was once much higher. The northern tributary (Ruaha, or Great Ruaha after the confluence with Kisiga) is completely different – an extremely narrow gorge is flanked by high mountains on both sides. The relatively simple shape of the gorge, with a big meander, leads one to see this as a case of antecedent drainage, which would imply the direction of flow predates the Rift Valley uplift.

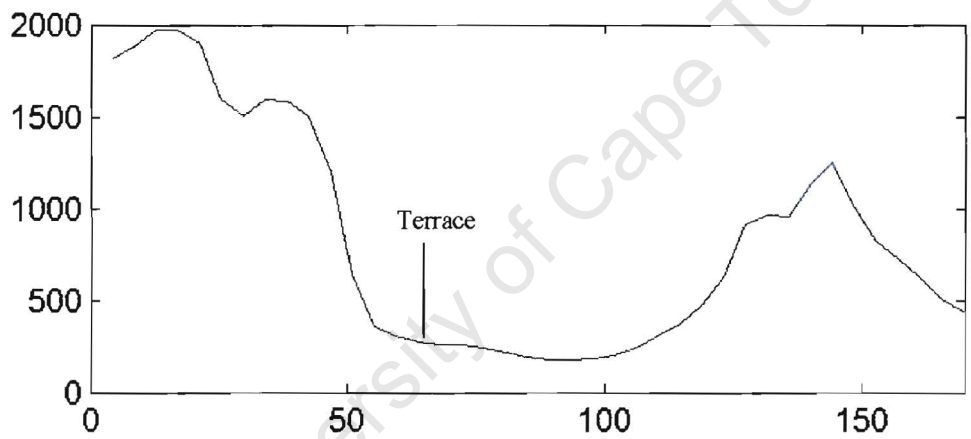

Fig. 8.10. Cross-section of the upper Rufiji valley. Horizontal scale in km, vertical in m. See Fig. 8.9 for location of section.

8.5. Northern and North-western flank of the Congo Basin: West African Rifts

South America and Africa have been fitted together by earth scientists since Antonio Snider's now famous engraving (1858). However, irrespective of whether the shorelines or continental margins were used, a tight fit could never be achieved – a tight fit between west Africa and northern Brazil, for instance, results in a major gap in the south Atlantic. To accommodate this Burke & Dewey (1974) first suggested that in the Cretaceous Africa behaved like two plates separated by rifting in the area of today's Nigeria,

Cameroon, Chad and Central African Republic. Pindell & Dewey (1982) show that distortion of the African Plate through such tectonic extensions could be the reason for the lack of a tight fit between continental margins of Africa and South America. De Wit *et al.* (1988) and Unternehr *et al.* (1988) further showed such plate deformations are also found in South America.

A tectonic model of this West and Central African rift system was presented by Fairhead (1988), and is superimposed here on the drainage system of the region in Figure 8.11. The structures relevant here are the southernmost in the regional setting. The Central African shear zone loosely follows the border between Chad and Central African Republic, and carries on into Sudan, arching northwards slightly. North-east Africa's move east along this shear zone was necessary to avoid compression or overlap in North-west Africa, which would result from South America's clockwise rotation (Reeves *et al.*, 2004). The South Sudan rift, recently found to be rich in oil deposits formed during the rifting, runs in Sudan roughly 200-300 km and parallel to its borders with CAR and Democratic Republic of Congo, into Kenya, possibly extending as far as the coast as the Anza Rift (Reeves *et al.*, 1986).

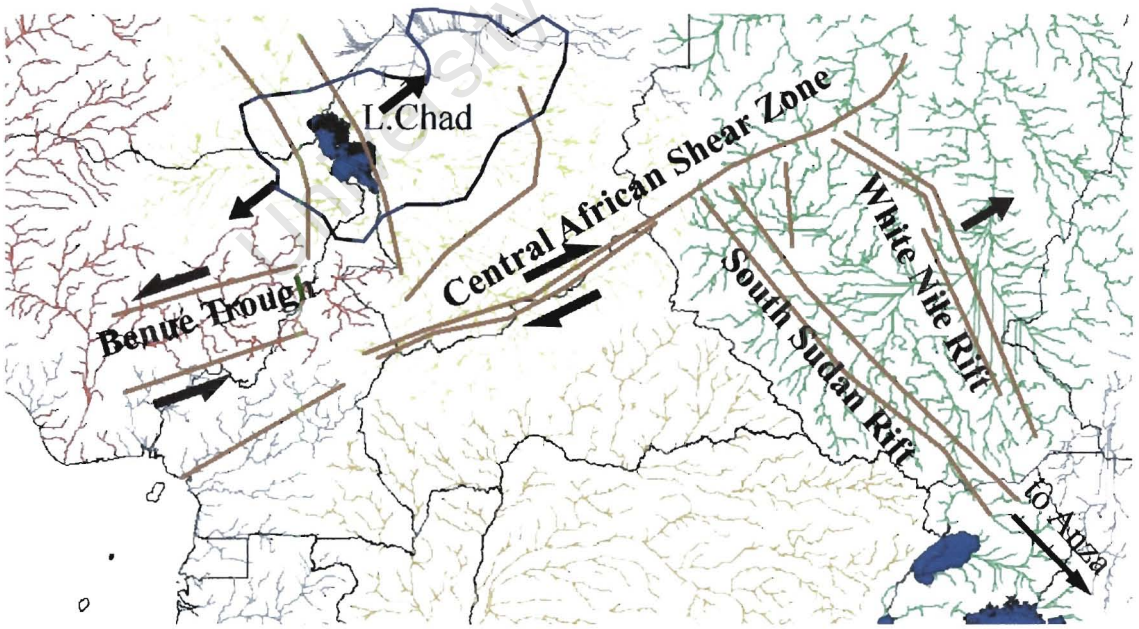

Fig. 8.11. Major structures of the West and Central African Rift, after Fairhead (1988). Possible extent of Lake Megachad has been drawn in after Burke (1976).

The rifts are dated as Mid-Upper Cretaceous between 125 and 80 Ma (Burke & Dewey, 1974, Fairhead, 1988), which is around the same time, or just prior to, the Congo Basin being elevated above sea level (Sahagian, 1988). The uplift associated with these structures would have produced drainage divides of the Cretaceous paleo-Congo. The shear zone would separate it from Lake Chad (which was much larger then than it is today, leading Burke (1976) to refer to it as Lake Megachad). This might have once been linked with the Benue river running in the rift related Benue Trough (Figure 8.11). The South Sudan rift would form the watershed between the Congo basin and what today is the upper Nile, but would in the Lower Cretaceous / Early Tertiary have been short rivers draining to the Indian Ocean that covered today's Ethiopia and eastern Sudan (Doucouré & de Wit, 2003; their Figure 9 reproduced as Figure 3.8 earlier in this thesis). A rift-related watershed has a steeper slope facing the rift than outside, and thus erosion rates will be greater into the rift valley, reducing the watershed's height and pushing it further out from the rift. This accounts for the Congo basin's northern boundary being tighter than the position of the tectonic structures in Figure 8.11. Furthermore, given that the Nile, the Congo and Chad drainage basins in that area exhibit fairly simple drainage patterns away from a linear divide, and it implies the watershed has not been breached since then, and if the Congo indeed drained into the Indian Ocean after the basin's uplift above sea level, its outlet could not have been in the northern part of the basin.

8.6. Flow Direction Reversal

Complete drainage reversal, or a case of a river changing its direction of flow, is a very rare, but not unheard of, phenomenon. Rivers in Alaska temporarily changed direction following the 1964 earthquake (Plafker, 1969), while Okay & Okay (2002) present a case for reversal of sections of the Maritsa river in Turkey and Greece. The section of Niger immediately 'downstream' from its inland delta in Mali might be the only present case of a river changing its flow direction seasonally (Burke, 1996).

The Zambezi model of Moore & Larkin (2001) summarized in Figure 8.8 assumes flow reversal of the middle section of the Zambezi (between today's Victoria Falls and the confluence with Luangwa, i.e. around the Gwembe Trough), which flows in opposite

directions in Figs. 8.8 b) and c). The authors attribute this reversal to headward erosion of the Lower Zambezi after its capture of the Luangwa. If such a reversal did take place, this is indeed the only factor that could have caused it. The section of the river is parallel to the OKZ flexural axis, while any uplift from East Africa could only stimulate southerly or south-westerly flow.

Thus consider the following scenario: in the Paleocene (Fig. 8.8b) a stream that used to be the lower-most Luangwa is flowing south-west towards Upper Zambezi. The land around the river will naturally slope the same way – it will obviously not be a constant gradient with no topographic features, but the first order trend should be clearly seen. If headward erosion by the Lower Zambezi, after it captured the Luangwa about halfway down its course, carries on along the Luangwa to its confluence with the Upper Zambezi and capturing it, the formerly-lower Luangwa would reverse its drainage, becoming the Middle Zambezi (Fig. 8.7). However, as no tectonic activity took place at the time, the land near the watercourse should still exhibit a trend lowering towards the south-west. Cross sections shown in Fig 8.12 show this is not the case – a trend down towards north-east is clear. The sections were taken on the north-western side (left bank) of the Middle Zambezi near the Lake Kariba, 30, 50 and 70 km from the river. The right bank was not considered, as the topography there is dominated by valleys of Zambezi's tributaries.

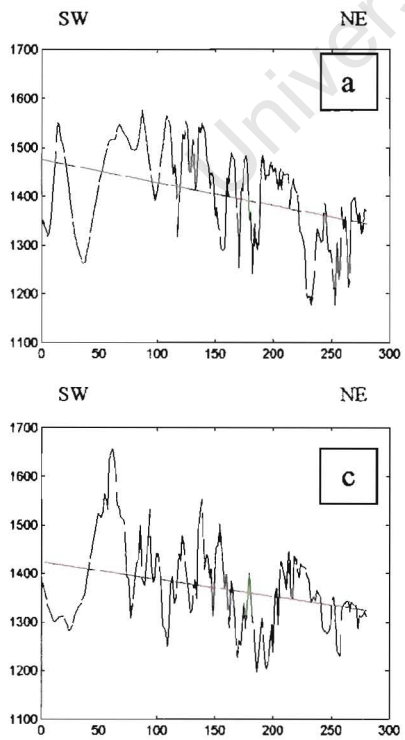

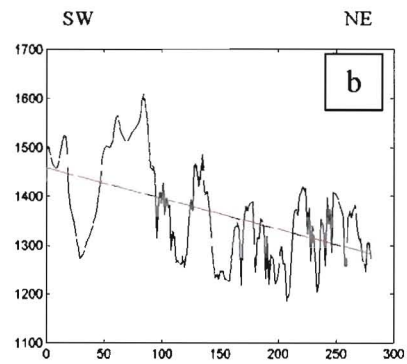

Fig. 8.12. Topography cross-sections parallel to the Middle Zambezi (going SW-NE) on the left bank of Lake Kariba. Distance from shore, and mean slope:

a) 30 km 0.469 m/km
b) 50 km 0.625 m/km
c) 70 km 0.351 m/km

Horizontal scale in km, vertical in m. Red lines show general trend slope towards the north-east, the direction of river flow today.

From these sections it seems unlikely that until recently the river flowed south-west. However, from the DEMs shown here it seems very plausible that the Middle Zambezi and the Luangwa were one river, as they are aligned in the same direction (Fig. 8.13). The suggestion made here is that they were indeed one river up to the Oligocene (~ 30 Ma), but flowing north-east rather than south west. During the uplift of East Africa in the Oligocene the area where Luangwa's headwaters are found today would have been uplifted enough to initiate a drainage reversal. This would have caused the Zambezi-Luangwa system to be landlocked, until Lower Zambezi's capture of the system. This suggestion is supported by the fact a number of tributaries of the lower Luangwa make obtuse angles with the main river – the same evidence Okay and Okay (2002) provide for their study of the reversal of the Maritsa river.

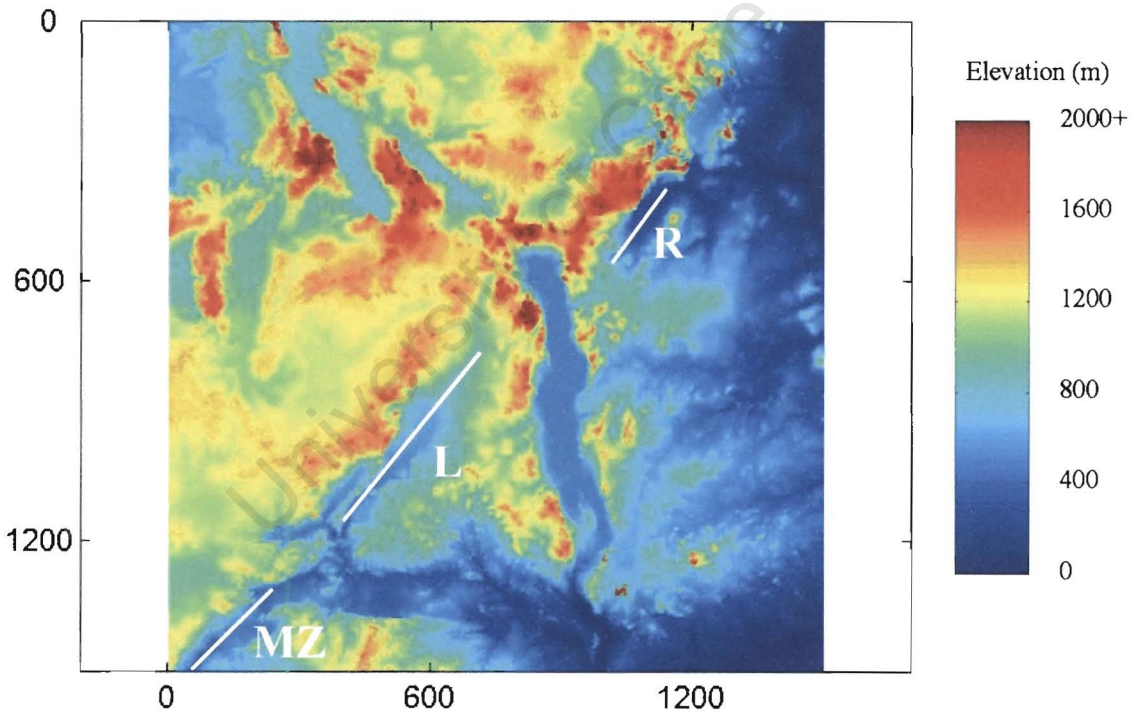

Fig. 8.13. DEM of the area between the Gwembe Trough (Lake Kariba) and Rufiji. White lines show how directions of Middle Zambezi (MZ), Luangwa (L) and Upper Rufiji (R) seem to be aligned. Horizontal distance in km, elevation truncated at 2000m.

8.7. Proposed Model for Drainage Evolution since the Cretaceous

Based on the observations discussed earlier, a model for drainage evolution in Central Africa is suggested here. Accepting that the Congo Basin drained to the Indian Ocean in the Cretaceous, the major trunk stream would have been located somewhere in the eastern side of the basin. The Lualaba (Fig. 8.3 and 8.4) seems to be the most likely candidate for that role. It follows a deep valley, slightly to the west and roughly parallel to Lake Tanganyika. The valley stretches farther east than any other in the region, and its size cannot be attributed to its drainage basin area today. It is therefore proposed the Lualaba drained south, towards its junction with Nonda (Fig. 8.3). It is furthermore suggested that the Nonda drained north-east even then. The combined streams then proceeded to flow first south-east, and then east, across where today the East African Rift Valley is found, following a course today taken by a upper Lualaba. This river then meandered to the Indian Ocean, the antecedent gorge of the Ruaha tributary of the Rufiji being the likely route, ending its journey at the Rufiji Delta, in turn explaining the Delta's size that is too big to have been built up by the present day Rufiji.

Shortly before reaching the Rufiji delta this Cretaceous river would be joined by a major tributary, the Middle Zambezi – Luangwa, which was likely to be the same river as the upper (southern) Rufiji. The Luangwa and Rufiji valleys are aligned in the same direction (Fig. 8.13), and the slight displacement can be attributed to separation during subsequent extensional spreading in the East African Rift. This would also account for the size of the upper Rufiji valley (Fig. 8.9 and 8.10). The Chambeshi (Fig. 8.7) is also likely to have flowed north-east at that time, either joining the Luangwa, or flowing directly into the pre-Congo. This proposed Cretaceous drainage pattern is shown in Figure 8.14.

At some stage during the uplift of East Africa, the Luangwa (except for its then lowest reaches), the flow direction of the Chambeshi, and the main trunk stream of the pre-Congo, would be reversed. The Luangwa would form a landlocked system with the Middle Zambezi until the capture by Lower Zambezi would redirect it into the present site of the Zambezi Delta. The lowest parts of the Luangwa, just before its confluence with the pre-Congo would have been on the eastern side of the uplift, and the drainage direction would not be affected. However, the drainage area reaching this valley would have been greatly reduced, leaving a relatively small river in a huge river valley – the

upper Rufiji seen today. The Chambeshi would also have its drainage reversed and become landlocked (possibly originating Lake Bangweulu). This system would be captured first by the Kafue to become part of the Zambezi network, and then by the Luapula, to become part of the new Congo network. The old trunk stream of the paleo-Congo would be a first-order stream draining the newly uplifted regions. Reversal of the Lualaba would make the Congo a huge inland draining basin. This is consistent with the hypothesis of Burke (1996) which suggests such a landlocked system was captured by a small west flowing river to produce the Congo Basin and the present delta of the Congo on the Atlantic coast as they are seen today.

Reeves *et al.* (2004) suggest that around the time of separation of Africa from South America (~ 110-130 Ma), the new Atlantic coastline was similar to the East African Rift system. Thus on either side of the proto-Atlantic a band of highlands would exist, like the branches on either side of the East African rift valley. These highlands on the African side would form the western boundary of the paleo-Congo. To the west of this divide short rivers would drain into the newly formed Atlantic Ocean. These would erode into the highlands, to form rivers like Oguoe and KNR. In due course one of these Atlantic-draining rivers would break through the divide, thus capturing the Congo Basin. It is possible that more than one stream broke through the watershed and different parts of the basin drained through different outlets. This might explain 2 active sources of deposition identified by Uenzelmann-Neben (1998). Such stream would compete with each other, and a series of captures would eventually produce the pattern seen today.

This drainage evolution model is summarized in Fig. 8.15. A possible way to test it further would be to analyse the sediment history of the Rufiji Delta, in a way similar to the seismic studies of Uenzelmann-Neben (1998) of the Congo Delta discussed earlier. Attempts to obtain such seismic sections to be included in this study were not successful.

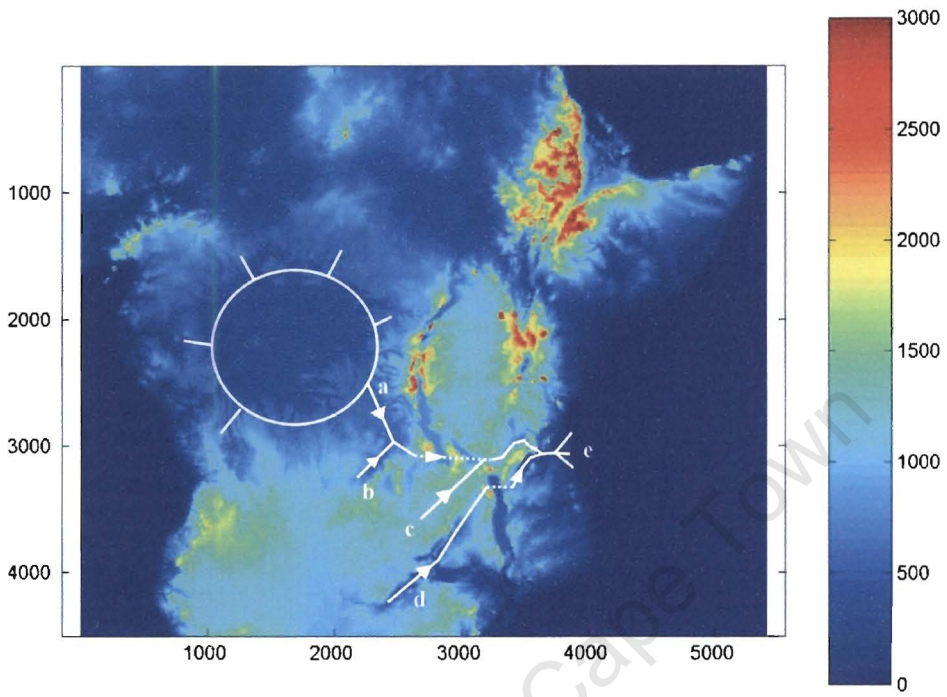

Fig. 8.14. Proposed drainage model for the Late Cretaceous Congo. Detailed drainage inside the Congo Basin (marked with a circle) is not clear, but the Basin would receive drainage from the older erosion surface (today at 610m). Solid lines mark rivers of today, dashed lines go across post-Eocene (< 35 Ma) volcanic highlands. Elevation in metres.

a) Lualaba
b) Nonda
c) Chambeshi
d) Middle Zambezi / Luangwa
e) Rufiji Delta

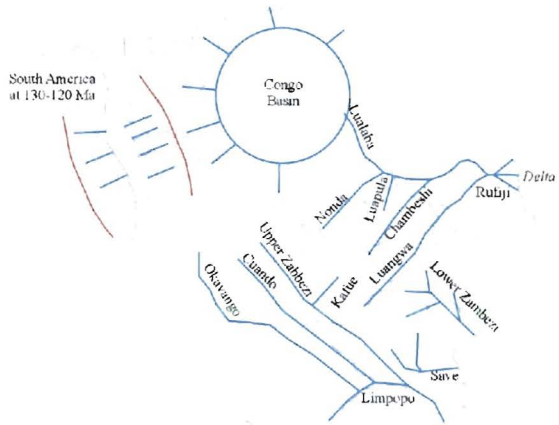

Upper Cretaceous (100-65 Ma)

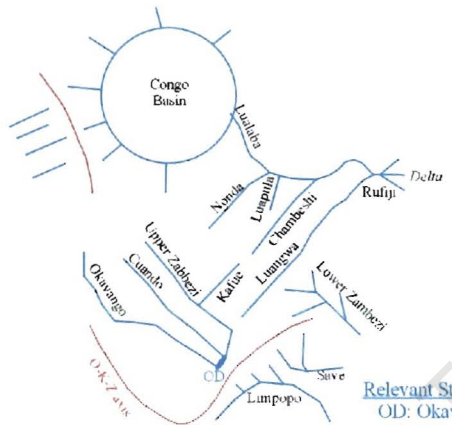

Paleocene (65-55 Ma)

Relevant Still Water Bodies:
OD: Okavango Delta
GT: Gwembe Tough
LB: Lake Bangweulu

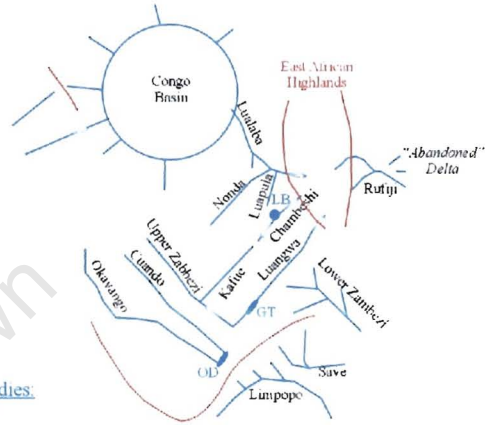

Pliocene (5-1 Ma)

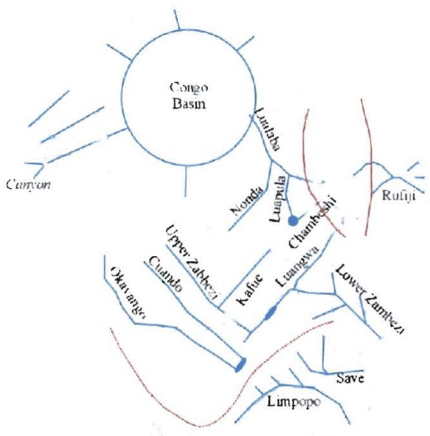

Pleistocene (~1 Ma)

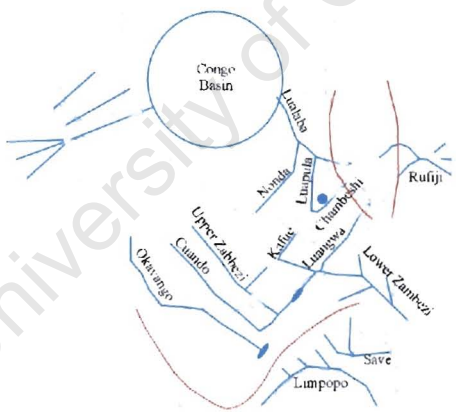

Present Day

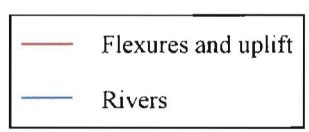

Fig. 8.15. Central African drainage evolution model proposed in this study. The Cretaceous drainage towards the new Atlantic coast would have had its "reflection" on the other side – the coast of South America has been included to show this in the first figure. The rift that led to the break-up of America and Africa was similar to the East African Rift ~100 million years later (Reeves *et al.* 2004). Major rivers and lakes occurred along this uplift until at least 120-110 Ma.

In the Paleocene the proposed Cretaceous drainage changes due to the OKZ flexuring, "beheading" Limpopo and transforming the Okavango-Cuando-Upper Zambezi into a landlocked system. At the same time the watershed separating the Congo Basin from the rivers draining into the new Atlantic Ocean moves eastwards.

During various rifting and uplift episodes in East Africa many changes would have taken place, but by the Pliocene Rufiji would be "beheaded", and Chambeshi and Luangwa (which would have earlier captured Upper Zambezi) would become landlocked. Lualaba would also be reversed due to the uplift, making the Congo Basin landlocked until the watershed to its west was breached. By the Pleistocene, the Chambeshi would be captured, first by Kafue, and then by Luapula (see also Fig. 10.4). Similarly, the Luangwa-Upper Zambezi would be captured by the Lower Zambezi. Further captures of the Cuando and Kafue would produce the pattern observed today.

Chapter 9

The Nile and Northern Africa

9.1. Introduction

The Nile (Fig. 9.1) is one of the longest river systems in the world. It is by far the longest river in Africa, at 6230 km nearly twice as long as the main streams of either the Congo or the Niger. Its basin area (3,360,000 km^2) is second only to the Congo on the African continent. The main tributaries of the Nile are the White Nile, originating in the western arm of the East African Rift Valley, and the Blue Nile, with its source around Lake Tana in the Ethiopian Highlands. Sometimes the upper reaches of the White Nile, upstream from the confluence with Bahr el Arab, are referred to as the Albert Nile (Fig. 9.1). The Nile basin is spread over 11 independent countries, with its watershed also partially forming the boundary of Central African Republic.

While most of the upper reaches of this river system are perennial (Fig. 9.2), the only perennial section in Egypt and northern Sudan is the main stream of the river, the tributaries only flowing episodically. Such tributaries, termed *wadis*, sometimes form extensive networks, and can be separated from the main stream by a considerable distance. An example of this is the Wadi Howar shown in Fig. 9.1 and 9.2. These *wadis* are remnants of ancient rivers, which could have in the past formed perennial networks with the Nile or another river system.

While some sections of the Nile network are claimed to have originated in the Cretaceous (Berry & Whiteman, 1968), the Nile as seen today is a young river. The uplands associated with the East African and Ethiopian rifts that form much of the basin have mostly originated in the Oligocene (e.g., Shackleton, 1978; Hofmann *et al.*, 1997). The opening of the Red Sea, and the uplift on the sea's west bank that separates it from the Nile, is even younger. In places streams originating less than 30 km from the Red Sea

flow in the opposite direction and reach the Mediterranean at the Nile Delta. Its south-western watershed with the Congo was suggested in an earlier chapter (using data of Fairhead, 1998) to be a result of the Cretaceous age West and Central African rifting, while very little is known about the Nile's western watershed with the Chad Basin (see McCauley *et al.*, 1982, for a review).

A feature always associated with the Nile is the ancient Egyptian civilization that relied on the river as a water source. Aspects of its history, including its sudden collapse, are by no means beyond the scope of Earth Science, and will be mentioned later.

9.2. Green Sahara

During the Holocene, the last 10 thousand years, the Earth's climate has changed significantly. North Africa, the area we are concerned with in this chapter, had a much wetter climate than today. Land-surface conditions and water balance evolution models (e.g. Yu & Harrison, 1996; Hoelzmann *et al.*, 1998) suggest the lake status in North Africa at 6 ka was as much as 15 times higher than at present. Over two-thirds of that mid-Holocene lake area would have been paleo-Lake Chad, which Schneider (1967, in Burke, 1976) estimated at 330,000 km^2, 13 times its size in 1967. Pollen and plant fossil reconstruction (Jolly *et al.*, 1998) shows the Sahara was covered by grasses at that time.

Obvious questions about the drastic change between the Sahara then and now are when it took place, how long the transition was, and what caused it. It has been suggested (Petit-Maire & Guo, 1996 in Claussen *et al.*, 1999) that this transition was not gradual, but occurred in two rapid arid episodes, between 6.7 and 5.5 ka, and between 4 and 3.6 ka. These episodes could correspond to two significant events in the history of ancient Egypt. In the Predynastic period most of North Africa was inhabited. At around 6 ka the population started to concentrat around the Nile, leading to the formation of the Old Kingdom. This might have been in response to the first arid episode, which would lead to drying up of smaller water bodies and leaving the Nile and its surrounding wetlands as the only source of water (Krom *et al.*, 2002). The Old Kingdom collapsed at 4.1 ka due to, among other factors, a drastic climate change, drying up of many lakes some as deep as 65 metres before, and the annual Nile flood failing for 30 years in a row (Hassan, 2001). This would have been in response to the second arid episode.

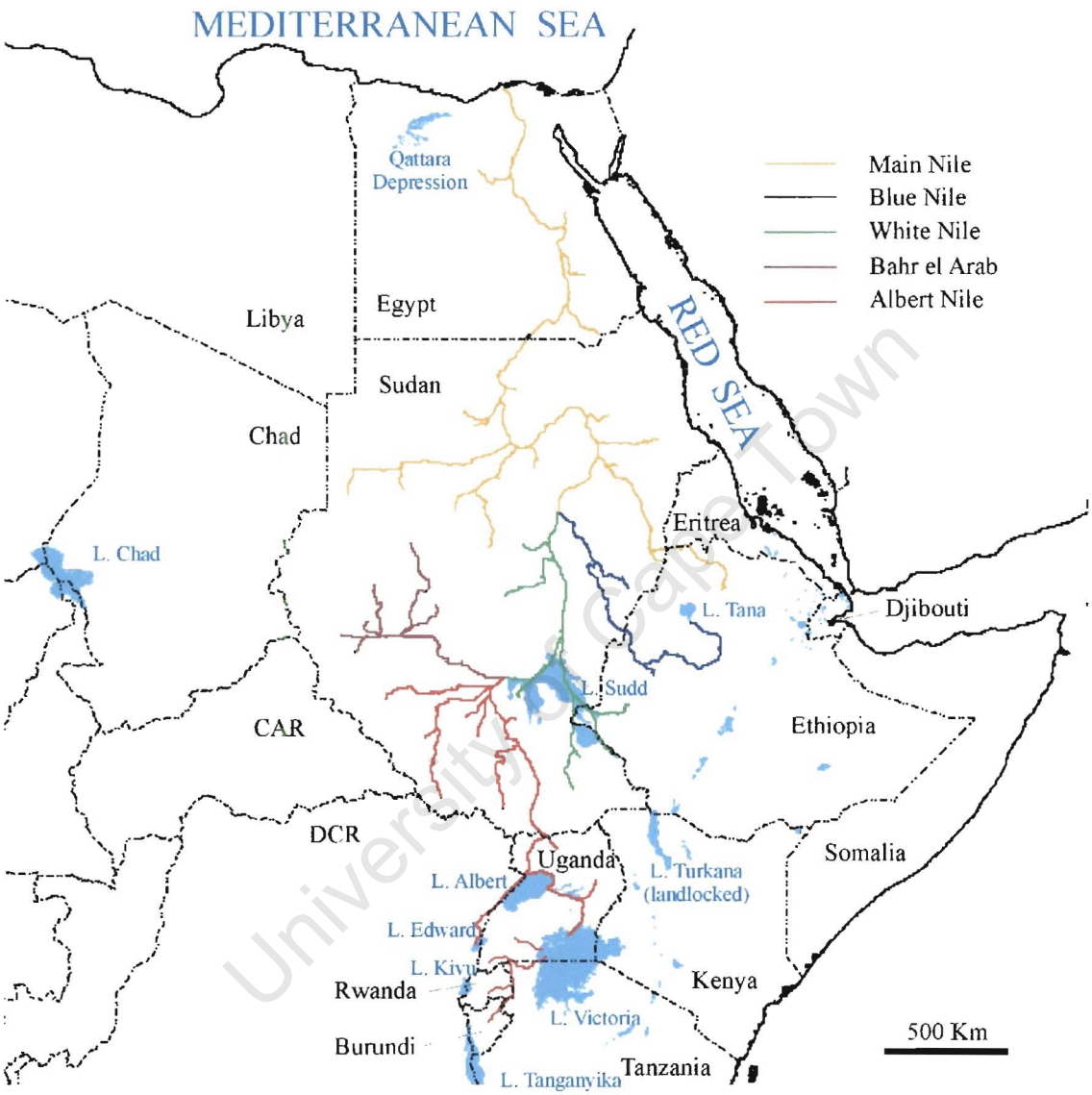

Fig. 9.1. Main streams in the Nile River basin. Lakes in the region are marked in blue, and major/important ones are labeled in the same colour. Note that some maps refer to White Nile, Albert Nile and Bahr el Arab collectively as the White Nile.

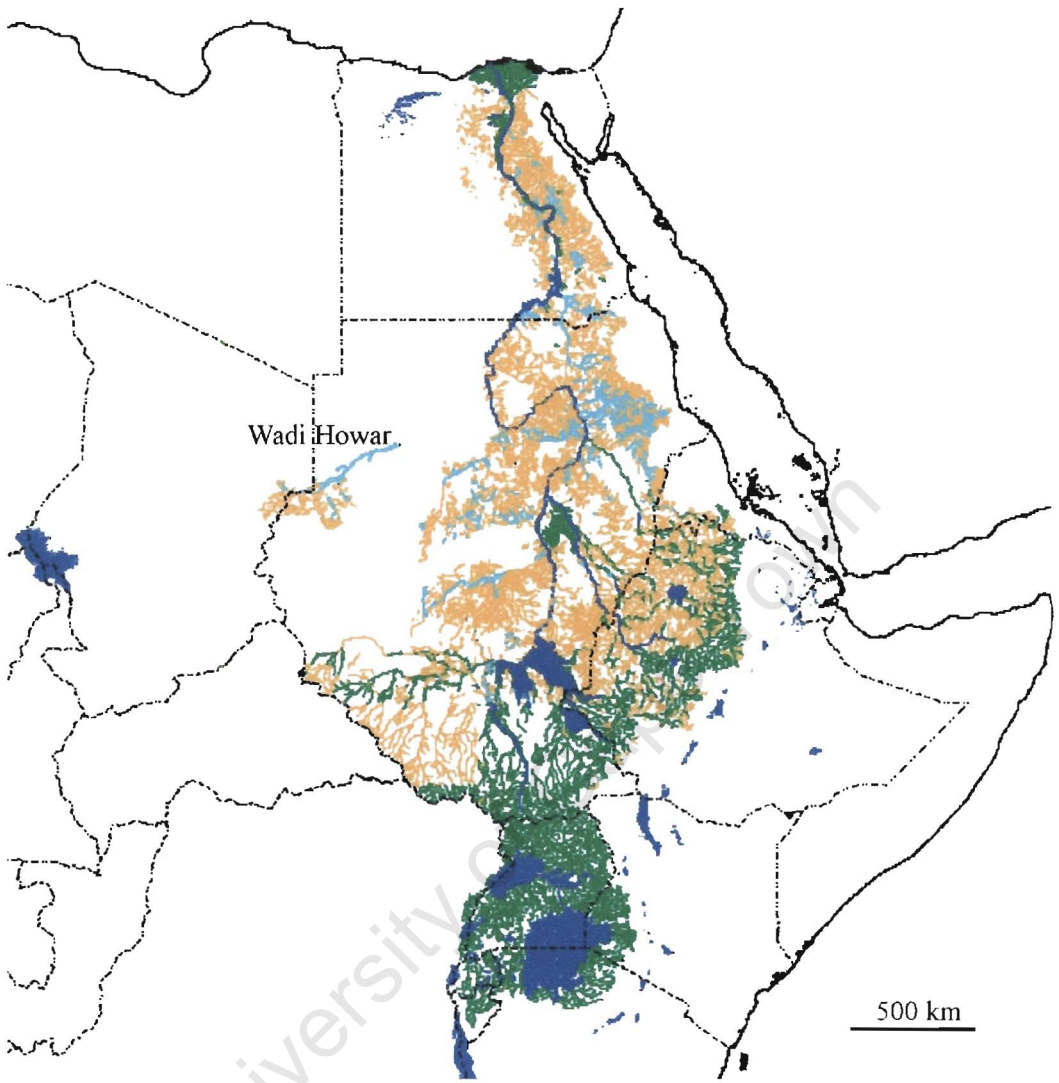

Fig. 9.2. Different types of waters in the Nile basin:
Green: perennial streams
Orange: non-perennial streams
Dark Blue: perennial shorelines
Light Blue: non-perennial shorelines

Note Wadi Howar originating on the Chad-Sudan border. There exists a channel linking in to the Nile (as in Fig. 9.1), but water has never been recorded in it, so here it is not even considered as a non-perennial stream, and the Wadi appears to vanish well short of the main Nile channel.

Holocene climate changes have been suggested to be a result of changes in the Earth's orbit and tilt axis (Kutzbach & Guetter, 1986). Claussen *et al.* (1999) use results of Berger (1978) to show that the mean summer insolation of the Northern Hemisphere has gradually decreased from 470 to 445 W/m^2 over the last 9000 years. The stronger insolation would amplify the summer monsoon. To explain how a gradual decrease in the insolation could result in abrupt changes in the climate and vegetation, Claussen (1997) proposed a feedback mechanism between climate and vegetation that would amplify the results of orbital forcing. This model is based on theory of Charney (1975) in which 'a desert feeds upon itself' due to the sandy barren areas having higher albedo than soil covered by vegetation, resulting in a desert reflecting more radiation than its surroundings. Furthermore, the desert surface is hotter, and the air above it less cloudy than in the surrounding vegetated areas. The combined effect of these factors is that the desert acts as a 'radioactive sink'. Missing from this model is the response of vegetation to the change in precipitation, and the reverse flux of atmosphere's response to a change in vegetation. This led Claussen (1997) to reassess the problem of desert dynamics by using a coupled atmosphere-biome model. To analyze the feedbacks, Ganopolski *et al.* (1998a, 1998b) performed a number of computer simulation experiments. The results for North Africa are presented in Claussen *et al.* (1999) for the last 9000 years (over which time the insolation drops steadily by 5%). They find the rainfall to decrease in discrete jumps between 6 and 4 ka, while the vegetation cover decreases from 70% of surface areas to near zero between 6 and 4.5 ka.

Thus there is evidence from scientific studies and models, as well as history, that the climate and vegetation on Northern Africa have changed drastically at a rate fast enough to affect the social structure of people inhabiting the area at the time. In an age where water constitutes one of the most essential natural resources, questions like "Will Sahara become green again" and "Will other regions become desertified" should be addressed very seriously by earth scientists.

9.3. Paleo-drainage in the Sahara

With the evidence presented above for a green Sahara as recently as 6000 years ago, it seems reasonable to assume that the area was drained by river networks in the past. Burke *et al.* (2003) present a map of possible African drainage pattern in the Upper Cretaceous (their Fig. 16), and the northern section of that map is reproduced here as Fig. 9.3. It clearly shows rivers draining most parts of the region. However, Doucouré & de Wit (2003) show in their reconstruction of the African topography that in the Cretaceous (their Fig. 9, discussed earlier in this thesis and reproduced as Fig. 3.8), the area of today's Nile (except its upper-most reaches) was below sea level. This is confirmed by the presence of Cretaceous and Paleocene marine sediments throughout North Africa, some as young as 55 Ma (Fig. 5a of Doucouré & de Wit, 2003). This is further supported by evidence for minimal global ice cover, and therefore high sea level, during the Cretaceous (e.g. Hubert *et al.*, 2002). Said (1981) suggested that sections of north-east Africa were submerged as recently as 40 Ma. It therefore seems unlikely there existed a well developed drainage network in North Africa prior to the onset on Cenozoic volcanism in north-east Africa.

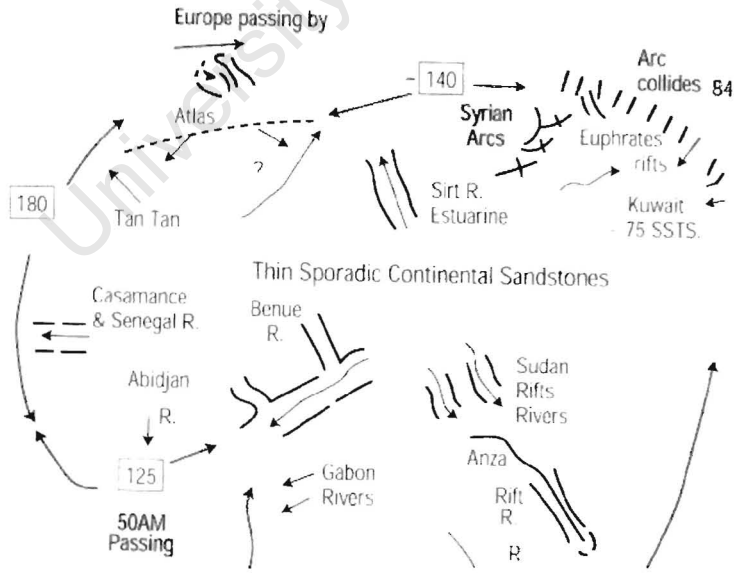

Fig. 9.3. Major rivers in North Africa and Arabian Peninsula in the Cretaceous, from Burke *et al.* (2003). Evidence from marine deposits and glacial levels referenced in the text suggests large parts of this area was submerged at least until the Eocene (~55 Ma, or possibly even ~40 Ma – see Chapter 3 and Fig. 3.8).

9.3.1. Cenozoic Volcanism in North Africa: Mantle Plumes, Rifting and Drainage

A careful examination of volcanism and tectonics in North and East Africa can be useful in attempting to reconstruct the paleo-drainage pattern. Cox (1989) shows what drainage patterns would develop as a result of plume-induced continental uplift. Moore & Blenkinsop (2002) readdress Cox's model and provide a more detailed one, which includes superposition of plumes of varying age. The plume-induced drainage was discussed in Chapters 3 and 4 (Orange and Limpopo drainage). Burke & Dewey (1973) show how 3 tectonic axes will develop over such uplift, meeting in the centre of the plume and separated by 120° – effectively a failed triple junction. In the South African example (Karoo Plume, ~180Ma) the 3 axes are the Sabi and Lebombo monoclines, and a dyke swarm linking the Okavango Delta with the Lower Limpopo. This dyke swarm marks the rift that would have been the valley of the Cretaceous Okavango-Cuando-Limpopo river system (Fig. 8.8). In theory, between these 3 tectonic axes, streams should flow radially outwards (downhill) from the elevated plume center (e.g., Cox, 1989). A schematic diagram of this model is shown in Fig. 9.4.

In North and East Africa, 2 such failed triple junctions have been identified (Fig. 9.5a). The Benue Rift, forming the valley of Benue River which joins the Niger about 200 km upstream from its delta, forms such a junction with the Niger valley and the coastline of Africa south of the delta (Burke *et al.* 1971). These authors date this as mid-Cretaceous (~ 100 Ma). Reeves *et al.* (1986) show a 'remarkable similarity' between the tectonic maps of the Benue valley and the Anza Trough between Kenya and Somalia. They interpret this as a Jurassic triple junction. The other 2 axes are the rifts along the coastlines of Kenya and Somalia, which led to the break-off of Madagascar. This break-off is described in detail by de Wit (2003). The Anza Trough was the site of much sediment deposition until its recent failure in the (Upper) Tertiary. Substantial delta-like sediment deposition has also taken place at the Lamu Embayment, where trough meets the Indian Ocean (Reeves *et al.*, 1986). This evidence, as well as the Anza Trough's similarity with the Benue Trough, suggests that until recently the trough contained a major river.

Another plume induced triple junction is currently developing in the region. The three axis/rifts here are the Red Sea, the Gulf of Aden and the Main Ethiopian Rift (MER) – Fig. 9.5a. Whereas the Ethiopian flood basalts associated with this plume (Richards *et al.*, 1989) have been dated at ~ 30 Ma (Hofmann *et al.*, 1997), most recent sea-floor spreading in the Gulf of Aden is only ~ 5 Ma old (Ebinger & Sleep, 1998).

Not all rifts in the area are failed triple junctions. The West/Central African Rift system was discussed in Chapter 8 of this thesis, and its features relevant here have been included in Fig. 9.5a. These are Cretaceous in age. During that rifting episode the older Anza Rift would be re-activated, and possibly join with the South Sudan and White Nile rifts (Browne & Fairhead, 1983). If this was the case, it is likely that once the area was elevated above sea level in the Eocene, rivers in these two Cretaceous rifts would join to form the Anza River, as implied by Burke *et al.* (2003; see Fig. 9.3). In all probability the Central African Shear Zone would form the north-western watershed of this system.

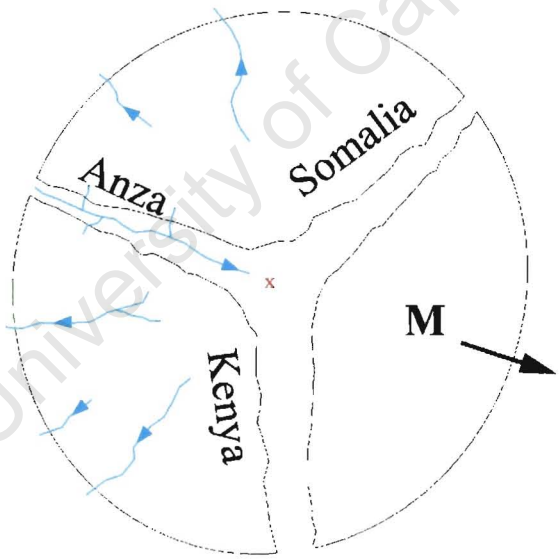

Fig. 9.4. Plume-induced drainage model of Cox (1989). The x marks the plume centre, and the circle the topographic extent of the uplift. It is broken by 3 axes separated by ~ 120° (Reeves, 1978). Blue lines indicate drainage: centripetal on the slopes of the induced uplift, and along the rift in the axis.
This example shows the case similar to the East African plume (Reeves *et al.* 1986). One axis becomes a river (Anza), the other 2 become coastlines (of Somalia and Kenya, respectively), as ⅓ of the area moves away like Madagascar (**M** and black arrow).

Fig. 9.5a. North-east Africa as seen today, showing selected (relevant) volcanic and tectonic structures, as well as the underground valleys in NW Sudan found by radar survey. Triple junctions discussed in the text are labeled TJ at the centre in the colour corresponding to their age. G.K.P. is the Gilf Kebir Plateau.

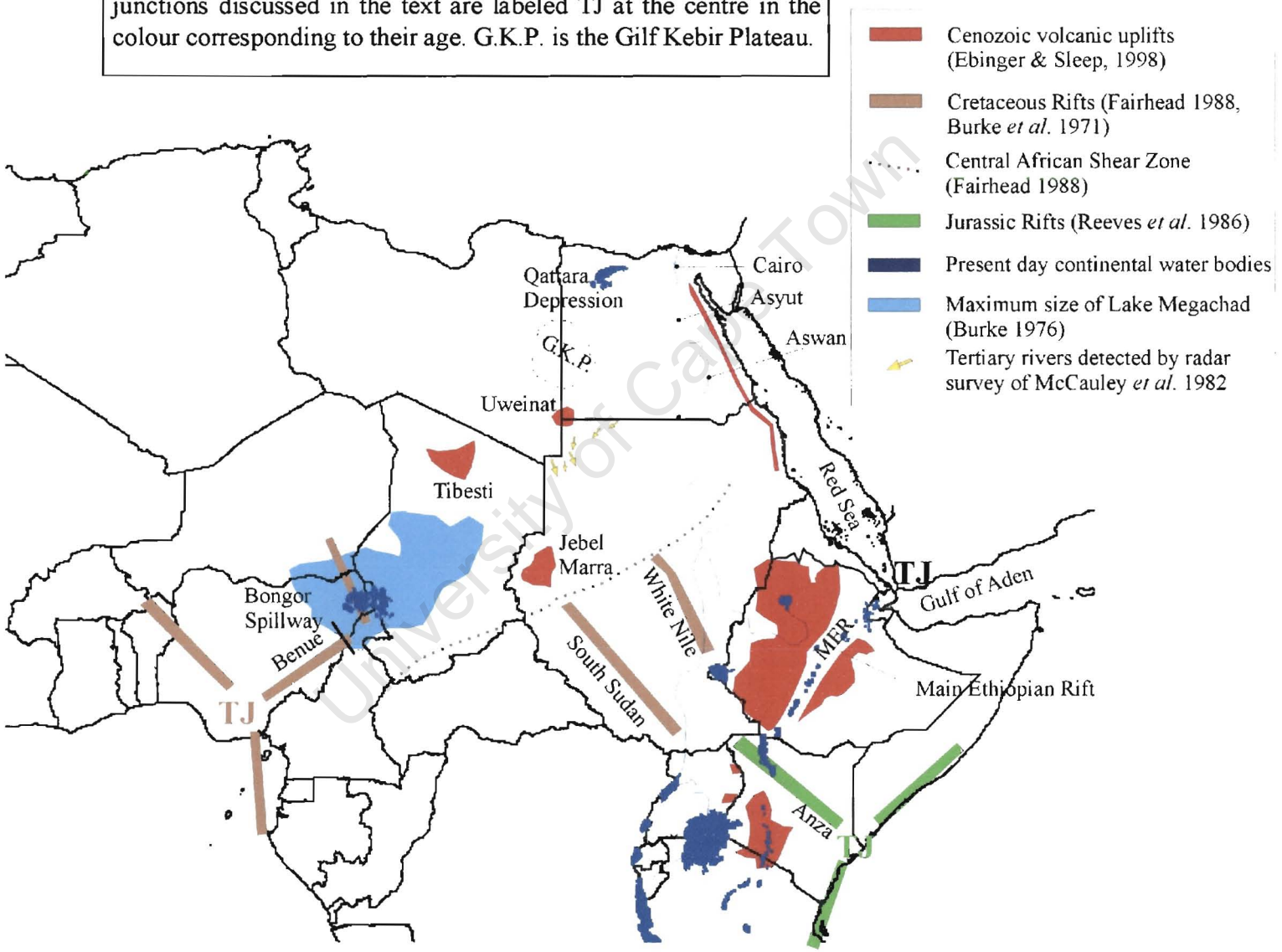

Fig. 9.5b. Proposed Late Eocene (~35 Ma) drainage in north-east Africa. Trans African Drainage System (TADS) and drainage north of the Abu Ballas divide are taken from McCauley *et al.* (1986). Size of arrows (flow direction) corresponds to approximate volume of flow. Green (proposed) and yellow (radar) arrows have different scales.

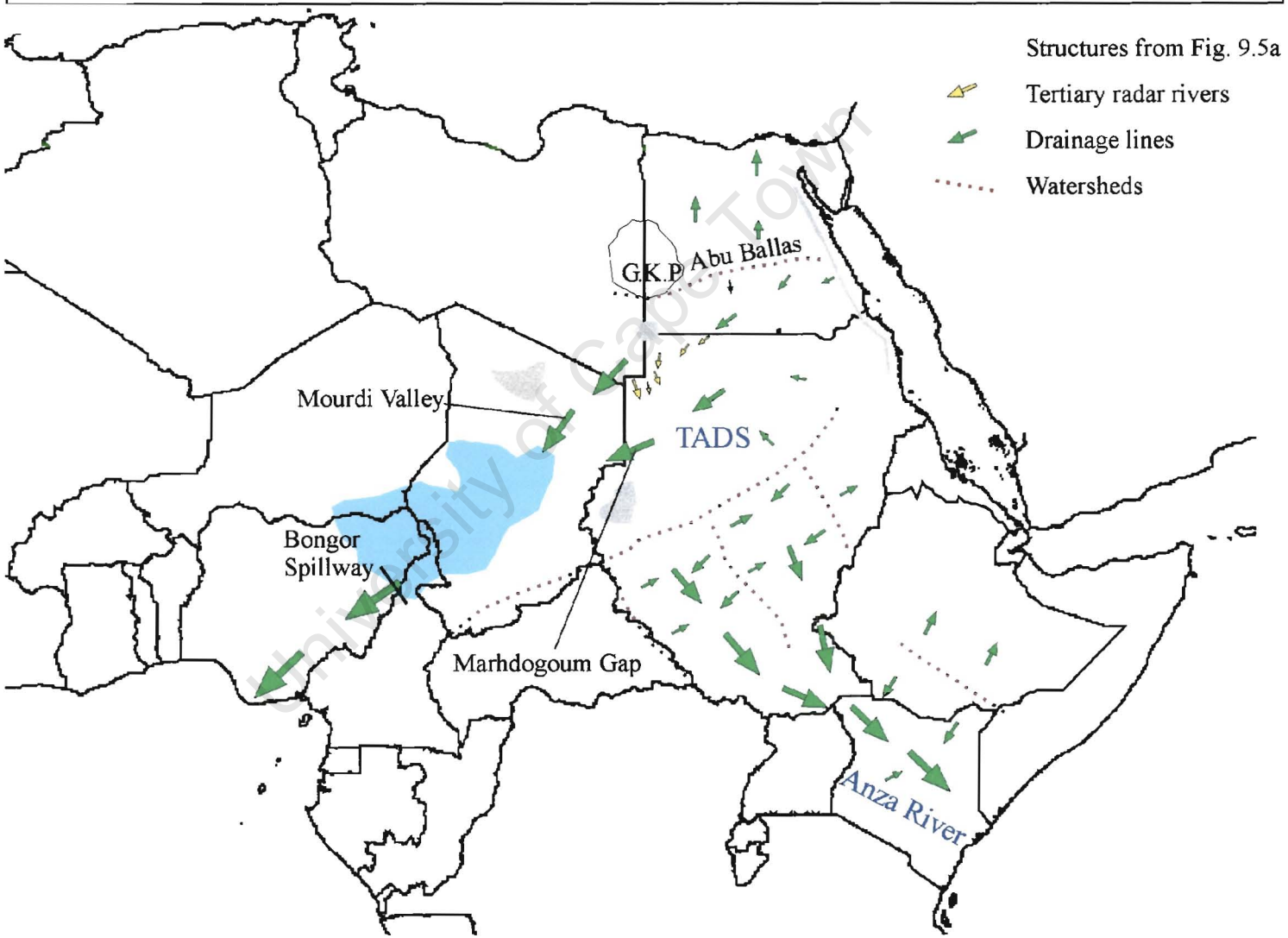

Fig. 9.5c. Proposed Oligocene (~24 Ma) drainage in north-east Africa. Note the beheading of Anza, resulting in deflection of "South Sudan Rift River" into the Congo Basin, and "White Nile Rift River" becoming landlocked.

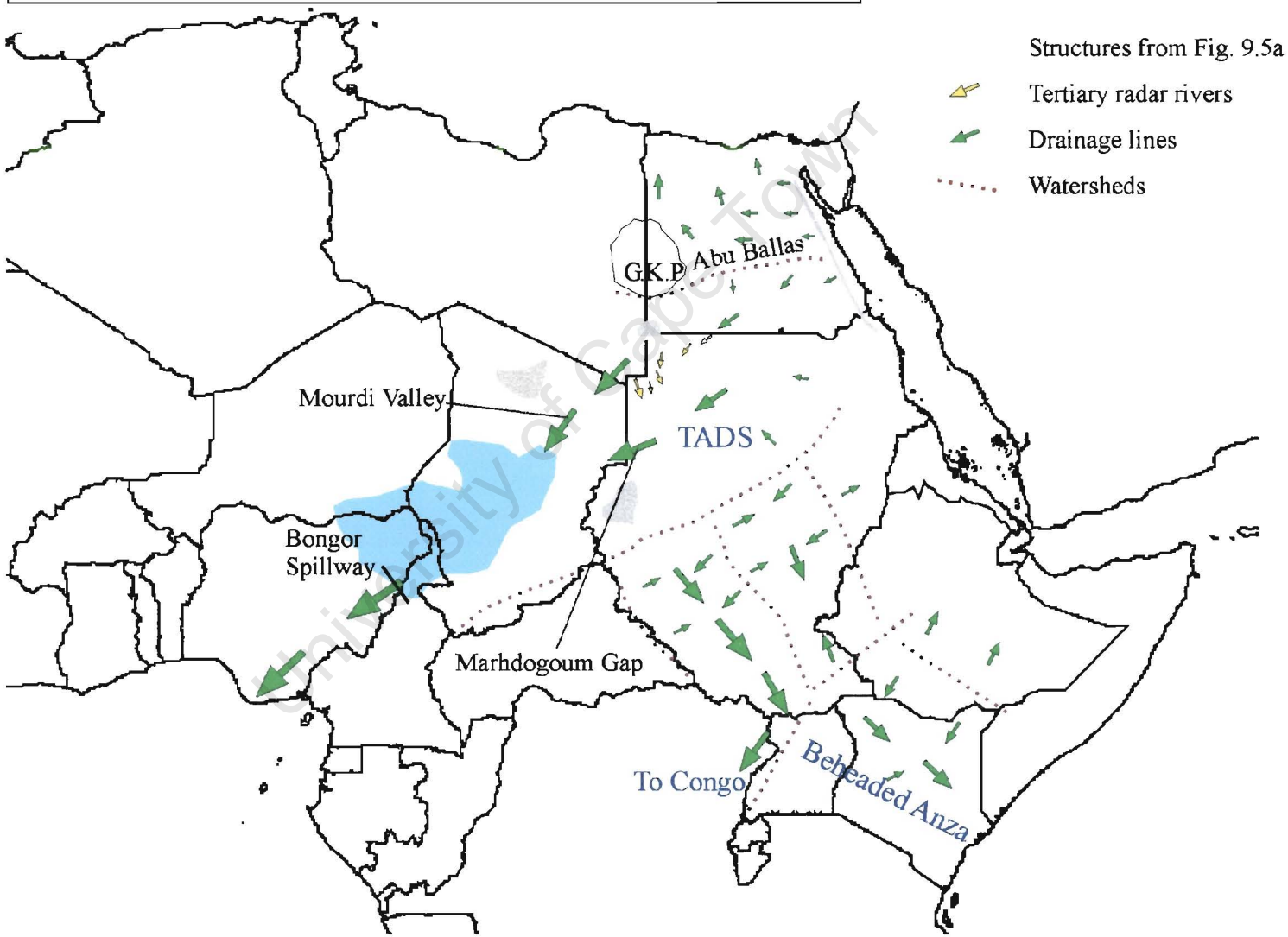

Fig. 9.5d. Proposed Late Miocene (~10 Ma) drainage in north-east Africa. Note development of south-flowing Qena in eastern Egypt, "South Sudan Rift River" becoming landlocked by the development of the western rift, and TADS and Chad basins becoming separated due to volcanism.

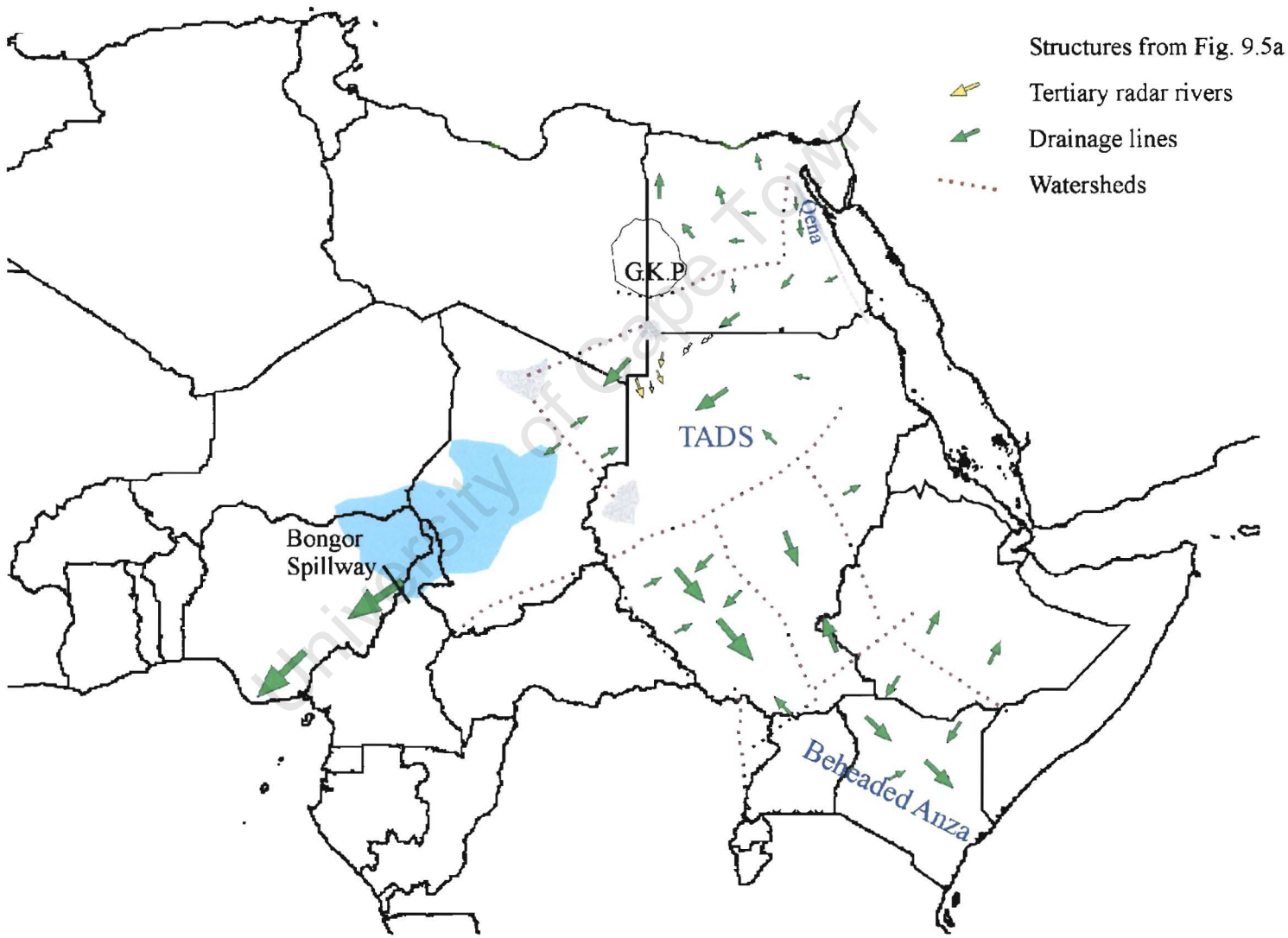

Fig. 9.5e. Proposed drainage in north-east Africa at ~0.4 Ma. Note the north-flowing Eonlie capturing the former TADS across the Abu Ballas, of which only Gilf Kebir Plateau remains. Qena still flows south, but after joining the Nile its waters turn north. White Nile Rift is occupied by a lake. The Anza rift is shown as blocked from the Indian Ocean with a landlocked Lake Turkana, but this status alternated.

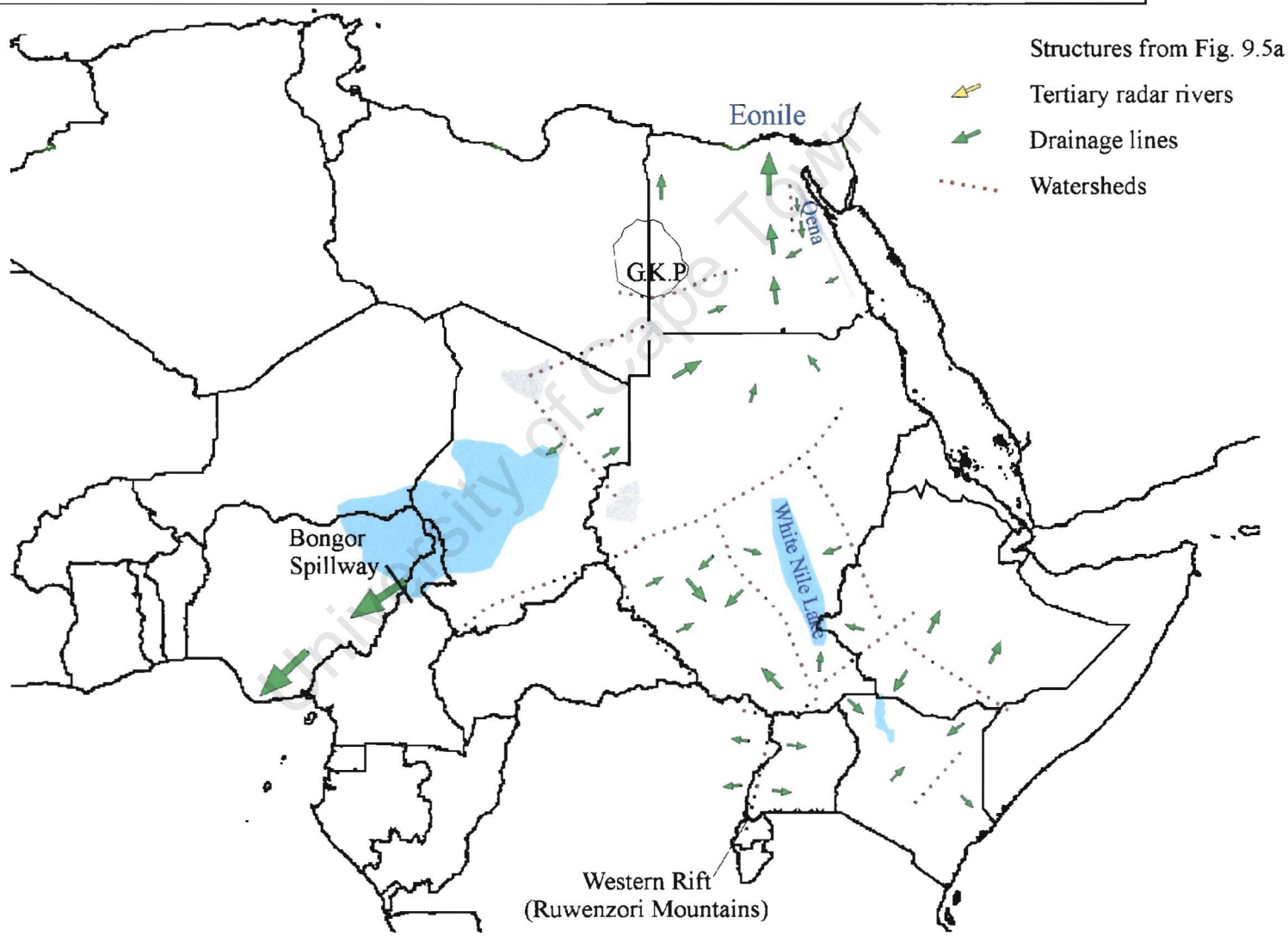

9.3.2. Subsurface River Valleys of the Eastern Sahara

A subsurface radar survey in Sudan and Egypt (McCauley *et al.*, 1982) found evidence for large valleys in north-western Sudan. Some of these subsurface valleys are nearly as wide as the main Nile channel today. These authors suggest these mid-Tertiary in age (~30 Ma). These valleys provide one of few clues for reconstruction of drainage in the Sahara. The valleys are included in Fig. 9.5a. However, this data must be treated with care. Hoelzmann *et al.* (1998) show that most of the postulated streams would have been occupied episodically, and it is unlikely that they were all flowing simultaneously.

9.3.3. Lake Megachad

It was already mentioned that in the past Lake Chad was much larger than today (Fig.9.5a). Burke (1976) shows that on reaching Schneider's (1967) estimated size of 330,000 km^2, the water level would reach 320 metres above (today's) sea level, and the waters would spill into the Benue River at Bongor (Grove & Warren, 1968). Burke (1976) goes on to suggest that the size of this Lake Megachad would fluctuate episodically, and the lake would alternate between being landlocked and draining to the Atlantic via the Benue.

9.3.4. Eocene-Miocene paleo-drainage

To explain the origin of the river valleys found by the radar survey of McCauley *et al.* (1982), McCauley *et al.* (1986) proposed the concept of an Eocene south-west flowing trans-African drainage system (TADS – Fig. 9.5b). A topographic study of Breed *et al.* (1982) showed that the Gilf Kebir Plateau was major drainage divide in the Eocene and that the Gilf Kebir is a small remnant of a major Tertiary divide that extended through south central Egypt (Fig. 9.5b), termed the Abu Ballas divide by McCauley *et al.* (1986), from which they propose the northern headwaters of TADS originated. To the East the system would be bound by the uplift associated with the Red Sea rifting, and in the south the Central African Shear Zone would separate it from the rift inherited Anza River system. The TADS would flow into Lake Megachad through the Mourdi Valley, or the Marhdogoum Gap, between the Tibesti and Jebel Marra volcanic uplifts, and, depending

on the water level of the lake, the waters would stay there, or carry on to the Atlantic via the Benue.

This model is severely criticized by Burke & Wells (1989), who propose a model in which the valleys found by the radar survey flow eastwards into a major north-flowing river much like the Nile today. According to this model the Nile-Chad watershed has existed since the beginning of the Tertiary. The main point of this critique is the assumption of the existence of a major north-flowing river in Sudan and Egypt, 'established by early Tertiary' and 'well established by mid-Tertiary'. One of the facts quoted in support of such a river is the result of Zaghloul *et al.* (1979) that the formation of a major delta in northern Egypt began in the late Oligocene (~25 Ma). Burke & Wells interpret this as the delta of a north-flowing proto-Nile, which would make it impossible for drainage from the Red Sea Hills to reach Lake Chad. Another point made by these authors is that volcanic uplifts of Uweinat, Jebel Marra and Tibesti (Fig. 9.5a) would present major obstacles for a west trending drainage system.

One of the key issues in determining the Sahara paleo-drainage is thus establishing the age of the major north-flowing river in Egypt. Burke & Wells (1989) quote a suggestion by Berry & Whiteman (1968) that such a river existed in Early Tertiary. Bown *et al.* (1982) examined local stratigraphy, sedimentology, and paleontology, and conclude there exists no evidence for the alleged Tertiary proto-Nile before the Miocene. McCauley *et al.* (1986), in developing the TADS, present north-flowing drainage north of their Abu Ballas extension of the Gilf Kebir. While some of these rivers reached the Qattara Depression (Said, 1981), it is possible that others originated the deposition of the proto-Nile delta near today's Nile Delta, explaining the results of Zaghloul *et al.* (1979) mentioned earlier. Issawi & McCauley (1992) identify 3 depocentres at ~24 Ma (Oligocene). They propose these to be outlets of rivers originating in the Red Sea Hills, flowing westwards and turning north to reach the Tethys Sea (~200 km inland of the current Mediterranean coast). The Oligocene drainage in the area is shown in Fig. 9.5c.

Since the Oligocene the TADS headwaters have been eroding the southern edge of the Abu Ballas. The most prominent erosion took place furthest east, parallel to the Red Sea rifting (Issawi & McCauley, 1992). Remnants of that river are clear to see today in the

form of Wadi Qena, over 300 km long. This valley would have beheaded the 3 streams flowing into the Tethys (Fig. 9.5d).

Another point that needs to be carefully addressed is the ages of Tibesti, Jebel Marra and Uweinat uplifts. McCauley *et al.* (1986) attribute the disruption of TADS and the formation of the Nile-Chad watershed to the formation of the two former massifs. Burke & Wells (1989), on the other hand quote the value of Schandelmeir *et al.* (1983) of 45 Ma for magmatism at Uweinat to argue this would be a formidable obstacle to the TADS. As can be seen from Fig. 9.5b the Uweinat is not necessarily an obstacle for TADS, and some of the radar valleys actually point outwards from this outcrop. Earliest volcanism in the region is indeed dated at ~ 45 Ma (the impact date of the single plume model of Ebinger & Sleep, 1998), but this is not the age at which all uplifts took place. Vincent (1970) describes the history of volcanism of Tibesti, where a series of episodes took place from Mid-Eocene (~ 40 Ma) to the Quaternary (< 2 Ma). The major phase of volcanism at Jebel Marra took place at 14-10 Ma (Wilson & Guiraud, 1998), with renewed activity at 4.3 Ma up until the Quaternary. These authors also point out that after a more detailed K-Ar analysis Schandelmeir *et al.* (1987) provided a value of 26-20 Ma for Uweinat. Thus it appears that if TADS was in place since the Eocene, as proposed by McCauley *et al.* (1986), it would be diverted in minor ways by successive eruptions and associated uplifts in the Uweinat and Tibesti regions, probably towards the present location of Jebel Marra. Between 14 and 10 Ma magmatism-induced uplift of the Darfur plateau, of which Jebel Marra is a part of, separated the TADS from the Chad basin. This new watershed has undergone minor changes is a series of stream captures (Adamson & Williams, 1980), but the Nile and Chad remained separated since ~10 Ma.

At the same time the Anza river system was undergoing changes south of the Central African Shear Zone. The volcanic and tectonic developments in the East African Rift Valley would repeatedly alter the drainage pattern. The development of the Eastern Rift at ~33 Ma (Ebinger & Sleep, 1998) would have severed the links between the rivers in the South Sudan and White Nile Rifts in Sudan with the Anza Rift in Kenya. The 'South Sudan River' would probably be deflected into the Congo Basin until the formation of the Western Rift at ~12 Ma, while the 'White Nile Rift River' (not to be confused with the White Nile of today) would have become landlocked (Fig. 9.5c, d).

9.3.5. Drainage evolution since the Miocene

In the Late Miocene (~ 7 Ma) a drastic drop in the Mediterranean Sea level caused a north-flowing river, called the 'Eonile', to cut a canyon from the present site of the Nile delta to Aswan (Said, 1981). A study comparing this canyon to the Grand Canyon of the Colorado River (Issawi & McCauley, 1992) showed that old ideas of superposition and antecedence are equally untenable for both rivers, and therefore the Eonile cannot be a descendant of the Eocene proto-Nile.

It was mentioned earlier that volcanics at ~ 15 Ma in Tibesti and Jebel Marra would have created a watershed similar to today's Chad-Nile divide. The thus disrupted system would become at least partially landlocked (Fig. 9.5d). At ~ 7 Ma the above-mentioned Eonile would cut its gorge at least as far as Aswan, beheading the former TADS headwaters in the Red Sea Hills. With the onset of aridity at ~ 2 Ma, fluvial sediment would be reworked into dune fields and sand sheets (McCauley *et al.* 1982). New low-order drainage lines after the end of the arid phase (~ 0.8 Ma, McCauley *et al.* 1986) would be directed towards the Eonile, i.e. in the opposite directions than in the TADS phase (Fig. 9.5e). McCauley *et al.* (1982) describe this as 'the final demise of the TADS'.

Very little is known about the history of White Nile. It is a very unusual river, as from Lake Sudd to its confluence with the Blue Nile (channel length of over 800 km) its level drops by less than 12 metres, with an average gradient of approximately 1:70,000. This led early workers in the area to believe the river was previously a huge lake. Berry & Whiteman (1968) give an account of these early studies. A recent study by Williams *et al.* (2003) suggest a lake from today's Sudd to the White-Blue Nile confluence, over 500 km long and up to 70 km wide. They propose this White Nile Lake formed ~ 400 ka (Fig. 9.5e). This lake would receive water from sources similar to those that feed the While Nile today. In particular, the Albert Nile formed as recently as Middle or even Late Pliocene (<700 ka, Berry & Whiteman, 1968) after a series of structural developments in the area (e.g. Bishop, 1966), including the recent rapid rise of the Ruwenzori Mountains (D. MacPhee, pers. comm., 2004). Climate induced changes in the level of Lake Victoria would cause it to alternate between being integrated with and separated from the Albert Nile – the last such separation period ended 12,500 years ago (Livingstone, 1980). The White Nile was captured by the continuous headward erosion of the main Nile as recently

as 10,000 years ago. This, combined with the Blue Nile flowing from the Ethiopian Highlands, produced one of the largest, and perhaps the most interesting of all, river basins in the world.

Further south, the isolated Anza river carried on being affected by the episodes in East African Rift. Today the Anza Rift is blocked – a landlocked Lake Turkana is found in the rift. Archeological studies in the area show that drainage in the Anza Rift changes episodically between being landlocked, and flowing into the Indian Ocean. In the last 5 Ma at least 3 separate episodes of landlocked drainage have been identified. Adamson & Williams (1980) also show evidence for Lake Turkana being drained north-west to the White Nile.

9.4. Discussion

The Nile is a river completely different to any other discussed in this thesis. A glance at a map of North Africa (Fig. 3.3) shows that the Eastern Sahara is almost completely devoid of surface drainage lines. It was remarked in Chapter 3 that the northern section of the Nile basin looks like a bottleneck, as it stops being fed by overland tributaries. The climate of the region has changed repeatedly between arid and non-arid in the last 2 Ma, with evidence for a green Sahara as recently as 6000 years ago. And yet evidence for the past drainage lines is buried underground, and radar technology is needed to uncover it. Clearly a comprehensive study of geometry of this 'radar drainage' will only be possible once a detailed map of it is available, and not just a few survey sections. Given the available technology such a map is certainly possible. This thesis showed how drainage patterns often give constraints on the underlying geology, and a detailed map of the past drainage would potentially give a lot of information about the geological history of the region. However, the costs and logistics associated with surveying the entire Sahara are both serious issues. Such a mapping project should only be undertaken if it is certain that the data produced by it will be of benefit not just to academics, but, much more importantly, to the population that experiences a continuous water shortage, and the primary goal of such a survey would be to identify perennial underground water. Studies of such 'radar drainage', combined with re-constructions of the climate, might also be of use in using climate forecasting to predic whether the Sahara could become green again.

Chapter 10

Conclusions and Discussion

10.1. Fractal properties of rivers

In chapters 3-6 of this thesis, scaling laws of African river networks were investigated. Attention was first given to the simplest of these, Horton's ratios of stream numbers, stream lengths and basin areas (eq. 3.1). These ratios were measured for different river basins in southern Africa (section 4.3). The scaling laws state that these ratios are independent of order – this was not the case in results presented here, though often the deviations in these ratios were very small. When investigating network geometry, it is important to note these deviations, as they may reflect the history of external influences on what is not a perfect fractal river basin. For example, the Cape Fold Belt rivers were noted to have some distinct anomalies in the form of very high Horton's ratios. It was explained (Fig. 4.6) how this is a direct result of the geology underlying the networks.

The next scaling law dealt with was the famous Hack's Law (eq. 3.2), according to which the stream length scales with its drainage area to an exponent, *h*. This Hack's exponent can be expressed in terms of Horton's ratios, if these are independent of order (eq. 3.6). Intuitively one would expect *h* to be ½, but this is not the case, as has been the discussed in section 3.2. Furthermore, there appears to be no uniform value for *h* – it varies between basins, as well as at different scales in a given basin. As with Horton's rations, these deviations might hold clues about the geomorphic evolution of the river network. A model of scaling regimes has been presented in section 4.5. Nonetheless, a mean value for *h* can be computed for sub-basins in a given maximal basin. For 6 main sub-basins of the Orange, this mean *h* was very strongly dependant on the mean basin slope (section 4.8). The correlation was negative, implying steep basins have lower *h*. In section 6.4.3 this analysis was extended to include 2 main sub-basins of Limpopo and 6

Cape Fold Belt rivers, and a similar trend was observed (Fig. 6.5). It must be kept in mind that a mean value for h is a serious simplification. We therefore return to the scaling regimes.

The smallest-scale regime consists of low order streams exhibiting non-convergent flow, where $h = 1$. To analyse this, drainage of linear mountain belts has been studied in Chapter 5. Such belts are drained by streams transverse to the structural trend. Three areas where such drainage is prominent have been identified: the Cape Fold Belt, the Drakensberg Escarpment, and valleys in the Lesotho Highlands. For Hack's Law to hold with a unity exponent, parallel first order streams should be equally spaced. The mean values for each of the three settings were found to be different. In each setting there were variations around the mean spacing, but these were independent of belt width, slope or height. This led us to conclude that Hack's Law hillslope regime (with $h = 1$) is observed in different settings, and these settings affect the constant of proportionality of the Law, but not the exponent. It is very interesting to note that while the Lesotho highlands and Drakensberg Escarpment have the same bedrock geology (basalt), their geomorphology is completely different. However, their spacing ratios were not significantly different. This suggests rock type is more important than geomorphology in determining stream spacing. Some of the variations in the Cape Fold Belt could be explained by variations in local bedding geometry. Not surprisingly, there exist random fluctuations in the stream distribution.

The next scaling regime is the short-range regime, where the streams begin to converge. This is followed by the random regime, which is not properly understood. The cross-over between these regimes for major networks in southern Africa was briefly analysed in section 4.7, and in more detail in Chapter 6. The value for h was found to decrease as one goes from the short-range to random. Hack's differentials (eq. 3.7) give an indication of the magnitude of this change in h for sub-basins of a given basin. This change was found to depend strongly on the maximal basin aspect ratio, κ. For long, narrow basins (high κ) the change was smaller than for wide basins. A detailed analysis in Chapter 6 showed there is no fixed threshold basin area where the cross-over takes place; instead it happens over approximately a natural order of magnitude. A quantity Δh was defined as the difference between h for sub-basins with areas below and above a given size. Three

different threshold sizes were used (see Fig. 6.2 for explanation). Strong negative correlation was found between this quantity and mean sub-basin slope, the slope of the maximal basin, and the roughness of the topography. These all suggest the change in the value of h across this threshold is smaller in steep basins than in flat ones. There are deviations from this relation in very steep basins (mean sub-basin slope >10 m/km), which have very high Δh. This might be due to the non-convergent hill-slope regime extending to larger basin sizes than usually, interfering what was believed to be the short-range regime. The change in h did not exhibit dependence on the fractal dimension of the topography.

Basins at the highest scale are allegedly controlled by geological constraints, and it has been suggested (see section 4.5) that in this regime the basins should be self-similar, and therefore the Hack's exponent, $h = 0.5$. The 11 largest basins in Africa have been presented in this thesis in section 3.4 (see also Table 3.1 and Fig. 3.9). It has been mentioned throughout this thesis that Africa's basins are all vastly different. It is therefore not surprising that the value for h using these 11 basins is not 0.5, as the basins are certainly not self-similar. The value of h, computed as the best-fit line for the 11 drainage areas and stream lengths, was in fact 0.576, with the correlation coefficient of the regression being 96.3 %. This value of h is higher than the exponents obtained for sub-basins of networks (e.g. Table 4.4), suggesting there is indeed a maximal regime with a higher value of h than the random one. The tectonic controls on the maximal basins in Africa are, however, different to those on other continents.

This study has shown that Hack's Law is much more complicated than a simple equation. The regional and scalar variations in the exponent clearly show there can be no universal value for h, and any attempts to provide such a value require a drastic simplification of river networks. Theoretical networks in a uniform setting, or even synthetic laboratory generated networks can lead theoreticians to believe in a single value, or perhaps 2 or 3 values separated by thresholds. However, real rivers cross boundaries between geological, geomorphological and climatic terrains, and furthermore dynamically evolve. The ever-present random fluctuations in any distribution put further error-bars on an already complicated 'Law'. Given how complicated the simplest scaling laws turned out to be, other laws were not considered here. Complicated distribution

functions are of value and interest in topology, but the variations in Africa's geological and climatic parameters will make any attempt to apply these to real networks very difficult to interpret. Table 10.1 summarizes different values of h obtained in this thesis, as well as values from other studies as comparison.

This thesis has also shown that results obtained using synthetic river networks are not necessarily observed in real river networks. In section 3.6 synthetic topographies were generated, and networks that would drain them were computed. Resulting values for h were all higher than any real network analysed. Furthermore, a linear relationship between h and the fractal dimension of the topography was found, while h seemed independent of topography slope. Results from real networks in (Chapters 4 and 6) showed that in fact topographic fractal dimensions do not correlate with h, but the mean slope does. This further illustrates that approximations used to compute theoretical networks make such networks unrealistic, and different to those found in nature.

It might be useful to list the conclusions of this thesis regarding Hack's exponent, h:

- h is usually not equal to ½ as might be expected from geometric intuition
- There is no universal value for h, it varies with scale and location
- There are up to 4 scaling regimes, with different values for h at different scales
- Small basins of mountain streams have $h \approx 1$
- At higher scales h can be correlated with topography roughness
- At these middle scales h is inversely correlated with network connectivity
- In some basins (e.g. Congo, but not southern African basins) h is inversely correlated with drainage density
- Maximal basins in Africa are not self-similar, as has been suggested for global maximal basins.

Table 10.1. Examples of values of *h* found in this study compared with other studies.

Description	Location	*h*	basin area (sq. km)	reference
Orange River	Southern Africa	0.685	1,040,000	Chapter 4 this study
Limpopo River	Southern Africa	0.642	386,000	Chapter 4 this study
CFB Rivers	Southern Africa	0.585-0.665	22,900-73,800	Chapter 4 this study
Mississippi River	North America	0.55	3,250,000	Dodds & Rothhman 2001
Kansas River	North America	0.57	63,000	Dodds & Rothhman 2001
Himalayan Rivers	Asia	0.50-0.54	~ 1,000-3,000	Pelletier 1999
Linear Belts	Southern Africa	~1	~ 4-10	Chapter 5 this study
Linear Belts	World	0.55	~ 230-3,300	Hovius 1997
Maximal Basins	Africa	0.576	192,000-3,690,000	Chapter 3 this study
Maximal Basins	World	0.50	~ 40,000-400,000	Dodds & Rothhman 2000

10.2. Drainage-Climate-Vegetation system as a function of time

While the fractal dimension of a river network might be of little importance to the people (and all other life) dependant on that river for their survival, the density of drainage, and the possible change in it, is of far grater importance. An example of this was the change in vegetation and population distribution in North Africa since 6,000 years ago (discussed in Chapter 9).

In Chapter 7 of this thesis, drainage density in Africa was analysed, in particular its variations with respect to local climatic conditions and vegetation. It was found that these three parameters (drainage density, climate, vegetation) form a complex system with thresholds. One of these thresholds is a mean annual rainfall value of between around 400 and 500 mm. Areas receiving less rainfall than that have virtually no perennial rivers, and are dominated by desert-type vegetation. Between 400 and 800 mm/y perennial density increases linearly with increasing rainfall, while the fraction of desert-vegetation decreases. Above 800 mm/y density becomes independent of rainfall, but exhibits strong correlation with the dominant vegetation type. In Africa two non-desert vegetation types are most dominant: woodlands and savanna. It was found the fraction containing woodlands is proportional to the density, while the fraction of savanna is inversely proportional. It is unlikely that either density or vegetation is an independent variable in this relationship – a change in either will produce a change in the other.

How then will a change in climate affect drainage density and vegetation? Let us assume the following simplified model for density-rainfall, ignoring vegetation. For areas receiving less than 400 mm/y the density is 0, for areas receiving more than 800 mm/y it is 0.08 km/km^2 (the mean value for high-rainfall regions found in Fig. 7.3), and between 400 and 800 it increases linearly from 0 to 0.08 km/km^2. Fig. 10.1 shows what percentage of the drainage would remain perennial if the mean annual rainfall dropped by 100 mm. For areas receiving less than 400 mm/y this percentage is obviously undefined, as they have no perennial rivers to begin with, but in the figure it was given a value of 0% for continuity. One can see that while high rainfall areas (receiving > ~900 mm/y) would not be directly affected, this is not the case for the dryer regions. Regions receiving 600 mm/y would have their perennial drainage cut by half, while ones with 500 mm/y would lose whatever little water they had. A glance at Fig. 4.16 shows most of southern Africa

is in the unstable section of the rainfall regime – while large parts are in the arid regime (< 400 mm/y), large sections of the sub-region receive between 400 and 600 mm/y (the most unstable regime), and other areas are in the slightly more stable 600-1000 mm/y range.

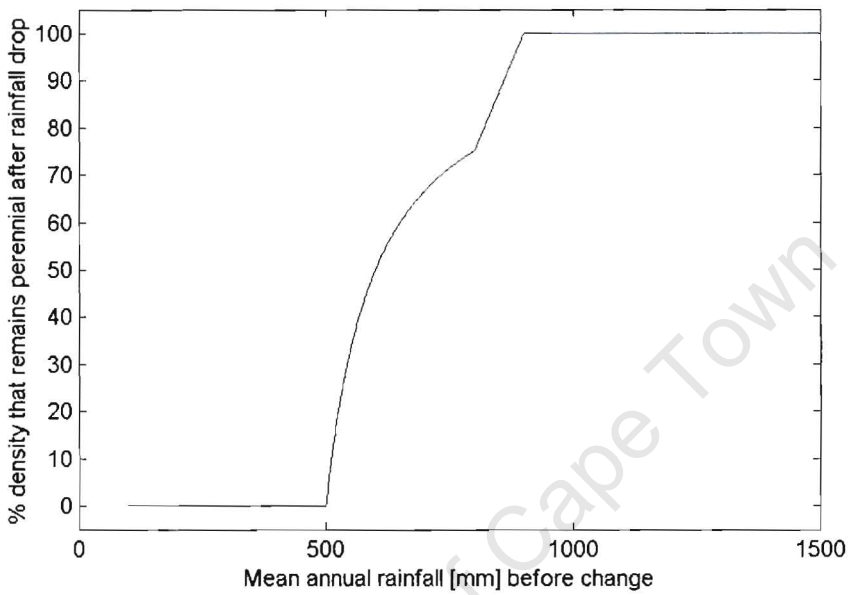

Fig. 10.1. Percentage of drainage that would remain perennial if mean annual rainfall in a region dropped by 100 mm.

While the existence of climate change is universally accepted, it is not clear how the climate will evolve across Africa for the rest of this century. Many different models are developed across the world using different techniques. Discussing these is beyond the scope of this study; a review can be found in the detailed report by CSAG[1] (2002). This report presents different scenarios for African climate at the end of this century. Recognizing the existence of different models, the CSAG presents results of 6 such models. As we are concerned with precipitation here, only this aspect of the models will be explored here. The changes in the rainfall are given as the difference between simulated future rainfall (mean monthly values between January 2070 and December 2099) and present rainfall (mean monthly values between January 1970 and December 1999). The grid size varied between models from 2.5° to 5.625°. Examples of the

[1] Climate System Analysis Group: www.csag.uct.ac.za

predicted rainfall changes are given below (Fig. 10.2 a-d). All models assume the A2 (high greenhouse gas emission – see the CSAG 2002 report) scenario.

From the examples presented here it is clear that the models not only give different estimates, but often disagree whether the rainfall in a given region will increase, decrease, or remain the same. The report also provides a mean value for all 6 models (assuming they are all equally good). This mean prediction is given in Fig. 10.3. According to this the mean rainfall in southern Africa will decrease by approximately 0.15 mm/day, or roughly 50 mm/y. The implications of such a change were mentioned earlier, but the uncertainty between models makes it difficult to provide a definite conclusion. The models used to compute this mean did not even all agree whether the rainfall will increase or decrease. The NCAR-CSM model, for example, predicts an increase of 0.2 mm/day (~ 70 mm/y) in South Africa. A detailed study of the individual models would be necessary to provide a prediction for future drainage.

It might, however, be useful to present a worst case scenario. The CCCMA model suggests the rainfall in most of southern Africa will drop by 0.2 mm/day (~70 mm/y). Fig. 4.16 in Chapter 4 shows that the western section of the sub-region receives less than 400 mm/y, and therefore has very little perennial drainage. A drop in precipitation would not change that. The western section receives between 400 and 1000 mm/y, so most of it would be affected. The CSIRO model predicts a decrease of over 0.4 mm/day (over 150 mm/y) in most of northern South Africa. Such a drop would make all drainage in areas receiving less than ~600 mm/y non-perennial, reduce perennial drainage by over 50 % in areas receiving between 600 and 800 mm/y, and affect all other areas in the region in a slightly less severe manner. It is therefore obvious that climate forecasting and drainage evolution are aspects that need to be taken very seriously.

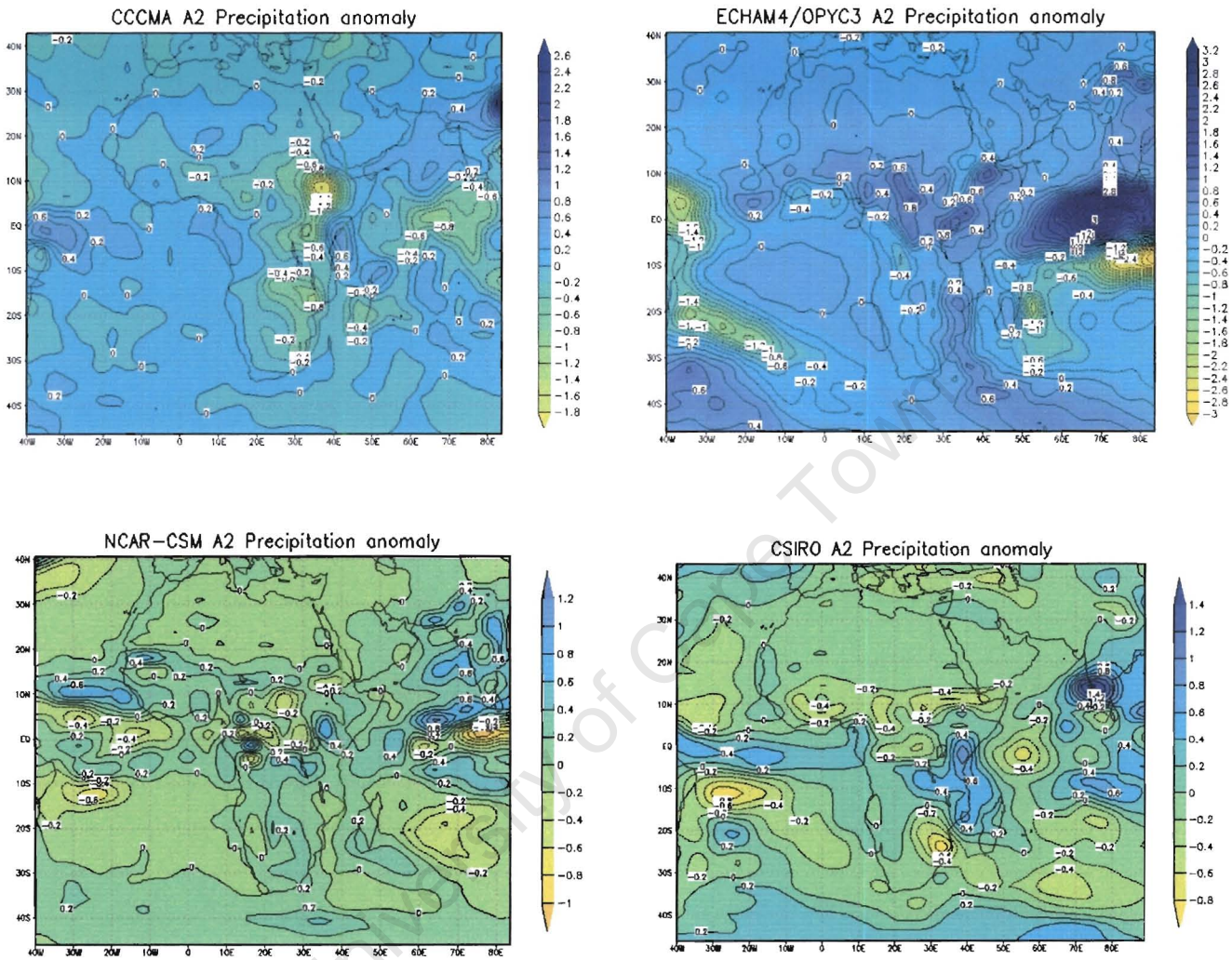

Fig. 10.2. Examples of predicted precipitation changes in Africa for the end of the 21st century. Changes given in mm/day. Positive numbers imply predicted increase in rainfall. Models by:

a) The Canadian Center for Climate Modeling and Analysis (CCCMA)
b) Max Planck Institute for Meteorology, Hamburg (model OPYC3)
c) National Center for Atmospheric Research (model CSM)
d) Commonwealth Scientific and Industrial Research Organisation (model MK2)

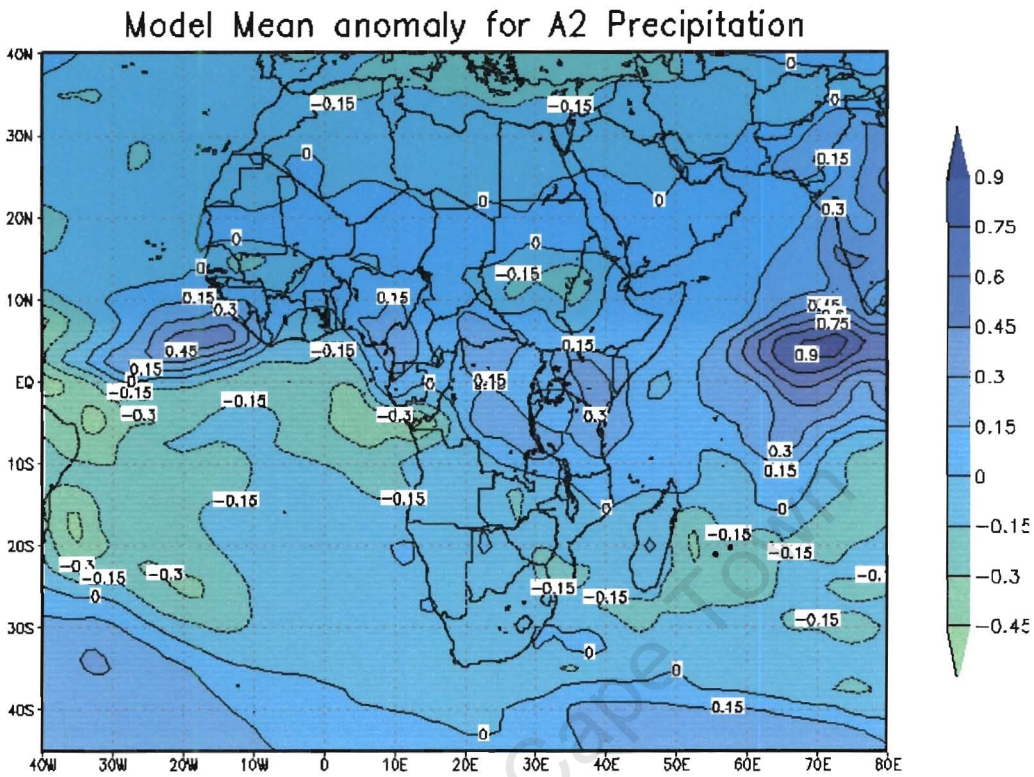

Fig. 10.3. Predicted change in mean annual precipitation in Africa. Mean data of the 6 models used by CSAG(2002).

The model relating drainage density and rainfall discussed above is obviously simplified. For one, it does not include vegetation cover, which is closely related to both climate and drainage. In fact, vegetation is the most likely reason for the existence of the 800 mm/y threshold above which density appears to be independent of rainfall. At that point a balance between erosive forces of precipitation and stabilizing forces of vegetative growth is reached (e.g. Moglen, 1998). If this balance was disturbed, changes in density and climate would result.

One way in which such disturbance can occur is a significant change in the vegetation cover. These can occur naturally due to climate changes and resulting feedback (such the Sahara in the last 6,000 years, described in detail in section 9.2), but can also be, and regularly has been, a result of human activity. Darkoh (1997) presents a case for human related desertification in Botswana, resulting mainly from an alarming increase in human and livestock population. If an area is totally overgrazed and no vegetation cover remains

on it, it will not necessarily re-grow naturally. In fact, Charney (1975) developed a model in which barren areas act as radiative heat sinks to their surroundings (e.g. albedo changes), and 'a desert feeds upon itself'. Using a refined version of this model, Claussen *et al.* (1997) show how a seemingly insignificant climate change can result in Sahara's vegetation cover decreasing from 70% to near zero in 1,500 years. During that desertification a climate change would constantly take place, amplifying the vegetation change. If such a runaway feedback can result from a small climatic change, can it also be triggered by destroying the vegetation of a seemingly small area? This study showed a strong inverse relationship between the percentage of land being a desert and rainfall, up to a mean rainfall value of around 500-600 mm/y (Fig. 7.12a). Thus it seems likely that an decreasing vegetation cover by a mere 10% would decrease the mean rainfall in the region by 50mm/y. As the rainfall in Botswana varies between 250 and 650 mm/y (Darkoh, 1997), this would significantly decrease the river water supply in any region of the country. If the desertified region then spreads, as predicted by Charney's (1975) model, the rainfall and water supply will both continue to dwindle.

Another way in which human activities can disturb the balance mentioned earlier is by deforestation. It was shown (Figs 7.7 and 7.12) that wooded areas are associated with higher drainage densities than savannas, due to trees providing a stronger stabilizing force in the equilibrium model of Moglen (1998). The forests also receive more precipitation. Thus if a large number of trees was to be cut down, and savanna became more prominent, a decrease in drainage density and precipitation would be observed. While in areas that do not experience water shortages such decreases might not appear significant, human and animal health can become an issue. Malaria, one of the deadliest diseases in Africa, is a parasite carried by mosquitoes. These insects need very specific climate conditions to survive well, and a very small change in climate can make an area very favourable or unfavourable for them, resulting in distribution of malaria being a function, amongst other things, of climate (Lindsay & Birley, 1996). A number of catastrophic malaria epidemics in East Africa have been attributed to slight climate changes associated with deforestation (e.g. Matola *et al.*, 1987; Malakooti *et al.*, 1997). Thus small changes in climate and vegetation can have far-reaching consequences through altering the perennial water supply.

10.3. Drainage Evolution and Biodiversity

As all animal life is dependent on water in some form or another, changes in the water supply will affect the distribution of the animal life. These changes can occur at different scales of both time and area, from daily variations in rainfall at a single site to species evolution as a result of continental drainage evolution over millions of years.

The most obvious example is presented by populations of fish. Moore & Larkin (2001) compared how many species of fish are the same in different sections of Okavango, Limpopo and Zambezi. Investigating this was one of the tools they used to decipher the history and the evolution of the drainage in the area (summarized in Fig. 8.8. in this thesis). Furthermore, a mixing of Congolian and Zambezian fish faunas is observed, suggesting the Chambeshi must have been a part of Zambezi system before the capture by Luapula made it a part of the Congo (Cotterill, 2003a). This is why in the model for Central African drainage evolution presented in this thesis (section 8.7, Fig. 8.15), it is necessary for the landlocked Pliocene Chambeshi to be captured first be the Kafue, and then by Luapula. The proposed evolution of that drainage is shown in detail in Fig. 10.4.

While observed biodiversities can help in the reconstruction of paleo-drainage, this process can be reversed. When drainage history is known (or at least suggested), it can be used to explain both distribution and diversity of animals. For example, Cotterill (2004) shows how drainage evolution in the south-central Africa can account for the distribution of different species and sub-species evolution of swamp dwelling birds. The concept of bird distribution is more subtle than that of the fish, as, quite obviously, birds can fly. They are, however, dependent on water, in particular the swamp dwelling birds that will have a propensity to stay in wetlands, and their distribution will be affected by the changes in these. As an example in southern Africa, consider a species that exists in the swamp in Fig. 10.4b. As the swamp dries up following the river capture, some of the birds will move to the Luapula swamp, while ones that lived further south will find homes on the banks of the Kafue. Over the next few millions of years it is suggested that the species will evolve differently, and 2 sub-species may develop. This is known as allotropic speciation.

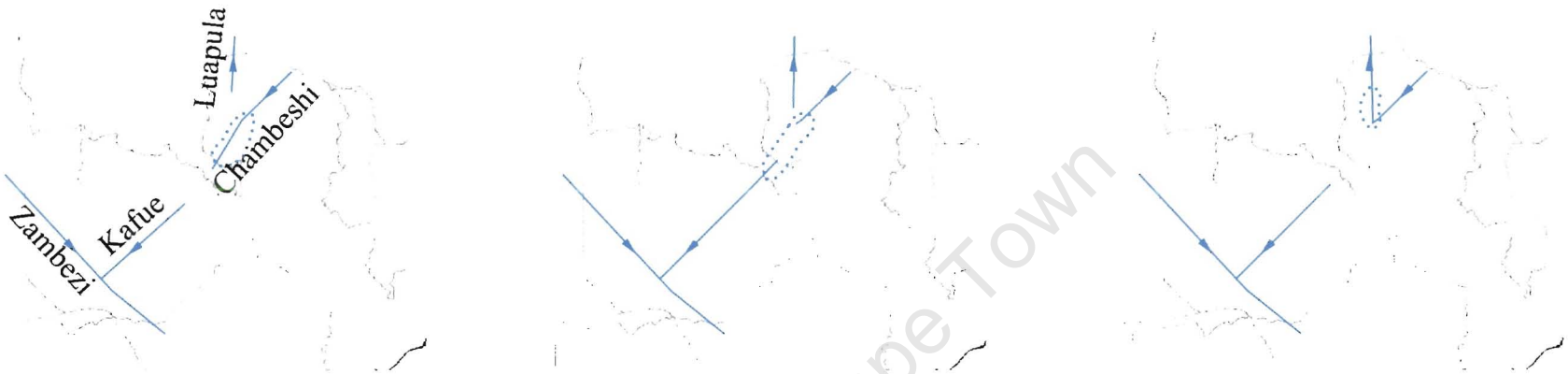

Fig. 10.4. Drainage evolution of the Cahmbeshi in the Pliocene (5-1 Ma), a model to accommodate Chambeshi belonging to both the Congo and Zambezi in that time. This is necessary to explain fish fauna similarities in the two basins (Cotterill, 2003a)

a) After uplifts in East Africa, the Chambeshi would become a landlocked system (section 8.7), and swamps associated with such a system would develop (dashed line).
b) Headward erosion by Kafue would capture the southern edge of the swamp. The wetlands would extend along the upper Kafue, as the captured waters would make these narrow valleys overflow.
c) Luapula captures the northern edge of the swamp, redirecting the upper Chambeshi into the Congo Basin. The wetlands would now be along the Luapuala, as the former surplus water in the Kafue is cut off.

This evolution is not restricted to birds. Cotterill (2003b, c) uses drainage evolution in his discussion of tsessebe antelope subspecies, while Broadley & Cotterill (2004) explore it to study reptile evolution. Perhaps the best example of sub-species evolution as a result of a change in drainage is the Black-faced Impala (*Aepyceros petersi*), a sub-species of the common Impala (*Aepyceros melampus*). The Black-faced impala is found south and east of the Cunene, extending to the Etosha Pan (a fossil lake), while the Impala is found in wet areas throughout Botswana, Zimbabwe, Zambia and South Africa. Capture of the Cunene in Early Pliocene (~5 Ma) by a river draining to the Atlantic cut off majority of the water input into Lake Etosha, creating a dry gap between Cunene and Okavango. The Impala near the Cunene were thus separated from the rest of the species, resulting in the evolution of the subspecies (Fig. 10.5).

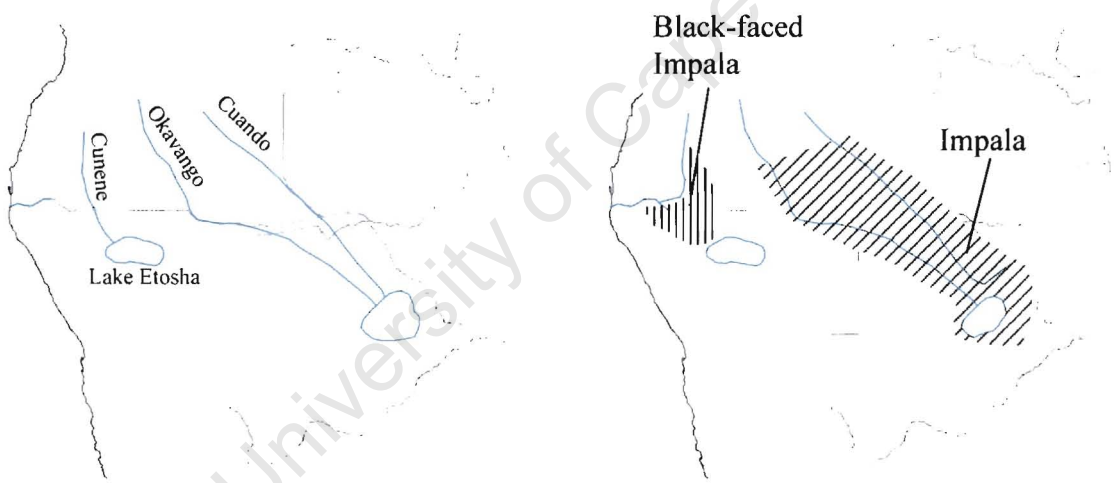

Fig. 10.5. Drainage evolution that may have caused the allotropic speciation of 2 sub-species of impala. In the Pliocene (left, ~5Ma) the Cunene river fed water into Lake Etosha. A capture of the Cunene left an arid gap north and around what is now Etosha Pan, resulting in a split of the Impala population, and a subsequent development of 2 sub-species. Distribution maps are not exact, they are drawn to illustrate the example in the text.

Both drainage and faunal evolution also occur at smaller scales. King & Schael (2001) analyse insect populations in 6 catchment areas (maximal basins) in the south-western Cape Province in South Africa: Table Mountain streams, Eerste, Palmiet, Berg, Breede and the southern section of Olifants basins (Fig. 10.6). These catchments coincide at least partially with the Cape Fold Belt mountains repeatedly mentioned in this thesis.

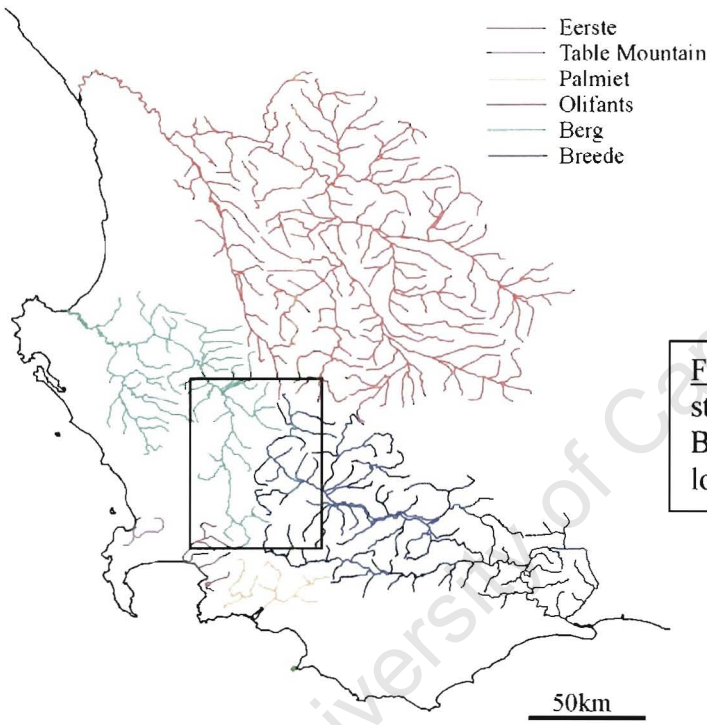

Fig. 10.6. The 6 catchment areas studies by King & Schael (2001). Black rectangle indicates the location of the area in Fig. 10.7.

Their results showed that usually sites in the same catchment area have similar biodata. At some sites, however, anomalies were observed. For example, sites along sections of the Breede river have similar biodata to those observed along sections of the Berg and Olifants rivers. The drainage patterns in the Cape Fold Belt are very dynamic, and one would expect a number of small-scale river captures to take place. A number of these captures, as well as other ways drainage evolution can take place, have been documented by Taljaard (1949). A classical example of such a river capture is at the Tulbagh kloof, where streams that were formerly part of the Breede river network are now joined with Berg river (Fig. 10.7). The sites chosen in the original study of King & Schael (2001)

were not picked with drainage evolution in mind, as this was not the primary aim of their project. However, a study to identify capture elbows on the area, and compare the biodata on either side of both the old and new watershed, is being planned (Dr. J. King, UCT Dept. of Zoology, pers. comm. 2004). Such a study will make it possible to verify the proposed river capture (e.g. Taljaard, 1949), and will also be of great use to studies of evolution of the species concerned.

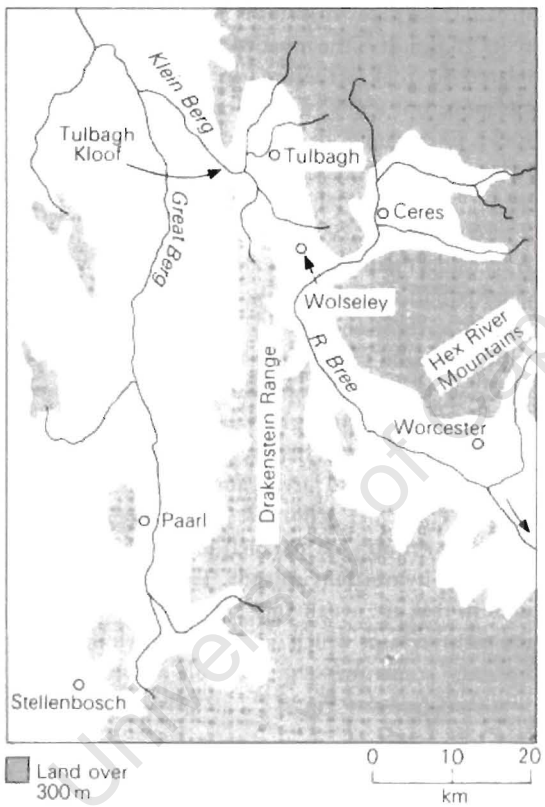

Fig. 10.7. Map of the Tulbagh kloof river capture. Streams from Tulbach flowed south past Wolsely into Breede before Berg river capture. From Buckle (1978), who uses Bree instead of Breede.

10.4. Concluding remarks

This study has shown that natural river networks very rarely form perfect fractal patterns. It was shown how at different scales different parameters control basin and network formation, but even over these scaling regimes deviations from 'perfection' occur. Some of these deviations are random fluctuations, but often they are results of different geologic and climatic environments the river flows through. These fluctuations hold information about the history of the river. This, apart from being a very interesting academic field, can be used to explain biodiversity, locate mineral placers, and even study human history (e.g., the history of Ancient Egypt is closely tied with the evolution of the Nile). Such analyses can be extended to attempt to predict aspects of the future drainage. Some of these are very important to humans and all other life, like the density of perennial drainage. A number of other social aspects, like health and agriculture are also closely related to drainage evolution. Water is a vital resource, and its proper management is vital to ensure its future availability to all. Such management must include forecasting of future drainage, and more detailed studies relating drainage with climate and vegetation, and how this complex system will interact with humans.

Appendix A: Topography as a Fractal

To begin with let us consider a 2 dimensional space, where the elevation function, z, is a function of just one parameter, x. This example is identical to studying a cross-section of a landscape. We are concerned with correlation between $z(x+x')$ and $z(x)$. The larger the value of x', the less the two values are expected to be correlated. For the series to be a self-affine fractal, it needs to satisfy the probability condition

$$p\left[\frac{z(x+x')-z(x)}{(x')^H} < z'\right] = F(z') \tag{A.1}$$

where H, the Hausdorff measure is constant. Point values of z are random, but the above equation correlates adjacent values. For $H = 0$ we get white noise.

Given that z is defined over an interval X, we specify a number of statistical properties. The mean value of z is

$$\bar{z}(X) = \frac{1}{X}\int_0^X z(x)dx \tag{A.2}$$

the variance of z is

$$V(X) = \frac{1}{X}\int_0^X \left[z(x)-\bar{z}\right]^2 dx \tag{A.3}$$

while the standard deviation is given by

$$\sigma(X) = \sqrt{V(X)} \tag{A.4}$$

A necessary condition for a series to be a fractal is that the variance has a power-law dependence on the interval X (e.g. Voss, 1985; Turcotte, 1988):

$$V(X) \sim X^{2H} \tag{A.5}$$

or

$$\sigma(X) \sim X^H \tag{A.6}$$

To compute the fractal dimension of the series we introduce a rectangular box with width X and height $\sigma_X = \sigma(X)$. Next divide X into n smaller intervals with length $X_n = X/n$. Then introduce n boxes of width X_n and height $\sigma_n = \sigma_X / n$. These boxes have the same

aspect ratio as the original box, but the standard deviation associated with an interval X_n is

$$\sigma_{Xn} = \sigma(X_n) = \sigma(X/n) \tag{A.7}$$

which is different from σ_n. The number of the smaller boxes required to cover the areas of width X and height σ_{Xn} is

$$N_n = \frac{X\sigma_{Xn}}{X_n\sigma_n} = n^2\frac{\sigma_{Xn}}{\sigma_X} \tag{A.8}$$

using (A.6)

$$\frac{\sigma_{Xn}}{\sigma_X} = \frac{\sigma(X/n)}{\sigma(X)} = \left(\frac{X/n}{X}\right)^H = \frac{1}{n^H} \tag{A.9}$$

and therefore

$$N_n = n^{2-H} = \left(\frac{X}{X_n}\right)^{2-H} \tag{A.10}$$

This is a power law defining a fractal relation, and it yields

$$D = 2 - H \tag{A.11}$$

This proves the relation stated in Chapter 1 (eq. 1.12 in a 2-dimensional space).

A series can expressed in the physical domain, or in the frequency domain using the amplitude $Z(f,X)$, which is a complex number indicating the phase of the signal:

$$Z(f,X) = \int_0^X z(x)e^{2\pi ifx}dx \tag{A.12}$$

The power spectral density of $z(x)$ is then given by

$$S(f) = \frac{1}{X}|Z(f,X)|^2 \tag{A.13}$$

For a time series to be a fractal S has a power law dependence on f (e.g. Turcotte, 1992):

$$S(f) \sim f^{-\beta} \tag{A.14}$$

To obtain a relationship between β and D consider two self-affine series related by:

$$z_2(x) = \frac{1}{r^H}z_1(rx) \tag{A.15}$$

defining $x' = rx$ we can write

$$Z_2(f,X) = \int_0^{rX} \frac{z_1(x')}{r^H} e^{2\pi i f x'/r} \frac{dx'}{r} \tag{A.16}$$

or

$$Z_2(f,X) = \frac{1}{r^{H+1}} Z_1\left(\frac{f}{r}, rX\right) \tag{A.17}$$

Using that we have

$$S_2(f) = \frac{1}{X}\left|X_2(f,X)\right|^2 = \frac{1}{r^{2H+1}} \frac{1}{rX} \left|Z_1\left(\frac{f}{r}, rX\right)\right|^2 = \frac{1}{r^{2H+1}} S_1\left(\frac{f}{r}\right) \tag{A.18}$$

Since z_2 is a rescaled version of z_1, their power spectral densities must be similarly scaled. Thus

$$S(f) = \frac{1}{r^{2H+1}} S\left(\frac{f}{r}\right) \tag{A.19}$$

and therefore

$$\beta = 2H + 1 = 5 - 2D \tag{A.20}$$

Having related these parameters to each other, it is possible to generate a synthetic series with a specified fractal dimension (Turcotte, 1992):

- Create a white noise series of N elements, h_1 to h_N.
- Perform a discrete Fourier transform on the series:

$$H_m = \Delta X \sum_{n=0}^{N-1} h_n e^{2\pi i n m / N} \tag{A.21}$$

  This will generate N complex numbers (H_m). Since $\beta = 0$ their amplitudes will be approximately equal.

- Filter the Fourier coefficients using

$$H_m' = \left(\frac{m}{N-1}\right)^{\beta/2} H_m \tag{A.22}$$

  where β can be obtained from (A.20). The amplitudes of the small-m coefficients correspond to short wavelengths, and large-m to long wavelengths.

- Perform an inverse Fourier transform on the filtered coefficients:

$$h_n' = \frac{1}{N\Delta T} \sum_{m=0}^{N-1} H_m' e^{-2\pi i n m / N} \tag{A.23}$$

The resulting series h_n will have a dimension $D = \frac{5-\beta}{2}$.

This approach can be extended to a function of 2 variables, like 3 dimensional topography (Dubuc *et al.*, 1989). Given an $N * N$ grid of equally spaced points denoted by h_{nm}, it possible to perform a 2 dimensional Fourier transform to obtain an array of complex coefficients H_{st}:

$$H_{st} = \left(\frac{L}{N}\right)^2 \sum_{n=0}^{N-1}\sum_{m=0}^{N-1} h_{nm} e^{-\frac{2\pi i}{N}(sn+tm)} \tag{A.24}$$

Each transform coefficient is then assigned a radial wave number

$$r = \sqrt{s^2 + t^2} \tag{A.25}$$

The complex coefficients are then filtered using the relation

$$H^*_{st} = \frac{H_{st}}{r^{\beta/2}} \tag{A.26}$$

An inverse transform of the new coefficients will yield a matrix with a dimension associated with β. While the equation $\beta = 2H + 1$ holds in all dimensions, eq.(A.11) is a special case of eq.(1.12), which for a function of two variables becomes

$$H = 3 - D \tag{A.27}$$

This gives

$$D = \frac{7-\beta}{2} \tag{A.28}$$

It is also possible to determine the fractal dimension of a given topography using spectral density (e.g. Voss, 1988; Turcotte, 1992). The 2 dimensional mean power spectral density S_{2j} for each radial wave number is given by:

$$S_{2j} = \frac{1}{L^2 N_j} \sum_{1}^{N_j} |H_{st}|^2 \tag{A.29}$$

where N_j is the number of coefficients satisfying $j < r < j+1$.

After obtaining the matrix of transform coefficients H_{st} using (A.24), each coefficient is assigned a wave number r using (A.25). The mean slope on a log-log plot of S_{2j} as a function of r will yield the fractal dimension D. It is important to note that D does not necessarily need to lie between 2 and 3. White noise ($\beta = 0$) has $D = 3.5$, and it also possible to have $D < 2$.

MATLAB scripts were written both to determine the dimension of a given landscape, and to produce a synthetic landscape of given size and dimension. Sample results are shown in Fig A.1. below:

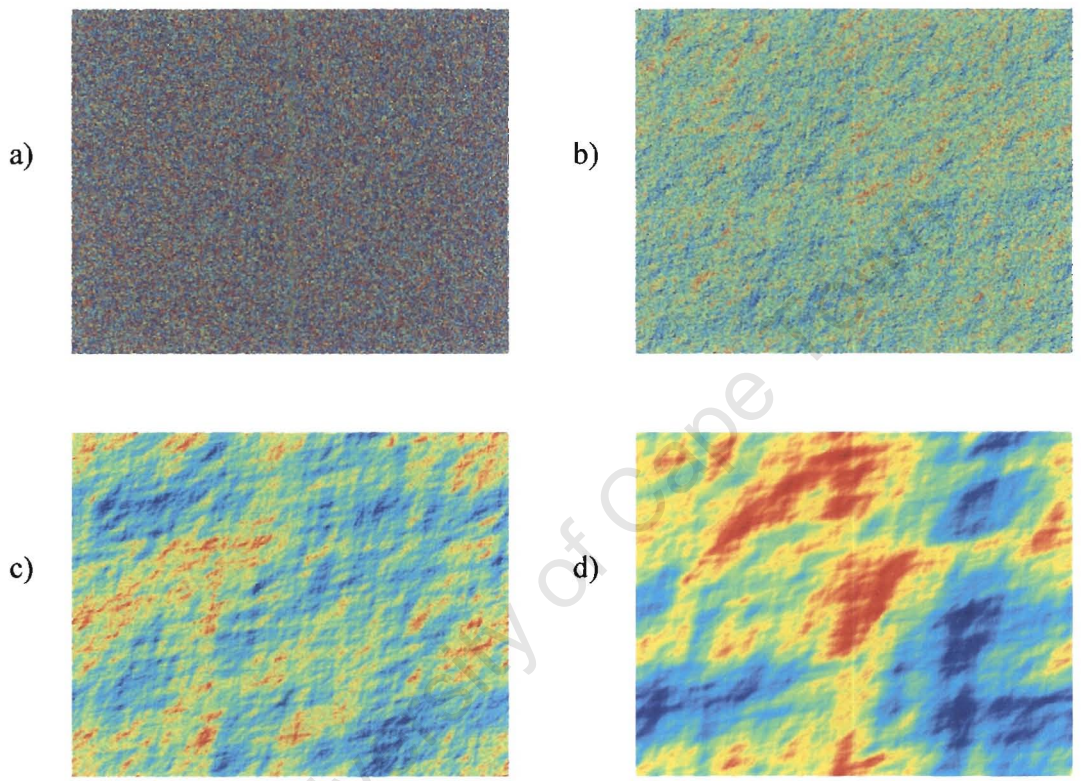

Fig. A.1. Synthetic topographies with fractal dimensions:
a) $D = 3.5$ (white noise) b) $D = 3$
c) $D = 2.5$ d) $D = 2$

Appendix B: Obtaining River Networks From DEMs

Digital elevation models (DEMs) were used in this study to, amongst other things, study river networks flowing over the given topography. This appendix gives the exact procedure used in determining the network from the given DEM. Below the elevation model for the South African coast near Port Elizabeth is shown (Fig B.1). This sample map is 250km wide in the north-south direction, and 300km in the east-west. It has a 1km resolution, and thus contains 75,000 data points. The elevation ranges from the Indian Ocean at 0 metres to 1852 in the north-eastern corner of the map, near Cradock. The Indian Ocean, with its obvious elevation of 0, takes up 19,770 of the data points.

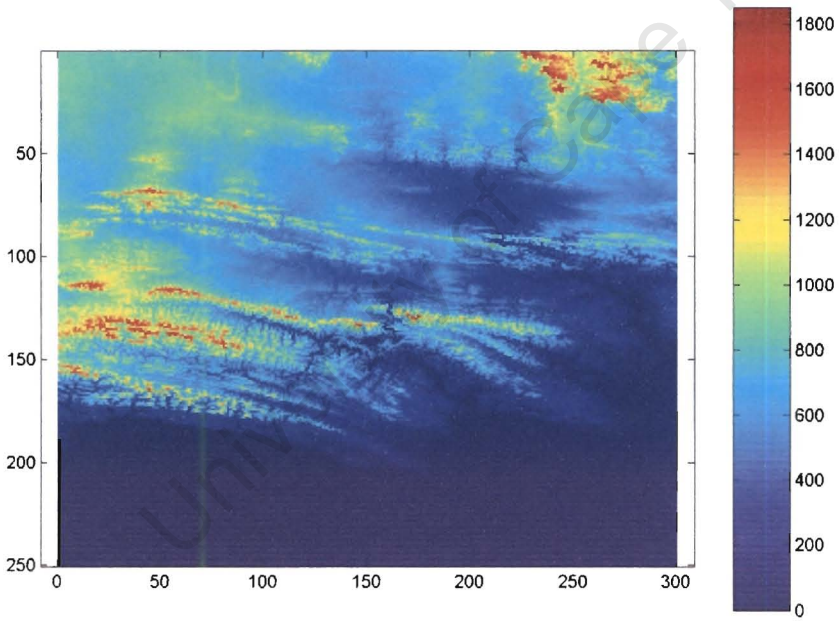

Fig. B.1. Sample DEM of the coast near Port Elizabeth. Units on map are kilometres, and on the elevation scalebar metres.

The first step in determining the river pattern is subdividing the area in question into individual drainage basins. This was done using the *watershed* function built into Matlab. The result is a matrix of the same size as the DEM in question, where every distinct watershed or significant change in slope has been traced, and the points on lines representing them been given the value of 0 in the matrix. All individual basins formed

by this division have then been labeled from 1 to *n*, where *n* is the total number of basins. The figure below (B.2) shows the resulting jigsaw, with dividing lines in black and basins in white. Not surprisingly the largest 'basin' is the portion of the Indian Ocean included in the map.

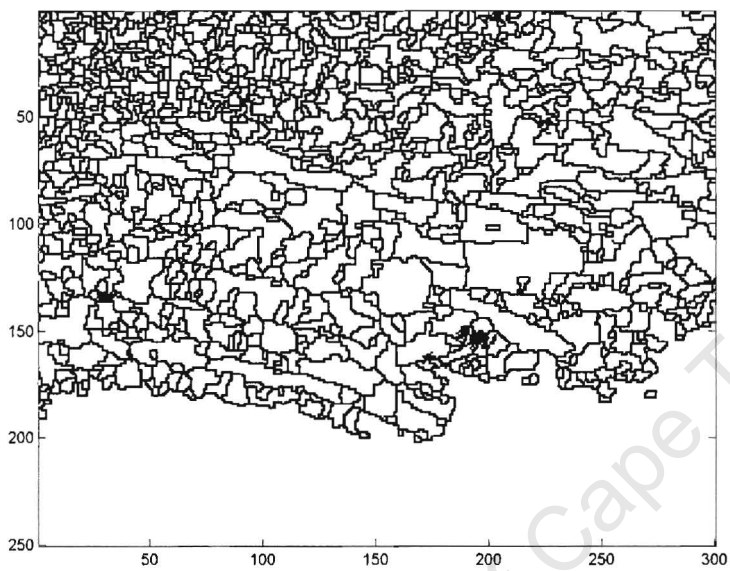

Fig. B.2. The are divided into basins using *watershed*

Following that, a number of arrays describing properties of each basin were computed. The index in each of them was the number from 1 to *n* assigned to each basin by *watershed.* Firstly, *area* was computed as the number of data points with a given basin index, or simply the area in km^2 of each basin. Next, *outlet* contained the co-ordinates and elevation of the lowest point in each basin which lies on the boundary of the basin in question.

Once the *outlet* array was computed, a program was written to determine to which of its neighbours each basin flows. This was done by checking points 2 pixels away in each direction from the basins lowest point. The basin index corresponding to the point that had the highest downhill slope from the outlet in question was considered to be the basin into which the original basin drains. The *onedown* array was computed in this way. In some cases points 2 pixels away were either on watersheds (basin = 0) or were all uphill from the outlet. In that case the distance was increased to 3, and then in increments of 1 up to 10. If no downhill basin was found, 0 was written into the *onedown* array, and the

basin was treated as an inland drainage terminal. The network was then constructed by joining the outlet of each basin with the outlet of its *onedown* basin by straight lines.

The *onedown* array enabled one to determine the total area draining into any given basin, or the true basin area. This is clearly the sum of areas all individual basins that pass through the individual basin in question on their way to the ocean. It is important to include the watershed points (black lines in the basin diagram) in this true basin area, as in reality they obviously have no surface area.

Once it was knows which basin flows into which, it was also possible to order them. First all basins were given order 1. Then it was calculated how many basins flow into each basin. All those receiving flow from more than one basin had their order increased to 2. Then first order basins were removed from the analysis, and the algorithm was repeated until only one basin (the ocean) was left, and a network ready for any further analysis was obtained. Example of an obtained network (for the sample DEM shown earlier) is shown below. This is a section of the entire Cape Fold Belt river system, and the analysis was done for a larger area, with just the sample area being shown in the figures – hence some rivers of higher orders enter the zoomed-in area. Colours correspond to orders: dark blue basins have order 1, increasing through light blue, green and yellow to red being order 5. The 2 major rivers are the Gamtoos and the Sundays.

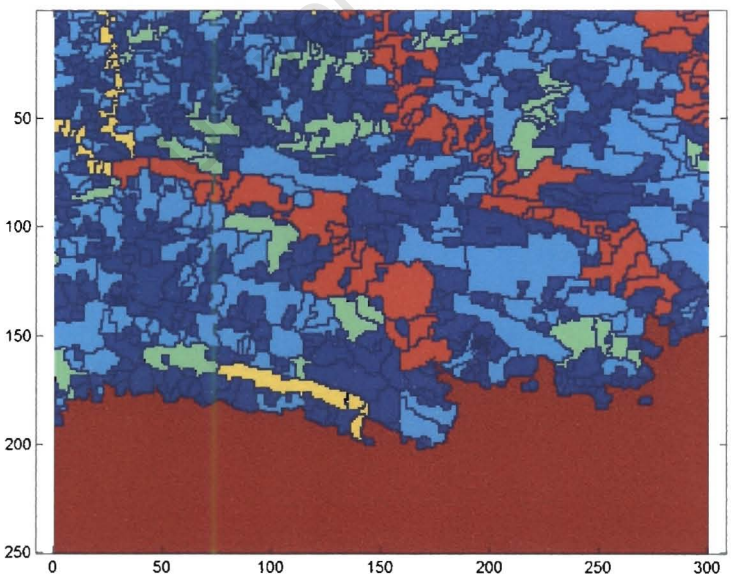

Fig. B.3. River networks obtained from the DEM

By far the biggest problem associated with obtaining river networks from DEMs is the problem of sinks. A sink is defined as any area on the DEM which is surrounded by points of greater elevation. While some of the sinks occur in nature and result in landlocked drainages (e.g., the Okavango Delta in Botswana, Lake Turkana in Kenya, Etosha Pan in Namibia, and many smaller scale craters), most of the ones in DEMs used here are not real. When a particular area is drained by a channel narrower than the resolution the DEM (1km in most cases in this study), it is possible the outlet will not be picked up by the model. If the area is in reality mostly surrounded by higher ground, it can then appear to be landlocked in the model.

As a result of that, some of the individual basins seemed to be surrounded by higher ground – it was already mentioned they were given the value of 0 in the *onedown* array, and were treated as inland drainages. Once the network could be drawn, it was possible to see all the 'landlocked' basins. Real topographic maps were then consulted as to the direction the river takes from there, and the index of the neighbouring basin in that direction was written into the *onedown* array. Thus it might appear in the model that the river has been pushed uphill, but this was necessary to have networks in the computer model resembling ones in reality.

Another problem associated with this model is inability to determine the length of first order streams. Remembering the stream length is defined here as the line joining outlets consecutive individual basins, it starts at the outlet of a first order basin. This is not a problem for higher order basins, as this few pixels become negligible, but any area – stream length relation would be meaningless for first order basins, and thus they have been excluded from the analysis. Furthermore, it is possible that a small scale watershed cannot be picked up by the DEM because of its resolution, and a first order basin might actually contain two mountain streams joining. On the other hand, a small basin picked up by the DEM might in reality not contain a stream. Thus the number of 1st order streams would also be difficult to determine. For second (and higher) order streams one can assume the feature size – map resolution ratio is high enough to produce reliable results.

Appendix C: Parameters of boxes in Chapter 7

Parameters of the boxes in Figure 7.1 (Entire Africa).

box	Area	rain	mean elev	roughness	channel dens.	perennial dens.	perennial
#	*1000 km²*	*mm/y*	*m*		*km/km²*	*km/km²*	*%*
1	631	265	853	27.5	0.070	0.015	22%
2	938	181	595	26.9	0.043	0.007	17%
3	690	144	362	26.7	0.066	0.006	9%
4	758	84	169	26.9	0.029	0.009	29%
5	497	140	234	26.8	0.042	0.000	0%
6	1000	50	341	23.8	0.031	0.000	0%
7	1000	51	535	27.6	0.067	0.000	0%
8	1000	50	678	27.5	0.063	0.000	0%
9	1000	50	502	27.1	0.030	0.000	0%
10	989	50	356	25.3	0.030	0.002	6%
11	903	462	1057	28.8	0.086	0.015	17%
12	584	844	114	25.8	0.063	0.032	50%
13	1000	660	316	26.1	0.055	0.020	37%
14	1000	549	328	27.3	0.066	0.030	45%
15	978	410	433	25.5	0.047	0.022	46%
16	1000	386	558	26.9	0.063	0.002	3%
17	1000	293	501	25.5	0.048	0.005	11%
18	636	1679	285	26.7	0.091	0.073	80%
19	501	1381	196	26.5	0.095	0.083	88%
20	893	1732	558	28.9	0.090	0.089	98%
21	1000	1483	522	28.5	0.104	0.097	93%
22	1000	1180	731	29.0	0.081	0.065	81%
23	1000	811	1007	30.1	0.075	0.033	44%
24	647	359	514	27.0	0.037	0.002	5%
25	659	1629	433	28.3	0.055	0.054	99%
26	1000	1819	545	27.4	0.083	0.082	100%
27	913	1296	1193	29.7	0.080	0.079	98%
28	656	731	743	31.2	0.090	0.065	72%
29	432	889	1029	28.1	0.078	0.077	99%
30	1000	1147	1146	24.3	0.083	0.083	100%
31	973	1093	1020	27.7	0.125	0.125	100%
32	599	1104	432	28.5	0.127	0.127	100%
33	692	292	1118	28.5	0.041	0.005	13%
34	1000	506	1073	29.1	0.037	0.023	61%
35	739	770	624	28.0	0.079	0.078	99%
36	720	231	876	27.5	0.083	0.044	53%
37	658	674	1214	27.5	0.109	0.101	93%
38	562	1455	568	27.8	0.093	0.091	97%

Vegetation zones in the continental study.

block #	wood	desert	savanna	grassland	floodplain
	%	%	%	%	%
1	45	55	0	0	0
2	10	90	0	0	0
3	15	85	0	0	0
4	5	90	0	0	5
5	0	100	0	0	0
6	0	100	0	0	0
7	0	100	0	0	0
8	0	100	0	0	0
9	0	100	0	0	0
10	0	90	0	0	10
11	5	35	60	0	0
12	20	20	60	0	0
13	10	35	45	0	10
14	5	45	50	0	0
15	5	50	40	0	5
16	0	55	45	0	0
17	0	50	40	0	10
18	55	0	45	0	0
19	55	0	45	0	0
20	60	0	40	0	0
21	60	0	40	0	0
22	40	0	60	0	0
23	5	0	95	0	0
24	0	40	60	0	0
25	55	0	45	0	0
26	75	0	25	0	0
27	70	0	30	0	0
28	20	0	80	0	0
29	65	5	30	0	0
30	90	0	5	0	5
31	90	0	5	0	5
32	85	0	15	0	0
33	10	45	45	0	0
34	20	5	70	0	5
35	70	0	30	0	0
36	15	75	10	0	0
37	30	5	15	50	0
38	65	0	35	0	0

Parameters of the boxes in Figure 7.8 (Congo).

block	density	n(1)	n(2)	n(3)	Rn	l(1)	l(2)	l(3)	Rl	h	elev	rough.
#	*km/km²*					*km*	*km*	*km*			*m*	
1	0.089	325	50	11	5.97	16.8	40.1	100.2	2.40	0.464	569	27.4
2	0.102	374	58	13	6.00	16.2	42.0	130.7	2.66	0.510	695	28.6
3	0.079	288	54	15	4.82	27.6	63.1	132.3	2.26	0.494	665	27.2
4	0.096	490	93	21	4.84	20.7	50.6	130.9	2.47	0.538	506	26.6
5	0.135	892	182	36	4.43	16.1	33.0	71.0	2.06	0.451	483	26.2
6	0.136	887	151	23	5.49	15.2	35.0	113.0	2.43	0.470	541	27.0
7	0.119	565	83	18	6.27	16.7	45.8	119.1	2.72	0.525	767	27.3
8	0.065	217	44	11	4.44	27.2	58.7	119.6	2.13	0.481	487	27.9
9	0.088	359	56	14	6.00	15.6	42.2	140.7	2.79	0.535	367	27.0
10	0.117	640	103	18	5.74	15.2	35.5	100.0	2.41	0.466	415	29.2
11	0.108	556	89	16	5.81	17.7	47.8	145.7	2.75	0.543	459	27.5
12	0.117	479	97	25	4.46	19.6	44.7	94.0	2.25	0.515	1009	28.4
13	0.096	372	70	13	4.78	22.5	52.8	104.0	2.29	0.511	396	24.0
14	0.091	392	85	15	4.26	19.6	50.2	132.8	2.58	0.616	451	26.4
15	0.086	320	67	14	4.58	22.3	53.1	192.5	2.59	0.554	563	26.2
16	0.080	348	63	15	5.22	21.9	57.9	203.5	2.77	0.567	1219	28.6
17	0.090	215	42	8	4.69	28.1	70.9	175.6	2.52	0.568	500	26.7
18	0.091	391	52	11	6.85	21.6	87.6	159.2	3.79	0.694	776	24.5
19	0.111	685	111	16	5.78	14.9	39.1	130.8	2.72	0.530	725	25.7
20	0.112	629	104	21	5.65	17.7	43.0	138.8	2.54	0.492	787	26.0
21	0.108	600	116	23	4.74	17.0	42.1	105.5	2.48	0.551	963	26.7
22	0.076	270	51	11	4.96	25.3	72.2	229.2	2.90	0.628	1164	27.0
23	0.093	363	75	19	4.49	20.4	56.7	159.3	2.79	0.650	1096	26.7
24	0.100	597	119	31	4.50	16.7	41.3	79.0	2.37	0.560	1215	27.3
25	0.119	776	163	40	4.91	14.7	33.8	85.4	2.47	0.536	1209	28.1

Vegetation zones in boxes in Figure 4.18 (southern Africa)

block #	wood	sav	des	grass	fluv
	%	%	%	%	%
A1	70	15	15	0	0
B1	75	25	0	0	0
C1	85	10	0	0	5
D1	90	0	0	0	10
E1	90	10	0	0	0
F1	90	10	0	0	0
A2	35	10	55	0	0
B2	10	85	5	0	0
C2	15	65	10	0	10
D2	40	50	10	0	0
E2	90	10	0	0	0
F2	90	10	0	0	0
A3	0	5	95	0	0
B3	0	35	65	0	0
C3	0	90	10	0	0
D3	10	80	0	10	0
E3	40	55	0	5	0
B4	0	0	100	0	0
C4	0	30	60	10	0
D4	5	5	0	90	0
E4	75	15	0	10	0
B5	60	0	40	0	0
C5	40	0	45	15	0
D5	70	0	0	30	0

References

Abrahams, A.D. (1984). Channel networks: a geomorphological perspective. Water Resour. Res., 20(2), 161-188.

Adams, J., (1985). Large scale tectonic geomorphology of the Southern Alps. In: Tectonic Geomorphology (ed. by M. Morisawa and J.T. Hack), 105-128. Allen & Unwin, Boston.

Adamson, D. & Williams, F. (1980). Structural geology, tectonics and the control of drainage in the Nile Basin. In: The Sahara and the Nile (ed. by M.A.J. Williams & H. Faure) 225-252. A.A. Balkema, Rotterdam.

Ashton, P., (2002). Water Wars in Africa? Science in Africa (online magazine): http://www.scienceinafrica.co.za/2002/november/water.htm

Ashwal, L.D. & Burke, K. (1989). African lithospheric structure, volcanism and topography. Earth Planet. Sci. Lett., 96, 8-14.

Bak, P. (1996). How nature works: the science of self-organized criticality. Springer-Verlag, New York.

Baker, B.H., Mohr, P.A. & Williams, L.A.J. (1971). Geology of the Eastern Rift System of Africa. Geol. Soc. Am. Spec. Paper 136, 1-67.

Bell, F.G. & Maud,R.R. (1994). Dispersive soils: a review from a South African perspective. Quarterly J. of Eng. Geol., 27, 195-210.

Berger, A. (1978). Long-term variations of daily insolation and quaternary climatic changes. J. Atmos. Sci., 35, 2362-2367.

Berry, L. & Whiteman, A.J., (1968). The Nile in Sudan. The Geographical Journal, 134(1), 1-35

Bishop, W.W. (1966). Stratigraphical geomorphology. In: Essays in geomorphology (ed. by G.H. Dury), 139-176, New York.

Bootsman, C.S. (1997). On the Evolution of the Upper-Molopo Drainage. S. Afr. Geogr. J., 79(2). 83-92.

Bown, T.M., Kraus, M.J., Wing, S.L., Fleagle, J.G., Tiffney, B.H., Simons, E.L., & Vondra, C.F. (1982). The Fayum Primate Forest revisited. J. of Human Evolution, 11, 503-560.

Breed, C.S., McCauley, J.F. & Grolier, M.J. (1982). Relict drainage, conical hills, and the eolian veneer in southwest Egypt: applications to Mars. J. Geophys. Res., 87, 9929-9950.

Broadley, D.G. & Cotterill, F.P.D. (2004). The reptiles of southeast Katanga, an overlooked 'hot spot'. Afr. J. Herpetology, submitted.

Browne, S.E. & Fairhead, J.D. (1983). Gravity study of the Central African Rift System: a model of continental disruption, 1. Tectonophysics, 94, 187-203.

Buckle, C. (1978). Landforms in Africa: An Introduction to Geomorphology. Longman Group, Essex, England.

Burke, K. (1976). The Chad Basin: An active intra-continental basin. Tectonophysics, 36, 197-206.

Burke, K. (1996). The African Plate. S. Afr. J. Geol., 99(4), 341-409.

Burke, K. & Wilson, J.T. (1972). Is the African Plate stationary? Nature, 239, 387-389.

Burke, K. & Dewey, J.F. (1973). Plume generated triple junctions: Key indicators in applying plate tectonics to old rocks. J. Geol. 81, 406-433.

Burke, K. & Dewey, J.F. (1974). Two plates in Africa during the Cretaceous? Nature, 249, 313-316.

Burke, K. & Wells, G.L. (1989). Trans-African drainage system of the Sahara: Was it the Nile? Geology, 17, 743-747.

Burke, K, Dessauvagie, T.F.J. & Whiteman, A.J. (1971). Opening of the Gulf of Guinea and geological history of the Benue Depression and Niger Delta. Nature Phys. Sci., 232, 51-55.

Burke, K., MacGregor, D.S. & Cameron, N.R. (2003). Africa's petroleum systems: four tectonic 'Aces' in the past 600 million years. In: Petroleum Geology of Africa, New Themes and Developing Technologies (ed. by T.J. Arthur, D.S. MacGregor & N.R. Cameron), 21-60. Geological Society Special Publication 207.

Cahen, L. & Snelling, N.J. (1984). The Geochronology and Evolution of Africa. Oxford University Press, Oxford.

Charney, J.G. (1975). Dynamics of deserts and draught in the Sahel. Quart. J. R. Met. Soc. 101, 193-202.

Claussen, M. (1997). Modeling bio-geophysical feedback in the African and Indian monsoon region. Clim. Dyn., 13, 247-257.

Claussen, M., Kubatzki, C., Brovkin, V., Ganopolski, A., Hoelzmann, P. & Pachur, H.-J. (1999). Simulation of an abrupt change in Saharan vegetation in the mid-Holocene. Geophys. Res. Lett., 24(14), 2037-2040.

Collins, R.O. (1990). The Waters of the Nile. Clarendon Press, Oxford.

Cotterill, F.P.D. (2003a). Geomorphological Influences an Vicariant Evolution in Some Africam Mammals in the Zambezi Basin: Some Lessons for Conservation. In: Ecology and Conservation of Mini-antelope: Proceedings of an International Symposium an Duiker and Dwarf Antelope in Africa (ed. By A. Plowman). Filander Verlag, 11-58.

Cotterill, F.P.D. (2003b). Insights into the taxonomy of tsessebe antelopes *Damaliscus lunatus* with the description of a new evolutionary species in south-central Africa. Durban Museum Novitates 28, 11-30.

Cotterill, F.P.D. (2003c). A biogeographic review of tsessebe antelopes *Damaliscus lunatus* in south-central Africa. Durban Museum Novitates 28, 45-55.

Cotterill, F.P.D. (2004) Drainage Evolution in South-Central Africa and Vicariant Speciation in Swamp-Dwelling Weaver Birds and Flycatchers. The Honeyguide 50, in press.

Cox, K.G. (1989). The role of mantle plumes in the development of continental drainage patterns. Nature, 342, 873-877.

CSAG (Climate System Analysis Group, 2002). Assessments of Impacts and Adaptations to Climate Change: Africa Climate Change Scenarios, Volume 1.

Daly, M.C., Chakraborty, S.K., Kasolo, P., Musiwa, M., Mumba, P., Naidu, B., Namateba, C., Ngambi, O & Coward, M.P. (1984). The Lufilian arc and Irumide belt of Zambia: results of a geotraverse across their intersection. J. Afr. Earth Sci. 2(4), 311-318.

Daly, M.C., Lawrence, S.R., Kimun'a, D. & Binga, M. (1991). Late Paleozoic deformation in central Africa: a result of a distant collision? Nature, 350, 605-607.

Daly, M.C., Lawrence, S.R., Diemu-Tshiband, K. & Matouana, B. (1992). Tectonic evolution of the Cuvette Centrale, Zaire. J. Geol. Soc, London, 149, 539-564.

Darkoh, M.B.K. (1997). Desertification in Botswana. *RALA* Report, 200, 61-74.

Davis, W.M. (1889). The Rivers and Valleys of Pennsylvania. National Geographic, 1, 183-253.

de Wit, M.C.J. (1990). Paleoenviromental interpretation of Tertiary sediments at Bosluispan, Namaqualand. In: Paleontology of Africa (ed. by K. Heine), 21, 101-118.

de Wit, M.C.J. (1993). Cainozoic Evolution of Drainage Systems in the North-Western Cape. Unpublished PhD thesis, University of Cape Town.

de Wit, M.C.J. (1999). Post-Gondwana Drainage and the Development of Diamond Placers in Western South Africa. Economic Geology, 94, 721-740.

de Wit, M.J. (2003). Madagascar: Heads it's a Continent, Tails it's an Island. Annu. Rev. Earth Sci., 31, 213-248.

de Wit, M.J., Jeffery, M., Bergh, H. & Nicolaysen, L. (1988). Geological Map of Sectors of Gondwana. Published by The American Association of Petroleum Geologists.

Dodds, P.S. & Rothman, D.H. (1999). Unified view of scaling laws for river networks. Phys. Rev. E, 59(5), 4865-4877.

Dodds, P.S. & Rothman, D.H. (2000). Scaling, Universality, and Geomorphology. Annu. Rev. Earth Planet. Sci., 28, 571-610.

Dodds, P.S. & Rothman, D.H. (2001). Geometry of river networks. I. Scaling, fluctuations, and deviations. Phys Rev. E., 63, 016115:1-13.

Doucouré, C.M & de Wit, M.J. (2003). Old inherited origin for the present near-bimodal topography of Africa. Journal of African Earth Sciences, 36, 371-388.

Dubuc, B., Zucker, S.W., Tricot, C., Quiniou, J.F. & Wehbi, D. (1989). Evaluating the fractal dimension of surfaces. Proc. Roy. Soc. London A425, 113-127.

Du Toit, A.L. (1933). Crustal movements as a factor in the evolution of South Africa. South African Geophysical Journal, 16, 3-20.

Ebinger, C.J. & Ibrahim, A. (1994). Multiple episodes of rifting in Central and East Africa: A re-evaluation of gravity data. Geol. Rundsch, 83, 689-702.

Ebinger, C.J. & Sleep, N.H. (1998). Cenozoic magmatism throughout east Africa resulting from impact of a single plume. Nature, 395, 788-791.

Fairhead, J.D. (1988). Mesozoic plate tectonic reconstructions of the central South Atlantic Ocean: The role of the West and Central African rift system. Tectonophysics, 155, 181-191.

Fairhead, J.D. & Binks, R.M. (1991). Differential opening of the Central and South Atlantic Oceans and the opening of the West African rift system. Tectonophysics, 187, 191-203.

Ganopolski, A., Rahmstorf, S., Petoukhov, V. & Claussen, M. (1998a). Simulation of modern and glacial climates with a coupled global model of intermediate complexity. Nature, 391, 351-356.

Ganopolski, A., Kubatzki, C., Claussen, M. Brovkin, V. & Petoukhov, V. (1998b). The Influence of Vegetation-Atmosphere-Ocean Interaction on Climate During the Mid-Holocene. Science, 280, 1916-1919.

Görgens, A.H.M. & van Wilgen, B.W. (2004). Invasive alien plants and water resources in South Africa: current understanding, predictive ability and research challenges. S. Afr. J. Sci. 100, 27-33.

Gratrix, S. & Elgin, J.N. (2004). Pointwise Dimensions of the Lorenz Attractor. Phys. Rev. Lett. 92(1), 014101-1:4.

Gregory, K.J. (1976). Drainage Networks and Climate. In: Geomorphology and Climate (ed. by E. Derbyshire), 289-315, John Wiley and Sons.

Grove, A.T. & Warren, A. (1968). Quaternary landforms and climate on the south side of the Sahara. Geographical Journal 134, 297-306.

Gutenberg, B. & Richter, C.F. (1954). Seismicity of the Earth and Associated Phenomenon, 2nd edition. Princeton University Press.

Hack, J.T. (1957). Studies of longitudinal stream profiles in Virginia and Maryland. US Geol. Surv. Prof. Pap. 294B, 45-97.

Halsey, T.C. & Jensen, M.H. (2004). Hurricanes and butterflies. Nature 428, 127-128.

Halsey, T.C., Jensen, M.H., Kadanoff, L.P., Procaccia, I. & Shraiman, B.I. (1986). Fractal measures and their singularities: The characterization of strange sets. Phys. Rev. A 33, 1141-1151.

Hassan, F. (2001). The Fall of the Egyptian Old Kingdom. BBC History Website Article: http://www.bbc.co.uk/history/ancient/egyptians/apocalypse_egypt_04.shtml

Hobbs, W.H. (1905). Examples of joint-controlled drainage from Wisconsin and New York. Journal of Geology 13, 363-374.

Hoelzmann, P., Jolly, D., Harrison, S.P., Laarif, F., Bonnefille, R. & Pachur, H.-J. (1998). Mid-Holocene land-surface conditions in northern Africa and the Arabian peninsula: A data set for the analysis of biogeophysical feedbacks in the climate system. Global Biogeochemical Cycles, 12(1), 35-51.

Hofmann, C., Courtillot, V., Féraud, G., Rochette, P., Yirgu, G., Ketefo, E. & Pik, R. (1997). Timing of the Ethiopian flood basalt event and implications for plume birth and global change. Nature, 389, 838-841.

Holmes, A. (1965). Principles of Physical Geology. 2nd edition. William Clowes and Sons, London.

Horton, R.E. (1945). Erosional development of streams and their drainage basins; hydrophysical approach to quantitative morphology. Bull. Geol. Soc. Am. 56(3) 275-370.

Hovius, N., (1996). Regular spacing of drainage outlets from linear mountain belts. Basin Research 8, 29-44.

Hubert, T., Norris, R.D. & MacLeod, K.G. (2002). Deep-sea paleo-temperature record of extreme warmth during the Cretaceous. Geology, 30, 123-126.

Issawi, B. & McCauley, J.F. (1992). The Cenozoic Rivers of Egypt: The Nile Problem. In: The followers of Horus: studies in memory of M.A. Hoffman (ed. by R. Friedman & B. Adams), 121-138. Egyptian studies publication 2, Oxbow Books, Oxford, England.

Jolly, D., Prentice, I.C., Bonnefille, R. & 30 associates (1998). Biome reconstruction from pollen and plant macrofossil data for Africa and the arabian peninsula at 0 and 6000 years. J. of Biogeography, 25, 1007-1027.

Jones, S.J., (2002). Transverse rivers draining the Spanish Pyrenees: large scale patterns of sediment erosion and deposition. In: Sediment Flux to Basins: Causes, Controls and Consequences (ed. by S. J. Jones & L.E. Frostick), 171-185. Geological Society Special Publication 191.

Kimani, M. (2004). The Nile Water Wars. The East African Standard, Nairobi: 13th March 2004. Available online: http://allafrica.com/stories/200403150239.html

King, J.M. & Schael, D.M. (2001). Assessing the ecological relevance of a spatially nested geomorphological hierarchy for river management. Water Research Commission Report # 754/1/01.

King, L.C. (1963). South Africa Scenery – a Textbook of Geomorphology. Third Edition – Revised, Oliver & Boyd, Edinburgh and London.

Krom, M.D., Stanley, J.-D., Cliff, R.A. & Woodward, J.C. (2002). Nile River sediment fluctuations over the past 7000 yr and their key role in sapropel development. Geology 30, 71-74

Kutzbach, J.E. & Guetter, P.J. (1986). The influence of changing orbital parameters and surface boundary conditions on climate simulations for the past 18,000 years. J. Atmos. Sci. 43, 1726-1759

Legates, D.R. & Willmot, C.J. (1990a). Mean seasonal and spatial variability in gauge-corrected global precipitation. Int. J. Climatology 10(2), 111-127.

Legates, D.R. & Willmot, C.J. (1990b). Mean seasonal and spatial variability in global surface air temperature. Theor. Appl. Climatol. 41, 11-21.

Lindsay, S.W. & Birley, M.H. (1996). Climate change and malaria transmission. Annals of Tropical Medicine and Parasitology, 90, 573-588.

Lister, L.A. (1967). African Landscape Studies. A.W. Bardwell & Co., Salisbury, Rhodesia.

Livingstone, D.A. (1980). Environmental changes in the Nile headwaters. In: The Sahara and the Nile (ed. by M.A.J. Williams & H. Faure) 339-359. A.A. Balkema, Rotterdam.

Lorenz, E.N. (1963). Deterministic nonperiodic flow, J. Atmos. Sci., 20, 130-141.

MacDonald, I.A.W. (2004). Recent research on alien plant invasions and their management in South Africa: a review of the inaugural research symposium of the Working for Water programme. S. Afr. J. Sci. 100, 21-26.

Malakooti, M.A., Biomndo, K. & Shanks G.D. (1997). Reemergence of epidemic high-land malaria in the highlands of western Kenya. Emerging Infectious Diseases, 4(4), 671-676.

Mandelbrot, B.B. (1967). How long is the coast of Britain? Statistical self-similarity and fractional dimension. Science, 156, 636-638.

Mandelbrot, B.B. (1975). Stochastic models for the earth's relief, the shape and the fractal dimension of coastlines, and the number-area rule for islands. Proc. Nat. Acad. Sci. USA 72, 3825-3828.

Maritan, A., Rinaldo, A., Rigon, R., Giacometti, A. & Rodriguez-Iturbe, I. (1996). Scaling laws for river networks. Phys. Rev. E, 53(2), 1510-1515.

Matola, Y.G., White, G.B., Magayuka, S.A. (1987). The changed pattern of malaria endemicity and transmission at Amano in the eastern Usambara mountains, north-eastern Tanzania. Journal of Tropical Medicine and Hygiene, 90 (3), 127-134.

Matthews, E. (1983). Global vegetation and land use: New high-resolution data bases for climate studies. J. Clim. Appl. Meteor., 22, 474-487.

Matthews, E. (1984). Prescription of Land-surface Boundary Conditions in GISS GCM II: A Simple Method Based on High-resolution Vegetation Data Sets. NASA TM-86096. National Aeronautics and Space Administration, Washington, D.C.

McCauley, J.F., Schaber, G.G., Breed, C.S., Grolier, M.J., Haynes, C.V., Issawi, B., Elachi, C. & Blom, R. (1982). Subsurface Valleys and Geoarcheology of the Eastern Sahara Revealed by Shuttle Radar. Science, 218, 1004-1020.

McCauley, J.F., Breed, C.S., Schaber, G.G., McHugh, W.P., Issawi, B., Haynes, C.V., Grolier, M.J. & El Kilani, A. (1986). Paleodrainages of the eastern Sahara – The radar rivers revisited (SIR-A/B implications for a mid-Tertiary trans-African drainage system). IEEE Transactions on Geoscience and Remote Sensing, v. GE-24, 624-648.

McClay, K. (1991). The Mapping of Geological Structures. Johm Wiley & Sons Ltd, UK.

McKenzie, D. & Weiss, N. (1975). Speculations on the thermal and tectionic history of the earth. Geophys. J. R. Astron. Soc., 42, 131-174.

Meakin, P., Feder, J. & Jøssang, T. (1991). Simple statistical models for river networks. Physica A, 176, 409-429.

Moglen, G.E., Eltahir, E.A.B. & Bras, R.L. (1998). On the sensitivity of drainage density to climate change. Water Resour. Res., 34(4), 855-862.

Montgomery, D.R. & Dietrich, W.E. (1988). Where do channels begin? Nature, 336, 232-234.

Moore, A.E. (1999). A reappraisal of epirogenic flexure axes in southern Africa. S. Afr. J. Geol. 102, 363-376.

Moore, A.E. & Blenkinsop, T. (2002). The role of mantle plumes in the development of continental-scale drainage patterns: The southern African example revisited. S. Afr. J. Geol. 105, 353-360.

Moore, A.E. & Larkin, P.A. (2001). Drainage evolution in south-central Africa since the breakup of Gondwana. S. Afr. J. Geol. 104(1), 47-68.

Mueller, J.E. (1973). Re-evalueation of the relationship of master streams and drainage basins: reply. Geol. Soc. Am. Bull. 84, 3127-3130.

Nel, J.L., Richardson, D.M., Rouget, M, Mgidi, T.N., Mdzeke, N., Le Maitre, D.C., van Wilgen, B.W., Schonegevel, L., Henderson, L. & Neser, S. (2004). A proposed classification of invasive alien plant species in South Africa: towards prioritizing species and areas for management action. S. Afr. J. Sci. 100, 53-64.

Nyblade, A.A. & Robinson, S.W. (1994). The African Superswell. Geophys. Res. Lett. 21, 765-768.

Nyblade, A.A., Pollack, H.N., Jones, D.C., Podmore, F. & Mushayandebvu, M. (1990). Terrestrial heat flow in east and southern Africa. J. Geophys. Res. 95, 17371-17384.

Okay, N. & Okay, A.I. (2002). Tectonically induced Quaternary drainage diversion in the northeastern Aegean. J. Geol. Soc, London. 159, 393-399.

Peckham, S.D. (1995). New results for self-similar trees with applications to river networks. Water Resour. Res. 31(4) 1023-1029.

Pelletier. J.D. (1999). Self-organization and scaling relationships of evolving river networks. J. Geophys. Res. 104(B4) 7359-7375.

Petit-Maire, N. & Guo, Z. (1996). Mise en evidence de variations climatiques holocenes rapides, en phase dans les deserts actuels de Chine et du Nord de lAfrique. Sciences de la Terre et des Planetes 322, 847-851.

Pfeiffer, P. & Olbert, M. (1989). Fractals: Basic concepts and terminology. In: The fractal approach to heterogeneous chemistry (ed. by D. Anvir), pp 11-43, Wiley, Chichester.

Pindell, J. & Dewey, J.F. (1982). Permo-Triassic reconstruction of Western Pangea and the evolution of the Gulf of Mexico / Caribbean domains. Tectonics, 1, 179-211.

Plafker, G. (1969). Tectonics of the March 27, 1964 Alaska Earthquake, 543-1. US Geological Survey Professional Paper.

Ramsay, J.G. & Huber, M.I. (1987). The techniques of modern structural geology. Volume 2: Folds and Fractures. Academic Press, Oxford.

Reclus, E. (1888). The Earth and its Inhabitants – Africa, Volume III, West Africa. D.Appleton & Co., New York.

Reeves, C.V. (1972). Rifting in the Kalahari? Nature, 237, 95-96.

Reeves, C.V. (1978). A failed Gondwana spreading axis in southern Africa. Nature, 273, 222-223.

Reeves, C.V., Karanja, F.M. & MacLeod, I.N. (1986). Geophysical evidence for a failed Jurassic rift and triple junction in Kenya. Earth and Planet. Sci. Lett., 81, 299-311.

Reeves, C.V., de Wit, M.J. & Sahu, B.K. (2004). Tight Reassembly of Gondwana Exposes Phanerozoic Shears in Africa as Global Tectonic Players. Gondwana Research 7(1), 7-19.

Richards, M.A., Duncan, R.A. & Courtillot, V.E. (1989). Flood basalts and hotspot tracks: plume heads and tails. Science 246, 103-107.

Rigon, R., Rodriguez-Iturbe, I., Maritan, A., Giacometti, A., Tarboton, D.G. & Rinaldo, A. (1996). On Hack's Law. Water Resour. Res., 32(11), 3367-3374.

Rigon, R., Rodriguez-Iturbe, I. & Rinaldo, A. (1998). Feasible optimality implies Hack's Law. Water Resour. Res., 34(11), 3181-3189.

Rodriguez-Iturbe, I. & Rinaldo, A. (1997). Fractal River Basins: Chance and Self-Organization. Cambridge, UK: Cambridge Univ. Press.

Rosso, R., Bacchi, B. & La Barbera, P., (1991). Fractal relation of mainstream length to catchment area in river networks. Water Resour. Res., 20(7) 914-920.

Sahagian, D. (1988). Epeirogenic motions of Africa as inferred from Cretaceous shoreline deposits. Tectonics, 7(1), 125-138.

Said. R. (1981). The Geological Evolution of the River Nile. Springer Verlag, New York.

Schandelmeir, H., Richter, A. & Franz, G. (1983). Outline of the geology of magmatic and metamorphic units between Gebel Uweinat and Bir Safsaf (SW Egypt / NW Sudan). J. Afr. Earth Science 1, 275-283.

Schandelmeir, H., Huth, A., Harms, U., Franz, G. & Bernau, R. (1987). The East Saharan craton in southern Egypt and northern Sudan: lithology, metamorphism, magamatism, geochronology and structural development. Berliner Geowissenschaftlichen Abhandlungen, A, 75, 25-48.

Schneider, J.L. (1967). Evolution du dernier lacustre et peuplements préhistoriques aux Bas-Pays du Tchad, bulletin. Association Sénégalaise pour l'Etude du Quaternaire en Afrique, Sénégaile.

Schorghofer, N., & Rothman, D.H., (2001). Basins of attraction on random topography. Phys. Rev. E 63(2), 026112-1:7.

Seeber, L. & Gornitz, V., (1983). River profiles along the Himalayan arc as indicators of active tectonics. Tectonophysics, 92, 335-367.

Shackleton, R.M., (1978). Structural development of East Africa rift system. In: Geological Background to Fossil Man (ed. by W.W. Bishop), Scottish Academic Press, Edinburgh.

Shreve, R.L., (1967). Infinite topologically random channel networks. J. of Geology, 75, 178-186.

Silver, P.G., Gao, S.S, Liu, K.H. and the Kaapvaal Seismic Group. (2001). Mantle deformation beneath southern Africa. Geophys. Res. Lett. 28, 2493-2496.

Snider, A. (1858). La Création et ses mystères dévoilés. Paris.

South African Geological Survey (1979). 1:250,000 Geological Series, map 3322 (Oudtshoorn).

Stankiewicz, J., Chevrot, S., van der Hilst, R.D. & de Wit, M.J. (2002). Crustal thickness, discontinuity depth, and upper mantle structure beneath southern Africa: constraints from body wave conversions. Physics of the Earth and Planetary Interiors 130, 235-251.

Strahler, A.N. (1957). Quantitative analysis of watershed geomorphology. EOS Trans. AGU 38(6), 913-920.

Stokes, S., Thomas, D.S.G. & Washington, R. (1997). Multiple episodes of aridity in southern Africa since the last interglacial period. Nature 388, 154-158.

Taljaard, M.S. (1949). Glimpse of South Africa. The University Publishers and Booksellers, Stellenbosch, South Africa.

Tankard, A.J., Jackson, M.P.A., Eriksson, K.A., Hobday, D.A., Hunter, D.R. & Minter, W.E.L. (1982). Crustal Evolution of southern Africa - 3.8 billion years of earth history. Springer-Verlag, Heidelberg.

Tarboton, D.G., Bras, R.L. & Rodriguez-Iturbe, I. (1988). The fractal nature of river networks. Water Resour. Res., 24(8), 1317-1322.

Thiessen, R., Burke, K. & Kidd, W.S.F. (1979). African Hotspots and their relation to the underlying mantle. Geology, 7, 263-266.

Thomas, D.S.G., & Shaw, P.A. (1991). The Kalahari environment. Cambridge University Press.

Tokunaga, E., (1978). Consideration of the composition of drainage networks and their evolution. Geogr. Rep., Tokyo Metrop. Univ., 13, 1-27.

Tooth, S., McCarthy, T.S., Brandt, D., Hancox, P.J. & Morris, R. (2002). Geological controls of the formation of alluvial meanders and floodplain wetlands: the example of the Klip River, Eastern Free State, South Africa. Earth Surface Processes and Landforms, 27, 797-815.

Tooth, S., Brandt, D., Hancox, P.J. & McCarthy, T.S. (2004). Geological controls on alluvial river behaviour: a comparative study of three rivers on the South African Highveld. J. Afr. Earth Sci., 38, 79-97.

Truswell, J. F. (1970). An Introduction to the Historical Geology of South Africa. Purvell Press, South Africa.

Tucker, G.E. & Bras, R.L. (1998). Hillslope processes, drainage density, and landscape morphology. Water Resour. Res., 34(10), 2751-2764.

Turcotte, D.L. (1986). Fractals and Fragmentation. J. Geophys. Res. 91, 1921-1926.

Turcotte, D.L. (1992). Fractals and chaos is geology and geophysics. Cambridge University Press.

Uenzelmann-Neben, G., Spiess, V. & Bleil, U. (1997). A seismic reconnaissance survey of the northern Congo Fan. Marine Geology, 140, 283-306.

Uenzelmann-Neben, G. (1998). Neogene sedimentation history of the Congo Fan. Marine and Petroleum Geology, 15, 635-650.

Unternehr, P., Curie, D., Olivet, J.L., Goslin, J. & Beuzart, P. (1988). South Atlantic fits and intraplate boundaries in Africa and South America. Tectonophysics, 155, 169-179.

Vale, P. (2004). Whatever happened to the post-appartheid moment? Past hopes and possible futures for southern Africa. Catholic Institute for International Relations, London, UK.

Vincent, P.M. (1970). The evolution of the Tibesti Volcanic Province, Eastern Sahara. In: African Magmatism and Tectonics (ed. by T.N. Clifford & I.G. Gass), pp 301-319, Oliver & Boyd, Edinburgh, UK.

Voss, R.F. (1985). Random fractals: characterization and measurement, In: Scaling Phenomena in Disordered Systems (ed. by R. Pynn & A. Skejeltorp), pp 1-11, Plenum Press, New York.

Voss, R.F. (1988). Fractals in nature: From Characterization to simulation. In: The Science of Fractal Images (ed. by H.O. Peitgen & D. Saupe), pp 21-70, Springer-Verlag, New York.

Wellington, J.H. (1955). Southern Africa – A Geographic Study. Volume I, Physical Geography. Cambridge University Press.

White, R. & McKenzie, D. (1989). Magmatism at rift zones: The generation of volcanic continental margins and flood basalts. J. Geophys. Res. 94, 7685-7729.

Williams, M.A.J., Adamson, D., Prescott, J.R. & Williams, F.M. (2003). New light on the age of the White Nile. Geology 31(11), 1001-1004.

Wilson, M. & Guiraud, R. (1998). Late Permian to Recent magmatic activity on the African-Arabian margin of Tethys. In: Petroleum Geology of North Africa (ed. by D.S. MacGregor, R.T.J. Moody & D.D Clark-Lowes), 231-263. Geological Society Special Publication 132.

Wolf, A.T., Stahl, K. & Macomber, M.F. (2003). Conflict and cooperation within international river basins: the importance of institutional capacity. Water Resources Update, 125, 1-10; Universities Council On Water Resources.

Yu, G. & Harrison, S.P. (1996). An evaluation of the simulated water balance of Eurasia and northern Africa at 6000 y BP using lake status data. Cim. Dyn. 12, 723-735.

Zaghloul, Z.M., Andrawis, S.F. & Ayyad, S.N. (1979). New contribution to the Tertiary sediments of Kafr El-Dawar Well No. 1, north-west Nile Delta, Egypt. Geological Survey of Egypt, Annals, v9, 292-307.

Zobler, L. (1986). A world soil file for global climate modeling. NASA TM-87802. National Aeronautics and Space Administration, Washington, D.C.